

Copyright Notices

Notice 1

Under the Copyright Act 1968, this thesis must be used only under the normal conditions of scholarly fair dealing. In particular no results or conclusions should be extracted from it, nor should it be copied or closely paraphrased in whole or in part without the written consent of the author. Proper written acknowledgement should be made for any assistance obtained from this thesis.

Notice 2

I certify that I have made all reasonable efforts to secure copyright permissions for third-party content included in this thesis and have not knowingly added copyright content to my work without the owner's permission.

**THE DEVELOPMENT OF INFRARED
MICROSPECTROSCOPY TECHNIQUES TO EXAMINE THE
EFFECT OF MONOCLONAL ANTIBODIES TO TYPE II
COLLAGEN IN A MURINE MODEL OF
RHEUMATOID ARTHRITIS**

A thesis presented for the degree of DOCTOR OF PHILOSOPHY

By

ALLYSON MICHELLE CROXFORD, B.Sc. Hons

(Monash University)

Supervisors: A/Prof. Merrill Joy Rowley

Prof. Donald McNaughton



Department of Biochemistry and Molecular Biology

Clayton Campus, Victoria 3800

AUSTRALIA

August, 2011

TABLE OF CONTENTS

<u>SECTION</u>	<u>PAGE NUMBER</u>
SUMMARY	i
GENERAL DECLARATION.....	vi
DECLARATION FOR RESEARCH PAPER 1	viii
DECLARATION FOR RESEARCH PAPER 2	x
DEDICATIONS.....	xii
ACKNOWLEDGEMENTS	xiii
PUBLICATIONS.....	xvii
CONFERENCE PRESENTATIONS	xviii
ABBREVIATIONS AND DEFINITIONS	xx
 Chapter One – Literature Review:	
<i>Infrared microspectroscopy to examine chemical changes to cartilage</i>	
Introduction	1
1.1. Structure of cartilage	2
1.1.1. Collagen	5
1.1.1.1. Structure of collagen.....	5
1.1.1.2. Cartilage collagens.....	8
1.1.1.3. Synthesis of collagen.....	10
1.1.2. Glycosaminoglycans	13
1.1.2.1. Aggrecan.....	13
1.1.2.2. Hyaluronan.....	17

1.1.2.3. Other smaller glycosaminoglycans	17
1.1.3. Chondrocytes	18
1.1.4. Current methods for analysing cartilage and the requirement for new techniques	21
1.2. Infrared spectroscopy	25
1.2.1. Fourier Transform Infrared Spectroscopy	27
1.2.2. Fourier Transform Infrared Microspectroscopy and the development of the focal plane array system	29
1.2.3. Sample preparation.....	30
1.2.3.1. Collection of data in Transmission mode.....	34
1.2.3.2. Collection of data in Transflection mode	35
1.2.4. Synchrotron Infrared Spectroscopy	35
1.2.5. The use of IR spectroscopy for the analysis of organic molecules	39
1.2.6. Analysis of secondary structure by FTIRS.....	43
1.2.7. Features of the spectra of cartilage components	48
1.2.7.1. Collagen.....	50
1.2.7.2. Proteoglycans	50
1.2.7.3. Hyaluronan.....	52
1.2.7.4. Combined spectral properties of cartilage.....	52
1.2.8. Methods of analysis	55
1.2.8.1. General chemometric analysis packages	55
1.2.8.2. Software for the analysis of spectral images	56

1.2.8.2.1. Cytospec analysis software	56
1.2.8.3. Unsupervised hierarchical cluster analysis	57
1.2.9. Applications of Fourier Transform Infrared Microspectroscopy.....	60
1.2.10. Applications of synchrotron radiation.....	62
1.3. The role of autoantibodies to collagen in the development of arthritis.....	64
1.4. Collagen Induced Arthritis.....	65
1.5. Collagen Antibody-Induced Arthritis	67
1.6. Epitope specificity of autoantibodies to CII in CAIA.....	70
1.7. A comparison of human RA and CAIA	73
1.8. <i>In vitro</i> studies on the effects of mAbs to CII.....	74
Aims of PhD	80
Chapter Two – The effects of monoclonal antibodies to CII on cartilage <i>in vitro</i>	
2.1. Preface	82
2.2. Research paper 1 – Specific antibody protection of the extracellular cartilage matrix against collagen antibody-induced damage	86
Chapter Three - The effects of monoclonal antibodies to CII on cartilage <i>in vivo</i>	
A. Chemical changes demonstrated in cartilage by synchrotron infrared microspectroscopy	
3.1. Preface	97

3.2. Research paper 2 – Chemical changes demonstrated in cartilage by synchrotron infrared Microspectroscopy in an antibody-induced murine model of rheumatoid arthritis101

Chapter Four -The effects of monoclonal antibodies to CII on cartilage *in vivo*

B. Histological changes

4.1. Preface 110

4.2. Research paper 3 – The role of collagen as the primary autoantigen in rheumatoid arthritis111

Chapter Five – General discussion..... 134

References..... 141

Appendix.....155

SUMMARY

Type II collagen (CII) is the major protein in cartilage. Collagen induced arthritis (CIA), that occurs in animals immunised with CII, is an experimental model of human rheumatoid arthritis (RA). The autoimmune response that develops in CIA includes the formation of antibodies to CII that provoke an acute destructive arthritis, collagen antibody induced arthritis (CAIA), on transfer to naïve mice. Although CAIA can be transferred by some single monoclonal antibodies (mAbs) to CII and by combinations of mAbs, not all are arthritogenic and arthritogenicity appears to be epitope related. The epitope specificity of arthritogenic mAbs has been mapped to regions of the CII molecule that are involved in structural interactions important to maintain cartilage stability. Several of these arthritogenic mAbs have been shown to affect collagen fibril formation, chondrocyte morphology and the synthesis of new cartilage matrix *in vitro*.

The aim of the present study was to examine the direct effects of combinations of mAbs to CII on pre-existing cartilage in the absence of inflammation *in vitro* in bovine cartilage explant cultures, and *in vivo* in mice that had not developed inflammation after injection with arthritogenic combinations of mAbs.

Because mAbs penetrate intact cartilage poorly, biochemical techniques used to examine new matrix formation in chondrocyte cultures were not suitable for such analysis. Instead, Fourier Transform Infrared Microspectroscopy (FTIRM) was used to examine chemical changes across the cartilage. FTIRM has been used previously in preliminary studies that indicate that some individual mAbs cause damage to pre-existing cartilage *in vitro*.

To test the effects of combinations of mAbs to CII on pre-existing cartilage *in vitro*, the morphology and chemical nature of the cartilage was examined using a standard combination of two mAbs M2139 and CIIC1 that are used to induce CAIA *in vivo*. Histological and FTIRM changes were examined in bovine cartilage explants

cultured with or without mAbs for up to two weeks *in vitro*. The effect of the addition of the non-arthritisogenic mAb ClIF4 to this combination of arthritisogenic mAbs was tested, noting that *in vivo* ClIF4 decreases the incidence and severity of CAIA induced by M2139 and ClIC1. To determine whether the effects of the mAbs were mediated by the mAbs alone or by cellular mechanisms, experiments were performed on cartilage containing viable or non-viable chondrocytes. The role of matrix metalloproteinases (MMPs) in mAb mediated cartilage damage and protection was examined by the addition of the MMP inhibitor GM6001 to cultures containing the arthritisogenic mAbs.

To test the effects of combinations of mAbs to CII on pre-existing cartilage *in vivo* the morphology and chemical nature of the cartilage was examined in mice injected with arthritisogenic mAbs that did not develop inflammation. Two different strains of mice were used, B10.Q mice that usually develop CAIA only after an additional injection of lipopolysaccharide (LPS) and B10.Q C5 δ mice that lack complement factor C5 and do not develop CAIA. Mice were injected with the standard mixture of two mAbs, ClIC1 and M2139 or a more arthritisogenic combination of four mAbs, M2139, ClIC1, UL-1 and ClIC2. Three days after injection, the mice were killed, and paws were decalcified and embedded in paraffin. The chemical nature of changes to the cartilage matrix and chondrocytes were examined by synchrotron FTIRM, and detailed histological examination of both matrix and chondrocytes was performed using a modified Mankin score, originally developed for scoring cartilage changes in osteoarthritis.

FTIRM analysis focused on the identification of changes to CII and proteoglycans. The amide 1 band, which is typically a measure of total protein content, was used for identification of changes to CII. The position of the amide 1 band when native triple helical CII is present is located above 1660 cm^{-1} , with a shift to a lower wavenumber upon denaturation of CII. Proteoglycan content was observed by examination of the height of the peak at 1076 cm^{-1} and compared with proteoglycan loss measured histologically by toluidine blue staining.

The results of the *in vitro* experiments on cartilage explants showed that the two arthritogenic mAbs M2139 and CIIC1 caused progressive degradation of the cartilage surface, including substantial loss of proteoglycans seen both by FTIRM and by toluidine blue staining, and denaturation and loss of CII demonstrable by FTIRM. The cartilage damage did not require living chondrocytes as the mAbs caused greater cartilage destruction in the absence of viable cells. By contrast, the non-arthritogenic mAb CIIF4 alone had no apparent effect on cartilage but when given with the arthritogenic mAbs prevented damage and caused apparent matrix regeneration, a process which only occurred in the presence of viable chondrocytes. The addition of the MMP inhibitor GM6001 reduced the cartilage damage caused by the arthritogenic mAbs M2139 and CIIC1 but did not mimic the protective effect of CIIF4. These results showed clearly that in addition to their adverse effects on the new synthesis of cartilage, CII reactive antibodies can cause direct damage to pre-existing cartilage. Moreover some antibodies could also be protective, depending on their epitope specificity, but the protection did not merely result from blocking binding of the damaging antibodies, as it required viable cells.

To determine whether the arthritogenic mAbs likewise cause non-inflammatory cartilage damage *in vivo*, strains of mice with impaired capacity to develop inflammation were injected intravenously with either two or four potentially arthritogenic mAbs, or with saline only as controls. Although none of the mice injected with mAbs showed visual or histological evidence of inflammation, in the presence of the mAbs that cause CAIA *in vivo* there were histological changes in the articular cartilage, including loss of proteoglycan and altered chondrocyte morphology. The changes seen were consistent with those previously observed *in vitro* in cartilage explants.

Synchrotron FTIRM at high lateral resolution revealed loss of CII and the appearance of a new peak at 1635 cm^{-1} at the surface of the cartilage within the cells and in the matrix, that coincided with regions in which chondrocytes were ringed with strong toluidine blue staining, consistent with new proteoglycan synthesis. The composition of the 1635 cm^{-1} band may represent the appearance

of a second band in the amide 1 region as a result of new synthesis of an unknown protein or from β -secondary structures within the globular telopeptides of newly synthesized collagen produced by activated chondrocytes; such telopeptides are normally removed prior to fibril formation.

Detailed histological analysis was performed on all paws from the mice. The cartilage in the joints was scored for cartilage structure, chondrocyte integrity and organization, and proteoglycan loss using toluidine blue. Cartilage damage was shown by marked loss of cartilage structure, chondrocyte hyperplasia and/or loss, loss of proteoglycans in all joints, and protrusion of the chondrocytes from the cartilage surface, particularly in the small phalangeal joints. These data demonstrate that arthritogenic mAbs to CII cause direct cartilage damage in mice *in vivo* in the absence of inflammation. Such changes in inflammation-intact mice would readily enhance the exposure of damaged collagen fibrils to immune complexes containing collagen antibodies, and to the degradative enzymes released by inflammatory cells. Hence antibody-induced cartilage damage is a potential mechanism for initiation and perpetuation of cartilage damage in both murine arthritis and, possibly, in human RA wherein anti-CII antibodies of the same specificity are known to be present.

These results amply demonstrate the utility of FTIRM for the analysis of localised changes in tissue. It has proved to be particularly useful for the analysis of cartilage, which is an unusual tissue made up of a small number of cells in an abundant extracellular matrix. It is the structure of this extracellular matrix that gives the cartilage its capacity to cushion the ends of joints. In contrast to most other tissues, the small number of chondrocytes in the tissue makes it difficult to examine changes in gene activity, and it is difficult to map changes based on histological techniques. Although there are other techniques available for the analysis of cartilage such as immunohistochemistry, this requires prior knowledge of the mechanisms involved in order to identify suitable neoepitopes of interest.

In the present study the use of FTIRM has allowed the definitive demonstration that mAbs to CII can cause direct cartilage damage in the absence of inflammation both *in vitro* and *in vivo*. The use of FTIRM has allowed examination of the localised chemical changes within the cartilage matrix without any prior knowledge of the likely mechanism of action of the mAbs. These studies suggest that antibodies to CII may participate in the cartilage damage that accompanies articular inflammation and that such cartilage damage is independent of, and possibly precedes damage that results from inflammation. . Since antibodies of similar epitope specificity to the mAbs used in these studies occur in RA the data presented in this thesis provide new evidence demonstrating the involvement of CII specific antibodies in the pathogenesis and possibly initiation of human RA.

A striking observation demonstrated in this thesis, is the protective effect of the non-arthritisogenic mAb CIIF4, which suppressed the degradative effects of the arthritisogenic mAbs. Although the mechanism of action of CIIF4 is at present unknown and cannot be elucidated by FTIRM alone, the observation has important implications, since antibodies of the same specificity have been associated with human arthritis but, notably, more abundantly in non-inflammatory osteoarthritis rather than associated with inflammation in rheumatoid arthritis. An understanding of the protective mechanism of CIIF4 could have important implications for the development of new treatments for RA.

In conclusion, these studies have clearly demonstrated the utility of FTIRM for the analysis of cartilage and should have wide applicability not only in RA but also in osteoarthritis, biomaterials and cartilage replacement therapies by identifying changes to the components of cartilage within its native state in the cartilage matrix.

GENERAL DECLARATION



Monash Research Graduate School

Declaration for thesis based or partially based on conjointly published or unpublished work

General Declaration

In accordance with Monash University Doctorate Regulation 17/ Doctor of Philosophy and Master of Philosophy (MPhil) regulations the following declarations are made:

I (**Allyson Michelle Croxford**) hereby declare that this thesis contains no material which has been accepted for the award of any other degree or diploma at any university or equivalent institution and that, to the best of my knowledge and belief, this thesis contains no material previously published or written by another person, except where due reference is made in the text of the thesis.

This thesis includes **(2)** original papers published in peer reviewed journals and **(1)** unpublished publication. The core theme of the thesis is: **The development of infrared Microspectroscopy techniques to examine the effect of monoclonal antibodies to type II collagen in a murine model of rheumatoid arthritis.** The ideas, development and writing up of all the papers in the thesis were the principal responsibility of myself, the candidate, working within the **Department of Biochemistry and Molecular Biology, Monash University** under the supervision of **A/Prof Merrill Rowley (50%) and Prof. Don McNaughton (50%)**

The inclusion of co-authors reflects the fact that the work came from active collaboration between researchers and acknowledges input into team-based research.

In the case of **chapters 2-4** my contribution to the work involved the following:

Chapter 2: Conception and design of the study, acquisition and interpretation of the data. Performed cartilage explant cultures and infrared experiments at the Australian Synchrotron including processing and interpretation of the data collected. Preparation of all figures for the manuscript. Drafting, revising and editing manuscript.

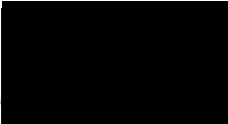
Chapter 3: Conception and design of the study, acquisition and interpretation of the data. Performed infrared experiments including processing and interpretation of the data collected. Preparation of all figures for the manuscript. Drafting, revising and editing manuscript.

Chapter 4: Conception and design of the study, acquisition and interpretation of the data. Performed infrared experiments at the Australian Synchrotron, processed and analysed data collected. Jointly with my supervisor A/Prof Merrill Rowley analysed histology sections of mouse joints and scored them as preparation for the data presented in this chapter. Involved in drafting, revising and editing of this chapter.

A description of the contributions of each co-author for the work involved in chapters 2 and 3 is presented in the declaration of co-authorship for each chapter.

Thesis chapter	Publication title	Publication status*	Nature and extent of candidate's contribution
2	Specific antibody protection of the extracellular cartilage matrix against collagen antibody-induced damage	Published	First author
3	Chemical changes demonstrated in cartilage by synchrotron infrared Microspectroscopy in an antibody-induced murine model of rheumatoid arthritis	Published	First author
4	The role of collagen as the primary autoantigen in rheumatoid arthritis	Prepared for publication	Solo author

I have re-numbered sections of submitted or published papers in order to generate a consistent presentation within the thesis.

Signed: .. 

Date: 16/8/11
(Handwritten date: 16/8/11)

DECLARATION FOR RESEARCH PAPER 1



MONASH University

Declaration for Thesis Chapter 2

Declaration by candidate

In the case of Chapter 2, the nature and extent of my contribution to the work was the following:

Nature of contribution	Extent of contribution (%)
Conception and design of the study, acquisition and interpretation of the data. Performed cartilage explant cultures and infrared experiments including processing and interpretation of the data collected. Preparation of all figures for the manuscript. Drafting, revising and editing manuscript.	80

The following co-authors contributed to the work. Co-authors who are students at Monash University must also indicate the extent of their contribution in percentage terms:

Name	Nature of contribution	Extent of contribution (%) for student co-authors only
Duncan Crombie*	Acquisition and interpretation of data for initial experiment. Reviewed manuscript	
Don McNaughton^	Study concept and design, analysis and interpretation of data. Reviewed manuscript	
Rikard Holmdahl#	Provided monoclonal antibodies. Study concept and design. Reviewed manuscript.	
Kutty Selva Nandakumar#	Provided monoclonal antibodies. Analysis and interpretation of data. Reviewed manuscript	
Merrill Rowley*	Initiated the study, interpretation and analysis of data. Editorial review of manuscript (Responsible author).	
Candidate's Signature	[Redacted Signature]	Date 16/8/11

Declaration by co-authors

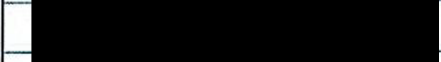
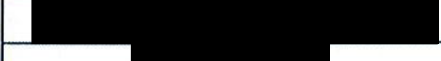
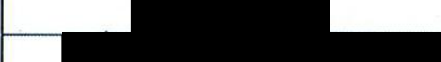
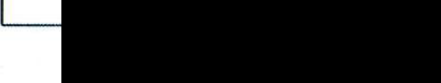
The undersigned hereby certify that:

- (1) the above declaration correctly reflects the nature and extent of the candidate's contribution to this work, and the nature of the contribution of each of the co-authors.
- (2) they meet the criteria for authorship in that they have participated in the conception, execution, or interpretation, of at least that part of the publication in their field of expertise;
- (3) they take public responsibility for their part of the publication, except for the responsible author who accepts overall responsibility for the publication;
- (4) there are no other authors of the publication according to these criteria;
- (5) potential conflicts of interest have been disclosed to (a) granting bodies, (b) the editor or publisher of journals or other publications, and (c) the head of the responsible academic unit; and
- (6) the original data are stored at the following location(s) and will be held for at least five years from the date indicated below:

Location(s)

*Department of Biochemistry and Molecular Biology, Monash University, Clayton, Melbourne, Australia
^Centre for Biospectroscopy and School of Chemistry, Monash University, Clayton, Melbourne, Australia
#Medical Inflammation Research, MBB, Karolinska Institute, Stockholm, Sweden

[Please note that the location(s) must be institutional in nature, and should be indicated here as a department, centre or institute, with specific campus identification where relevant.]

Signature 1		Date 100808
Signature 2		23 Aug 11
Signature 3		110808
Signature 4		110808
Signature 5		16 08 2011

DECLARATION FOR RESEARCH PAPER 2



MONASH University

Declaration for Thesis Chapter 3

Declaration by candidate

In the case of Chapter 3, the nature and extent of my contribution to the work was the following:

Nature of contribution	Extent of contribution (%)
Conception and design of the study, acquisition and interpretation of the data. Performed infrared experiments including processing and interpretation of the data collected. Preparation of all figures for the manuscript. Drafting, revising and editing manuscript.	80

The following co-authors contributed to the work. Co-authors who are students at Monash University must also indicate the extent of their contribution in percentage terms:

Name	Nature of contribution	Extent of contribution (%) for student co-authors only
Kutty Selva Nandakumar [#]	Performed experiments on mice and provided sections of joints for analysis. Analysis and interpretation of data. Study concept and design Reviewed manuscript	
Rikard Holmdahl [#]	Performed experiments on mice and provided sections of joints for analysis. Analysis and interpretation of data. Study concept and design. Reviewed manuscript.	
Mark Tobin [!]	Provided expert assistance with infrared experiments. Analysis and interpretation of infrared data. Reviewed manuscript.	
Don McNaughton [^]	Analysis and interpretation of infrared data. Reviewed manuscript	
Merrill Rowley [*]	Initiated the study, interpretation and analysis of data. Editorial review of manuscript (Responsible author).	

Candidate's Signature

[Redacted Signature]

Date

16/8/11

Declaration by co-authors

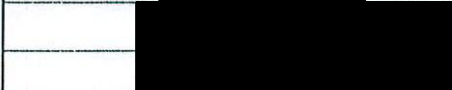
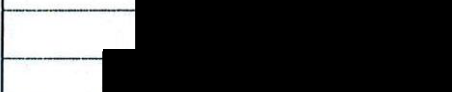
The undersigned hereby certify that:

- (1) the above declaration correctly reflects the nature and extent of the candidate's contribution to this work, and the nature of the contribution of each of the co-authors.
- (2) they meet the criteria for authorship in that they have participated in the conception, execution, or interpretation, of at least that part of the publication in their field of expertise;
- (3) they take public responsibility for their part of the publication, except for the responsible author who accepts overall responsibility for the publication;
- (4) there are no other authors of the publication according to these criteria;
- (5) potential conflicts of interest have been disclosed to (a) granting bodies, (b) the editor or publisher of journals or other publications, and (c) the head of the responsible academic unit; and
- (6) the original data are stored at the following location(s) and will be held for at least five years from the date indicated below:

Location(s)

*Department of Biochemistry and Molecular Biology, Monash University, Clayton, Melbourne, Australia
 ^Centre for Biospectroscopy and School of Chemistry, Monash University, Clayton, Melbourne, Australia
 #Medical Inflammation Research, MBB, Karolinska Institute, Stockholm, Sweden
 !Australian Synchrotron, Clayton, Melbourne, Australia

[Please note that the location(s) must be institutional in nature, and should be indicated here as a department, centre or institute, with specific campus identification where relevant.]

Signature 1		110808
Signature 2		110808
Signature 3		10 th August 2011
Signature 4		23 Aug 2011
Signature 5		16 08 2011

*This thesis is dedicated in loving memory to my
wonderful Aunty Judy and my hero,
Uncle Bob.*

*You both believed in me so much, this thesis is
for you. xx*

ACKNOWLEDGEMENTS

There are so many people I am indebted to for their overwhelming support, assistance and advice over the course of my PhD and I will be eternally grateful to each one of them.

Firstly to two of the best supervisors a PhD student could ask for, Associate Professor Merrill Rowley and Professor Don McNaughton who have both been awesome supports.

I would firstly like to extend my sincere gratitude to my main supervisor, Merrill, truly the best supervisor a student could ever ask for. Merrill's continued support, honesty, assistance and sincerity through both the trying times I have endured over the course of my PhD and as a whole will be forever appreciated. I would describe Merrill as being a 'caring mentor', her dedication to not only her research and me as a student is something to be admired. You have been there by my side to guide, support and encourage me through my studies and I feel very privileged to have had the opportunity to have you as my supervisor.

I also owe a great deal of appreciation to my co-supervisor Don, who has been instrumental in helping me gain an understanding of the fundamentals of infrared spectroscopy. Don is a wonderful, supportive supervisor, who always looks up with a smile from his desk when you knock at his door for some assistance, regardless of how often that is. I truly appreciate your guidance and support throughout my studies and in making sure we get the most out of infrared spectroscopy.

Thankyou to Dr Senga Wittingham and Professor Ian Mackay for always keeping me on my toes and pushing me to be the best scientist I can be. Your, sometimes critical advice has been instrumental in making my thesis the best possible. Senga, I always enjoy our little chats and your welcoming ear to hear my problems and offer wise advice. Ian, I love when you walk into my office and pull

up a chair for a little chat. Thankyou both for your continuous support and belief in me.

I would like to extend my sincere gratitude to Professor Rikard Holmdahl and Associate Professor Kutty Selva Nandakumar for kindly providing our laboratory with the antibodies to collagen, without which, none of the experiments would have been possible, thankyou very much. I would also like to thank, Duncan Crombie for his assistance in setting up the first cartilage cultures and for teaching me everything about culturing cartilage. I would like to thank Dr Mark Tobin, Dr Lili Puskar and Dr Danielle Martin from the Australian Synchrotron for their unwavering assistance with infrared experiments and data analysis, and for our endearing chats. Without their assistance it may have been even longer days and nights I spent on the beam.

Thank you to the people who along the way have kept me sane and provided me with comfort over the course of my PhD. To Leigh Hill, Anne Chow and Deb Truin for their endearing chats, wise advice and wonderful friendship. Thank you to my honorary lab members (or they would say I'm their honorary lab member), Dr Dalibor Mijaljica, Craig Don Paul, Jion Battad, Dr Gavin Higgins, Dr Heling Higgins and Tanya D'Cruze who took me under their wing when our lab was diminishing and provided me with a friendly place for lunch, great laughs and all round great company. You have all provided me with tremendous support particularly over the last couple of years which were tough personally and I will be forever grateful for the lasting friendships that have been formed.

Thank you to Professor Rachelle Buchbinder for providing me with ongoing support and encouragement. To Justin Gardner for his continued confidence in me to succeed an unwavering support. A huge thank you to the 'teaching ladies', Dr Janet Macaulay, Dr Caroline Speed, Dr Nirma Samarawickrema and Mrs Wilma Checkley for their endearing ears and unwavering support and guidance, you have all been such a wonderful support and I truly thank each of you.

To Kristen Robinson and Lauren Kenny, two of my oldest friends who have always believed in me. You have provided me with more confidence to keep going in my studies because each time I told you about something positive at uni you made me feel even better by being so proud and excited for me, thanks for a wonderful friendship thus far and for the many more years to come.

I owe a great deal of gratitude to Rhondda Curtis, I know you would say it is your job to listen, but you have been a tremendous support and kept me on track to seeing that light at the end of the tunnel. I will be eternally grateful to you for the wonderful chats, great advice and support you have given me.

A massive thank you to my best friend Kristina Youngs, for always being there for me, whether it be to listen, to provide a shoulder to cry on, for endless fun, laughs and gossip and for just being an all round wonderful friend. You provided me with the courage and perseverance to continue and get this thesis finished. Also to Phil, Isabella and Oscar Youngs for providing me with good fun and laughs. Bella, I love when I come to visit you make me feel welcome and provide me with some relaxing time.

Last but definitely not least, to my family. Mum you have been the rock that holds me together. Your continued support and confidence in me has kept me going and made me all that more determined to finish my PhD. You are not only my mum, but my friend, when I needed de-stressing or relaxing you were always there, when something is up you are always the first to ask 'what's wrong'. I will be forever grateful for the ongoing strength and support you have provided me with and I hope I've made you proud. To my dad, Bill, you have always said you would be proud whatever I did and have always provided me with unwavering support so thank you very much, I look forward to showing you the finished product. To my sister Katie, you have not only provided me with ongoing support, you have helped me relax and de-stress. I love our little shopping adventures; they are always great sisterly fun and distraction when I need it the most, thank you. A huge thank you to Tom, you are not only my loving partner, but a huge support. I guess I could say the

journey has been somewhat easier to have you by my side, someone who understands the stress and pressure we go through and to have you to bounce ideas off, look to for support and care has been absolutely amazing, so thank you from the bottom of my heart.

To my beloved Aunty Judy and Uncle Bob, you were always so very proud of me in my studies and this made me more determined to make you proud. Uncle Bob, you were always so excited I would be the first Dr. Croxford, so here it is. The love and support you both always gave me without question really meant a great deal to me, and I only wish you were both here to see the finished product. R.I.P xx

PUBLICATIONS DERIVED FROM THIS THESIS

Croxford AM, Crombie DE, McNaughton D, Holmdahl R, Nandakumar KS, Rowley MJ (2010). Specific Antibody Protection of the Extracellular Cartilage Matrix Against Collagen Antibody-Induced Damage. *Arthritis & Rheumatism*. **62**: 3374-3384

Croxford AM, Nandakumar KS, Holmdahl, R, Tobin MJ, McNaughton D, Rowley MJ (2011). Chemical changes demonstrated in cartilage by synchrotron infrared microspectroscopy in an antibody-induced murine model of rheumatoid arthritis. *Journal of Biomedical Optics*. **16**: 066004-1-066004-9

CONFERENCE AND SEMINAR PRESENTATIONS

(Presenting author in bold)

ORAL PRESENTATIONS

Croxford AM, Wood BR, McNaughton D, Holmdahl R, Nandakumar KS, Rowley MJ (2007). Monoclonal antibodies to type II collagen modify extracellular matrix in cartilage explants *in vitro*. 11th Australasian Autoimmunity Workshop, Melbourne, Australia.

Croxford AM (2009). The effects of antibodies to type II collagen on cartilage. Monash University Research Week 3 minute thesis competition, Monash University, Melbourne, Australia.

*Won 1st prize overall

Croxford AM, Rowley MJ, McNaughton D, Nandakumar KS, Holmdahl R (2010). The use of synchrotron IR- microspectroscopy to demonstrate cartilage damage in mice *in vivo* in the absence of inflammation. The meeting of Biology and Synchrotron Radiation, Melbourne, Australia.

Croxford AM (2010). Synchrotron IR microspectroscopy to examine chemical changes to cartilage. Invited speaker for seminar program at the O'Brien Institute, Melbourne, Australia.

Croxford AM (2011). Infrared spectroscopy to examine chemical changes to cartilage in a murine model of rheumatoid arthritis. Invited speaker for seminar program at the Australian Synchrotron, Melbourne, Australia.

POSTER PRESENTATIONS

Croxford AM, Wood BR, McNaughton D, Rowley MJ (2006). Infrared spectroscopy to examine changes to cartilage. Australian Health and Medical Research Congress, Melbourne, Australia.

Croxford AM, Wood BR, McNaughton D, Rowley MJ (2007). Monoclonal antibodies to type II collagen modify extracellular matrix in cartilage explants *in vitro*. 7th Pan-Pacific Connective Tissue Societies Symposium, incorporating the 31st Annual meeting of the MBSANZ, Cairns, Australia.

*Also presented at the Department of Biochemistry and Molecular Biology Annual Postgraduate conference 2008, Melbourne, Australia winning 1st prize for 3rd and 4th year student posters.

Croxford AM, McNaughton D, Holmdahl R, Nandakumar KS, Rowley MJ (2009). Analysis of the effects of monoclonal antibodies to type II collagen on cartilage *in vitro* using Fourier Transform Infrared Microspectroscopy. 5th International Conference on Advanced Vibrational Spectroscopy, Melbourne, Australia.

Croxford AM, McNaughton D, Holmdahl R, Nandakumar KS, Rowley MJ (2009). Monoclonal antibodies to type II collagen modify extracellular matrix in cartilage explants *in vitro*. Monash University research week, Melbourne, Australia.

*Also presented at the Department of Biochemistry and Molecular Biology Annual Postgraduate conference 2009, Melbourne, Australia winning 2nd prize for 3rd and 4th year student posters.

ABBREVIATIONS AND DEFINITIONS

This is a compiled list of abbreviations used throughout this thesis, (including those used in the publications)

δ	Bending vibration
λ	Wavelength
$1/\lambda$	Wavenumber in cm^{-1}
ANOVA	Analysis of variance
ATR	Attenuated Total Reflectance
CI	Type I collagen
CII	Type II collagen
CIX	Type IX collagen
CXI	Type XI collagen
CVI	Type VI collagen
CIA	Collagen Induced Arthritis
CAIA	Collagen Antibody Induced Arthritis
CS	Chondroitin sulfate
DNA	Deoxyribose nucleic acid
ECM	Extracellular matrix
ER	Endoplasmic reticulum
ELISA	Enzyme Linked Immunosorbent Assay
FTIRM	Fourier Transform Infrared Microscopy
FTIRS	Fourier Transform Infrared Spectroscopy
FcRs	Fc Receptors
FACIT	Fibril-associated collagen with interrupted triple-helix
GlcA	(1→4)- β linked D-glucuronic

Abbreviations and Definitions

GlcNAc	(1→3)-β linked A-acetyl-D-glucosamine
Gn	Glycogen deposits
GAG	Glycosaminoglycans
H&E	Haemotoxylin and Eosin
HA	Hyaluronan
IR	Infrared
IRS	Infrared spectroscopy
IL-1	Interleukin-1
IGD	Interglobular domain
KS	Keratin sulfate
LPS	Lipopolysaccharide
mAbs	Monoclonal antibodies
MHC	Major Histocompatibility Complex
MMPs	Matrix Metalloproteinase's
MACIT	Membrane associated collagen with interrupted triple helices
MULTIPLEXINS	Multiple triple helix domains and interruptions
NC	Non collagenous
NOD	Non-obese Diabetic
PBS	Phosphate Buffered Saline
RA	Rheumatoid Arthritis
RNA	Ribonucleic acid
SCID	Severe combined immune deficiency
SNR	Signal to noise ratio
TNF	Tumour Necrosis Factor
UHCA	Unsupervised Hierarchical Cluster Analysis

Abbreviations and Definitions

v	Stretching vibrations
v_{as}	Asymmetrical stretch
v_s	Symmetrical stretch

CHAPTER ONE
LITERATURE REVIEW

**INFRARED MICROSPECTROSCOPY TO EXAMINE
CHEMICAL CHANGES TO CARTILAGE**

1. Introduction

Autoimmunity to type II collagen (CII), an integral component of cartilage, is implicated in the development of rheumatoid arthritis (RA). An autoimmune response to CII which develops in patients with RA is demonstrable in blood, synovium and cartilage⁽¹⁾. RA is a chronic autoimmune inflammatory disease affecting the synovium and leading to joint damage and bone destruction⁽²⁾. The pathology of RA extends throughout the synovial joint, which is infiltrated with neutrophils, macrophages, T lymphocytes and dendritic cells⁽³⁾. Collagen antibody induced arthritis (CAIA) is an animal model of human RA which is induced by injection of monoclonal antibodies (mAbs) to CII and causing an inflammatory response and joint damage⁽⁴⁻⁶⁾. The cartilage loss and joint damage may be explained by the degradative enzymes produced by the inflammatory cells. However, although various mAbs to CII induce CAIA not all such mAbs are arthritogenic. The hypothesis that led to this work was that antibodies to CII affect cartilage stability by interfering with the interactions of CII within the extracellular matrix (ECM). Using standard biochemical and histological techniques various mAbs to CII that were arthritogenic *in vivo* were shown to adversely affect the formation of collagen fibril *in vitro*⁽⁷⁾ and the synthesis of matrix by bovine chondrocytes *in vitro* in cell culture^(8,9). However, as cartilage is an avascular tissue in which there is minimal collagen synthesis in adults⁽¹⁰⁾ and antibodies penetrate cartilage poorly⁽⁴⁾, it was uncertain whether the mAbs could damage pre-existing cartilage. As the biochemical methods used for the analysis of cartilage synthesis were not appropriate to examine cartilage damage that could vary across the tissue according to the penetration of mAbs. The novel technique of Fourier Transform Infrared Microspectroscopy (FTIRM) was applied to the examination of chemical changes in the cartilage matrix where there was penetration of the arthritogenic mAbs, and the antibodies were shown to have degradative effects⁽¹¹⁾.

In this thesis, FTIRM has been utilized to examine the effects of combinations of CII-specific mAbs, aiming to replicate the polyclonal antibody

response that would occur in the serum and synovial fluid in CAIA and human RA using cartilage explants *in vitro*, and examining cartilage damage *in vivo* in the joints of mice treated with arthritogenic mAbs that did not develop inflammation.

To provide the background for this work, this literature review can be divided into three sections. The first describes the structure of cartilage, and the problems associated with examining cartilage changes using conventional biochemical and histological techniques. The second describes the use of IR spectroscopy and the development of FTIRM as a technique to examine chemical changes in tissues, and its applicability to analyse cartilage and its components. The third section provides a brief introduction to the animal model, Collagen Antibody Induced Arthritis that is the subject of the work in this thesis.

1.1. Structure of cartilage

Articular cartilage belongs to the hyaline group of cartilages⁽¹²⁾, the most widely distributed cartilage type characterized by a glassy, sometimes translucent appearance⁽¹³⁾. Hyaline cartilage cushions the ends of bone against compression stresses and provides a virtually frictionless movement across the smooth articular surfaces allowing joints to move smoothly and without pain⁽¹⁴⁻¹⁶⁾. Cartilage is an avascular, aneural and hypocellular tissue that consists of sparsely located individual chondrocytes in an abundant highly hydrated extracellular matrix (ECM) that makes up 95% of cartilage tissue volume⁽¹⁷⁾ and comprises a network of collagen fibres, mainly type II collagen (CII), in which are enmeshed sulphated glycoproteins, particularly aggrecan and the polysaccharide hyaluronan^(10, 17). As cartilage is avascular, its nutrition depends on diffusion from outside, which may limit the number of cells that may be sustained in a given volume and there is an inverse relationship between cell density and cartilage thickness, irrespective of an animal's size^(10, 13).

The arrangement of the cartilage components within the ECM varies across the tissue. The superficial zone of cartilage contains thin closely packed collagen fibres that run parallel with the surface and flattened chondrocytes. In the intermediate layer, the collagen content is higher and the fibres form a network. The deep layer of cartilage contain collagen fibres and rounded chondrocytes arranged vertically either individually or in clusters^(12, 13). The concentration of aggrecan also increases with depth within the tissue⁽¹⁰⁾. The arrangement of the chondrocytes and collagen fibrils within the cartilage matrix is shown in **Figure 1.1**. One of the major components of the articular cartilage, large aggregating proteoglycans, contribute the negative charges to the tissue making it metachromatic⁽¹²⁾.

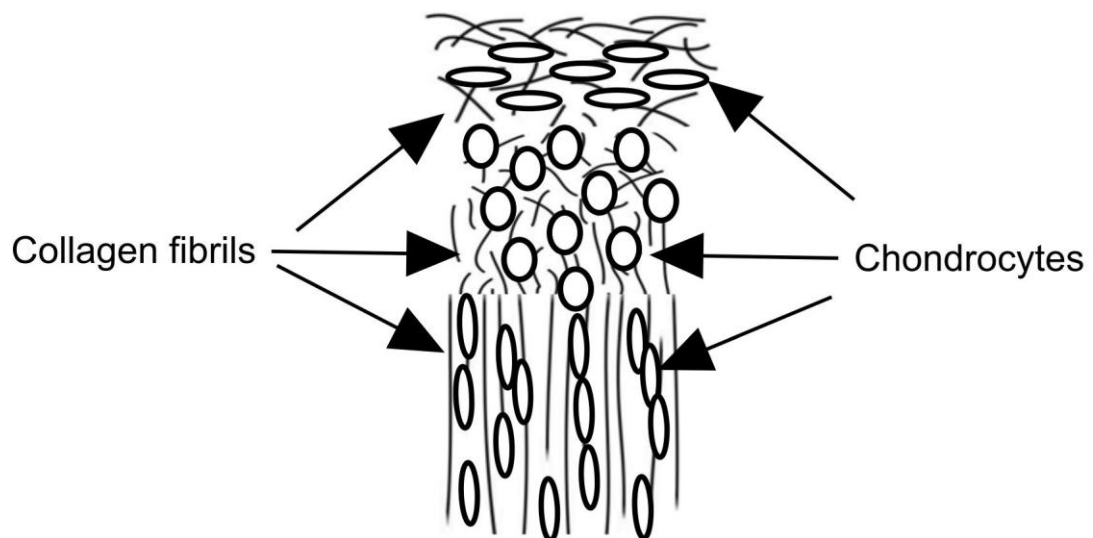


Figure 1.1. Schematic illustrating the arrangement and orientation of chondrocytes and collagen fibrils within the cartilage matrix. The superficial zone (top layer) contains flattened chondrocytes and collagen fibres which run parallel to the cartilage surface. The intermediate layer contains a dense collagen network and rounded chondrocytes. The deepest layer comprises collagen fibres arranged vertically and chondrocytes arranged individually or in clusters.

The matrix in close proximity to the chondrocytes, termed the territorial matrix is surrounded by a dense collagenous network which forms a structure often referred to as a “basket” or chondron. These individual chondrons are separated by matrix components including proteoglycans and hyaluronan⁽¹²⁾ which are shown in **Figure 1.2**.

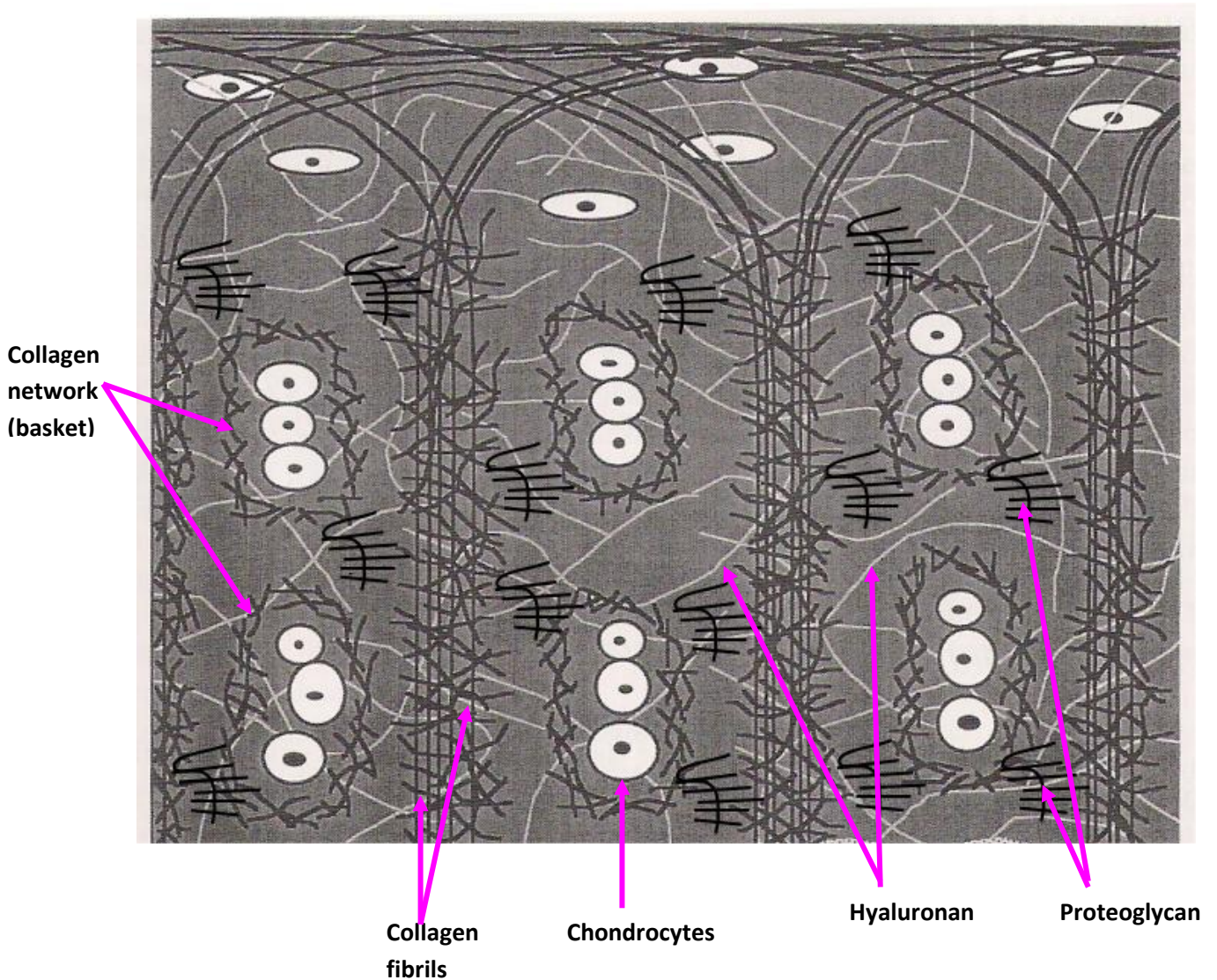


Figure 1.2. Schematic representation of the cartilage matrix. The territorial matrix, surrounding the chondrocytes is surrounded by a dense collagen network, which form “basket” conformations and are separated by the matrix components; hyaluronan and proteoglycans. (Adapted from Buckwalter *et al.*, 1999⁽¹⁸⁾).

1.1.1. Collagen

1.1.1.1. Structure of collagen

The term “collagen” refers to a wide range of molecules with the basic structural motif of three polypeptide chains wound in a triple helical conformation containing a Gly-X-Y repetitive motif, in which X or Y are frequently the imino acids proline or hydroxyproline. Almost all such proteins are structural proteins, and collagen is the most abundant structural protein in animals, but one exception is the complement component C1q that comprises a collagen-like triple helix at the N-terminus, with C-terminal globular heads⁽¹⁹⁾. The structure of the complement component C1q has been described as a hexameric structure with an appearance much like a bunch of tulips. Studies on its sequence, indicate that C1q contains 18 polypeptide chains of three type, A, B and C, and each of the chains is approximately 226 amino acids in length and one copy from each amino acid chain comprised the monomeric unit of C1q^(20, 21). In the N-terminus, the 81 residues in the A, B and C chains form a collagen triple-helix, which terminates at the C-terminus with 6 globular heads which each contain 136 amino acids⁽²⁰⁾.

To date, 28 different types of collagen have been identified in vertebrates⁽²²⁾. The collagen types, their class and distribution within the body are outlined in **Table 1**. The most widely studied collagens are fibrillar collagens, in which a single triple helical domain constitutes 95% of the molecule. These include types I, II, III, V and XI, and provide the structural support for most tissues of the body. Of these, types I, II and III are the most common, and form the characteristic collagen fibres which are seen in tissues. Type I and III form the bulk of the fibrils in tissues other than cartilage, whereas fibrils in cartilage are made up of type II collagen, with small amounts of type IX and type XI⁽²²⁾.

The non-fibrillar collagens contain one or several triple helical domains interrupted by short non-helical domains of various sizes, and can be divided into several subfamilies, including the FACIT (fibril-associated collagen with interrupted triple-helix) collagens, network-forming collagens, MACIT (membrane-associated

collagen with interrupted triple helices, and MULTIPLEXINS (Multiple triple helix domains and interruptions)⁽²²⁾. These collagens do not form fibrils alone, but may associate with particular fibrillar collagens. In particular, FACIT collagens are multidomain molecules that are usually associated with the fibrous collagens CI or CII and project their amino-terminal globular domains out into the matrix. They appear to be involved in linking fibrils to each other or modulating interactions with other matrix components.

Table.1. Collagen types identified in vertebrates (Adapted from Shoulders *et al.*, 2009)⁽²²⁾

Type	Class	Distribution in the body
I	Fibrillar	Abundant and widespread: dermis, bone, tendon, ligament
II	Fibrillar	Cartilage, vitreous
III	Fibrillar	Skin, blood vessels, intestine
IV	Network	Basement membranes
V	Fibrillar	Widespread: bone dermis, cornea, placenta
VI	Network	Widespread: bone, cartilage, cornea, dermis
VII	Anchoring fibrils	Dermis, bladder
VIII	Network	Widespread: dermis, brain, heart, kidney
IX	FACIT	Cartilage, cornea, vitreous
X	Network	Cartilage
XI	Fibrillar	Cartilage, intervertebral disc
XII	FACIT	Dermis, tendon
XIII	MACIT	Endothelial cells, dermis, eye, heart
XIV	FACIT	Widespread: bone dermis, cartilage
XV	MULTIPLEXIN	Capillaries, testis, kidney, heart
XVI	FACIT	Dermis, kidney
XVII	MACIT	Hemidesmosomes in epithelia
XVIII	MULTIPLEXIN	Basement membrane, liver
XIX	FACIT	Basement membrane
XX	FACIT	Cornea (chick)
XXI	FACIT	Stomach, kidney
XXII	FACIT	Tissue junctions
XXIII	MACIT	Heart, retina
XXIV	Fibrillar	Bone, cornea
XXV	MACIT	Brain, heart, testis
XXVI	FACIT	Testis, ovary
XXVII	Fibrillar	Cartilage
XXVIII	Contains von Willebrand factor A domain	Dermis, sciatic nerve

Abbreviations: FACIT: Fibril-associated collagen with interrupted triple helices; MACIT: Membrane associated collagen with interrupted triple helices; MULTIPLEXIN: Multiple triple helix domains and interruptions. All information contained in the table was sourced from^(23, 24) except information on collagen XXVIII which was sourced from⁽²⁵⁾.

1.1.1.2. Cartilage collagens

The articular cartilage matrix consists of an organized network of fibrils of CII and other less abundant collagens, type IX, type XI and type VI that entrap negatively charged matrix components^(15, 16). Collagen comprises approximately 10-20% of the wet weight of cartilage, where CII makes up 90% of the collagen content⁽¹⁷⁾ and provides the tensile strength of the cartilage matrix^(17, 26). Collagen types II, IX and XI are organized into matrix fibrils, where type II constitutes the bulk of the fibril, type XI regulates fibril size and type IX facilitates fibril interaction with proteoglycan macromolecules⁽¹⁶⁾. Collagen types IX and XI are cartilage specific molecules but are found in smaller quantities (3-10%) than CII.

Various other collagens may occur in cartilage in small quantities including collagen type X which is generally found in the calcified zone of cartilage (interfacing with bone) and in the hypertrophic zone of the growth plate⁽²⁷⁾. Collagen type III is rare in cartilage, and is more usually associated with type I collagen in other tissues, however, it can be found in both normal and osteoarthritic human articular cartilage⁽²⁷⁾. In osteoarthritic cartilage it is concentrated within the superficial and intermediate zones and is synthesized by chondrocytes in the absence of CI expression. CIII has also been found to colocalise with CII, assisting CII in retaining its N-propeptide domain⁽²⁷⁾. CVI is concentrated in fibrocartilages such as in the meniscus and intervertebral disc⁽²⁷⁾ and within the structure of chondrons⁽²⁸⁾.

Distinguishing each collagen type is the amalgamation of different α -chains combining to form homotrimeric or heterotrimeric superhelices. For example, heterotrimeric type I collagen contains 2 $\alpha 1$ chains and 1 $\alpha 2$ chain, or $[\alpha 1(I)]_2\alpha 2(I)$, whereas type II is a homotrimer of 3 $\alpha 1$ chains, or $[\alpha 1(II)]_3$ ⁽¹⁰⁾ shown in **Figure 1.3**. CIX and CXI are heterotrimers. CIX is a FACIT collagen contains a large globular noncollagenous (NC) domain N-terminus and contains two short NC segments creating a “kink” in the molecule which is the site of chondroitin sulphate glycosaminoglycan chains extending from $\alpha_2(IX)$ ⁽¹⁶⁾. CXI on the other hand,

resembles CII in structure due to the helices of both molecules being uninterrupted by NC domains. The main difference though between CII and CXI, is the ability of CXI to retain an $\alpha_3(XI)$ N-propeptide projecting from the fibril⁽¹⁶⁾. A higher degree of glycosylation of $\alpha_3(XI)$ indicates differences in the post-translational modifications between CII and CXI. CX is a cartilage-specific homotrimer which is most abundant in areas of hypertrophic chondrocytes, particularly at the site of healing fractures and found only sparingly in normal adult cartilage^(16, 29).

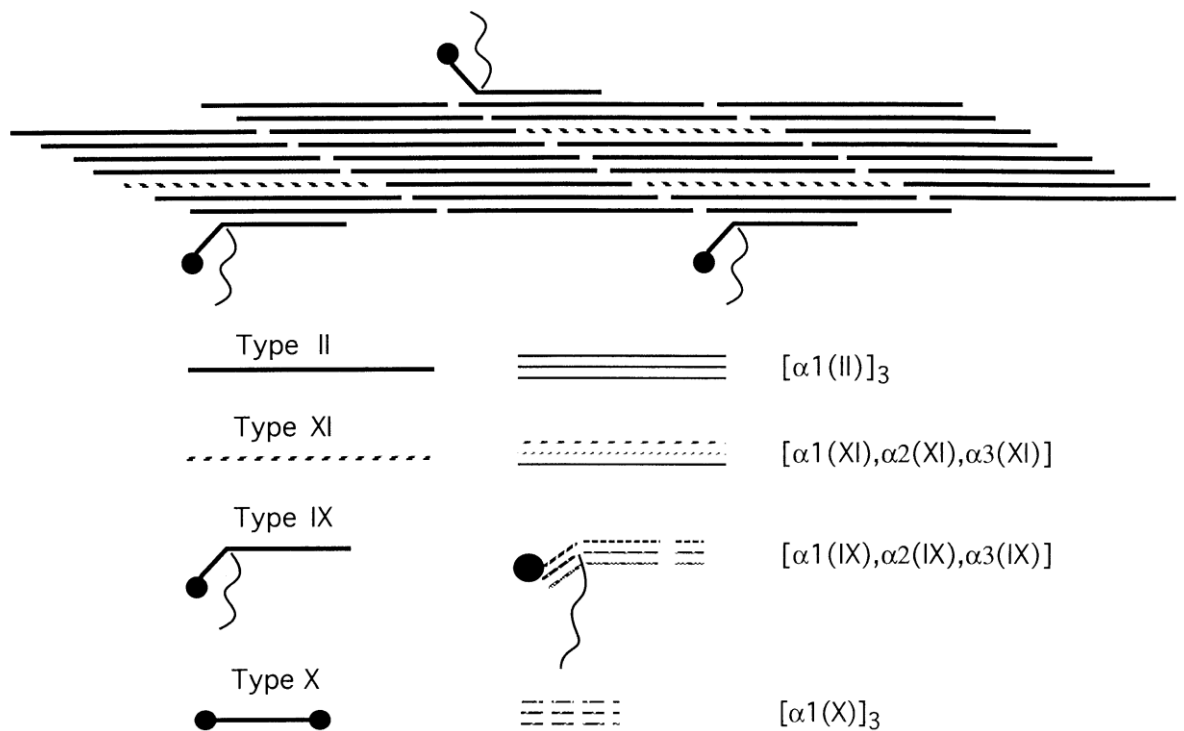


Figure 1.3. Representation of a cartilage-collagen fibril and the collagen molecules which are specific to cartilage outlining the differences in structure of the α -chain. Cartilage fibrils consist primarily of type II collagen. CXI is found within fibrils, CIX is found on the surface and CX is not a component of the fibril but found in the cartilage matrix in close proximity to the hypertrophic zone (Figure from Cremer *et al.*, 1998^(16, 26)).

1.1.1.3. Synthesis of collagen

Collagen pre-cursors are synthesized with large C-terminal and N-terminal extensions which are involved in the chain assembly necessary for the triple helical formation. These pro-peptides are cleaved by specific peptidases after secretion but prior to fibril formation. Collagen fibrils are then stabilized by cross linking residues including lysine. The biologically functional form of collagen, its fibrillar form, results from both intra- and extracellular post-translational modifications⁽¹⁰⁾.

The collagen molecule (tropocollagen) is a subunit of larger collagen aggregates, fibrils. CII is comprised of three chains, each in polyproline II-like conformation, each of which consists of a 280 nm long polypeptide chain. Three left-hand polyproline II-like helical chains are wound around each other to form a tightly packed right-handed triple-helix. The three chains are staggered by one residue with respect to each other and stabilized by interchain hydrogen bonding⁽²²⁾. This conformation requires that every third residue must be glycine, generating a repeating (Gly-Xaa-Yaa)_n pattern, where a high proportion of residues are the imino acids proline and hydroxyproline^(17, 26). This triple-helix in its native form allows the structure to be highly resistant to proteolytic degradation.

The tropocollagen subunits self assemble into D-periodic cross striated fibrils, often termed a quarter staggered array, where D (period) is 67nm, the axial periodicity of collagen⁽³⁰⁾. An electron micrograph of a collagen II fibril illustrating the characteristic banding pattern of collagen fibrils is shown in **Figure 1.4**. The fibril forming collagen molecules consist of an uninterrupted triple helix of 300 nm in length as mentioned above and 1.5 nm in diameter flanked by short extra-helical telopeptides. These telopeptides, do not have a repeating (Gly-X-Y)_n structure or a triple helical confirmation and account for 2% of the molecule but are critical for fibril formation⁽³⁰⁾. An important feature of fibril forming collagens is that they are synthesized as soluble procollagens which are then converted into collagens by procollagen metalloproteinase enzymatic cleavage of the terminal propeptidases⁽³⁰⁾. These proteinases are critical for the synthesis of the collagen

fibrils. **Figure 1.5** illustrates the synthesis of fibrillar collagens. In brief, as described above, the procollagen which is comprised of three α -chains each of approximately 1000 residues is secreted from cells and converted to collagen by the removal of the N- and C-propeptides by procollagen N-proteinase and procollagen C-proteinase. The collagen produced then spontaneously self-assembles into cross-striated fibrils which occur in the extracellular matrix of connective tissues. The fibrils are stabilized by covalent cross-linking which is initiated by oxidative deamination of specific lysine and hydroxylysine residues within the collagen by lysyl oxidase⁽³⁰⁾.

In healthy cartilage, the turnover of the matrix is normally very slow, and the half-life of CII in adult cartilage has been estimated to be 1000 days⁽¹⁰⁾, although there is some loss and repair of the ECM evidenced by turnover of proteoglycans, particularly aggrecan, at the joint surface, and this may be accelerated up to 10-fold within 2 weeks after joint injury^(10, 27, 31).

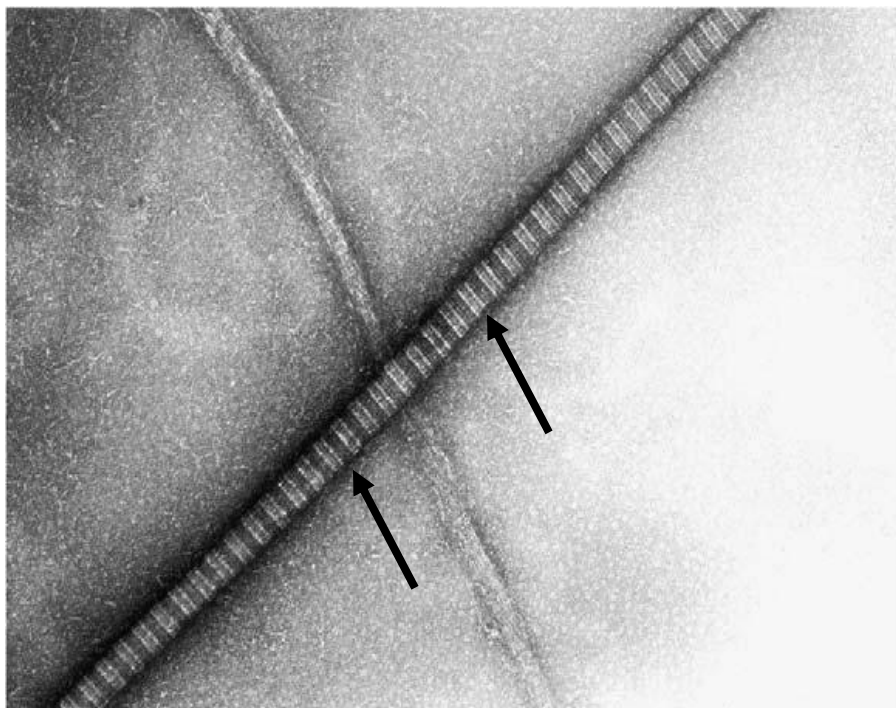


Figure 1.4. Electron micrograph of a type II collagen fibril, showing the characteristic banding pattern, indicated by the arrows. (Figure from Gray *et al.*, 2004⁽⁷⁾)

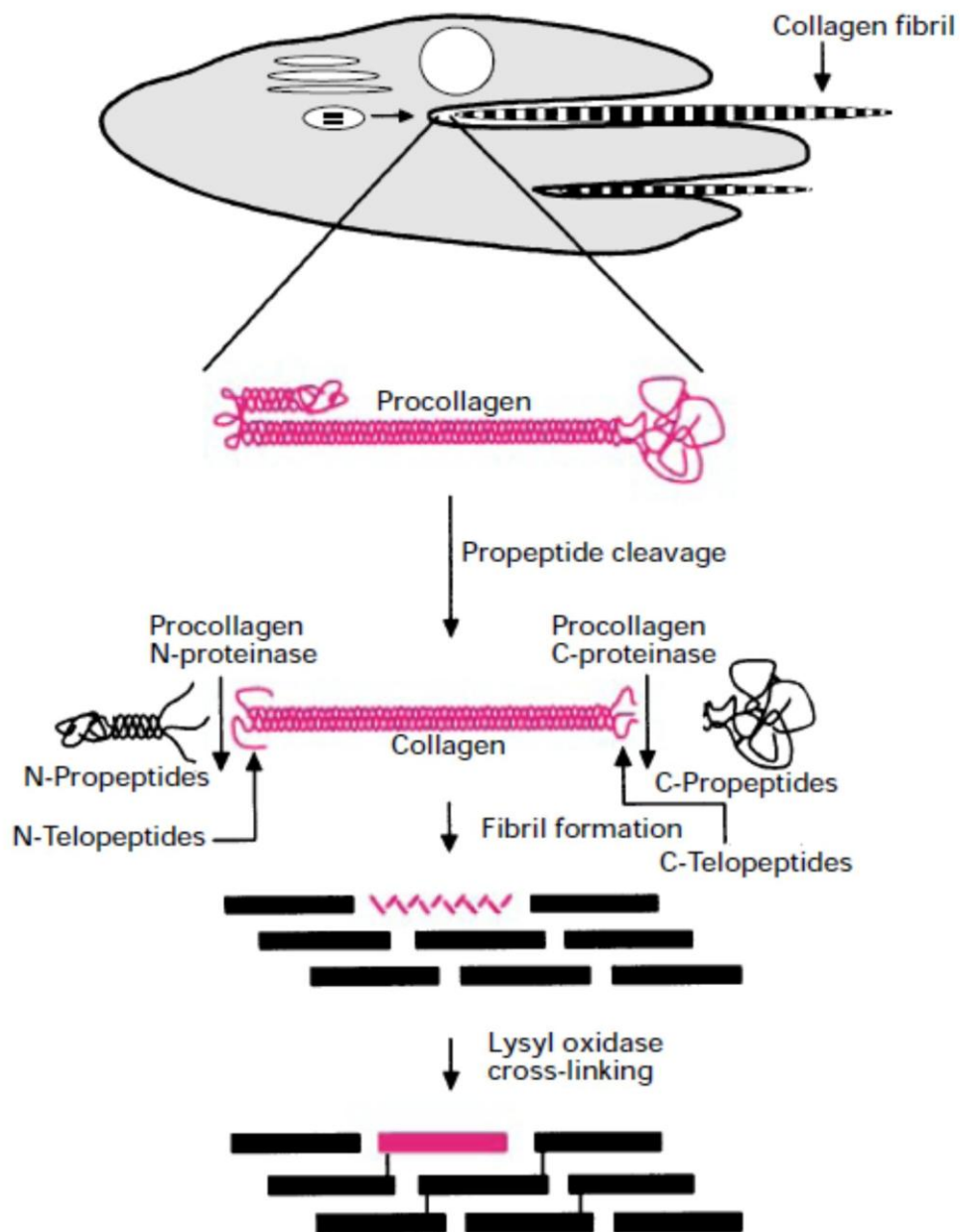


Figure 1.5. Synthesis of collagen fibrils. The procollagen molecule is secreted from cells and converted to collagen by propeptide cleavage of the N- and C-propeptides. The collagen produced spontaneously self-assembles into cross-striated fibrils. The fibrils are stabilized by covalent cross-linking which is initiated by oxidative deamination of specific lysine and hydroxylysine residues within the collagen by lysyl oxidase (Figure from Kadler *et al.*, 1996⁽³⁰⁾).

1.1.2. Glycosaminoglycans

Cartilage contains up to 10% proteoglycan (PG) content⁽¹⁴⁾. Proteoglycans are a diverse group of heterogeneous macromolecular glycoconjugates which are abundant in the body, most prominently in the ECM and connective tissues especially cartilage⁽²⁶⁾. They contain a central core protein to which one or more glycosaminoglycan (GAG) side chains are covalently linked⁽¹⁴⁾. In articular cartilage, PGs are highly hydrophilic macromolecules which are embedded in a compressed form within the fibrillar network and provide cartilage with the ability to undergo reversible deformation⁽²⁶⁾.

1.1.2.1. Aggrecan

The load bearing function of cartilage depends primarily on the properties of the large cartilage specific proteoglycan, aggrecan. It is a large aggregating chondroitin sulphate proteoglycan with a bottle brush appearance (**Figure 1.6**) and containing a protein core (M_r 215 kDa), to which GAG side chains and both N- and O-linked oligosaccharides are covalently attached^(10, 26). The glycosaminoglycan chains which comprise approximately 90% total mass of aggrecan are keratan sulphate (KS), a sulphated dimer of N-acetyl-glucosamine and galactose and chondroitin sulphate (CS), a dimer of N-acetylgalactosamine with a sulphate ester on either the fourth or sixth carbon atom and glucuronic acid⁽²⁶⁾. The core protein, contains three globular and two extended interglobular domains. The amino terminal region contains two of the globular regions, G_1 , G_2 , which are separated by a 21 nm extended segment and G_3 which is at the carboxy-terminal end and separated from the G_2 by the extended region, approximately 260 nm, carrying more than 100 CS chains and approx. 20-50 KS chains along with O-linked oligosaccharides⁽²⁶⁾. A representation of the structure of aggrecan, showing the main constituents, chondroitin sulphate, keratan sulphate, the globular domains and core protein is shown in **Figure 1.7**.

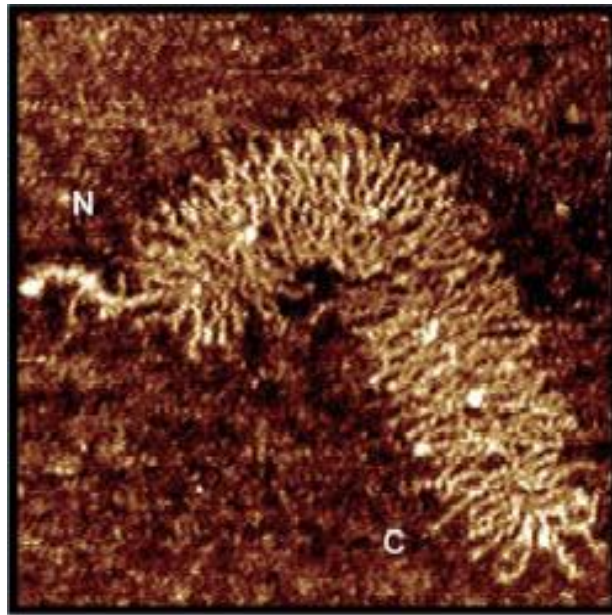


Figure 1.6. “Bottle brush” structure of aggrecan. “N” and “C” indicate the N- and C- termini of the proteoglycan respectively (Figure from Ng *et al.*, 2003⁽³²⁾)

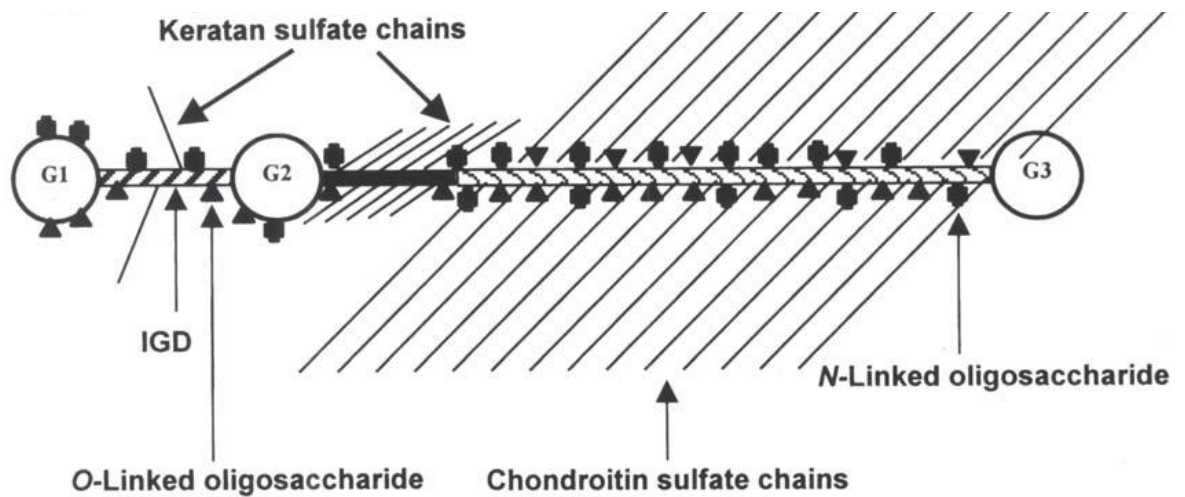


Figure 1.7. Structure of aggrecan, highlighting the main constituents; chondroitin sulphate, keratan sulphate and a core protein. G1, G2 and G3 refer to the globular domains. IGD refers to the interglobular domain. ▲ refers to the O-Linked oligosaccharides and ■ refers to the N-Linked oligosaccharides (Adapted from Kiani *et al.*, 2002⁽¹⁴⁾).

In cartilage, proteoglycans at high concentration create an osmotic swelling pressure and draw water into the tissue. This is due to the negatively charged anionic groups on the GAG chains of aggrecan carrying ions such as Na^+ , which creates a difference in ion concentration between the cartilage and the surrounding tissue and hence an imbalance of free anions and cations⁽¹⁴⁾. Water is then drawn into the tissue caused by an osmotic imbalance and due to the large size of aggrecan, it is immobile to redistributing itself and the water causes the aggrecan rich cartilage matrix to expand and swell⁽¹⁴⁾. When combined with hyaluronan, which is known to bind water 1000-fold its own weight, the presence of the sulphated complexes provides cartilage one of its characteristic features, where 70% of its total content is water^(10, 16)

Together, the collagen/aggrecan network allows cartilage to resist sudden impact loading and maintain its structure. A depiction of the combined properties of collagen, hyaluronan and aggrecan in cartilage and how they contribute to the swelling pressure and tension of cartilage is shown in **Figure 1.8**.

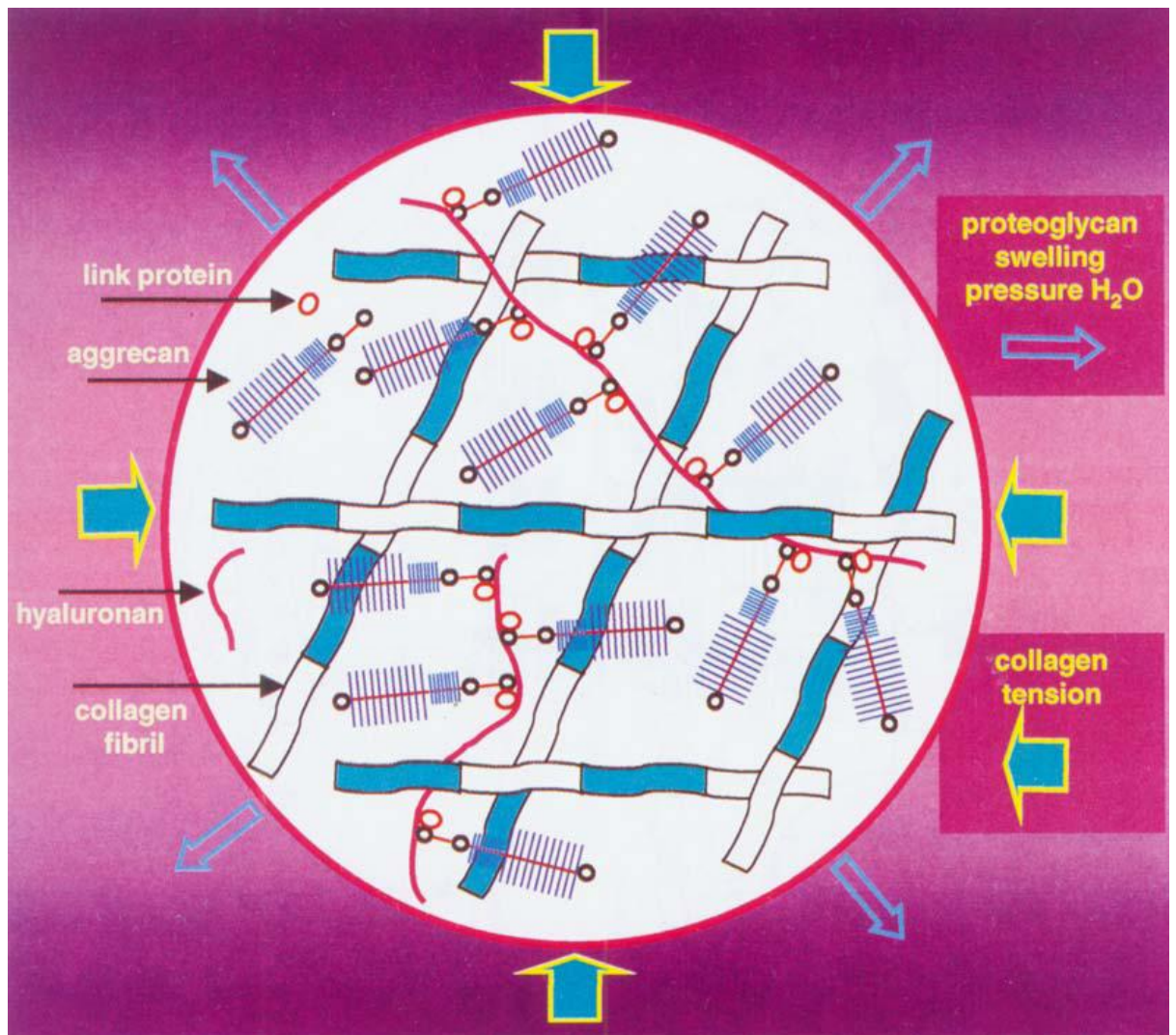


Figure 1.8. Combined properties of the cartilage components. Aggrecan, hyaluronan and the collagen network provide cartilage with its swelling pressure and strength to resist impact. When pressure is exerted to cartilage, the matrix components contract and the highly sulphated proteoglycans exert swelling pressure causing water to be released to protect the cartilage. Once the pressure is released the water is drawn back into the cartilage (Figure from Kiani *et al.*, 2002⁽¹⁴⁾).

1.1.2.2. Hyaluronan

Hyaluronan (HA), also termed hyaluronic acid or hyaluronate is a ubiquitous non-sulphated GAG. It is a linear polysaccharide of 2000-25000 repeating units of the disaccharide (1→4)-β linked D-glucuronic (GlcA) and (1→3)-β linked N-acetyl-D-glucosamine (GlcNAc) residues^(33, 34). HA is the only non-sulphated GAG and the only GAG which is not synthesized by the golgi apparatus, it is instead synthesized on the cytoplasmic surface of the plasma membrane as a free glycan, not attached to a protein, with either Mg²⁺ or Mn²⁺ being essential for synthesis and is translocated to the pericellular space^(33, 35, 36).

HA is widespread in normal mammalian connective tissues and some bacteria^(13, 36). The highest concentrations of HA are found in connective tissues including the umbilical cord, skin, vitreous body and synovial fluid, but it is also found in the lungs, kidneys, brain and muscle, with the lowest known concentration in the blood serum⁽³⁶⁾. The estimated half life of HA in skin is approximately one day, in the eye it ranges between one to one and a half hours, in the vitreous body it is 70 days and in cartilage it is estimated to be between one and three weeks⁽³³⁾. HA degradation occurs in the lysosomes which contain hyaluronidases and other such degradative enzymes.

Several proteins, the hyaladherins recognize HA and these interactions bind HA with proteoglycans stabilizing the structure of the cartilage matrix⁽³⁶⁾. The binding of aggrecans and HA is reinforced by small link proteins, to which some may be attached to HA chains which are linked to binding sites on chondrocytes. The completed aggregates are deposited between collagen fibres and attract water by osmosis in the ECM⁽³⁶⁾.

1.1.2.3. Other smaller glycosaminoglycans

Two small chondroitin sulphate proteoglycans have been found in developing human bone⁽³⁷⁾. These are termed decorin (PG II) and biglycan (PG I), which are

members of the leucine rich proteoglycan family. Both of these proteoglycans possess chondroitin sulphate or dermatan sulphate chains as their GAG components⁽³⁸⁾. Biglycan consists of a core protein of Mr 42,510 with two chondroitin sulphate chains whereas decorin has a core protein of similar size but only one chondroitin sulphate chain⁽³⁷⁾. Decorin and biglycan are ubiquitous despite their different localization within tissues. Decorin is associated with all major type I and II collagen-rich connective tissues whereas biglycan is expressed and localized in a range of cell types including that of connective tissue and epithelial cells^(37, 39). Decorin is thought to be important in regulating collagen fibrillogenesis and biglycan is believed to be related to cell regulation due to its core protein being localized at the cell surface particularly on keratinocytes⁽³⁷⁾. Biglycan is also thought to be important in the cartilage's ability to withstand pressure⁽⁴⁰⁾.

1.1.3. Chondrocytes

Chondrocytes, the only cells found within the cartilage matrix, are responsible for producing the matrix and are derived from mesenchymal cells which differentiate during development⁽¹⁰⁾. The chondrocyte is responsible for the longitudinal growth that occurs within the epiphyseal growth plate⁽⁴¹⁾. Chondrocytes comprise 5% of the cartilage and synthesize and assemble the components of the macromolecular framework⁽²⁶⁾. Chondrocytes are unique in that they are generally cytoplasmically isolated from their neighbouring cells and have no readily available access to the vascular system⁽⁴¹⁾. Unlike parenchymal cells found in other systems, cell-cell interactions within the cartilage matrix is minimal and signalling occurs via cell-matrix interactions⁽¹⁵⁾.

Chondrocytes are encapsulated in basket like networks of fine fibrils of collagen termed a chondron⁽¹⁰⁾. Chondrons are compression-resistant, fluid filled cavities that reduce mechanical, osmotic and physio-chemical changes that are induced by dynamic loading⁽¹⁰⁾. In normal cartilage, chondrocytes are metabolically

inactive, and where once growth has ceased there is no detectable cell division in healthy adult articular cartilage^(10, 17, 42, 43). Chondrocytes are long-lived cells, which survive usually as long as the person or animal, unless the metabolic state of arrested cell division breaks down, as in osteoarthritis or RA when the integrity of the collagen network is compromised⁽¹⁰⁾. The ECM of cartilage is structured by few cells, where the proportion of cells to matrix is much less in cartilage compared with other tissues. In adult femoral head cartilage there are only 10,000 cells/mm³^(10, 44). Chondrocytes are also able to withstand very low oxygen tensions and metabolize glucose primarily by glycolysis producing lactate, which is maintained also under aerobic conditions^(10, 13).

Chondrocytes are typically rounded or polygonal cells except when they exist at tissue boundaries where they become flattened such as at the articular surface of joints⁽⁴¹⁾. An electron micrograph of a typical articular chondrocyte is shown in **Figure 1.9**. Features commonly present within a chondrocyte, include rough endoplasmic reticulum, Golgi apparatus, deposits of glycogen and primary cilium⁽⁴¹⁾, all of which are shown more closely in **Figure 1.10 and 1.11**.

Chondrocytes may have a specialized form of cell process, termed the single cilium (**Figure 1.11**). In chondrocytes, only one cilium per chondrocyte has ever been documented. The frequency of finding a cilia attached to a chondrocyte declines with growth, as cilia are most commonly found in fetal and immature cartilage but may occasionally be present in young adult cartilage⁽¹³⁾.

Chondrocyte cell size varies considerably, the largest diameter ranging from 10-30 μm or more. Several factors influence the shape and size of chondrocytes, including the type of cartilage, position of the cell within the tissue, cell density and the age of the organism to which the chondrocyte resides⁽¹³⁾. The organization and morphological appearance of chondrocytes within the cartilage matrix varies according to the zones of cartilage in which they reside. Within the superficial zone, at the surface of the articular cartilage, chondrocytes are typically flattened

and in the deeper layers of the cartilage chondrocytes are more rounded and are arranged vertically⁽¹⁰⁾ (see Figure 1.2).

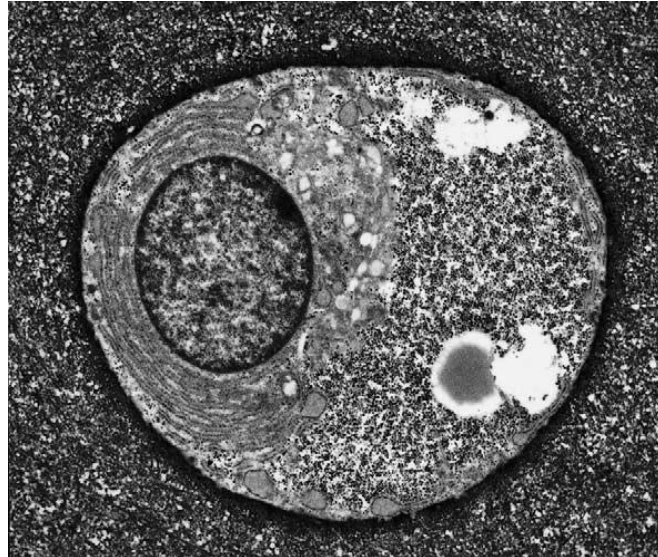


Figure 1.9. Electron micrograph of an articular chondrocyte. Chondrocytes are typically rounded or polygonal in appearance and range from 10-30 μm in size. (Figure from Archer *et al.*, 2003⁽⁴¹⁾).



Figure 1.10. Electron micrograph illustrating the cell contents of a chondrocyte in human articular cartilage. G refers to the Golgi apparatus, ER refers to the endoplasmic reticulum. The F represents the surrounding fibrous network and the arrow is illustrating the presence of lysosomes. Original magnification x 13000 (Figure from Stockwell *et al.*, 1979⁽¹³⁾).

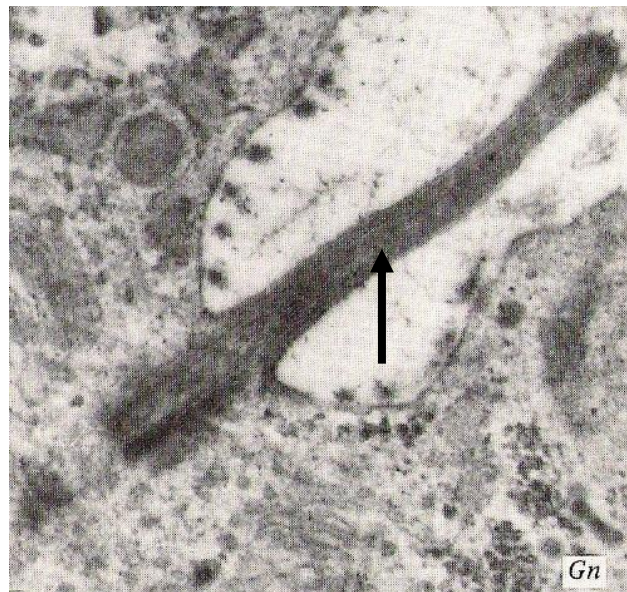


Figure 1.11. Electron micrograph from sheep fetal cartilage showing a single cilium (arrow) protruding from the chondrocyte and the presence of glycogen deposits (Gn), original magnification x 30000 (Figure from Stockwell *et al.*, 1979⁽¹³⁾).

1.1.4. Current methods for analysing cartilage and the requirement for new techniques

Although there are a number of methods currently available for the analysis of cartilage, all of them have limitations. Techniques can be divided into those that are applicable to studying chondrocyte metabolism and synthesis of new cartilage, or those that can be applied to examination of changes in pre-existing cartilage, but few are applicable to the detection of chemical changes to the intact cartilage or chondrocytes which may be occurring either in normal or diseased cartilage.

The location of chondrocytes within an abundant ECM, and their relative scarcity within the ECM has made the study of chondrocyte metabolism and cartilage synthesis difficult. To isolate chondrocytes, the cartilage must be finely minced, then digested extensively with collagenase and trypsin⁽⁴⁵⁾. This digestion removes surface markers and receptors from the chondrocytes which are normally held in culture for 2-3 days before analysis, by which time they have begun to

synthesize new matrix, and become difficult to isolate once more⁽⁴⁶⁾. The matrix is essential to maintain their phenotype, and cells removed from the matrix rapidly undergo dedifferentiation, losing their chondrocytic phenotype, becoming fibroblastic and producing type I collagen rather than type II^(47, 48). Although various chondrocytic cell lines have been developed⁽⁴⁹⁻⁵³⁾ it is unlikely that any of them represent phenotypically normal chondrocytes.

To prevent the de-differentiation of primary cultures of chondrocytes, various methods have been developed. The simplest is the use of high density cultures, in which chondrocytes are seeded at a density in which chondrocytes are already confluent: as they grow and divide and produce matrix the culture becomes thicker, and “rubbery” analogous to normal cartilage as matrix is produced. This has been the technique used in previous studies of the effects of mAbs to CII on cartilage synthesis from our laboratory described in section 1.8. Other techniques have involved seeding autologous chondrocytes in an artificial matrix, such as agarose scaffolds⁽⁵⁴⁾, alginate beads⁽⁵⁴⁾ or similar polymer scaffolds⁽⁵⁵⁾ and this is the subject of extensive on-going research in biomaterials development in the field of cartilage replacement⁽⁵⁶⁻⁵⁸⁾.

Such chondrocyte preparations have been extensively used for the analysis of cartilage synthesis and metabolism using a variety of biochemical techniques, such as metabolic labelling to measure the synthesis of matrix components, using ³H-proline incorporation into newly synthesized collagen, or ³⁵S-sulphate that is incorporated into proteoglycans. In each case, the matrix synthesised must be further processed to purify the components and demonstrate incorporation of the radioactive label. These techniques have been used in our laboratory by Amirahmadi and colleagues^(8, 9), who examined primary cultures of bovine chondrocytes grown in high density after treatment with known arthritogenic mAbs, for new collagen synthesis in the matrix produced and surrounding the chondrocytes and released into the medium and proteoglycan synthesis in the matrix and released into the medium. In the same studies, the chondrocytes and

matrix were examined histologically and by electron microscopy to determine whether there were changes in the morphology of the chondrocytes, or the structure of the collagen fibrils produced (see section 1.8). Such experiments are expensive and time consuming, for instance for metabolic labelling, each analysis needs to be performed separately and only one form of analysis may be performed on each sample. Multiple replicates are also required for statistical significance, and morphometric analysis using electron microscopy is not readily available.

Similar techniques have also been applied to the analysis of cartilage degradation, such as that which occurs in diseases such as osteoarthritis, rheumatoid arthritis and joint injuries suffered by sports people and is characterised by loss of cartilage. For metabolic labelling, the metabolism of chondrocytes from osteoarthritic cartilage has been compared to that of chondrocytes from healthy cartilage⁽⁵⁹⁾, and there have been several studies of the morphology of osteoarthritic cartilage⁽⁶⁰⁻⁶²⁾, but other techniques are also used. In particular, histological staining is a widely accepted method for identifying loss of particular components of the cartilage matrix. Glycosaminoglycans bind cationic dyes electrostatically and therefore the use of metachromatic dyes such as toluidine blue and methylene blue have proven useful for semi quantitative measurement of proteoglycan loss in cartilage⁽⁶³⁾. Cartilage has also been analysed morphologically, and various methods of scoring cartilage damage based on appearance have been developed and attempts have been made to correlate morphological damage with biochemical changes⁽⁶²⁾. These scoring systems are based on the Mankin score which was developed in 1971⁽⁶²⁾, and assesses structure, cellular abnormalities, matrix staining and tidemark integrity in cartilage.

Direct analysis of cartilage damage has been extended by the use of immunohistochemistry, using antibodies of varying specificity to localise changes. Immunohistochemistry is considered a valuable technique for studies of bone, cartilage matrix and cellular studies. Biological substances of interest are localised by the precise attachment of a label or complex which may subsequently be

visualised in the tissue or cell of interest⁽⁶⁴⁾. For example collagen damage may be revealed using a mAb that recognises a neoepitope on denatured collagen⁽⁶⁵⁾ or several mAbs can be used that identify neoepitopes resulting from degradation of aggrecan with matrix metalloproteinases or aggrecanase⁽⁶⁶⁻⁶⁸⁾. Several mAbs have also been developed which detect neoepitopes to cartilage components including CII and proteoglycans⁽⁶⁹⁻⁷¹⁾. Although the use of immunohistochemistry can be useful in provide information of the release of matrix components some knowledge of the likely changes occurring in the tissue is required to select the antibodies that may be of use, which also requires a new section of tissue for each specific antibody of interest.

All of these methods provide some information on the release or distribution of matrix components or loss of cartilage components but many require destruction of the tissue prior to analysis, and most of the current assays do not allow analysis of several components and changes within a single piece of tissue and correlation of the chemical composition with the location within the cartilage. Moreover most of the current techniques for cartilage analysis require some knowledge of the possible effector mechanism involved for an accurate detection of cartilage changes.

The recent development of the technique of Fourier Transform Infrared Microspectroscopy (FTIRM) which provides a new method of chemical analysis of tissue changes at the microscopic level and examination of localised chemical changes within tissue sections has prompted a re-examination of cartilage analysis. Recently, Camacho and colleagues^(72, 73) used infrared spectroscopy to analyse the main components of cartilage, CII and proteoglycans offering a non-destructive technique for analysis of cartilage and this will be discussed in further detail in section 1.2.7.4. Infrared spectroscopy therefore has the potential to offer a novel approach for the analysis of cartilage and will be investigated further as the subject of this thesis.

1.2. Infrared spectroscopy

Infrared spectroscopy (IRS) involves the measurement of absorption or reflection at different IR frequencies by a sample when positioned in an IR beam⁽⁷⁴⁾. It utilises the infrared region of the electromagnetic spectrum with wavenumber (defined below) values ranging from 13,000 to 10 cm^{-1} ⁽⁷⁴⁾. Signals reflect the vibrations within molecules, generating information on the chemical composition of samples in the form of absorption or reflection spectra⁽⁷⁵⁾. IR spectroscopy has broad applicability and can be used to analyse samples such as gases, liquids and solids, to identify organic and inorganic compounds, to determine molecular functional groups in materials and chemicals and in the quantitative determination of compounds in mixtures and hence provides an important tool for identification of compounds and identification of chemical structures⁽⁷⁴⁾. It is widely used by chemists, biochemists and material scientists and is one of the oldest and most established spectroscopic experimental techniques⁽⁷⁴⁾.

The IR region of the spectrum is typically divided into three smaller subregions, near IR (13,000-4,000 cm^{-1}), mid IR (4,000-400 cm^{-1}) and far IR (400-10 cm^{-1}). Of these, the most frequently used region is the mid IR region. In the mid-infrared region, there are absorption bands observed from two main types of fundamental vibrations, those along chemical bonds termed stretching vibrations (ν) which involve changes to the bond-length and vibrations with changes to the bond angles⁽⁷⁵⁾. Infrared radiation is absorbed and the associated energy is converted into vibrational energy. Examples of the vibrational modes are shown in **Figure 1.12**. The resultant spectra reflect all the infrared active vibrational motions in a molecule. A simple molecule made up of only two atoms would only have one fundamental mode peak in the IR spectrum, but more complex molecules have many bonds and bending angles, and their vibrational spectra are correspondingly more complex, with several peaks in their IR spectra. IR spectra result from transitions between quantized vibrational energy states and hence the molecular vibrations are represented by the degrees of freedom, $3N-6$, where N is the number

of atoms. Molecules with N atoms have $3N$ degrees of freedom, three of these represent the translational motion along the x , y and z -axes and three represent rotational motion around the x , y and z -axes. The remaining $3N-6$ degrees of freedom indicate the number of vibrational modes⁽⁷⁶⁾.

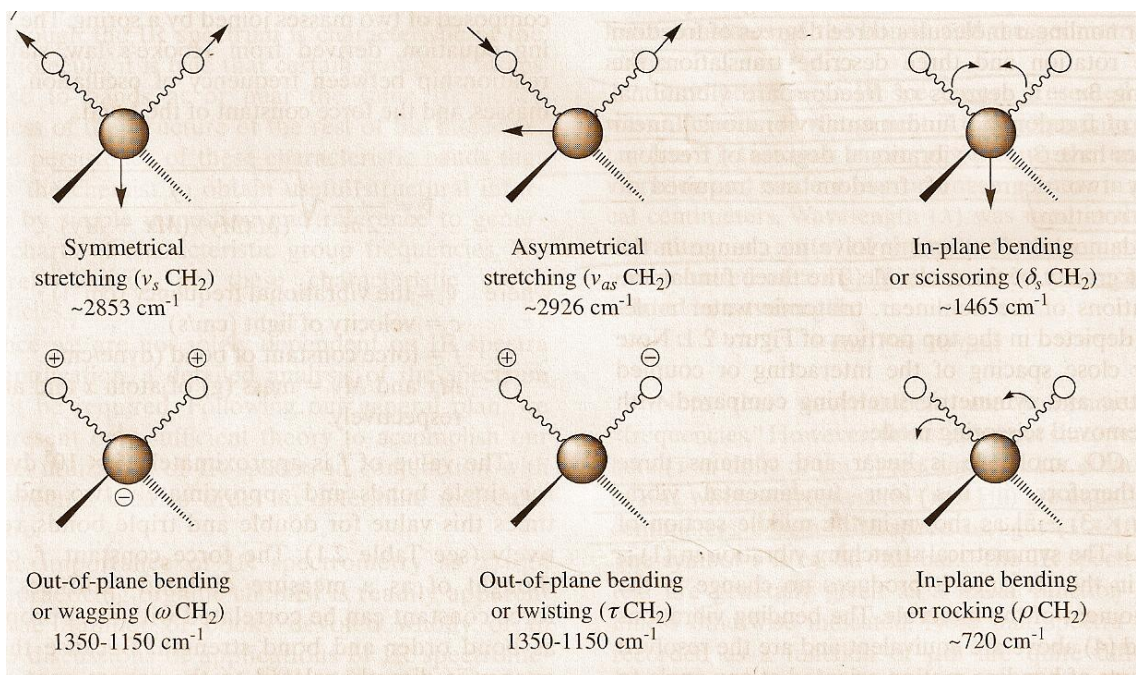


Figure 1.12. Major vibrational modes for a non-linear group, CH₂ and their associated wavenumbers. + indicates a motion away towards reader and – indicates motion away from reader. (Adapted from Silverstein *et al.*, 2005⁽⁷⁷⁾)

The far and near IR regions are not commonly employed. For the near infrared only secondary vibrations (overtones and combinations) occur and these produce generally weak spectra that are more difficult to interpret⁽⁷⁸⁾. The far IR region where fundamental vibrations involving heavy atoms and low amplitude bends give rise to absorptions is generally used for the analysis of organic, inorganic and organo-metallic compounds and also provides useful information for structural studies such as conformational analysis. Near IR spectroscopy is primarily a

quantitative rather than qualitative technique⁽⁷⁹⁾, which requires minimal or no sample preparation and offers high speed quantitative analysis without destruction of the sample⁽⁷⁴⁾. It is typically used for the quantitative determination of water, phenols, alcohols, amines, unsaturated hydrocarbons and other groups of compounds which contain the O-H, N-H or C-H groups⁽⁷⁹⁾ that give rise to observable overtone bands. Quantification however within the near IR region requires building chemometric models. The use of IR spectroscopy utilising these regions will not be discussed further.

1.2.1. Fourier Transform Infrared Spectroscopy

The development of a stable and powerful calibration laser has led to the modern development of the Fourier transform methods for IR data acquisition. This coupled with modern computers has enabled rapid and powerful FTIR-spectroscopy (FTIRS) data processing and conversion⁽⁸⁰⁾. This has led to the technique being recognised as an invaluable tool for not only the determination of protein conformation and structure, but also in the analysis of liquid and gaseous samples and for analysis of biological tissue.

The main components in a FTIR system are a radiation source, interferometer, and detector. Mid-IR spectrometers use a Michelson interferometer. A schematic of a Michelson interferometer is outlined in **Figure 1.13**. Light from an infrared source is focused onto the aperture, which limits the size of the source visualised by the interferometer. The beam is coupled into the interferometer via a collimating mirror, which, together with the aperture limits the divergence angle seen by the interferometer. The light is then directed into the beamsplitter, which in the mid-IR is a thin layer deposited on a substrate, where the light is then split into two beams of ideally equal intensity. The substrate, however changes the optical pathlength in one arm of the interferometer, therefore a compressing plate is positioned on the opposite arm of

the interferometer to compensate. One of the two beams then passes to a fixed mirror and is reflected and returns to the beamsplitter. The other beam passes to a mirror which is mounted on a drive that allows it to be displaced along the optical axis and once reflected also returns to the beamsplitter where it is combined with the beam from the fixed mirror. From the beamsplitter, approximately half of the light returns along the optical path to the source and the other half is directed to the sample by a focusing mirror. The light is then focused onto a detector after either transmission through the sample or reflection from the sample. The beam from a HeNe laser is also passed through the interferometer and its interference pattern is detected by one or more laser detectors to provide a optical pathlength calibration⁽⁷⁶⁾. A mathematical algorithm known as Fourier Transformation converts the interferogram (plot of signal intensity versus optical path difference) to a raw spectrum and an IR transmission spectrum is generated by ratioing the sample spectrum against a background spectrum⁽⁷⁴⁾.

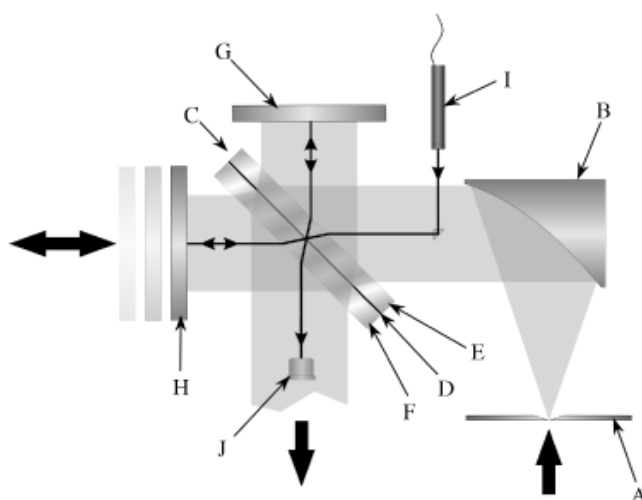


Figure 1.13. Schematic of a Michelson interferometer. Light from an infrared source is focused onto the aperture (A) and directed through the optical elements of the interferometer as described in the text and eventually focused on to a detector after passing through a sample placed after the interferometer. B represents the mirror, C and D are the beamsplitter, E is the substrate, F is the compressing plate, G is fixed mirror, H is mirror, I is the HeNe laser and J is the laser detector. The arrows indicate the direction of travel of the light. Figure from Chalmers *et al.*, 2002⁽⁷⁶⁾.

There are several distinct advantages of FTIRS over conventional IR spectroscopy. A complete spectrum may be obtained during a single scan of the moving mirror with the detector examining all frequencies simultaneously. An FTIR instrument can achieve the same signal to noise ratio (SNR) of a dispersive spectrometer with heightened sensitivity in a fraction of the time (1 sec or less with FTIRS vs. 10-15 mins using a dispersive instrument)⁽⁷⁴⁾, however there is one drawback in that FTIR spectroscopy requires a pre or post recorded background spectrum. The superiority of FTIR has led to the technique being considered as the norm in infrared spectroscopy.

1.2.2. Fourier Transform Infrared Microspectroscopy and the development of the focal plane array system

Although FTIRS has been extensively used for the examination of a single pure substance or a mixture of substances and the determination of secondary structure, it has also led to the development of IR microspectroscopy, imaging and focal plane array imaging to examine chemical characteristics at the microscopic level.

Microscopic infrared mapping was typically performed with a conventional reflective or transmissive raster-scanned infrared microscope which is coupled to a step-scan or rapid scan FTIRS⁽⁸¹⁾ and termed Fourier transform infrared microspectroscopy (FTIRM). In FTIRM, the Michelson interferometer discussed earlier is coupled to a microscope to allow for infrared microspectroscopy and mapping. Spatial resolution with an FTIRM instrument is however limited, however, as the microscopy is achieved by simply introducing an aperture to select a small proportion of the radiation and therefore the sample size is restricted to approximately 30 μ m, below which the SNR is very poor and does not produce useful spectra.

While there are clear advantages of FTIRM over conventional FTIRS in analysing heterogeneous tissues there are also limitations. The main disadvantage

is due to the fact that the images are constructed by mapping the substance of interest a single pixel at a time which makes it very time consuming for all but very small samples.

In the late 1990's, multichannel IR imaging detectors, termed focal plane array detectors (FPA), which were originally developed for military applications were made commercially available⁽⁸¹⁾. The use of a FTIRM coupled to a FPA detector, has led to the development of a powerful mid-infrared spectroscopic chemical imaging technique⁽⁸¹⁾. A typical system allows for the collection of 4096 individual spectra simultaneously over a 400 x 400 μm^2 area in a single sample of tissue at a spatial resolution to ca. 10 μm , which reduces the time by a factor of 1000 required to collect spectra and allows for the examination of multiple parameters in each sample⁽⁷²⁾. Fourier transform infrared spectra can thus be used for fingerprinting of particular areas/organelles/features and then taking the chemical information obtained one step further by examining chemical changes within a tissue which contain a range of components from the single sample hence aiding in the determination of the relative content, molecular nature, distribution and orientation of the individual components of histological sections of tissues⁽⁷³⁾.

FTIR microscopes coupled to FPA detectors were originally developed using step scan techniques however the current systems used are rapid scan. Rapid-scan interferometry does not require a time delay for the stabilization of the moving mirror, as the mirror motion is constant. This allows modern FPAs sufficient time required to acquire high quality data.

1.2.3. Sample preparation

FTIRS can be used for the analysis of a variety of samples, including liquids, gases and solids. Sample preparation is one of the most important components for a successful IR spectroscopy experiment and it is therefore crucial that the appropriate methods for the sample of interest are used.

Liquids may occur either as pure liquids or solutions and are sampled in sealed cells or demountable cells regardless of their initial state⁽⁸²⁾. Generally for pure liquids, more polar samples require a thinner cell thickness and materials in solution use a cell thickness ranging from 0.1mm to several tenths of a millimetre⁽⁸²⁾. Sealed cells for liquid sampling are constructed using two windows one of which has holes to allow for filling with the sample of interest. These two windows are separated by a lead or silver spacer which is then sealed to the windows. The window/spacer cell is held in a metal frame with two ports sealed with polytetrafluoroethylene. Demountable cells have the benefit of being able to assemble and disassemble them with every sample. Either one or two windows may be used depending on the sample. A thin film may be placed on one window or alternatively, two windows may be used to hold the liquid between⁽⁸²⁾.

Due to the low density of gaseous samples, absorption spectra of gases may be measured in gas cells which range from a few centimetres to several metres in path length^(83, 84). These cells may be constructed from other glass or metal, although metal cells are more convenient for very small or very large volumes or for studies at high temperatures.

Unlike gases and liquids, solid samples may be prepared in a variety of ways. Solids may occur as thin films, for example polymer films, large or small particles or in solution. If the particles are very large or very minute compared with the infrared wavelength, measurements are relatively easy. However, if the particle size is of the order of the wavelength, the sample often needs to be ground to a particle size which is less than the wavelength or to incorporate the particles into a medium of similar refractive index⁽⁸²⁾. This grinding is usually carried out using a mortar and pestle. A drop of mulling fluid, either mineral oil (Nujol) or chlorofluorocarbon (Fluorolube) is mixed with the ground sample until the sample is dispersed into the mulling fluid. Mulling fluid has a refractive index of approximately 1.5 which is very similar to most organic materials in absorption regions and as a result scattering is substantially reduced⁽⁸²⁾. This resultant mixture

is applied as a thin film to an infrared window and a second window is placed on top⁽⁸²⁾. The windows are then placed into a demountable cell for measurements, typically in transmission mode.

Attenuated total reflection (ATR) is an internal reflection technique which may be used to analyse solids or liquids. ATR is the most useful and generally accepted sampling method for analysing most simple solid and liquid samples. An ATR accessory, measures the changes that occur in an internally reflected infrared beam when the beam comes into contact with the sample. Internal reflection occurs when radiation moves through a higher refractive index material and imposes on the interface with a lower refractive material at angles at or above the critical angle⁽⁸²⁾. ATR only has a small penetration depth and hence the sample must be in close contact with the internal reflection crystal⁽⁸²⁾. Maintaining close contact between the sample and the crystal is relatively simple for soft materials but more challenging for harder materials. Pressure can be applied to improve contact between sample and crystal, however great care must be taken not to crack or distort the crystal. Because the penetration depth of ATR is so small, a few micrometers or less, only the surface of the sample is being measured, however because most internal reflection accessories produce multiple reflections, the surface layer is sampled several times and as a result, spectra are produced with significant intensity for interpretation⁽⁸²⁾. Several different internal reflection crystals are available for ATR. The most common are Zinc Selenide (ZnSe) and Germanium(Ge). ZnSe is relatively inexpensive and is ideal for analysing liquid samples, however it scratches quite easily and care must be taken when using ZnSe crystals. Ge is often used to analyse weak acids and alkalis due to its wider working pH range. Diamond is the most durable ATR crystal, however it is more expensive than ZnSe or Ge.

Typically, an infrared beam is directed onto an optically dense crystal which has a high refractive index at certain angles. The internal reflectance from the crystal creates an evanescent wave which extends beyond the surface of the crystal

and in to the sample which is placed in close contact to the crystal⁽⁸⁵⁾. In areas of the infrared spectrum where the sample absorbs energy, the evanescent wave is attenuated. This attenuated energy from each evanescent wave is passed back into the IR beam which exits at the opposite end of the crystal and is passed in to the detector in the IR spectrometer, which then generates an infrared spectrum⁽⁸⁵⁾. A typical schematic of an ATR crystal is shown in **Figure 1.14**.

Sample in contact with evanescent wave

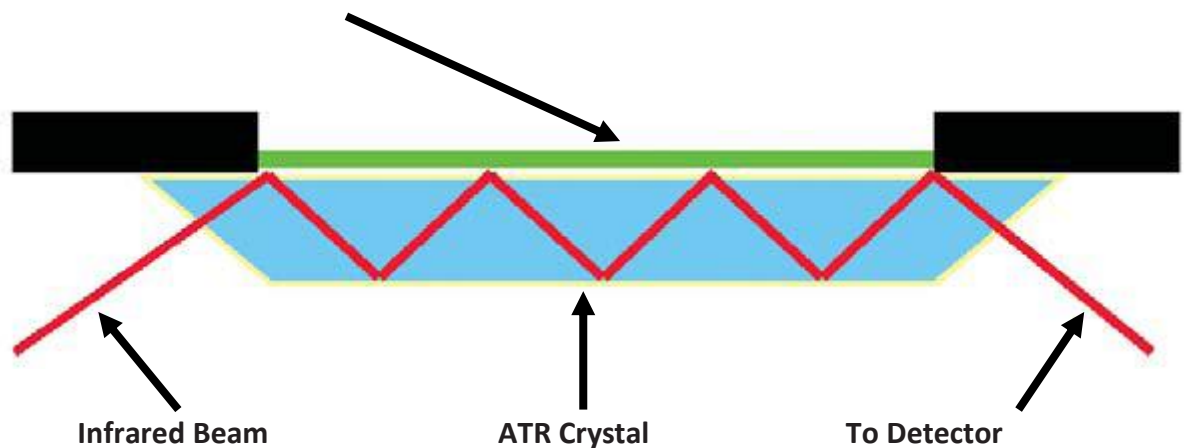


Figure 1.14. Schematic of ATR crystal. The infrared beam is directed onto the ATR crystal and the internal reflectance from the crystal creates an evanescent wave which extends beyond the surface of the crystal and in to the sample, placed in close contact to the crystal. In regions of the infrared spectrum where the sample absorbs energy, the evanescent wave is attenuated and this attenuated energy from each evanescent wave is passed back into the IR beam which exits at the opposite end of the crystal and is passed in to the detector in the IR spectrometer, which then generates an infrared spectrum (Figure adapted from Perkin Elmer⁽⁸⁵⁾).

IR analysis may also be performed on most biological tissues or plant samples and the examination of such samples has a distinct advantage in that the preparation method can be the same for both light microscopy and FTIRS or FTIR

microscopy (FTIRM), which will be discussed in further detail in section 1.5. Biological samples are commonly fixed in paraformaldehyde or formalin and embedded usually in paraffin blocks. Paraffin has advantages for embedded biological tissues, as its most intense absorption features are limited mainly to the C-H stretch region ($2800-3000\text{ cm}^{-1}$)⁽⁸⁶⁾, and do not interfere with the important biological spectrum region. Thin sections of paraffin embedded tissue are cut and adhered to IR reflective substrates, or transmissive non hygroscopic substrates or transfection slides such as KevleyTM slides which consist of a glass slide coated with a dispersed thin Ag layer and over coated with SnO₂ for protection. The latter slides have the advantage of transmitting visible light for visible microscopy but reflecting infrared light. The tissue is then dewaxed in xylene and rehydrated through a graded series of ethanol baths and distilled water. Although such processing allows for a direct comparison of FTIR measurements and standard histology, fixation of the tissue alters the chemical bonds within the cell⁽⁸⁶⁾ and the dewaxing process removes cellular lipids. Alternatively, to avoid this interference, unfixed frozen sections of tissue which have been embedded in optimum cutting medium (OCT-Tissue-Tek) may be used. This method best preserves the original state of the tissue, if the OCT is not removed; otherwise any water soluble components of the tissue will also be removed. The thin sections are air-dried onto the substrates. Biological samples can be examined in either transmission or transfection modes.

1.2.3.1. Collection of data in Transmission mode

Transmission is the oldest and most common method used for FTIRS studies⁽⁸⁷⁾. The typical thickness of sections for measurement in transmission mode is 5-30 μm , however it is very sample dependent⁽⁸⁶⁾. Polymers, un-mineralized biological tissues and other organic molecules are generally prepared at a thickness of 10-15 μm . Minerals are more variable, for example mineralized bone is usually sectioned at 3-5 μm ^(86, 88). Samples are placed on an infrared transparent surface where the thickness of the substrate surface ranges from micrometres to millimetres.

Biological samples are most commonly placed on transparent, water insoluble substrates such as CaF_2 and BaF_2 ⁽⁸⁶⁾.

1.2.3.2. Collection of data in Transflection mode

Another common method for collecting IR spectra is in transflection mode. Samples probed in reflection mode are usually cut to thin sections and are placed on an IR-reflective substrate, such as a Kevley slide. In transreflectance mode, the IR beam penetrates through the sample, reflects off the substrate and passes back through the sample again⁽⁸⁶⁾. As the beam passes through the sample twice, there is a significant requirement for the thickness of the sample to be about half that used for transmission measurements. Diffuse reflectance and attenuated total reflectance are other methods of collecting data in reflectance mode and attenuated total reflectance is described in section 1.2.3. Unfortunately, most of the IR-transparent substrates have some degree of dispersion in the visible or infrared region of the spectrum which must be considered when collecting measurements.

1.2.4. Synchrotron Infrared Spectroscopy

The capacity of FTIRM to non-destructively and rapidly detect functional groups makes it a powerful technique for studying biological specimens⁽⁸⁹⁾, but despite its wide applicability and use for the analysis of biological tissues, the lack of brilliant, bright light sources and/or detector sensitivity⁽⁹⁰⁾ and the restricted lateral resolution to ca. $10\mu\text{m}$ has limited the depth of study in certain biological systems. The use of a synchrotron radiation (SR) source was therefore considered.

SR significantly improves the spatial resolution of an infrared microspectrometer, allowing data to be obtained a high SNR of $3\text{-}5\mu\text{m}$ within the mid-infrared region⁽⁹¹⁾. The spatial resolution obtained using conventional FTIRM is

controlled by an aperture stop in the beam. For a global source with a large angular distribution of light the beam cannot be focused efficiently on to a small aperture yielding a low SNR. The superior brightness of synchrotron light with its narrow angular distribution allows almost all of the light to be transmitted through even a small aperture leading to a high SNR at spatial resolutions down to the diffraction limit^(92, 93).

Synchrotrons are accelerator facilities which provide extremely bright, high-flux electromagnetic radiation at energies ranging from X-ray, Ultraviolet and infrared regions⁽⁹⁴⁾. The electron beam is first accelerated in a linear accelerator, boosted to relativistic speeds in a booster ring and then stored in a storage ring. The storage rings are designed to maintain 'bunches' of electrons in a circular orbit by bending magnets⁽⁹⁴⁾. As the electrons pass through the magnetic fields, they are bent to maintain orbit and as a result, photon energy is expressed over a wide frequency range, hence at each of the bending magnets around the ring, beam ports are installed to enable radiation to pass through in a confined vacuum and into an experimental chamber⁽⁹⁴⁾.

Third generation of synchrotrons developed in the 1980s included the insertion of devices such as multipole wigglers and undulator magnets which were specifically designed to optimize SR brightness in the X-ray region, better beam stability and longer scanning durations between injections^(90, 95). Synchrotron infrared light still relies on bending magnets where both edge and bending radiation provide a source that is 1000 times brighter than a conventional infrared source⁽⁹⁶⁾ which allows data collection that is approximately 30 times faster than with a Global source and permitting small microscopic apertures close to the diffraction limit of the light to be used in microspectroscopy^(90, 96) (**Figure 1.15**). Fourth generation synchrotrons (free electron lasers) are capable of providing greater IR output but will not be discussed further.

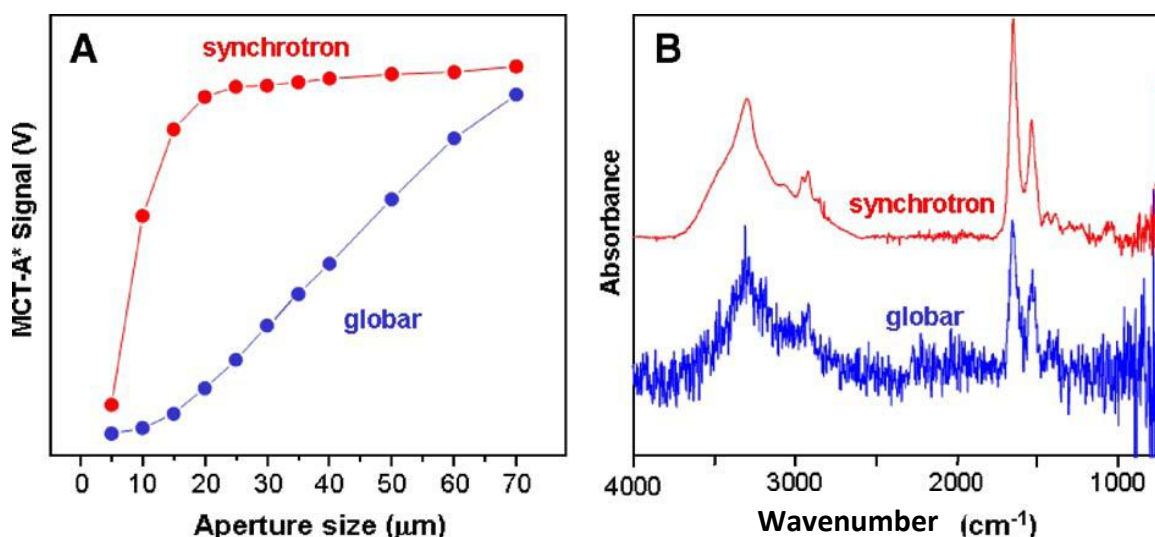


Figure 1.15. A Infrared signal through aperture sizes ranging from 5 – 70 μm using a synchrotron source versus a globar source, showing the difference in brightness as a function of aperture size. The globar source transmits little light through a 10 μm aperture, unlike more than 80% of the synchrotron IR light passing through the same aperture size. **B** Infrared spectra of a single red blood cell collected using a 5 x 5 μm aperture, demonstrating the advantage of the bright synchrotron IR source and the drastically improved SNR (Figure from Miller *et al.*, 2006⁽⁸⁶⁾).

The first instance of coupling an FTIRM with a synchrotron IR source was in the early 1990s at the National Synchrotron Light Source in New York and since then IR microscopes have been installed on over 15 beamlines at synchrotrons worldwide⁽⁸⁶⁾. The collimated beam of synchrotron IR light follows the same beam path as a conventional IR source, the synchrotron radiation brightness is however far greater than conventional sources and enables to the beam size to be reduced to below 10 μm without significant loss of photons. While synchrotron FTIRM

instruments provide the highest possible spatial resolution, measurements are still time consuming because they utilise the confocal arrangements with a single element IR detector and hence raster scanned images of a single biological cell may take over an hour to collect and some areas of subcellular imaging in tissue may take several days⁽⁸⁶⁾.

The addition of FPA detectors at synchrotron radiation facilities worldwide extends the performance and applicability of infrared beamlines for soft tissues and cell analysis^(90, 94). Due to the superior SNR characteristic of SR emission, smaller and more dilute samples and those that are thicker can be studied whilst still maintaining superior spatial resolution^(90, 96, 97). The first successful experiments utilizing an FPA detector (64 x 64) with SR was performed in Germany at ANKA, the synchrotron facility at the Karlsruhe Institute of Technology in 2005⁽⁹⁰⁾ and the use of FPA detectors optimised in the mid-IR range appeared to be the most appropriate way to collect fast IR images over large areas due to the sensitivity and readout speed available at a SR source⁽⁹⁰⁾.

More recently, the University of Wisconsin Synchrotron Radiation Center have developed a multi-beam infrared beamline termed IRENI (Infrared Environmental Imaging) is specifically designed to achieve broad wide-field illumination and spatial oversampling required to obtain high quality IR images with the highest spatial resolution (at the diffraction limit for mid-IR) within minutes⁽⁹⁸⁾. The recent design is able to achieve a geometric pixel size of $0.54 \times 0.54 \mu\text{m}^2$ compared with $6.25 \times 6.25 \mu\text{m}^2$ which is currently the best pixel size available⁽⁹⁹⁾ for synchrotron FTIR spectroscopy. In the developing beamline, a set of 12 identical paraboloidal mirrors with 250 mm focal lengths, which collimate the beams and deflect them 90° in the horizontal plane. These collimated beams are then combined and rearranged to form a 4 x 3 matrix from 12 plane mirrors. This group of beams is then directed by a single flat mirror into the FTIR interferometer through the microscope. It is here that the beams overlap before the microscope condenser in order to uniformly illuminate the sample⁽⁹⁹⁾. The IRENI beamline is

postulated to provide the next step in IR imaging by coupling the brilliant light from a synchrotron source with a FPA detector and thus providing very high spatial resolution at the diffraction limit for all wavelengths, very short acquisition times and high SNR and hence high quality data⁽⁹⁸⁾.

1.2.5. The use of IR spectroscopy for the analysis of organic molecules

IR spectroscopy in the mid IR region is most commonly used to determine the chemical functional groups in a sample, as different functional groups produce characteristic absorption frequencies of IR radiation (**Table 2**). It is a non-destructive technique that requires less sample preparation than conventional biochemical or chemical techniques and may be used under a wide variety of conditions for a wide variety of samples⁽⁸⁰⁾. It has been applied to the identification of compounds by matching spectral fingerprints from unknown samples with reference spectra for example in the identification of polymers, plastics and resins and in the analysis of insecticides and copolymers^(74, 100). In biological systems, the IR spectrum is the sum of all contributions from all the biomolecules⁽⁹⁰⁾ and will show small changes when the chemical structure of a functional group is modified, thus providing molecular fingerprints in the form of absorption spectra.

Table.2. Infrared band assignments identified in biological systems

Vibrational mode	Wavenumber (cm ⁻¹)	References
DNA marker bands	890, 830	(101)
RNA, ribose-phosphate	815,870,880,915,970	(101)
Nucleic acid, ribose	965	(102)
RNA, ν and δ ring of uracil	996	(102)
DNA, ν_{C-O} ribose	1015	(102)
Glycogen, ν_{C-O}	1025, 1047	(103)
DNA and RNA ribose C-O	1050	(101)
Nucleic Acids, $\nu_s PO_2^-$	1080-1090	(101)
RNA, ribose ν_{C-O}	1120, 1160	(102)
ν_{C-O} of proteins and carbohydrates	1171-1154	(104)
DNA, $\nu_{as} PO_2^-$	1230	(101)
RNA, $\nu_{as} PO_2^-$	1244	(101)
Proteins, Amide III (CN stretching, NH bending)	1250-1300	(80)
DNA and RNA conformational markers	1330-1530	(102)
ν_{COO^-} of fatty acids and amino acid side chains	1400	(105)
Proteins	1450	(106)
$\delta_{as} CH_3$ of cellular proteins	1457	(104)
Lipids, CH_2 scissoring	1474-1520	(107)
Proteins, Amide II (CN stretching, NH bending)	1530-1545	(80, 108)
DNA and RNA, $\nu_{C=N}$ imidazole ring vibrations	1578	(102)
DNA, δ_{NH_2}	1603-1605	(109)
DNA and RNA, $\nu_{C4=C5}$	1610	(102)
Proteins, Amide I (C=O stretching)	1650	(80, 83, 108)
$\nu_{C=O}$ from purine and pyrimidine bases	1720-1666	(102)
B-DNA base pairing vibration ($\nu_{C=O}$ & $\nu_{C=N}$)	1708	(110)
A-DNA base pairing vibration ($\nu_{C=O}$ & $\nu_{C=N}$)	1715	(110)
$\nu_s CH_2$ acycl chain lipids	2852	(111)
$\nu_s CH_3$ acycl chain lipids	2874	(111)
$\nu_{as} CH_2$ acycl chain lipids	2922	(111)
$\nu_{as} CH_3$ acycl chain lipids	2956	(111)

ν = stretch, ν_{as} = asymmetrical stretch, ν_s = symmetrical stretch, δ = bending vibration

IR absorption is typically shown in the form of spectra with wavelength (λ) or wavenumber ($1/\lambda$) in cm^{-1} as the x-axis and absorbance on the y-axis⁽⁷⁴⁾. The details obtained from infrared spectroscopy are obtained by careful monitoring of the spectral wavenumber, intensity and line-width parameters which, with great sensitivity reflects a sample's molecular structure. Quantitative information within the IR region is derived from absorbance values and the application of Beer's law⁽⁸¹⁾.

A typical IR spectrum of a cell in a biological system will exhibit contributions from cellular macromolecules including proteins, lipids, carbohydrates and nucleic acids and a typical example is shown in **Figure 1.16**. Although spectra of macromolecules are complex, each of the above mentioned components provide characteristic contributions to the IR spectrum⁽⁷⁸⁾. Within the mid-infrared region, 4,000-400 cm^{-1} , particularly within the 1800-700 cm^{-1} region, the average protein spectrum is dominated by the amide I band at $\sim 1650 \text{ cm}^{-1}$, which is primarily associated with the stretching motion of the C=O group, and is sensitive to the environment of the peptide linkage and the protein's overall secondary structure. The amide II band associated with C-N stretching and CNH deformation occurs at $\sim 1530 \text{ cm}^{-1}$.

The infrared absorption spectra of nucleic acids, both nuclear and mitochondrial DNA, and also RNA depends on the hydration state and the nature of the secondary structures of the DNA and RNA. They exhibit absorption peaks between 1580 and 1700 cm^{-1} due to the aromatic base and C=O stretching vibrations. The ionized PO_2^- and ribose groups demonstrate three peaks at 1071, 1085 and 1095 cm^{-1} . In DNA, these peaks have almost identical intensities, and DNA also shows peaks at 965 and 1245 cm^{-1} which are the phosphodiester vibration⁽¹¹²⁾. In RNA, the peak at 1085 cm^{-1} is stronger than the other two peaks at 1071 and 1095 cm^{-1} .

Carbohydrates, usually in the form of glycoproteins or polymeric sugars also occur in cells and tissues and these are characterized by peaks in the region 1140-985 cm^{-1} ⁽¹¹³⁾. Glycogen, a glucose polymer, exhibits a strong absorption spectrum due to the C-O and C-C stretching and C-O-H deformation motions with peaks at 1151, 1078 and 1028 cm^{-1} ⁽¹¹²⁾.

Molecules which make up the cell membrane lipid bilayer are termed phospholipids. Distinctive C-H vibrations of lipids occur at around 3000 cm^{-1} as outlined in table 2, however C-H stretching vibrations which are associated with methyl and methylene groups are also generally observed within the region 2960-2850 cm^{-1} , where methylene and methyl groups originating from lipids and methyl groups from proteins both contribute to a strong band at 2930 cm^{-1} ⁽¹¹⁴⁾. The most prominent feature within this spectral region and relevant to the spectra of lipids is the C-O stretching vibration at $\sim 1735\text{-}1740$ cm^{-1} which originates from the ester linkage of the fatty acid tail and the triglyceride polar group, where a shoulder at 1740 cm^{-1} is observed in some cells or tissues due to phospholipids⁽¹¹²⁾.

Biological samples are typically embedded in paraffin which also displays a prominent IR absorption within the C-H stretch region usually within the 2800-3000 cm^{-1} region⁽⁸⁶⁾, and do not interfere with the important biological spectrum region which is shown in **Figure 1.16**.

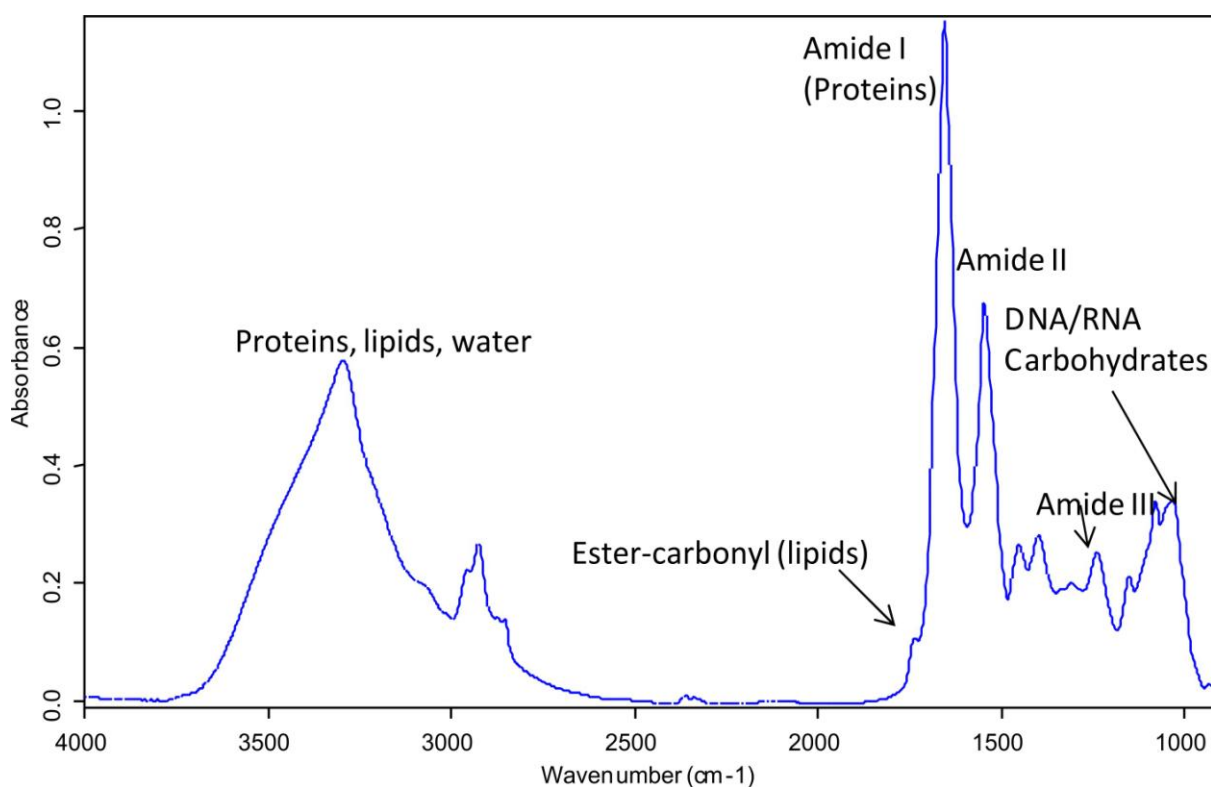


Figure 1.16. Region of the IR spectrum illustrating four prominent features of biological samples (protein, lipid, nucleic acid and carbohydrate), highlighting the main features of each. Amide I and amide II bands typically represent protein, lipids show a distinct ester-carbonyl band at ~ 1740 , nucleic acids are represented by the P=O stretch and carbohydrates by the C-O stretch (Unpublished data from our lab).

1.2.6. Analysis of secondary structure by FTIRS

Considerable information about the secondary structures of proteins can be derived from FTIRS. The extraction of information on the secondary structure of biological samples and the limitations of the various techniques have been extensively reviewed^(19, 115-117) and are only briefly outlined here.

FTIRS is sensitive to conformational changes in proteins due to the strong IR absorption of peptide carbonyl groups. FTIRS allows direct probing of the vibrational properties of almost all cofactors, amino-acid side chains and of water

molecules, making it a useful molecular probe for the analysis of secondary structure of polypeptides and proteins^(80, 108).

The infrared spectra of proteins and polypeptides are characterised by a number of amide bands which represent different vibrations of the peptide moiety⁽¹¹⁷⁾. Of all the amide modes of the peptide group, the most widely used in studies of protein secondary structure is the amide I band, originating from the C=O stretching vibration of the amide group and coupled to the bending of the N-H bond and the stretching of the C-N bond⁽¹¹⁷⁾. The relationship between the position of the amide I band and the type of secondary structure it may represent, is best derived from the analysis of the spectra of relatively simple proteins of well defined structure, e.g., α -helical or β -sheet, and this is increasingly providing the background for studies of more complex molecules^(115, 117). Since proteins are complex structures made up of regions folded into different structures, the amide I band is itself a composite of a series of overlapping component bands representing these structural elements, such as α -helices, β -sheets, turns and non-ordered or irregular structures⁽¹¹⁷⁾. The main difficulty in analysing these composite bands is due to the width of the contributing component bands which is usually greater than the difference between the maxima of the adjacent peaks, making the individual component bands difficult to identify.

Extensive mathematical manipulations of the infrared data collected including extraction of data based on band narrowing and deconvolution of the amide I band into its underlying components are used to gain structural information from the infrared bands. Deconvolution and second derivative analysis may be used to identify the positions of the components of the amide I band, from which the secondary structure may be cautiously identified.

One of the most frequent approaches to extracting information on the protein secondary structure from the infrared spectra collected is Fourier deconvolution⁽¹¹⁸⁾. Deconvolution in spectroscopy, utilises mathematical

algorithms to reverse the optical distortion from the instrument. This decreases the width of infrared bands which then allows for better separation and identification of the bands which were previously overlapping^(116, 119). This process does not increase the resolution of the data collected but it increases the degree to which contributing component lines may be distinguished. Fourier deconvolution does not affect the integrated intensities or areas of the individual bands⁽¹¹⁷⁾.

Analysis of second derivative spectra is another method of extracting vital spectra information within composite bands and has been described for identification of protein structure by Kennedy *et al.*, 1991⁽¹¹⁸⁾, where different amide I regions were assigned to secondary structures by comparison to a set of proteins of known structure^(118, 120). Second derivative spectroscopy is an analysis technique by which the obtained spectrum is differentiated twice. This analysis eliminates sloping baselines which arise in heterogeneous samples and enables resolution of bands contributing to shoulders or inflection points in the original spectra⁽¹⁰⁹⁾. It allows more specific band assignments to be made by correlating the minima peaks in the second derivative spectra with the maxima peaks in the non-derivatized spectra, thereby increasing the specificity of absorption peaks for certain molecules within a tissue.

There are however disadvantages associated with deconvolution and derivatization of spectra. Both of these processes amplify the noise in the spectra significantly and hence the degree to which bands may be narrowed is limited to the SNR of the spectrum and care must be taken to avoid amplified noise being misinterpreted as a real band⁽¹¹⁷⁾. Derivatization of spectra produces faster spectral degradation than deconvolution and therefore information may be partially lost⁽¹²¹⁾.

Table 3 illustrates the major bands, generated by either deconvolution or derivatization of spectra that are attributed to structural components in proteins which contain a triple helix. It is interesting to note that in most of the examples given in the table, the location of the triple helix of collagen differs from most assignments of collagen which is usually above 1660 cm^{-1} . George and Veis⁽¹²²⁾

made an observation that the amide I region of the spectrum of native collagen is particularly interesting as the type I collagen triple-helix conformation does not fit the standard α -helix, β -sheet and β -turn conformation as most other proteins and Payne and Veis⁽¹¹⁵⁾ showed that the broad amide I band of the native type I collagen molecule can in aqueous solution be deconvoluted into three distinct bands with maxima at 1660, 1643 and 1633 cm^{-1} .

Table.3. Relative intensities of the components of the amide I band in proteins which contain a triple helix

Protein and method of extraction	Form	Amide I band location (cm ⁻¹)	Main bands identified by deconvolution (by decreasing intensity (cm ⁻¹))	Reference
Type I collagen (Acetic acid, NaCl precipitation from lathyrus calf skin)	Native monomer	1650	1660, 1643, 1633	(115, 116)
Type I collagen (calf skin gelatine, 50°C)	Denatured	1643	1633, 1643, 1660	(115)
Gelatine renatured at 4°C	Variable triple helix formation	1643	1643, 1656, 1634	(115)
C1q intact	Large globular domain, short triple helix	1638	1637, 1661, 1683	(19)
C1q stalks (pepsin digested)	Triple helix	1652	1655, 1636	(19)
Type I collagen (pepsin digested)	Triple helix	1654	1657, 1632, 1682	(19)
Type III collagen (pepsin digested)	Triple helix	1655	1659, 1632, 1682	(19)
Type IV collagen (pepsin digested)	Triple helix	1653	1659, 1633, 1682	(19)
Rat & cod skin collagen		1656 (native), 1647 (denatured)	1656, 1630, 1670	(123)
Collagen related polypeptides (synthetic)	Disordered (Gly-X-Y) _n	1630	1630, 1650	(123)
Collagen related polypeptides (synthetic)	Helical polytripeptides	1643	1632-7, 1650-5, 1669-1687	
Type I collagen (rat skin collagen, acetic acid preparation)	Native monomeric	1660.1	1660, 1645, 1631	(122)
Type I collagen (rat skin collagen, acetic acid preparation)	During fibrillogenesis	1660.1	1660, 1644, 1630	(116, 122)
Type I collagen (rat tail fibres)	Native, fibrillar	1658	1658 (α-helix), 1638 (triple helix), 1668 (β-turns), 1647 (unordered)	(124)
Type IV collagen	Native, fibrillar	1658	1658 (α-helix), 1638 (triple helix), 1668 (β-turns), 1625 (parallel β-sheets), 1612 (β-turns)	(124)
Type II collagen (chicken)	Native	1655	1655	(72)
Type II collagen (bovine, pepsin digestion)	Native	1666	1666	(11)
Type II collagen (bovine, pepsin digestion)	Denatured at 50°C	1652	1652	(11)

1.2.7. Features of the spectra of cartilage components

As described in section 1.1, cartilage is primarily composed of a network of collagen fibrils in which are enmeshed proteoglycans and hyaluronan. FTIRS has been used to examine the individual spectra of the main cartilage components, CII^(122, 123, 125), proteoglycans⁽¹²⁶⁻¹²⁹⁾ and hyaluronan⁽¹³⁰⁾ three major components of the cartilage matrix. FTIRS analysis of the individual components of cartilage has lead to the identification and designation of particular bands present in the IR spectrum which are characteristic of cartilage or the individual components of cartilage. **Table 4** outlines the band assignments for each of the major components of the cartilage matrix⁽⁷²⁾.

Table.4 Band assignments for the components of the cartilage matrix

Bond vibrations	Wavenumber (cm⁻¹)	References
Collagen		(131) (11, 73) (72, 132)
Amide A N-H stretch	3330	
Amide I C=O stretch	>1660, 1655	
Amide II C-N stretch, N-H bend combination	1500 1338	
Amide III C-N stretch, N-H bend, C-C stretch	1250	
Proteoglycan		(126-129)
Amide I C=O stretch	1640	
Amide II C-N stretch, N-H bend combination	1545	
Sulphate stretch	1245	
C-O-C, C-OH, C-C ring vibrations	1125-920	
C-O-S stretch	850	
Hyaluronan		(128-130)
Amide I C=O stretch	1640-1550	
Amide II C-N stretch, N-H bend combination	1545	
Carboxylate group –COOH	1420-1400	
Carboxylate group –COOH	1370	
R-C-O-CR	1150, 1000	

1.2.7.1. Collagen

The major protein component of cartilage is CII, a fibril forming collagen which is synthesized by chondrocytes and is comprised of three chains, each in polyproline II-like conformation, each of which consists of a 280 nm long polypeptide chain. The three chains are staggered by one residue and stabilized by interchain hydrogen bonding⁽²²⁾. There is little information on the IR spectrum of CII but it is very similar in structure and sequence to type I collagen, the major structural protein of most tissues which has been extensively examined^(115, 123, 124). The amide I peak of the native collagen helix is characteristically above 1660-1658 cm^{-1} , appearing in deconvoluted or second derivative spectra as three distinct bands at 1657-1661, 1630-37 cm^{-1} and above 1670 cm^{-1} ^(18, 29,30, 32).

The deconvoluted native CI spectrum at 4°C shows three prominent bands at 1660, 1643 and 1633 cm^{-1} spectrum with the 1660 cm^{-1} being the most intense⁽¹¹⁵⁾. Upon heat denaturation, the 1660 cm^{-1} band is markedly diminished and the 1633 cm^{-1} band is more intense. The three most intense peaks however, remain at 1660, 1643 and 1633 cm^{-1} whether in the native or denatured states. This prominence of the 1660 cm^{-1} component in both the native spectrum and the denatured state suggest that this peak contains a component which is directly related to the native triple helix formation⁽¹¹⁵⁾.

These bands also occur in other molecules that contain a collagen-like triple helix, including the non-fibrillar collagens that contain one or several small triple-helical domains interrupted by short non-helical domains, and the complement component C1q that comprises a collagen-like triple helix at the N-terminus, with C-terminal globular heads⁽¹⁹⁾.

1.2.7.2. Proteoglycan

Camacho *et al.*⁽⁷²⁾, characterised the spectrum of aggrecan, which is a molecule containing chondroitin and keratan sulphate molecules linked to a protein core

containing features derived from the sulphate, sugar and protein entities of the spectrum. Considerable overlap between the spectrum of pure CII and aggrecan also occurred within the spectral region $1800\text{-}800\text{ cm}^{-1}$ and this is shown in the spectrum of both CII and aggrecan in **Figure 1.17**. The most prominent features of the cartilage spectrum are the amide I, II and III which are shown to contribute to the collagen spectrum (refer to **Table 4**). The most prominent features of the aggrecan spectrum are the large sulphate and sugar peaks. Camacho and colleagues identified the spectral region from $1185\text{-}960\text{ cm}^{-1}$ to be representative of aggrecan⁽⁷²⁾. This is validated by Bychkov *et al.*,^(128, 129) who examined individual preparations of several chondroitin sulphate molecules including chondroitin-4-sulphate and chondroitin-6-sulphate and identified absorption bands at 1125 and 1245 cm^{-1} which are only present in sulphate containing proteoglycans.

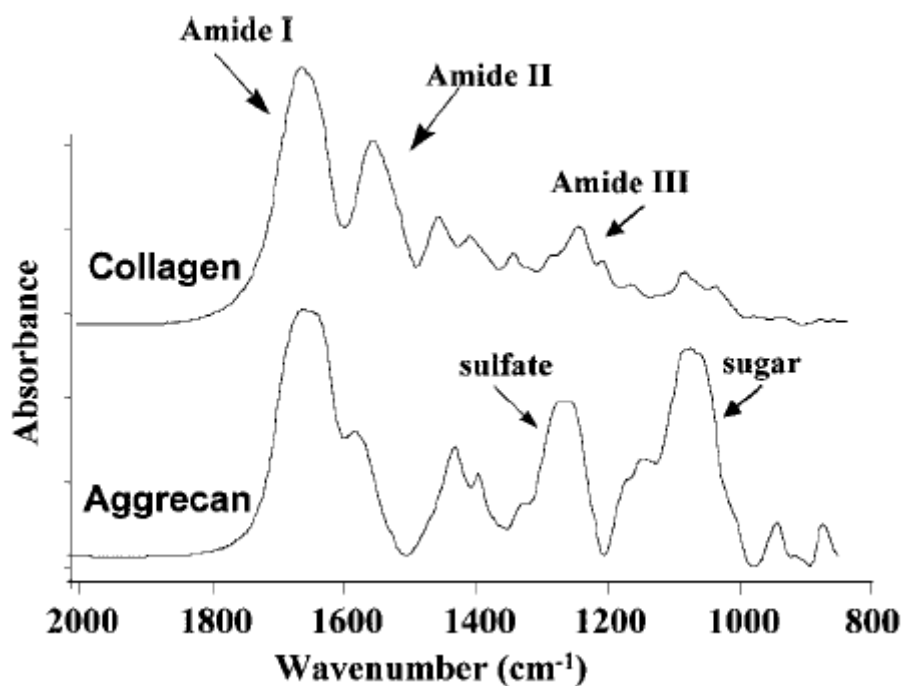


Figure 1.17. FTIR spectra of type II collagen and aggrecan. The spectra of both these individual components shows considerable overlap within the spectral region from $1800\text{-}800\text{ cm}^{-1}$. The most prominent features of the CII spectrum are the amide I, II and III which are shown to contribute to the collagen spectrum. The most prominent features of the

aggrecan spectrum are the large sulphate and sugar peaks. (Figure from Camacho *et al.*, 2001⁽⁷²⁾)

1.2.7.3. Hyaluronan

Bychkov *et al.*,^(129, 130) have performed extensive studies on the identification of infrared absorption bands of hyaluronan, or hyaluronic acid. Bands were identified within the amide I ($1640\text{-}1550\text{ cm}^{-1}$) and amide II region (1545 cm^{-1}) as well as at 1400 , 1380 and $940\text{-}925\text{ cm}^{-1}$. There were weak bands observed at 1305 , 1225 and 1200 cm^{-1} and the strongest absorption recorded at $1080\text{-}1030\text{ cm}^{-1}$ ⁽¹³⁰⁾. Bands within the $1420\text{-}1400\text{ cm}^{-1}$ region and a shoulder at 1370 cm^{-1} were later identified by the same group as belonging to the carboxylate group ($-\text{COOH}$) and the R-C-O-CR structure revealed absorptions at 1150 and 1000 cm^{-1} ^(128, 129).

1.2.7.4. Combined spectral properties of cartilage

Camacho *et al.*,⁽⁷²⁾ characterised collagen and proteoglycan content in articular cartilage, whereby the integrated absorbance of the amide I peak ($1720\text{-}1585\text{ cm}^{-1}$) was used as a representation of collagen content and the absorption within the carbohydrate region ($985\text{-}1140\text{ cm}^{-1}$) was used for proteoglycan analysis. The infrared spectrum of cartilage therefore characteristically focuses on two regions, the amide I region, which appears at a higher wavenumber than that for most proteins, above 1650 cm^{-1} and the collagen triplet, with bands at 1203 , 1234 and 1280 cm^{-1} . The collagen triplet however also coincides with a peak at $1240\text{-}1245\text{ cm}^{-1}$, which is derived from the sulphated glycosaminoglycan side chains of proteoglycans^(72, 133). The position of the amide I peak above 1650 cm^{-1} has been attributed to hydrogen bonding between polypeptide chains of collagen, as a spectral shift occurs between 40°C and 43°C , the temperature at which collagen denatures⁽¹¹⁵⁾. The position of the amide I band therefore provides a useful marker of helical (native) collagen in cartilage.

The spectrum of the major components of cartilage, CII, proteoglycans and hyaluronan was also studied by Crombie *et al.*,⁽¹¹⁾ where it was shown that each of the components demonstrated a characteristic IR spectrum and the resultant spectrum is shown in **Figure 1.18**. The amide I band, 1600-1700 cm^{-1} is present in the spectrum of all three components, whereas a triplet of bands at 1200-1300 cm^{-1} is only present in the spectrum of CII, and bands within the spectral region 960-1175 cm^{-1} resulting from sugars are seen in the spectrum of proteoglycan and hyaluronan.

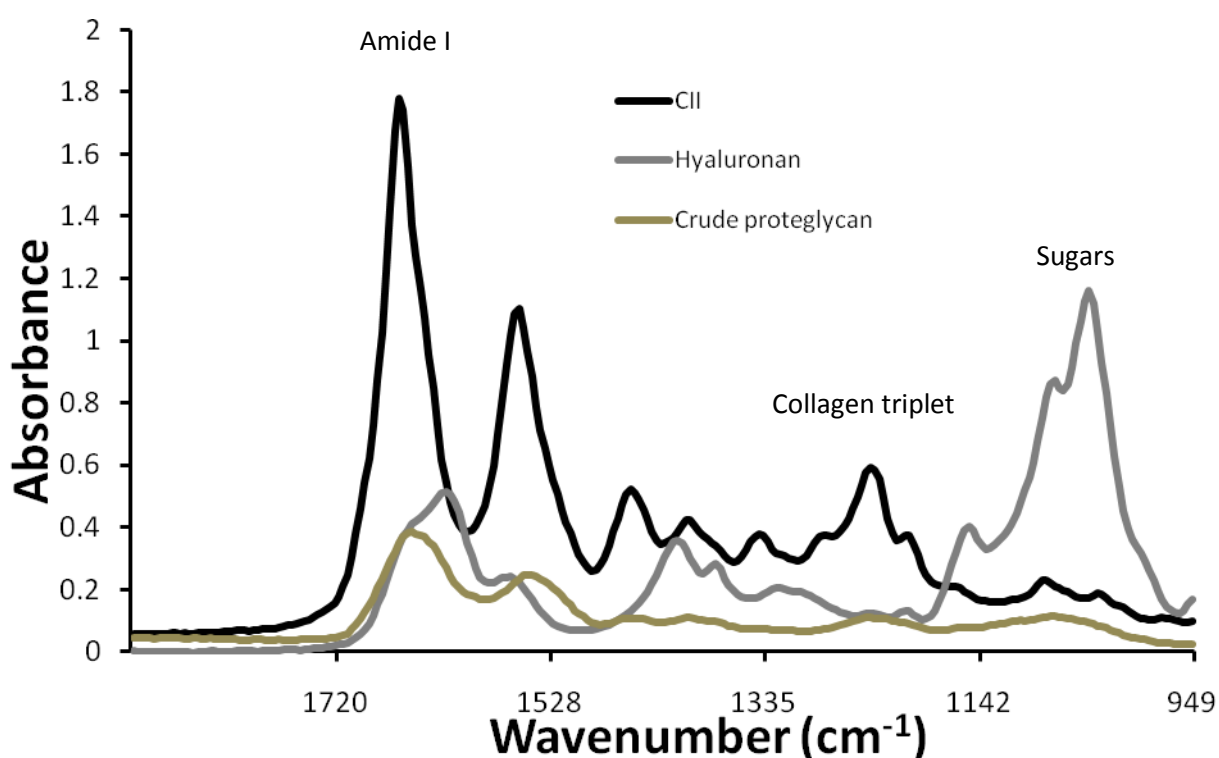


Figure 1.18. FTIR spectra of the individual components of the cartilage matrix, CII, proteoglycan (shown here as crude PG) and hyaluronan. The amide I band 1600-1700 cm^{-1} is present in each of the components but with different profiles and intensities. A triplet of bands from 1200-1300 cm^{-1} is present only within the spectrum of CII and bands within the 960-1175 cm^{-1} resulting from sugars are present in both the proteoglycan and hyaluronan spectrum. (Unpublished data from our lab).

A combined typical IR spectrum of articular cartilage comprises 55% CII, 40% proteoglycan and 5% hyaluronan⁽¹¹⁾ and has been published by both Rieppo *et al.*,⁽¹¹³⁾ and Crombie *et al.*,⁽¹¹⁾ and is shown in **Figure 1.19**. The main spectral features of cartilage are a prominent amide I peak ($>1655\text{ cm}^{-1}$) as well as sulphate peak derived from the side chains of glycosaminoglycans ($1240\text{-}1245\text{ cm}^{-1}$) and the collagen triplet ($1203, 1234$ and 1280 cm^{-1}).

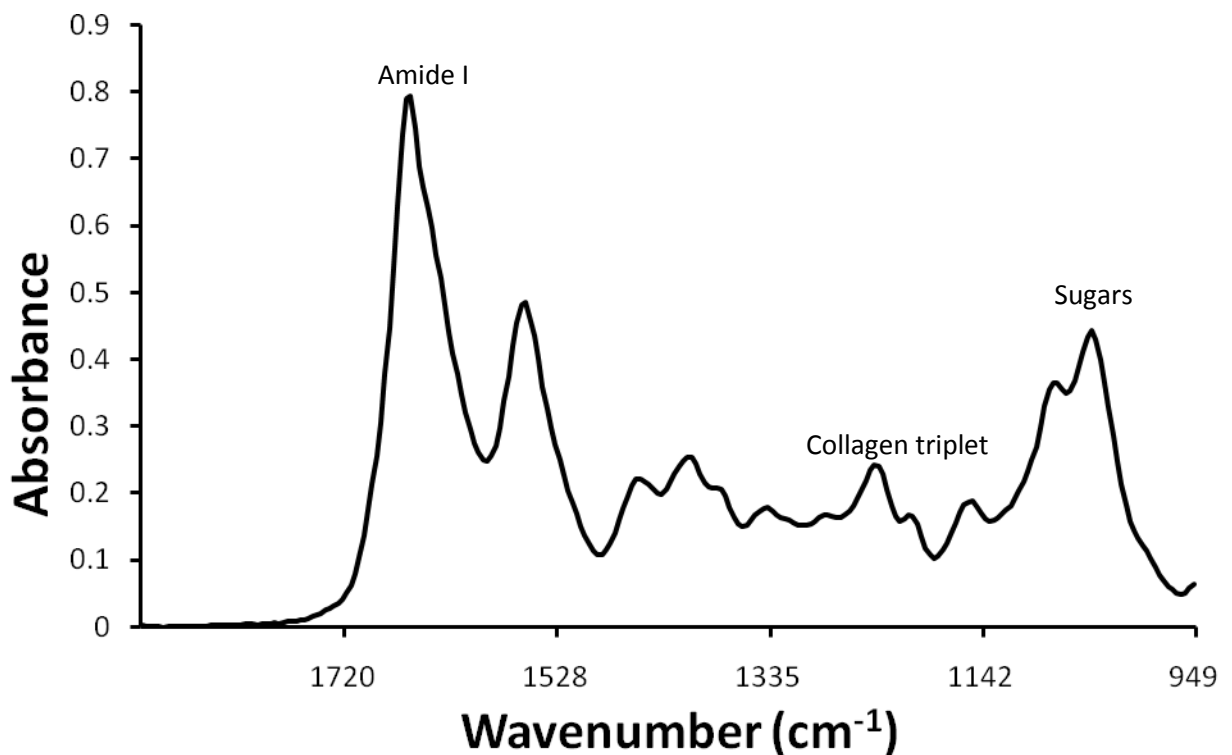


Figure 1.19. Typical IR spectrum of articular cartilage. The spectrum of cartilage shows a prominent amide I peak ($>1655\text{ cm}^{-1}$) as well as sulphate peak derived from the side chains of glycosaminoglycans ($1240\text{-}1245\text{ cm}^{-1}$) and the collagen triplet ($1203, 1234$ and 1280 cm^{-1}). (Unpublished data from our lab).

1.2.8. Methods of Analysis

Infrared spectrometers produce large data sets which require high speed computing for further analysis and interpretation of the spectra data collected. Various programs have been developed for this purpose and can be separated into three categories.

OPUS, developed by Bruker is another software program available for analysis of spectral data. OPUS was first developed for analysis of single point spectra which are commonly collected on infrared beamlines which use Bruker instruments at Synchrotrons worldwide. It allows for such functions as baseline correct, averaging of several individual spectra, second derivative analysis and peak integrations. It also contains a search package which may be useful in identifying unknown compounds by searching a database of known spectra and comparing to that of the unknown sample. The OPUS software has the ability to generate both two and three dimensional representations of spectra data and allowing single spectra to be selected from a large map. The OPUS software package contains pre-processing functions and false colour maps of spectral data inputs; however OPUS only contains univariate methods of analysis, therefore another chemometric program, Cytospec is often employed in conjunction to OPUS to analyse data sets depending on the users' preferences and needs. Cytospec will be discussed in section 1.2.8.2.1.

1.2.8.1. General chemometric analysis packages

MATLAB® (MathWorks, Inc, <http://www.mathworks.com>) is a general purpose mathematical based program which is used for algorithm development, data visualisation, data and analysis and numeric computation. MATLAB uses mathematical modelling which is of use for such applications as signal and image processing, communications, financial modelling and analysis and computational

biology. It contains mathematical functions for Fourier analysis which makes it useful for analysis of infrared spectra.

Unscrambler® is a software package used for spectroscopic analysis. It is equipped with a toolkit for spectral transformations including, smoothing and derivatives, scatter correction and normalisation and baseline correction of spectra. It also contains modelling tools capable of performing principal component analysis and cluster analysis.

1.2.8.2. Software for the analysis of spectral images

1.2.8.2.1. Cytospec analysis software

One of the most widely used software packages for spectral imaging analysis is Cytospec™. Originally developed in 2000 as a specialized software package for FTIRS imaging, it now encompasses an array of pre-processing options and imaging methods. The major advantage of Cytospec over other infrared analysis programs is its ability to manipulate hyper-spectral data cubes and not just individual spectra, allowing all operations to be carried out on the entire spectra map collected. Cytospec contains basic manipulation functions including rotation or flipping of images, exporting and defining regions of interest and capturing of spectral images. The software contains standard pre-processing manipulations including smoothing, scaling and normalization, baseline correction, cutting to a spectral region of interest and calculation of derivative spectra. Pre-processing of spectral grids may also be performed to remove poor quality spectra based on such factors as SNR and sample thickness to eliminate spectra which may be influenced by variations in the thickness of the sample or unevenness to the sample. Cytospec also allows for more specialized univariate and multivariate approaches.

Univariate methods include pseudo-colour mapping of 3-dimensional spectral imaging data sets through statistical methods and utilizing the entire spectra information. This allows the user to manually select spectral regions of

interest which can then be integrated with the multivariate analysis approaches. These create spectral correlations and maps again using the entire spectra information. Multivariate methods include principal component analysis, k-means clustering and unsupervised Hierarchical Cluster Analysis, which will be outlined in section 1.2.8.3.

The infrared analysis undertaken and reported in this thesis was performed using both OPUS, as the spectra collected were taken on Bruker instruments and Cytospec, particularly the use of the UHCA method because it is the optimum program for spectral image analysis.

1.2.8.3. Unsupervised hierarchical cluster analysis

IR data generated from FTIRM can be analysed using a variety of techniques. Unsupervised Hierarchical Cluster Analysis (UHCA) is a multivariate approach that was applied for spectral image analysis in 2000⁽¹³⁴⁾. It is a technique that can be applied to analysing a data set collected by FTIRM and has been well described in literature⁽¹³⁴⁻¹³⁶⁾. UHCA is commonly used to assign a set of subset spectra into specific groups based on similarity. These groups of similar spectra can then be used to generate pseudo colour images. Researchers commonly use UHCA as a means of discriminating differences in the spectra of composite tissues, providing an objective means for determining variations in the tissue without any prior knowledge of changes that may be occurring.

Using UHCA, a matrix is calculated that expresses the similarity, or “distance”, between each spectrum and all other spectra within the data set. For two spectra S and R in the spectral hypercube, this distance is defined as the correlation coefficient C_{SR} according to the following equation⁽¹³⁴⁾.

$$C_{SR} = \frac{\sum_i (S_i - \bar{S})(R_i - \bar{R})}{\sqrt{\sum_i (S_i - \bar{S})^2} \sqrt{\sum_i (R_i - \bar{R})^2}} \quad [i=1 \dots M]$$

The spectra denoted by S and R are represented by 1-dimensional vectors of M absorption values, and \bar{S} and \bar{R} are the mean values for each vector. The resulting C_{SR} matrix, also known as the correlation matrix, contains N^2 entries, where N is the total number of spectra within the data set. Since the matrix is symmetric, only $N(N - 1)/2$ spectral distance elements C_{SR} need to be computed. Therefore, the two most similar spectra in the hypercube are merged into a “cluster”, and a new distance matrix column is calculated for each new cluster and all existing spectra. The process of merging spectra or clusters into new clusters continues, and the C_{SR} is recalculated until all spectra have been combined into a user defined number of clusters. Pseudo-colour maps based on cluster analysis are created by assigning a colour to each spectral cluster, and displaying this colour at the coordinates at which each spectrum was collected. The mean spectra may then be extracted corresponding to each of the clusters and used for interpretation of the chemical or biochemical differences between clusters and related to the pathology of the tissue. A schematic representation of the algorithm and the false colour map generated from the spectra data is shown in **figure 1.20**.

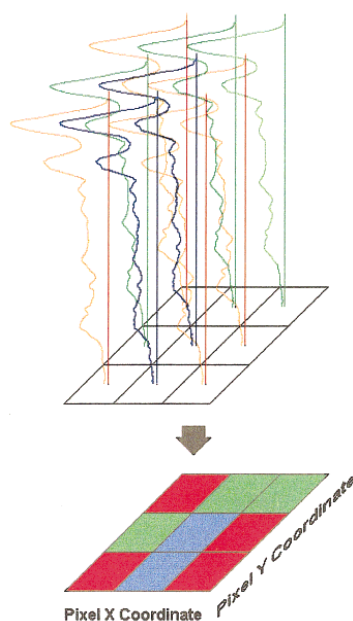


Figure 1.20. Schematic representation of the algorithm used to perform UHCA. The top is a 4-dimensional representation of raw data where the dimensions for each pixel point are pixel coordinates X and Y, the wavenumber and intensity axis. The bottom is a false colour map of the same spectral data (Figure from Diem *et al.*, 2000⁽¹³⁴⁾).

The use of UHCA is well illustrated by a study of liver fibrosis^(134, 137). One of these studies⁽¹³⁷⁾ applied UHCA to analyse levels of both type I collagen and glycogen in liver biopsies. In this study serial sections of a liver biopsy were collected where one section was stained with Masson's trichrome, a stain which is designed to distinguish cells from connective tissue, in which type I collagen stains blue and liver cells stain pink. The second section was used for FTIRM and analysed using Cytospec to derive a chemical map based on the region of the collagen triplet, 1203, 1234 and 1280 cm^{-1} . UHCA was then applied to the spectral region of the collagen triplet which was clearly able to distinguish between the liver cells and the type I collagen in the liver biopsy. **Figure 1.21** outlines the results of this study coupling FTIRM and UHCA to further understand the chemical changes that occur in a liver biopsy to coincide with the histological staining.

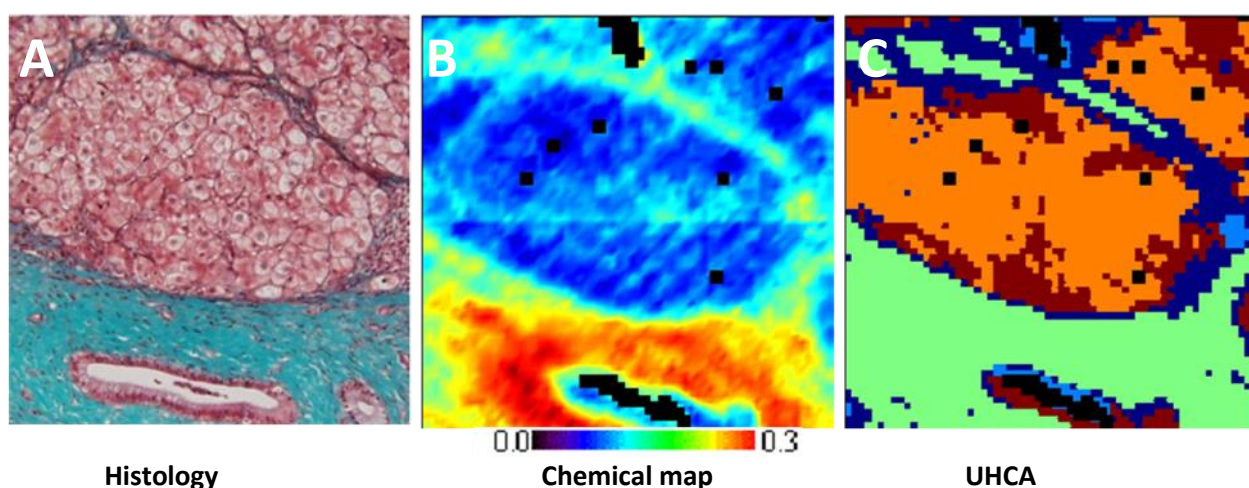


Figure 1.21. **A.** Masson's trichrome stained section of a liver biopsy. The pink area denotes the liver cells and the fibrous tissue, which contains type I collagen is shown in blue. **B.** chemical map of based on the collagen triplet region, 1203, 1234 and 1280 cm^{-1} of the infrared spectrum. The shading in this image indicates the strength of the signal, where red indicates a high concentration and blue indicates an area of low concentration of signal within the collagen triplet region of the spectrum. **C.** cluster analysis based on the collagen triplet, 1203, 1234 and 1280 cm^{-1} which has distinguished between the liver cells (brown/orange) and the fibrous tissue, type I collagen (green) in the liver biopsy (Adapted from Crombie *et al.*, 2005⁽¹³⁷⁾).

1.2.9. Applications of Fourier Transform Infrared Microspectroscopy

The ability of IR spectroscopy to distinguish between different tissue types and between healthy and diseased states has enabled IR spectroscopy to be applied in studies of pathology and cytology⁽¹³⁴⁾. FTIRM has been particularly useful in the study of cancer. For example, FTIRM has been used to examine cancerous and pre-cancerous changes in cervical cancer^(136, 138, 139). In one of these studies⁽¹³⁶⁾, cervical biopsies were examined by UHCA and the results were compared with histological changes detected by light microscopy. Particular clusters in areas of the biopsies were identified by light microscopy in which there were chemical changes detected within the amide I and amide II region, glycogen, carbohydrates and the phosphodiester bands of nucleic acids that corresponded to histological cancerous

changes and these chemical changes extended beyond the region of histology, indicating the appearance of pre-cancerous changes. Specifically, spectra from areas of a cervical intraepithelial neoplasia classed as CIN II/CIN III showed unique features including pronounced symmetric and asymmetric phosphate bands at 1078 and 1240 cm^{-1} and a significant reduction in the intensity of glycogen bands and a small amide I/II band ratio. By using UHCA this study was able to demonstrate subtle differences within the amide I/II region which correlated well with leukocyte proliferation which is otherwise difficult to observe using standard spectra. **Figure 1.22** shows the tissue section, a UHCA map of the corresponding section and a 2nd derivative spectrum from selected areas of the UHCA map, showing these changes to the amide I/II region and the reduced glycogen bands illustrating the capacity of UHCA to detect pre-cancerous changes.

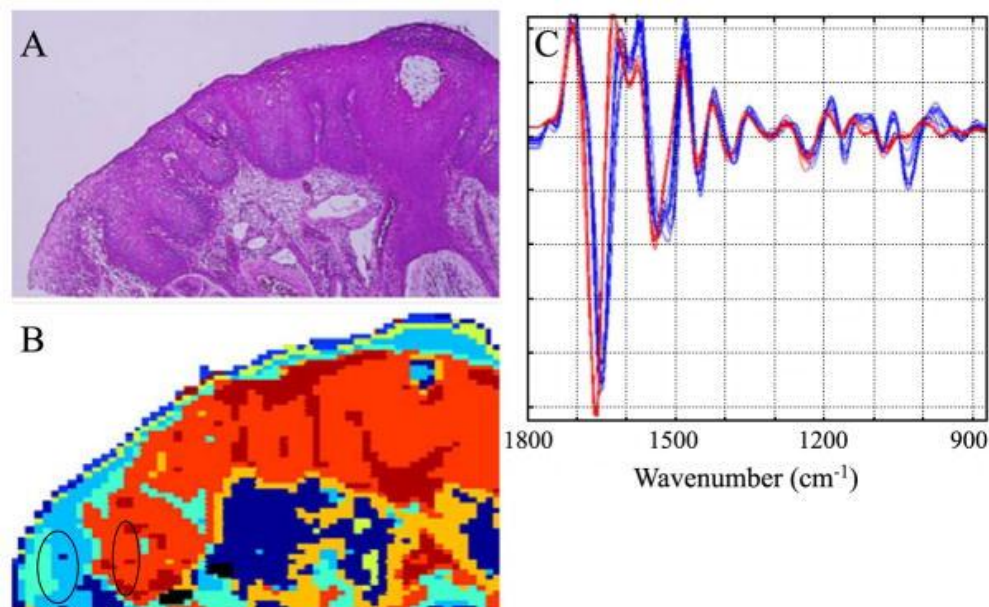


Figure 1.22. **A.** Haematoxylin and Eosin stained section of glandular epithelium from a patient diagnosed with high grade squamous intraepithelial lesions. The dark stained areas are associated with cervical intraepithelial neoplasia classed as CIN II/CIN III. **B.** A 9 cluster map constructed using 2nd derivative spectra within the spectral region (1800-800 cm^{-1}). **C.** Individual 2nd derivative spectra of the UHCA is **B**. The blue trace is selected from the circled regions of **B**. and the red trace is from the red area of the diseased state. (Figure from Wood *et al.*, 2004⁽¹³⁶⁾)

FTIRM has more recently been applied to the examination of chemical changes in cartilage^(11, 72, 115, 140-142). The first application of FTIRM to examine cartilage and its components as an entity was in 2001⁽⁷²⁾. In this study, FTIRM was used to examine normal bovine cartilage and identify the molecular components that contribute to the cartilage IR spectrum. Spectra of mixture of compounds which contained the main components of the cartilage matrix, CII and aggrecan were also analysed to identify any spectra markers could be potentially used for quantitative analysis of the components within the complete cartilage. This study provides information of the band assignments of the components of cartilage, which are outlined in **Table 4**. Specifically, that the main bands of collagen arise from the peptide bond vibrations of the Amide I, II and III and the spectrum of aggrecan exhibits spectral features which arise from the sulphate, sugar and protein entities⁽⁷²⁾. The identification of specific bands arising from the components of cartilage illustrates the potential for the use of FTIRM as a valuable tool in understanding bone and cartilage damage that occurs in the joints particularly in such diseases as RA⁽¹³²⁾ and osteoarthritis^(73, 141-143), joint injuries⁽¹⁴⁰⁾ and osteoporosis⁽¹⁴⁴⁾.

This information has lead the way for more recent IR studies applied in our laboratory to the investigation of the chemical changes to the major components of the cartilage matrix, CII and proteoglycans in the presence of monoclonal antibodies to CII⁽¹¹⁾ these changes are detailed in section 1.8.

1.2.10. Applications of synchrotron radiation

Whilst it is still an emerging technique, SR has been used successfully to examine a range of biological samples and more recently for live cell imaging⁽¹⁴⁵⁾. The synchrotron IR source has been successfully utilized to map the distribution of functional groups including proteins, lipids and nucleic acids from inside a single living cell, for example *Micrasterias hardyi*⁽¹⁴⁵⁾ with a spatial resolution of a few microns⁽¹⁴⁶⁾. Synchrotron IR has been used most frequently to examine bone⁽¹⁴⁷⁻¹⁵²⁾,

chondrocytes⁽¹⁴⁹⁾, cancer cells, all of which together encompass investigations into clinical pathology of Osteoarthritis, Osteoporosis, Cancer, Alzheimer's disease and heart disease^(86, 152). Studies have shown, that a SR infrared source at high current, coupled to an FTIR microscope provides information on cellular organic contents that is not accessible from spectra that are collected using a standard Global source. One such study demonstrated a band that was due to absorption by fatty acyl chains in a human glioma cell line that was not demonstrable with a Global source⁽¹⁵³⁾.

One of the limitations to the examination of living cells has been the challenge of positioning them within the IR beam to gain a clear signal. Various techniques and experimental cells are being developed for this. Thus, in 2005 a flow cell was developed at the SR source in Daresbury⁽¹⁴⁵⁾, which consisted of two separate windows, one made from CaF₂ and the other from ZnSe. This flow cell allowed medium to be supplied continuously using *Micrasterias hardyi* cells which are up to 300 µm in diameter but less than 12µm thick. In 2009 another flow cell was developed, using as a model and using diamond windows which are water insoluble, non-toxic, transparent and colourless in the visible and mid IR range, exhibiting a low dispersion in the mid IR region and tested using *Micrasterias sp.*⁽⁸⁹⁾.

Each of these experiments conducted using a SR source clearly demonstrate the superior advantage of the SR-IR source for FTIR imaging at high sensitivity and spatial resolution compared to that of conventional FTIRM. Specifically, the spatial resolution of SR-IR, down to ca. 3µm vs. ca. 10µm using FTIRM systems allows users to gain important spectral information at the cellular level.

1.3. The role of autoantibodies to collagen in the development of arthritis

Human RA is a chronic inflammatory destructive disease of the joints, in which there is an inflammatory outgrowth of the synovial membrane over the cartilage surface (pannus) with accompanying cartilage destruction and loss⁽²⁾ (**Figure 1.23**). RA is an autoimmune disease, and various autoantibodies can be detected in the serum and synovial fluid of patients. In particular, related to the present thesis, antibodies to CII have been described in serum and synovial fluid of patients with RA^(1, 154). In 1970, Steffen proposed that an autoimmune response to collagen was a cause of RA⁽¹⁵⁵⁾. Rats⁽¹⁵⁶⁾, mice⁽¹⁵⁷⁾ and primates⁽¹⁵⁸⁾ immunized with CII in complete or incomplete Freund's adjuvant all produce a strong antibody response to CII, and develop an inflammatory arthritis termed CIA that shares clinical and histological features with human RA⁽¹⁵⁹⁾.

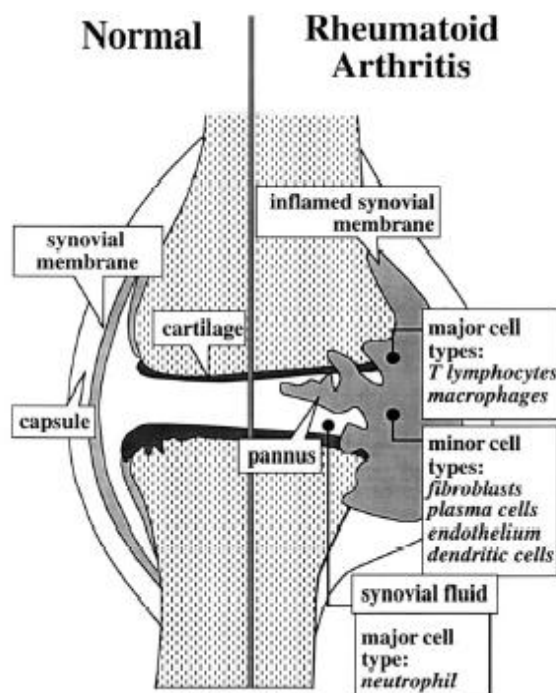


Figure 1.23. Comparison of a normal joint versus an RA afflicted joint. In the RA afflicted joint (right), the acellular synovial fluid is invaded by immune cells, and a destructive pannus migrates into and over the cartilage, where there is an infiltration of T lymphocytes and macrophages into the joint (Figure from Feldmann, *et al.*, 1996⁽³⁾).

1.4. Collagen Induced Arthritis

CIA is the most widely studied model of human RA. CIA is an inflammatory joint disease, characterized by synovial hyperplasia, mononuclear cell infiltration into the synovium and the development of pannus and cartilage and bone destruction within the joint^(157, 160) similar to those seen in human RA. Both T and B cell immunity to CII are required for disease development, and disease development is restricted by Major Histocompatibility Complex (MHC) genes, and only certain strains of mice develop the disease^(161, 162) The details of the pathogenesis and induction CIA have been extensively reviewed⁽¹⁶³⁻¹⁶⁶⁾ and will not be covered in detail in this thesis.

Following immunization of mice, the preferred model, with heterologous CII, the course of CIA is characterized by a severe, acute phase with no further occurrences⁽¹⁶⁷⁾. The first signs of inflammation in the paws may occur at day 9 post immunization, however in the most commonly used mouse strain (DBA/1 Lac J), onset of inflammation typically occurs between 14 and 21 days post immunization⁽¹⁶⁸⁾, the time at which the animals are developing high titres of antibodies to CII. The initial inflammation typically occurs in one or more digits on the paws of the mice, progressing rapidly over several days, often progressing to ankle or wrist joints⁽¹⁶⁸⁾. Within a week of maximal swelling occurring in affected paws the inflammation gradually subsides⁽¹⁶⁸⁾.

Although the arthritis induced with heterologous CII is usually monophasic, immunization with homologous CII produces an arthritis with a course that is similar to that which occurs in human RA with regular acute inflammatory flare ups including progression of the disease into both affected and previously unaffected joints^(163, 167). The reason for the differences observed in arthritis induced by heterologous CII as opposed to homologous CII is unclear, but arthritis induced using homologous CII closely resembles human RA not only in the similarity of the clinical presentation in affected joints, but also in regard to the appearance of true autoantibodies to CII, as mice immunized with murine CII develop antibodies to

murine CII, whereas in mice immunized with heterologous CII, most anti-CII population may react only with the immunizing CII, and not with murine CII⁽¹⁶⁷⁾.

Furthermore, susceptibility of mice and rats to develop CIA has been linked to the class II molecules of the major histocompatibility complex (MHC) and the immune response to CII is characterized by the production of high levels of circulating antibody specific for both heterologous CII (immunogen) and mouse CII (autoantigen) and the stimulation of collagen specific T-cells⁽¹⁵⁹⁾. The development of arthritis following immunization with either heterologous or homologous CII is restricted to mouse strains with H-2^q, H-2^q related or H-2^r haplotype strain⁽¹⁶³⁾.

Both T and B cells are involved in the pathogenesis of CIA. However the antibody-response is T-cell dependent, as the primary B cell response is only present in H-2^q strains such as DBA/1, SWR and B10G and not in the H-2^p B10P strain, indicating that the B-cell response depends on the activation of MHC-restricted T cells⁽¹⁶⁴⁾. Although T cells are essential for the development of CIA, the disease is not completely mediated by T cells and both B and T cells are required in CIA autoimmunity⁽¹⁶⁸⁾. There is also a close association between the development of both B and T-cells with the onset of polysynovitis seen macroscopically⁽¹⁶⁹⁾. The T cell mediated activation of macrophages and fibroblasts within the joints may be important leading to cartilage destruction in the joints.

B cells are also directly involved in the development of arthritis. Immunization of CIA response DBA/1 mice with rat CII induces the activation of high numbers of autoantibody-producing B cells as early as 9-11 days post immunization, where approximately 20% of all antibody-producing B cells in the lymph node of the DBA/1 mice produce anti-CII reactive antibodies 9 days post immunization⁽¹⁶⁴⁾. The majority of antibody producing B-cells, which are CII reactive, produce IgG reactive with epitopes common to CII and the anti-CII reactive B cells produce antibodies encoded from several different V_H and V_L genes⁽¹⁶⁴⁾. Furthermore, the very strong B-cell response to autologous CII in draining lymph

nodes 9-11 days post immunization with heterologous CII, suggests that the anti-CII B cells have been primed prior to the *in vivo* immunization of CII⁽¹⁶⁴⁾.

The B cell response observed in CIA is targeted towards a series of epitopes on triple helical CII which are also conserved and recognized in RA^(4, 170-172). The antibody response to CII is dependent on the triple-helical structure of CII, as denatured CII is non-arthritogenic and induces a weak antibody response⁽¹⁷³⁾. The major epitopes on triple helical CII have been identified within peptides derived from cyanogen bromide (CB) cleavage of the triple helix and include C1, J1, U1 which share a common arginine-glycine-hydrophobic amino acid motif^(6, 172, 174, 175). The major immunodominant epitope is C1 and is located within CB11, a region which also contains a major T cell epitope^(173, 174, 176, 177). A more detailed description of the major epitopes and monoclonal antibodies to CII will be discussed in section 1.6.

Studies on autoimmunity to CII in CIA have been important in developing an understanding of the aetiology and pathogenic mechanism of RA⁽¹⁷⁸⁾ and for testing new therapies⁽¹⁶⁰⁾. However the process of the development of arthritis following injection of CII involves both inductive processes involved in the development of an immune response to CII, and effector processes that lead to the development of the arthritis, particularly the role of antibodies to CII in the development of arthritis. The role of antibodies can be studied in more detail in collagen antibody-induced arthritis (CAIA).

1.5. Collagen Antibody-Induced Arthritis

Certain mAbs to CII, produced from mice with CIA, can on passive transfer, induce arthritis in naïve mice^(4-6, 156) and this model is termed CAIA. CAIA may be transferred to naïve mice using either serum from arthritic mice with either a single CII-specific mAb or a combination of CII-specific mAbs^(6, 156, 179). A similar arthritis has also been induced in mice by using antibodies to CII from patients with RA⁽¹⁸⁰⁾.

The particular advantage of studying CAIA as opposed to CIA is that there is no requirement for T helper cells in the induction of the disease. The disease resembles human RA including bone erosions, influx of neutrophils and deposition of IgG and complement components on articular cartilage⁽¹⁸¹⁾. The transfer of a combination of mAbs to CII induces a severe arthritis with a rapid onset which damages the architecture of cartilage and bone, which is shown in **Figure 1.24**⁽¹⁸¹⁾.

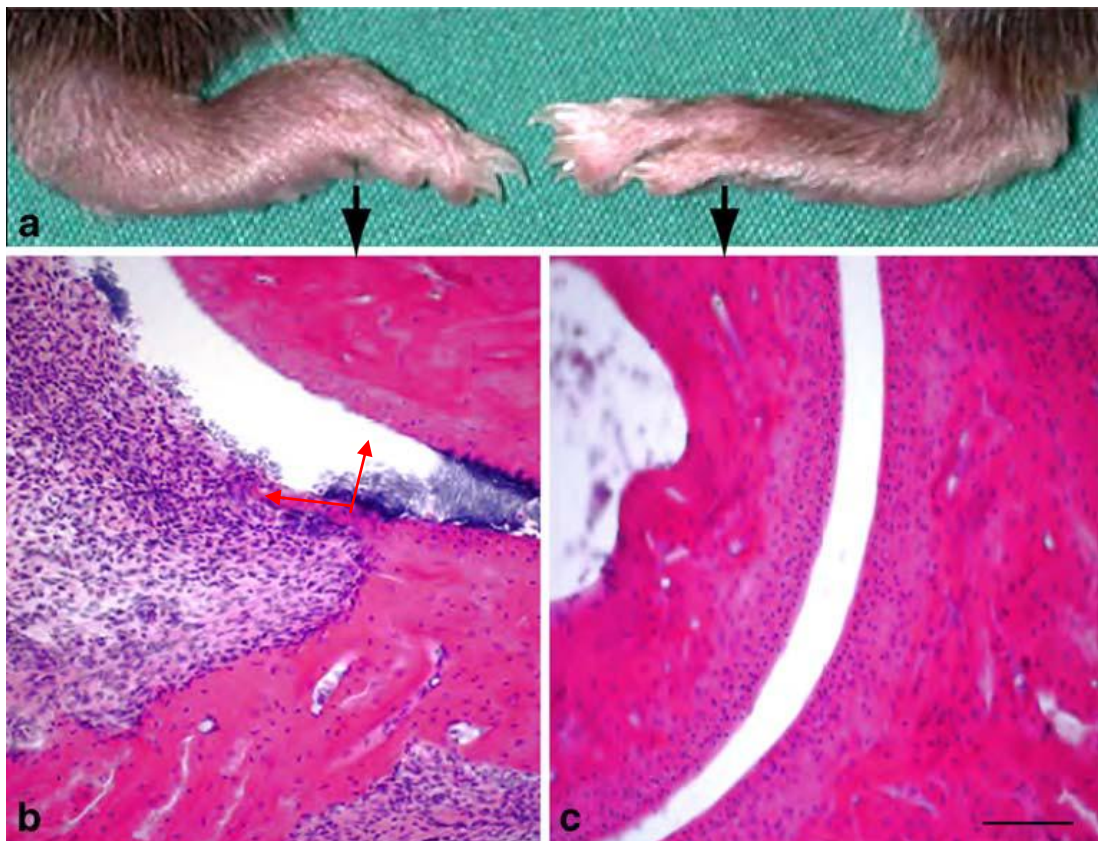


Figure 1.24. CAIA induced in naïve mice. **A.** representative image of macroscopic arthritis on day 10 following transfer of two mAbs to CII, showing inflammation in an arthritic paw on the left and a normal paw on the right. **B.** Histology of CAIA on day 17 following antibody transfer illustrating an infiltration of inflammatory cells and cartilage damage (red arrows). **C.** Histology of a normal paw showing an even cartilage surface and no inflammatory cells. Both **B** and **C** are haematoxylin and Eosin stained sections with original magnification of x20 and the scale bar represents 40 μm . (Figure from Nandakumar *et al.*, 2010⁽¹⁸¹⁾).

Although CAIA shares several characteristics with CIA, CAIA has a much more rapid onset (24-48 hours) where the use of lipopolysaccharide (LPS) enhances the incidence and severity of the CAIA which usually subsides completely after a month⁽⁵⁾. The increase in severity and incidence of CAIA in the presence of LPS may occur by decreasing the threshold required for induction of arthritis and bypassing epitope specificity, increasing pro-inflammatory mediators, and activation of complement components via the toll like receptor 4 signalling⁽⁵⁾. It is also possible to induce relapsing arthritis in mice that have previously developed chronic CIA, using single mAbs to CII⁽¹⁸²⁾. This highlights the role of antibodies in relapses during the chronic phase of arthritis⁽⁵⁾.

A detailed study of factors affecting the development of CAIA was carried out by Nandakumar and colleagues in different strains of mice⁽⁶⁾. They showed that CAIA may be initiated using mAb in most mouse strains, including strains in which CIA could not be induced by direct injection. Susceptibility of mice to CAIA is independent of MHC and severe combined immunodeficient (SCID) mice⁽⁵⁾. CAIA allows the inflammatory phase of arthritis to be studied.

The contribution of CII antibodies to CAIA is initiated by the direct binding of the antibodies to CII and involves immune complex formation, complement deposition and activation and binding of Fc receptors (FcRs)⁽⁵⁾. Both Fc γ receptor and complement are critical for induction of disease and interleukin-1 (IL-1) and tumour necrosis factor (TNF)- α are critical mediators in the inflammatory process of arthritis⁽⁵⁾. Neutralization of these effector cytokines (TNF- α and IL-1) have been used successfully in treatment of RA^(183, 184). Complement activation and Fc γ R engagement are required for the onset of the clinical disease⁽⁵⁾, and an absence of activating Fc γ receptors makes mice resistant to CAIA, whereas a deficiency in the inhibitory Fc γ RIIb exacerbates the antibody induced disease^(185, 186). Neutrophils macrophages and mast cells are all classed as effector cells of the innate immune system, which induce inflammation, cause cartilage damage and perpetuate the

ongoing immune responses by secreting cytokines and proteases in the disease course of CAIA⁽⁵⁾.

1.6. Epitope specificity of autoantibodies to CII in CAIA

The major arthritogenic B cell epitopes on CII have been identified and mapped to specific cyanogens bromide (CB) fragments. These include the C1 epitope (aa 359-369) of the CB11 fragment with the epitope sequence ARGLT, J1 (aa 551-564) of the CB10 fragment with the epitope sequence GERGAAGIAGPK, U1 (aa 494-504) of the CB8 fragment with the epitope sequence GLVGPRGERGF, D3 (aa 687-698) of the CB10 fragment with the epitope sequence RGAQGPPGATGF⁽¹⁸⁷⁾ and the F4 epitope (aa 926-936) of the CB9 fragment with the epitope sequence RGLKGHRGFT^(170, 172-174, 187). The C1 epitope is recognized by the mAb CIICI, UL1 recognizes the U1 epitope, CIIC2 recognizes the D3 epitope and CIIF4 recognizes the F4 epitope. M2139, CIICI, CIIC2 and UL1 are designated arthritogenic mAbs to CII, whereas CIIF4 is termed a non-arthritogenic anti-CII mAb as it fails to induce arthritis on passive transfer to mice. The binding sites of the epitopes of the mAbs described is shown in **Figure 1.25**.

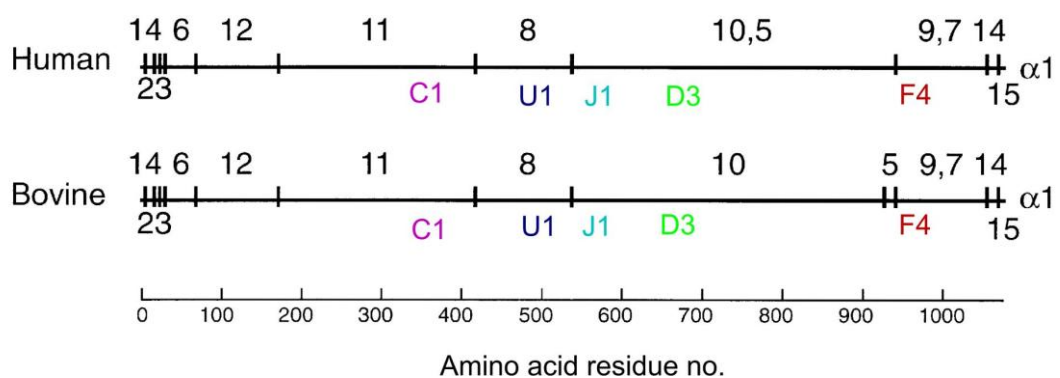


Fig 1.25. Identification of CB peptides of CII, showing the location of the methionine residues (vertical bars) in both human and bovine CII and the resultant CB peptides (numbered) derived by methionine cleavage. The epitopes of the mAbs described are indicated on each of the human and bovine collagen molecules.

The U1 epitope has been found to co-localise with an $\alpha 1/\beta 1$ integrin binding site and is recognized by high antibody titres in serum from patients with a late-stage chronic arthritis^(172, 188). The J1 epitope is within the region on CII which is involved in the binding between type IX collagen (CIX) and CII⁽¹⁷⁴⁾. The C1 epitope which is close to the binding site of chondroadherin is the major epitope in the immune response to CII and dominates the response to CIA in mice and rats^(9, 187). The lysine residue at amino acid position 930 on the CII molecule is in close proximity to the F4 epitope (932-963) which is one of the two hydroxylysines in CII triple helices which is involved in intermolecular cross-linking^(174, 189). It could, therefore be postulated that the mAb CIIF4 does not react with non-cross linked protein but it has been shown previously to bind *in vivo*⁽¹⁷⁰⁾.

A combination of the arthritogenic mAbs M2139 and CIICI has been shown to induce a clinically severe arthritis in mice *in vivo*^(6, 186, 190-192). Burkhardt and colleagues⁽¹⁷⁰⁾ investigated the effects that combinations of mAbs have on the development of experimental CIA, and found that with the combination of M2139 and CIICI, there was an increase in the severity of arthritis. However when CIIF4 was added to this cocktail, inhibition of mAb-induced arthritis was observed, suggesting that CIIF4 may elicit a protective role in CIA. A depiction of the effects of the combination of the two arthritogenic mAbs and the addition of the non-arthritogenic mAb CIIF4 is shown in **Figure 1.26**. This “protective” effect of CIIF4 may be due to the fact that the binding region of CIIF4 to the CII molecule is shared with the stromelysin; a metalloproteinase, and in binding to the stromelysin binding site, the antibody may subsequently inhibit the binding and degradative activity of this metalloproteinase⁽¹⁷⁰⁾. These studies illustrate an important aspect in the pathogenesis of RA whereby it is possible, that the binding of the monoclonal antibodies may block important interactions between chondrocytes and CII, as well as other ECM components, thereby inducing changes in the regulation of cartilage turnover and initiating a destructive autoimmune response.

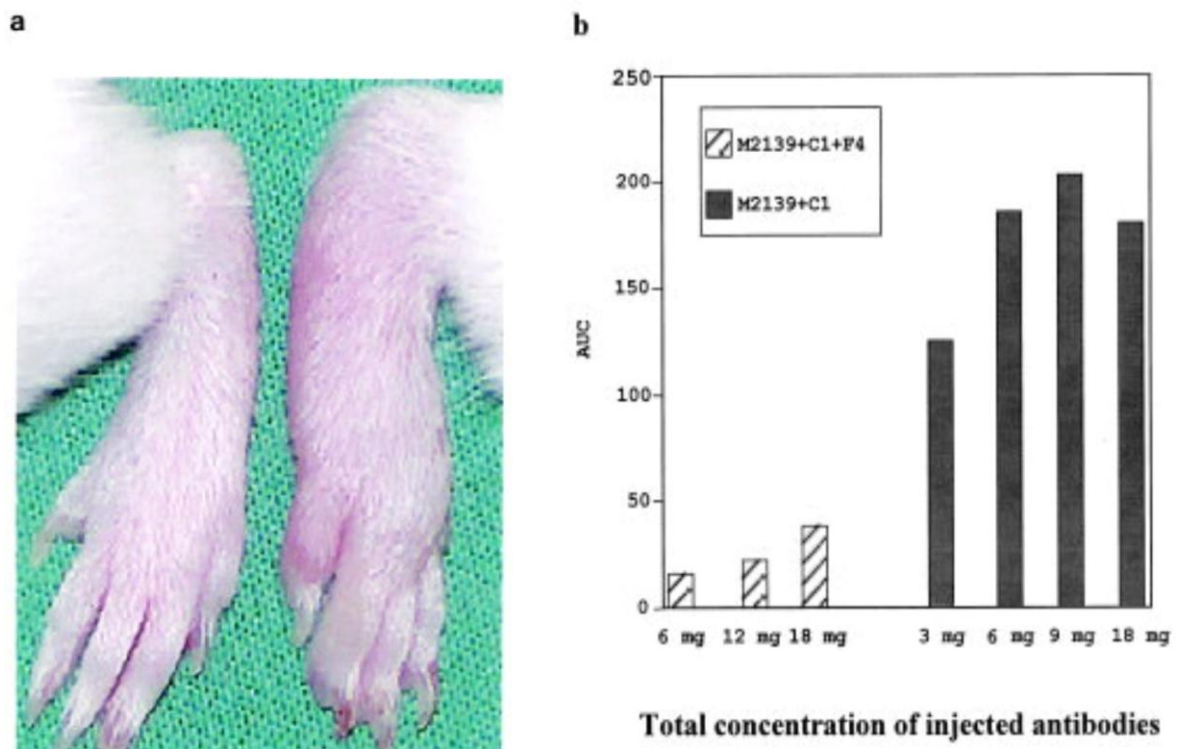


Fig 1.26. Effects of combinations of mAbs in mice with CAIA. **A.** A paw from a control mouse injected with phosphate-buffered saline (left) compared with a paw from a mouse which has been injected with the arthritogenic mAbs M2139 and CIIC1 (right) which has become red and inflamed compared with the normal. **B** Chart illustrating the increasing severity of arthritis represented as area under the arthritis curve (AUC) with M2139 and CIIC1 whereas the addition of the non-arthritogenic mAb CIIF4 appears to have a protective effect, decreasing arthritis severity (Figure from Burkhardt *et al.*, 2002⁽¹⁷⁰⁾).

1.7. A comparison of human RA and CAIA

As noted there are important similarities between RA and CIA and CAIA, and CII-specific autoimmunity has been suggested as a possible initiator in the pathogenesis of RA⁽¹⁵⁵⁾. As in CIA, there is a strong Class II MHC association in human RA, particularly with alleles of the Human Leukocyte Antigen (HLA) DR4⁽¹⁾. Moreover CII autoantibodies and CII-specific T cells and immune complexes are detectable in RA.

Evidence for autoantibodies to CII in RA is of particular note. Serum antibodies to CII are present in up to 70% of cases of early RA⁽¹⁹³⁻¹⁹⁵⁾, however there is a decline in the frequency and level of these anti-CII antibodies in patients with erosive disease⁽¹⁾, possibly due to the sequestering of the anti-CII antibodies within immune complexes that are deposited on the cartilage surface which becomes progressively more eroded as the disease progresses, exposing more CII for further attack⁽¹⁸¹⁾. The presence of anti-CII antibodies may precede the appearance of rheumatoid factor or radiological changes^(194, 196).

Importantly, antibodies of the same specificity to the same conformational epitopes of CII, which are recognized by autoantibodies in rodents are also identified in synovium, sera and cartilage of patients with RA^(170, 188, 197). Interestingly, whereas antibodies to the C1, J1 and U1 epitopes are positively associated with the development of RA antibodies to the F4 epitope, which protect against the development of CAIA following passive injection of other arthritogenic mAbs, occur more frequently in osteoarthritis than in RA, and are negatively associated with RA⁽¹⁷⁰⁾.

1.8. *In vitro* studies on the effects of mAbs to CII

There is widespread acceptance that the pathogenic effects of antibodies to CII are non-specific, and primarily related to the binding of immune complexes, complement activation, and cellular activation leading to inflammation, and that cartilage damage results from the degradative effects of enzymes produced by inflammatory cells⁽¹⁸¹⁾. However it is notable that various arthritogenic mAbs react with particular regions of the collagen fibril that may be involved in molecular interactions important for functional stability of the cartilage. Moreover the observation that not all mAbs to CII are arthritogenic, and that one, CIIF4, is non-arthritogenic although it is of similar affinity, and similar IgG subclass to CIIC1 that is arthritogenic, raised the possibility that some antibodies to CII could damage cartilage directly. To test this hypothesis, the mAbs to CII shown in **Table 5** have also been tested for their effects on newly synthesised cartilage by chondrocytes *in vitro*. Moreover the arthritogenic mAbs caused inhibition of collagen fibrillogenesis *in vitro*⁽⁷⁾.

Studies using anti-CII mAbs on synthesis of matrix *in vitro* have shown that various of the above mentioned mAbs, used individually in high density cultures of bovine chondrocytes are pathogenic to chondrocytes, causing impaired cartilage formation, and disorganisation of CII fibrils in the ECM in the absence of inflammatory mediators^(8, 9, 187). The effects of the mAbs differed according to the specificity of the mAb. Thus, the addition of the arthritogenic mAb CIIC1 to chondrocyte cultures caused impaired matrix synthesis, with thin and uneven collagen fibrils, detectable by electron microscopy (**Figure 1.27**)⁽⁸⁾ but little change in chondrocyte morphology. By contrast, in similar experiments mAb M2139 caused major morphological changes to the chondrocytes, and the collagen fibrils were thickened (**Fig 1.27**). By contrast mAb CIIF4 had no apparent effect on chondrocyte morphology or matrix synthesis.

These anti-CII mAbs also have destructive effects on pre-formed cartilage, also in the absence of any inflammatory mediators, causing loss of proteoglycans

from the cartilage surface where the mAb directly penetrates and a progressive denaturation and loss of CII from the surface⁽¹¹⁾. Studies investigating the effects of two of the arthritogenic mAbs, CIICI and M2139 and the non-arthritogenic mAbs CIIF4 on cartilage explants. They showed that each of the mAbs penetrated the cartilage matrix to varying degrees during culture and remained bound to the tissue, shown by immunofluorescence (**Figure 1.28**). Light microscopy and toluidine blue staining (**Figure 1.29**) revealed that in the presence of the non-arthritogenic mAb CIIF4, the cartilage remained healthy for up to 21 days, however the two arthritogenic mAbs, caused profound changes in the structure of the cartilage progressively over increasing time in culture. Specifically, M2139 caused loss of toluidine blue staining from the surface of the cartilage representing loss of proteoglycans and the development of a layer of cells on the surface of the explant after 14 days in culture⁽¹¹⁾. A summary of the effects of mAbs to CII particularly *in vitro* and specific details regarding the background on each of the antibodies is outlined in **Table 5**.

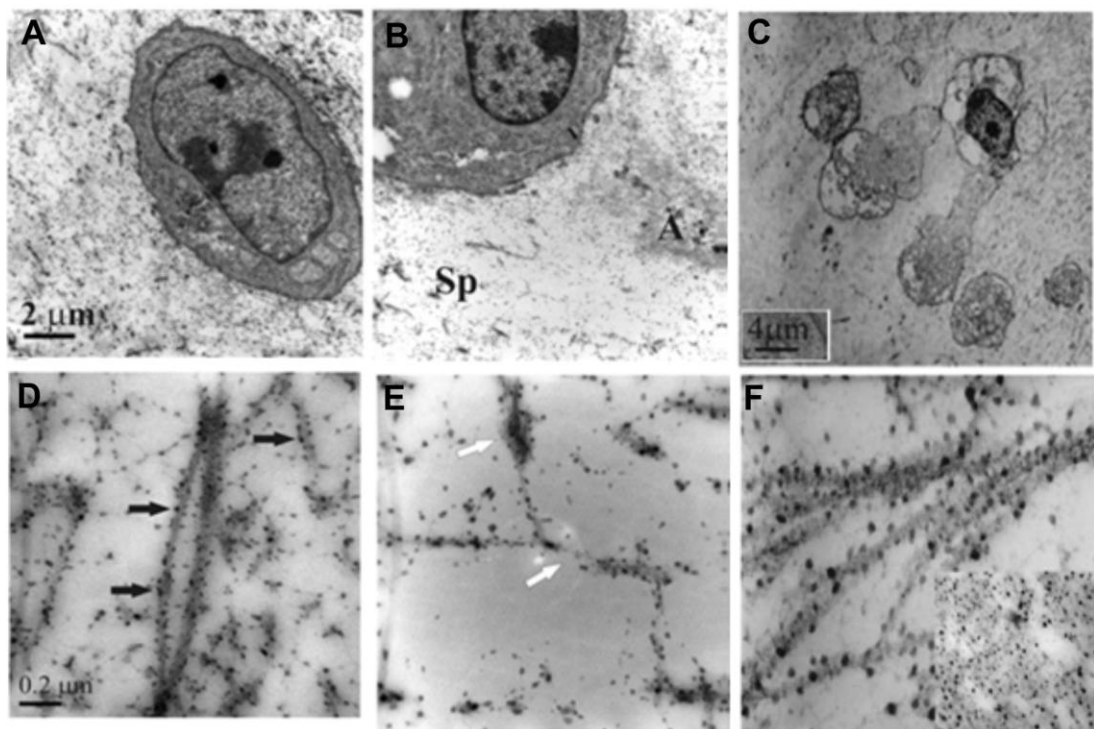


Figure 1.27. Electron micrographs of chondrocytes and ECM in either control cultures (**A**, **D**), those cultured with the arthritogenic mAb CIIC1 (**B**, **E**) or the arthritogenic mAb M2139 (**C**, **F**). The chondrocytes have a rounded appearance and the perichondrocyte matrix is even and regular in control cultures (**A**), however with the addition of CIIC1 (**B**) the perichondrocyte matrix is uneven and sparse (sp) with prominent areas of amorphous material. The addition of M2139 caused chondrocytes to become pleomorphic (**C**). (**D**) shows uniform collagen fibrils with ordered proteoglycans (black arrows) and (**E**) disordered collagen fibrils of variable thickness shown by the white arrows and unevenly distributed proteoglycans appearing as black dots. (**F**) shows a disordered network of thick fibrils between chondrocytes and the inset shows complete disorganisation of the matrix which was seen at the top and bottom surfaces. (Figure adapted from Amirahmadi *et al.*, 2004, 2005^(8,9))

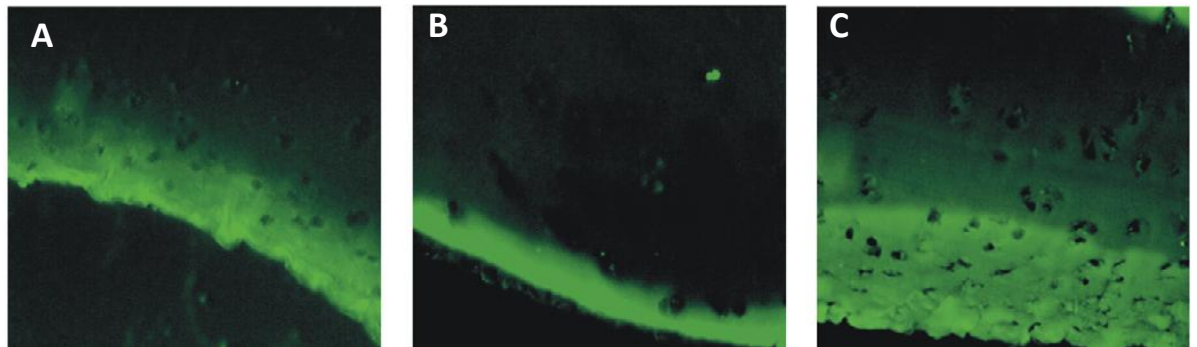


Figure 1.28. Immunofluorescence illustrating penetration of the mAbs CIIF4, CIIC1 and M2139. The green areas of fluorescence indicate antibody binding (Figure from Crombie *et al.*, 2005⁽¹¹⁾).

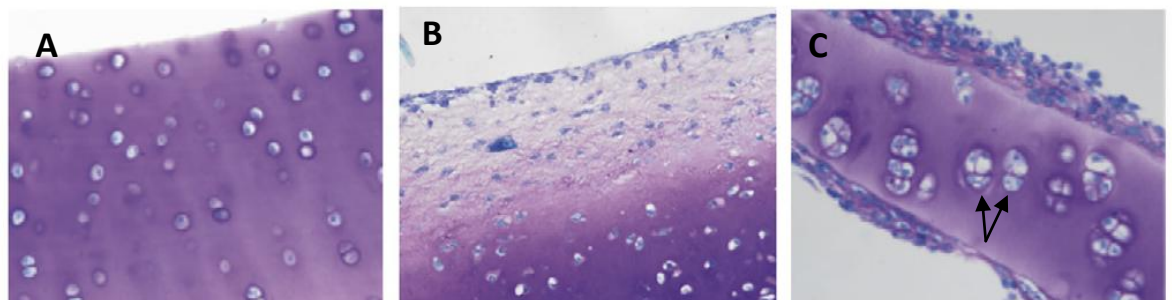


Figure 1.29. Toluidine blue stained sections of cartilage cultured with CIIF4 (**A**) remains healthy and displays an evenly stained cartilage matrix with typical rounded chondrocytes even after 21 days in culture. Cartilage incubated with M2139 for 7 days (**B**) shows abnormal matrix morphology and a loss of proteoglycans indicated by the loss in toluidine blue staining at the cartilage surface and (**C**) cartilage cultured for 14 days with M2139 shows the development of a cellular layer at the cartilage surface and hypertrophic chondrocytes indicated by the arrow. (Figure from Crombie *et al.*, 2005⁽¹¹⁾).

Table 5. Effects of mAbs to CII both *in vivo* and *in vitro* (Table adapted from Amirahmadi *et al.*, 2005⁽⁹⁾ and Rowley *et al.*, 2008^(1, 181)).

Properties	mAb			
	CIIC1	M2139	UL-1	CIIF4
IgG subclass	IgG2a	IgG2b	IgG2b	IgG2a
Epitope	C1 ¹	J1	U1	F4
Amino acids	359-363	551-564	494-504	926-936
Binding site	Chondroadherin	CIX, Integrin	Integrin	Stromelysin
Binds cartilage <i>in vivo</i>	Yes	Yes	Yes	Yes
Arthritogenic <i>in vivo</i>	Yes	Yes	Yes	No/Protective
Antibodies present in human RA	Yes, RA>OA*	Yes RA	Yes, severe RA	Yes, OA>RA
<u>Effects in vitro on chondrocyte cultures</u>				
Chondrocyte morphology	Normal	Pleomorphic	Vacuolated	Normal
Collagen fibrils	Thin	Thick, aggregated	Normal	Normal
Matrix synthesis	Increased	Normal	Normal	Normal
<u>Effects in vitro on explant cultures</u>				
Proteoglycan loss at cartilage surface	Yes	Yes	Yes	No
Collagen denaturation	Yes	Yes	Yes	No
Collagen loss	Yes	Yes	Yes	No

* OA is Osteoarthritis

Previously published results on the effects of mAbs to CII on cartilage *in vitro* clearly demonstrate that these anti-CII mAbs may be important in initiating the pathogenic events that occur in CAIA. Moreover, as antibodies of similar epitope specificity also occur in human RA, they may also play a role in the human disease. The studies highlight the requirement for further analysis into the effects of these mAbs and the possible mechanisms of both degradation caused by the arthritogenic mAbs and the protective effect of the mAb ClF4.

AIMS OF PhD

CII is the major protein in cartilage. CIA, induced in animals immunised with CII, is an experimental model of human RA. The autoimmune response that develops in CIA induces the formation of antibodies to CII that provoke an acute destructive arthritis on transfer to naïve mice (CAIA). Although CAIA can be transferred by some single mAbs and by combinations of mAbs to CII, not all are arthritogenic and arthritogenicity appears to be epitope related.

The epitope specificity of arthritogenic mAbs has been mapped to regions of the CII molecule that are involved in structural interactions important to maintain cartilage stability^(6, 169, 171, 172). Several of these arthritogenic mAbs have been shown to affect collagen fibril formation, chondrocyte morphology and the synthesis of new cartilage matrix *in vitro*⁽⁷⁻⁹⁾. Preliminary data has also indicated that some individual mAbs also caused damage to pre-existing cartilage *in vitro*⁽¹¹⁾.

The aim of the present study was to use FTIRM and standard histological techniques to examine the direct effects of combinations of mAbs to CII on pre-existing cartilage in the absence of inflammation *in vitro* in bovine cartilage explant cultures, and *in vivo* in mice injected with arthritogenic combinations of mAbs that had not developed inflammation.

To test the effects of combinations of mAbs to CII on pre-existing cartilage *in vitro* the morphology and chemical nature of the cartilage was examined in the following experiments:

1. A standard combination of two mAbs M2139 and CIIC1 that are used to induce CAIA *in vivo* was examined for their effects on bovine cartilage explants.

2. The effect of the addition of the non-arthritisogenic mAb ClIF4 to this combination of arthritisogenic mAbs was tested, noting that *in vivo* ClIF4 decreases the incidence and severity of CAIA induced by M2139 and ClIC1.
3. The arthritisogenic and/or the protective effects of the mAbs mediated by the mAbs alone or by cellular mechanisms were determined by performing experiments on cartilage containing viable or non-viable chondrocytes.
4. The role of MMPs in mAb mediated cartilage damage and protection was examined by the addition of the MMP inhibitor GM6001 to cultures containing the arthritisogenic mAbs.

To test the effects of combinations of mAbs to CII on pre-existing cartilage *in vivo* the morphology and chemical nature of the cartilage was examined. Two different strains of mice were used, B10.Q mice that usually develop CAIA only after an additional injection of lipopolysaccharide and B10.Q C5 δ mice that lack complement factor C5 and do not develop CAIA. Mice were injected with the standard mixture of two mAbs, ClIC1 and M2139 or a more arthritisogenic combination of four mAbs, M2139, ClIC1, UL-1 and ClIC2 and 3 days after injection, paws were compared using extensive histological examination and FTIRM to examine the chemical nature of changes to the cartilage.

CHAPTER TWO

THE EFFECTS OF MONOCLONAL ANTIBODIES TO CII ON CARTILAGE *IN VITRO*

2.1. Preface

This chapter describes work performed to determine whether the antibodies to CII that can be used to transfer CAIA in mice can directly damage cartilage *in vitro*. Bovine cartilage explants were cultured for periods of up to 2 weeks in the presence of mAbs, and morphological changes which were identified by histology were correlated with chemical changes observed by FTIRM using a Stingray Digilab FTS 7000 series spectrophotometer coupled to a UMA 600 microscope equipped with a 64 X 64 focal plane array detector.

Three particular mAbs were tested, M2139, CIIC1 and the non-arthritis-inducing mAb CIIF4. These mAbs each react with three different, well-defined conformational epitopes on the CII molecule^(168, 170-172, 185), which are depicted in figure 1.25 and all react strongly with bovine CII by ELISA⁽¹⁹⁰⁾. These mAbs have been tested *in vivo* for their ability to induce arthritis. M2139 and CIIC1 are weakly arthritis-inducing alone, although arthritis-inducing is enhanced by the injection of LPS after transfer of the mAb^(6, 185). However the mAbs caused a more severe arthritis in combination and the mixture of M2139 and CIIC1 have been used in several studies to induce CAIA in naïve mice *in vivo*^(6, 184, 187-189). By contrast, the mAb CIIF4 does not induce arthritis in mice *in vivo*, and the addition of CIIF4 to the mixture of M2139 and CIIC1 has been shown to reduce and even prevent the development of CAIA⁽¹⁶⁸⁾.

The three mAbs have been tested for their effects on the synthesis of new matrix in high density bovine chondrocyte cultures *in vitro* and they each have varying effects. The arthritis-inducing mAb M2139 caused major morphological changes to the chondrocytes and uneven matrix formation with thickened collagen fibrils^(8, 9). CIIC1 caused decreased matrix synthesis, with thin and uneven collagen fibrils but had no effect on chondrocyte morphology^(8, 9). The non-arthritis-inducing mAb CIIF4 had no apparent effect on chondrocyte cultures^(8, 9). The two

arthritogenic mAbs M2139 and CIIC1 but not CIIF4 have also been shown to inhibit collagen fibrillogenesis *in vitro*⁽⁷⁾.

The effects of the arthritogenic mAbs M2139 and CIIC1 on pre-existing cartilage explants *in vitro* have also been tested⁽¹¹⁾. Unlike chondrocyte cultures where the mAbs are present throughout the culture before the production of new cartilage matrix, in cartilage explant cultures the mAbs penetrate the cartilage poorly⁽¹⁹⁵⁾ and it is necessary to distinguish changes in the immediate area of mAb penetration from changes beyond the region of penetration. In this study, FTIRM was established as a suitable technique for examination of cartilage, particularly for identification of changes to the cartilage in the areas of direct mAb penetration. FTIRM for examination of cartilage was validated using purified cartilage components and results from the exterior of the cartilage based on mAb penetration and proteoglycan loss measured by toluidine blue were compared with the FTIRM spectra from the interior of the cartilage where mAb did not penetrate.

The specific effects of the mAbs were examined using FTIRM to identify chemical changes to the major components of the cartilage matrix, CII and proteoglycans. Both of the arthritogenic mAbs caused loss of proteoglycans particularly at the cartilage surface where direct mAb penetration occurred. In cultures containing M2139, an abnormal layer of chondrocytes with an increased proportion of empty chondrons developed on the cartilage surface. FTIRM showed denaturation and loss of CII at the cartilage surface in the presence of either M2139 or CIIC1. The non-arthritogenic mAb CIIF4 had no effect⁽¹¹⁾. Notably, the use of FTIRM also identified that the mAb-mediated damaging effects on cartilage matrix were increased with f(ab)₂ mAbs alone, causing deeper mAb penetration, loss of CII and complete loss of proteoglycans, excluding the possibility that the mAb-mediated cartilage damage is due to Fc binding.

In this chapter I describe work carried out to further explore the nature of the effects. Specifically, I examined the effects of combinations of the two

arthritogenic mAbs to CII, M2139 and CIIC1 on pre-existing cartilage *in vitro* compared with normal cartilage held in culture. This combination of mAbs has been used in passive transfer experiments to understand the factors affecting the effector phase of the immune response to CII leading to the development of arthritis. The experiments described above using single mAbs were performed at a concentration of 50 µg/ml. My preliminary experiments (refer to appendix) indicated that in the range of 25 µg/ml to 100 µg/ml, increasing concentrations of the mAbs caused an increase in cartilage damage. In this study, 25 µg/ml of each of the arthritogenic mAbs M2139 and CIIC1 were chosen to give a final concentration of 50 µg/ml corresponding to the 50 µg/ml of a single mAb used in previous experiments.

Furthermore, the effect of the non-arthritogenic mAb CIIF4 individually and in combination with the two arthritogenic mAbs was examined on pre-existing cartilage *in vitro*. The effect of CIIF4 in culture alone was compared with normal cartilage to first confirm that this mAb did not cause damage alone. The effect of the combination of M2139 and CIIC1 was then compared with the effect of M2139, CIIC1 and CIIF4 in cartilage explants. Cartilage changes observed in the presence of the two arthritogenic mAbs with and without the addition of CIIF4 were then compared in both cartilage containing living chondrocytes and cartilage which had been freeze-thawed to kill the chondrocytes, to ascertain whether the mAbs are able to have a direct effect on cartilage damage or whether the damage is mediated by living chondrocytes. Furthermore, the role of MMPs both latent in the cartilage matrix and produced by chondrocytes in mAb mediated cartilage damage was investigated to identify whether inhibition of MMPs using a broad spectrum MMP inhibitor GM6001 protects the cartilage against mAb mediated damage and whether this inhibition mimics the protective effect of CIIF4.

The mAbs were provided by Prof. Rikard Holmdahl and A/Prof. Kutty Selva Nandakumar from the Karolinska Institute, Stockholm, Sweden. The mAbs were derived from hybridomas developed from CII immunised mice⁽⁴⁾. The mAbs were

prepared and purified in Sweden. I obtained them as freeze-dried components and reconstituted them in sterile distilled water and filter sterilised using a 0.22 μm syringe filter.

The results are presented in the form of a published manuscript describing the use of the mixture of arthritogenic mAbs, M2139 and ClIC1 with and without the addition of the non-arthritogenic mAb ClIF4.

Specific Antibody Protection of the Extracellular Cartilage Matrix Against Collagen Antibody–Induced Damage

Allyson M. Croxford,¹ Duncan Crombie,¹ Donald McNaughton,¹ Rikard Holmdahl,² Kutty Selva Nandakumar,² and Merrill J. Rowley¹

Objective. The type II collagen (CII)–specific monoclonal antibodies (mAb) M2139 and CIIC1 induce arthritis in vivo and degrade bovine cartilage explants in vitro, whereas mAb CIIF4 is nonarthritogenic and prevents arthritis development when given in combination with M2139 and CIIC1. To determine the nature of the protective capacity of CIIF4 antibody, we examined the effects of adding CIIF4 to cartilage explants cultured in vitro with M2139 and CIIC1.

Methods. Bovine cartilage explants were cultured in the presence of M2139 and CIIC1, with or without CIIF4. Histologic changes were examined, and chemical changes to collagens and proteoglycans were assessed by Fourier transform infrared microspectroscopy (FT-IRM). Fresh cartilage and cartilage that had been freeze-thawed to kill chondrocytes cultured with or without the addition of GM6001, a broad-spectrum inhibitor of matrix metalloproteinases (MMPs), were compared using FTIRM analysis.

Results. M2139 and CIIC1 caused progressive degradation of the cartilage surface and loss of CII, even

in the absence of viable chondrocytes. CIIF4 did not cause cartilage damage, and when given with the arthritogenic mAb, it prevented their damage and permitted matrix regeneration, a process that required viable chondrocytes. Inhibition of MMP activity reduced cartilage damage but did not mimic the effects of CIIF4.

Conclusion. CII-reactive antibodies can cause cartilage damage or can be protective in vivo and in vitro, depending on their epitope specificity. Since CII antibodies of similar specificity also occur in rheumatoid arthritis in humans, more detailed studies should unravel the regulatory mechanisms operating at the effector level of arthritis pathogenesis.

Rheumatoid arthritis (RA) is a chronic autoimmune inflammatory disease that affects multiple joints, leading to articular damage and bone destruction (1). There is increasing evidence that B cells and secreted antibodies may play an important role in RA, and depleting B cells by use of monoclonal antibodies (mAb) to CD20 (rituximab) ameliorates RA. Since autoantibody levels are not completely depleted, even in RA patients undergoing B cell depletion therapy with rituximab (2), understanding the regulatory mechanisms at the effector level becomes all the more important in designing better treatments for RA patients.

An autoimmune response to native type II collagen (CII) develops in some patients, with IgG antibodies to CII demonstrable in the blood, cartilage, and synovium (3). In collagen-induced arthritis (CIA), which is induced by immunization of animals with CII (4,5), there is destruction of the articular cartilage matrix as occurs in RA in humans, with accompanying T cell and B cell immune responses to CII that are seen as requisite for disease initiation and development (6). Certain anti-CII mAb produced from mice susceptible to CIA can, on passive transfer to naive mice, cause an acute arthritis known as collagen antibody–

Supported by the National Health and Medical Research Council of Australia, the Barbara Cameron Memorial Grant, Arthritis Australia (project grant), the Swedish Rheumatism Association, the Swedish Research Council, the Swedish Foundation for Strategic Research, the European Union Seventh Framework Programme (project Masterswitch; HEALTH-F2-2008-223404), the Monash University Centre for Biospectroscopy, and the Australian Synchrotron, which allowed us free access to the infrared microspectroscopy beamline for part of this study.

¹Allyson M. Croxford, BSc (Hons), Duncan Crombie, BSc (Hons), Donald McNaughton, PhD, Merrill J. Rowley, PhD: Monash University, Clayton, Victoria, Australia; ²Rikard Holmdahl, MD, PhD, Kutty Selva Nandakumar, PhD, DrMedSci: Karolinska Institute, Stockholm, Sweden.

Address correspondence and reprint requests to Merrill J. Rowley, PhD, Department of Biochemistry and Molecular Biology, Monash University, Wellington Road, Clayton, Victoria 3800, Australia. E-mail: Merrill.Rowley@monash.edu.

Submitted for publication March 8, 2010; accepted in revised form July 15, 2010.

induced arthritis (CAIA) (7–10). Since CAIA occurs independently of the direct activity of B cells and T cells, it allows for the study of effector processes without consideration of events in the inductive phase (8).

The articular inflammation that characterizes the effector stage is customarily attributed to the formation and deposition of immune complexes and the activation of complement and Fc receptors (FcR) (11). Interestingly, cleavage of arthritogenic mAb at the hinge region *in vivo* (12) or selective removal of carbohydrate moieties in the C_{H2} domain *in vitro* (13) were shown to completely abrogate the development of antibody-mediated arthritis. Not all CII-specific antibodies are equally arthritogenic, however. CIIF4 mAb is inert after passive transfer and, indeed, is even protective against articular damage *in vivo* when transferred together with a combination of the normally potent arthritogenic mAb M2139 and CIIC1 (14), but the mechanism of this protection has not yet been identified.

Using *in vitro* systems based on cartilage explant cultures, we have previously shown that mAb M2139 and CIIC1, which are arthritogenic *in vivo*, adversely affect cartilage matrix integrity, whereas the nonarthritogenic mAb CIIF4 has no effect (15). In the present study, we extended these observations to show that *in vitro*, CIIF4 is counterdestructive/protective against the degradative effects of these arthritogenic mAb when used in combination. Notably, in the culture system we used, cartilage damage by antibody occurs independently of immune cells or their small-molecule mediators. Our enquiries were directed toward the mechanism(s) whereby the physical interaction of antibody with a collagen epitope is transduced to matrix degradation, and how mAb CIIF4 could interfere with such processes. We addressed these questions by assessing whether there was a requirement for living chondrocytes in the cultures for these effects of the CIIF4 mAb and whether attachment of CIIF4 to its epitope site might sterically interfere with the binding of matrix metalloproteinase 3 (MMP-3; stromelysin 1) at its catalytic site on CII.

MATERIALS AND METHODS

Monoclonal antibodies. The mAb we used were derived from hybridomas developed from CII-immunized mice, as described previously (10). All of the mAb were affinity purified from culture supernatants using γ -bind plus columns. M2139 and CIIC1 are arthritogenic mAb that bind to separate well-defined conformational epitopes of native CII: the J1 epitope (MPGERGAAGIAGPK; amino acids [aa] 551–564) and the C1 epitope (ARGLTGRPGDA; aa 359–369). CIIF4 is

a nonarthritogenic mAb that binds to the conformational F4 epitope (ERGLKGHRGFT; aa 926–936) (16).

Analysis of the *in vitro* effects of monoclonal antibodies with the use of bovine cartilage explants. Articular cartilage samples extracted from adult bovine metacarpophalangeal joints and cartilage shavings (5 × 5 × 1 mm) were cultured for up to 14 days in Dulbecco's modified Eagle's medium plus 20% (v/v) fetal calf serum and 25 μ g/ml ascorbic acid, with the appropriate concentrations (25 μ g/ml, 50 μ g/ml, or 100 μ g/ml) of mAb or in medium alone (15). Medium was changed every 2 days, and fresh ascorbic acid and mAb were added at each change. Cartilage samples were tested in duplicate, and all experiments were performed at least twice.

On selected days, cartilage explants were harvested, fixed in 4% paraformaldehyde, and embedded in paraffin (oriented to allow sectioning across the full depth of the cartilage) for histologic analysis and Fourier transform infrared microspectroscopy (FTIRM) or were processed for indirect immunofluorescence to measure antibody penetration (15,17). For histologic examination, 5- μ m sections of tissue were stained with hematoxylin and eosin and with toluidine blue to examine proteoglycan loss.

Analysis of changes in the chemical composition of the cartilage by FTIRM. Sections of paraffin-embedded tissue (5 μ m) were placed onto MirrIR low-e microscope slides (Kevley Technologies), and adjacent sections were stained with toluidine blue. FTIR images were recorded with a Stingray Digilab FTS 7000 series spectrometer coupled to a UMA 600 microscope equipped with a 64 × 64 focal plane array detector or were recorded using the infrared beamline at the Australian Synchrotron. For each spectrum, 16 scans were co-added at a resolution of 6 cm⁻¹. The spectra were analyzed using Cyto-Spec imaging software. A quality test was performed to remove spectra with poor signal-to-noise ratios and spectra containing obvious artifacts. The spectra were further analyzed using 2 different methods.

Initially, spectra were analyzed as described in our previous publications (15,17), in which spectra from the antibody-exposed surface of the cartilage were compared with those from the interior of the cartilage. Raw chemical maps were generated from the integrated intensities of specific functional groups identified in the spectra, and 10 spectra from the surface of the explant and 10 from the interior were extracted from the raw chemical maps. The mean spectra for "surface" and "interior" were calculated to assess the effects of antibody penetration on the peaks characteristic of collagen and of proteoglycans. An FTIRM spectrum from tissue containing collagen characteristically contains a triplet of peaks at 1203 cm⁻¹, 1234 cm⁻¹, and 1280 cm⁻¹. However, since this collagen triplet coincides with a peak at 1240–1245 cm⁻¹ derived from the sulfated glycosaminoglycan side chains of proteoglycans (18,19), analysis was directed particularly to the location of the amide 1 peak (1640–1670 cm⁻¹), which represents total protein, which for cartilage, is primarily collagen. The amide 1 peak for the native triple-helical collagen is unusual, being >1660 cm⁻¹, as compared with most other proteins, for which the peak is ~1650 cm⁻¹, and there is a characteristic shift to a lower wave number on denaturation (15,20–25). For proteoglycans, analysis was based on the height of the peak at 1076 cm⁻¹, within the region of 1175–960 cm⁻¹ derived from carbohydrate moieties (15). Since according to the Beer-Lambert law, the concentration of a particular chemical is proportional to the

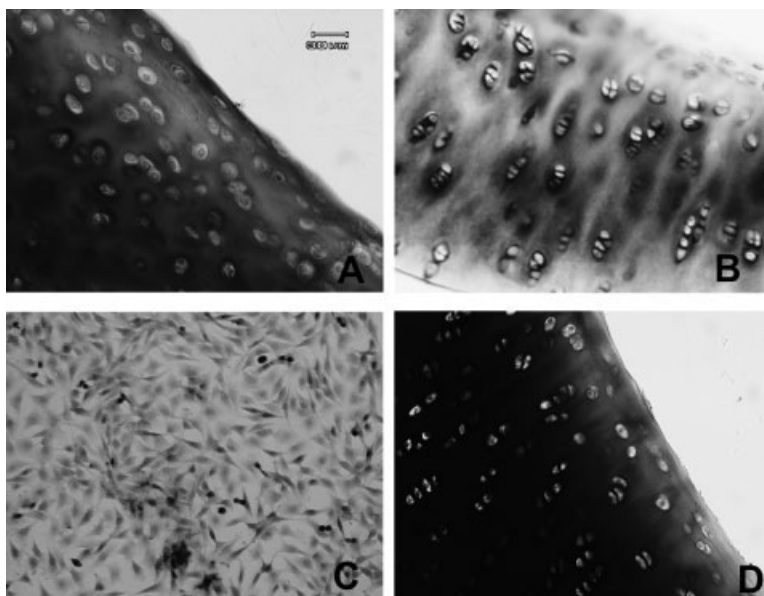


Figure 1. Toluidine blue–stained cartilage samples cultured with various monoclonal antibodies (mAb). **A**, Cartilage sample cultured for 14 days with CIIF4, showing even staining and regular distribution of chondrocytes. **B**, Cartilage sample cultured for 14 days with a combination of arthritogenic mAb M2139 and CIIC1, showing uneven loss of proteoglycan staining and clumping of chondrocytes. **C**, Appearance of fibroblast-like cells on the base of the culture plate of cartilage explants cultured with M2139 and CIIC1. **D**, Cartilage sample cultured for 14 days with the combination of M2139, CIIC1, and CIIF4 mAb. (Original magnification $\times 200$.)

absorbance of the particular band, this characteristic peak provides a direct measure of the proteoglycan content.

Analysis was also performed using second derivatives, which measures changes in the slope of the spectra, where minima peaks in the second derivative spectra correlated with the maxima peaks in the nonderivatized spectra (26). This provided more information about the changes in cartilage components by allowing the resolution of bands that contribute to inflection points or shoulders in the original spectra, which represent the total of the spectra of all of the chemical components scanned within each pixel. It also eliminated problems with sloping baselines arising from loss of cartilage components, but at the expense of loss of information about relative amounts of components. To analyze changes across the cartilage, unsupervised hierarchical cluster analysis, a technique that identifies areas with similar spectral properties (27), was performed on the chemical maps derived using the second derivative spectra.

Requirement for living chondrocytes in damage or protection of cartilage. To determine whether the changes observed in the presence of the mAb to CII required degradative enzymes or other factors produced by chondrocytes, experiments were conducted on explants in which chondrocytes were killed by freeze-thawing the cartilage explants 3 times in liquid nitrogen (28). Experiments were conducted on explants cultured with the combination of the mAb M2139 and CIIC1, with or without CIIF4, and on control explants cultured without mAb, which were then cultured as normal for 7 or 14

days (15). The results obtained were compared with those obtained in the same experiments in which cartilage contained living chondrocytes.

Contribution of matrix metalloproteinases to cartilage destruction in vitro. The changes observed in cartilage cultured with arthritogenic mAb (see Results) resembled those induced by chondrocyte-derived degradative enzymes, particularly the MMPs, including collagenases (MMPs 1, 8, and 13), gelatinases (MMPs 2 and 9), and stromelysins and aggrecanases (MMPs 3, 7, 10, 11, 12, and 18) (29). Since the epitope for mAb CIIF4 in the C-terminal region of CII in the aggregated collagen fibrils is close to the cleavage site of MMP-3 in the N-terminal telopeptide of CII (30), the protective effect of CIIF4 could be attributed to steric inhibition of MMP-3 activity. Hence, to examine the effects of MMPs on the cultures, experiments were performed using the commercially available broad-spectrum MMP inhibitor GM6001 (Millipore). GM6001 was added to cultures in varying concentrations (15 μM , 25 μM , and 35 μM) together with 25 $\mu\text{g}/\text{ml}$ each of mAb M2139 and CIIC1. Controls without mAb were included, and the effects were assessed histologically and by FTIRM.

Statistical analysis. Statistical analyses were performed using Statistica for Windows, version 4.5 (StatSoft). Analysis of variance (ANOVA) or the nonparametric Kruskal-Wallis ANOVA by ranks was performed to determine whether there were significant differences between all groups in the experiment. Student's *t*-test or the Mann-Whitney U test was

Table 1. Location of the amide 1 peak and the height of the proteoglycan peak at the surface and in the interior of cartilage explants cultured in the presence and absence of arthritogenic mAb*

Treatment, vital status of cells, and location	Day 7		Day 14	
	Amide 1 peak, median (range) cm ⁻¹	Proteoglycan peak, maximum \pm SD absorbance	Amide 1 peak, median (range) cm ⁻¹	Proteoglycan peak, maximum \pm SD absorbance
No mAb				
Alive				
Surface	1666 (1639–1670)	0.37 \pm 0.06	1662 (1662–1662)	0.39 \pm 0.06
Interior	1666 (1639–1670)	0.37 \pm 0.04	1666 (1635–1670)	0.41 \pm 0.05
CIIF4 100 μ g/ml				
Alive				
Surface	1666 (1639–1670)	0.32 \pm 0.08	1662 (1654–1670)	0.38 \pm 0.03
Interior	1666 (1639–1670)	0.40 \pm 0.05	1662 (1650–1670)	0.30 \pm 0.06
M2139 25 μ g/ml + CIIC1 25 μ g/ml				
Alive				
Surface	1658 (1643–1658)	0.28 \pm 0.05	1643 (1639–1650)	0.15 \pm 0.02
Interior	1666 (1662–1670)	0.32 \pm 0.08	1651 (1639–1666)†	0.11 \pm 0.02†
M2139 25 μ g/ml + CIIC1 25 μ g/ml + CIIF4 50 μ g/ml				
Alive				
Surface	1666 (1654–1670)	0.30 \pm 0.09	1658 (1639–1670)	0.55 \pm 0.06
Interior	1662 (1647–1662)	0.25 \pm 0.05	1666 (1646–1677)	0.37 \pm 0.04
M2139 25 μ g/ml + CIIC1 25 μ g/ml				
Dead				
Surface	1643 (1631–1658)	0.16 \pm 0.03	1635 (1631–1643)	0.15 \pm 0.04
Interior	1666 (1658–1666)	0.39 \pm 0.03	1654 (1646–1658)†	0.22 \pm 0.03†
M2139 25 μ g/ml + CIIC1 25 μ g/ml + CIIF4 50 μ g/ml				
Dead				
Surface	1647 (1643–1650)	0.07 \pm 0.02	1639 (1631–1639)	0.05 \pm 0.18
Interior	1666 (1666–1670)	0.29 \pm 0.01	1650 (1643–1654)†	0.39 \pm 0.05†

* Fourier transform infrared microspectroscopy was used to determine the location of the amide 1 peak and the height of the proteoglycan peak at 1,076 cm⁻¹ at the cartilage surface, where the monoclonal antibody (mAb) penetrates, and in the interior of cartilage explants cultured for 7 or 14 days under the indicated conditions (see Materials and Methods for details). Analyses were performed in cartilage containing living chondrocytes or in cartilage in which the chondrocytes had been killed by repeated freezing and thawing.

† Cartilage damage extends to the interior.

used to analyze differences between specified groups. *P* values less than 0.05 were considered significant.

RESULTS

Effect of anti-CII mAb on cartilage morphology in explant cultures. Cartilage explants cultured in medium alone or with CIIF4 concentrations of up to 100 μ g/ml appeared normal throughout the culture period, and the matrix stained strongly with toluidine blue (Figure 1A). The mAb bound to the cartilage, and on day 7, CIIF4 had penetrated $32 \pm 12 \mu\text{m}$ (mean \pm SD), M2139 plus CIIC1 had penetrated $45 \pm 16.5 \mu\text{m}$, and M2139 plus CIIC1 plus CIIF4 had penetrated $29 \pm 4 \mu\text{m}$. The use of mixtures of M2139 and CIIC1 resulted in profound changes in the explant structure, including marked loss of toluidine blue staining, gradual loss of the matrix integrity at the cartilage surface, with increasing mAb penetration, and chondrons containing several cells, suggestive of hyperplasia as a compensatory re-

sponse to mAb-mediated damage (Figure 1B), and more so with increasing concentrations of mAb or with increasing times in culture.

From day 9 to day 10, cartilage degradation was associated with a migration of cells from the surface of the cartilage, and fibroblast-like cells began to appear on the base of the plate (Figure 1C). Such cells, which were taken to represent chondrocytes undergoing dedifferentiation as a result of matrix loss from the cut surface of the tissue, also appeared in control cultures by day 14, but their numbers were quite sparse. The addition of 50 μ g/ml of CIIF4 to cultures containing 50 μ g/ml of the arthritogenic mAb reversed the degenerative changes, as judged by a reduced loss of toluidine blue staining of proteoglycans at the cartilage surface, normal architecture of the tissue, albeit with a slight increase in multicellular chondrons, and even increased proteoglycan synthesis, particularly at the cartilage surface, after 14 days in culture (Figure 1D). Also, the appearance of

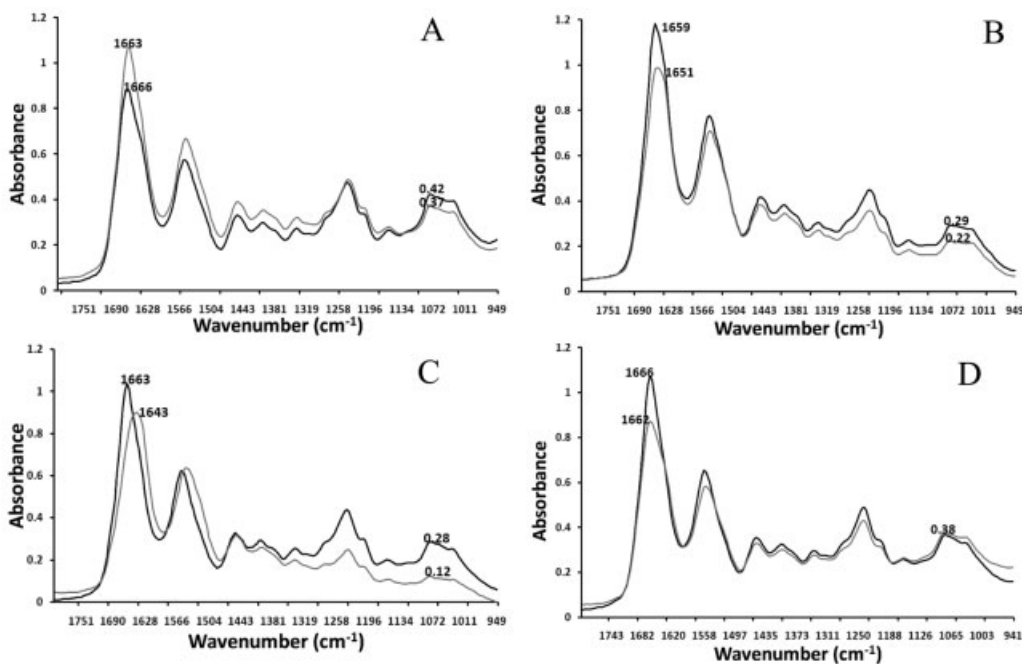


Figure 2. Fourier transform infrared microspectroscopy spectra of cartilage sections cultured with various antibodies. The results shown are the mean of 10 measurements taken from the central areas (thick line) and near the surface of the tissue (thin line). Shown in each panel is the location of the amide 1 peak, which represents the total protein content of the tissue, in the region 1600–1700 cm^{-1} , and the height of the peak at 1076 cm^{-1} , representing proteoglycans. **A**, Spectra of cartilage cultured for 14 days with 100 $\mu\text{g}/\text{ml}$ of monoclonal antibody (mAb) CIIF4. **B**, Spectra of cartilage cultured for 10 days with 25 $\mu\text{g}/\text{ml}$ each of mAb M2139 and CIIC1. **C**, Spectra of cartilage cultured for 10 days with 50 $\mu\text{g}/\text{ml}$ each of mAb M2139 and CIIC1. **D**, Spectra of cartilage cultured for 10 days with 25 $\mu\text{g}/\text{ml}$ each of mAb M2139 and CIIC1 with the addition of 50 $\mu\text{g}/\text{ml}$ of mAb CIIF4.

fibroblast-like cells on the base of the plates was reduced to that seen in normal cultures.

Role of chondrocytes in antibody-mediated cartilage damage in vitro. By light microscopy, freeze-thawed cartilage cultured for up to 14 days without mAb or with CIIF4 appeared normal, with rounded chondrocytes distributed within a matrix that stained evenly with toluidine blue. Histologically, freeze-thawed cartilage cultured with the combination of mAb M2139 and mAb CIIC1 showed changes similar to or greater than those observed in the cartilage containing living chondrocytes (Figure 1B), although the chondrocyte pairing and clumping seen in the living cartilage was not observed in the freeze-thawed tissue. The addition of CIIF4 to cultures of freeze-thawed cartilage did not protect from the damaging effects of the arthritogenic mAb.

Chemical changes in cartilage matrix as measured by FTIRM. Histologic differences were confirmed by FTIRM, a technique that provides information on the nature of the chemical changes that have occurred. Spectra obtained from 5 samples of cartilage cultured for 14 days with up to 100 $\mu\text{g}/\text{ml}$ of CIIF4 resembled

spectra from control cartilage cultured without mAb. In each case, the amide 1 peak at the cartilage surface after incubation with CIIF4 was located above wave number 1660 cm^{-1} (range 1662–1670), which was comparable with that in the controls (1662–1666 cm^{-1}), and the areas under the curve for the amide 1 and proteoglycan peaks were similar to those in the controls. Spectra derived from the cartilage surface and the cartilage interior were similar (Table 1 and Figure 2A).

In contrast to the lack of effect of CIIF4 on the FTIRM spectra of cartilage, there were striking differences in spectra obtained from cartilage cultured in the presence of CIIC1 and M2139 (Table 1 and Figure 2B). Beyond the region of penetration by mAb, the spectra were generally similar to those of controls cultured without mAb, but spectra from the surface of the cartilage showed substantial changes that increased with time in culture or with higher concentrations of mAb (Figure 2C). There was a progressive shift in the location of the amide 1 peak from $>1660 \text{ cm}^{-1}$ to as low as 1643 cm^{-1} or 1639 cm^{-1} , which is suggestive of progressive

denaturation of the collagen, and these changes gradually became evident deeper within the cartilage (Table 1).

Initially, there was loss of the proteoglycan peak, but no loss of protein, as judged by the area under the curve for the amide 1 peak, but with increasing time in culture, there was a substantial decrease in the amide 1 peak and, indeed, across the whole spectrum, indicating a total loss of matrix. The data indicated that the arthritogenic mAb caused initial denaturation of collagen and loss of proteoglycans, with ongoing progressive denaturation and loss of collagen over the period of culture. These changes were antibody mediated and did not require viable chondrocytes or new synthesis of degradative enzymes because similar or even greater effects were seen in cartilage that had been freeze-thawed (Table 1).

The addition of CIIF4 to cultures with combinations of the arthritogenic mAb counteracted these changes (Table 1 and Figure 2D), although the protective effect was somewhat delayed. On day 7, there was often some degradation, and the changes observed in explants cultured with CIIF4 in combination with any of the arthritogenic mAb were not significantly different from those seen in explants cultured with the arthritogenic mAb alone. However, by days 10–14 in cultures that contained CIIF4, the position of the amide 1 peak at the cartilage surface had normalized to that for the control cartilage (above wave number 1660 cm^{-1}), and there was an equivalent normalization, or even an increase, in the proteoglycan content at the cartilage surface, as measured by the height of the proteoglycan peak at 1076 cm^{-1} . In contrast to the degradative effects of the combination of arthritogenic mAb, which did not require living chondrocytes, the protective effect of CIIF4 was observed only when the cartilage contained viable cells (Table 1).

FTIRM analysis using second derivatives. The results obtained using second derivative spectra confirmed those obtained by comparison of direct spectra, and second derivative minima were, as expected, located similarly to the peak maxima on the original spectra. In freeze-thawed cartilage, the use of second derivatives confirmed that the major change in chemical composition in the cartilage cultured with the arthritogenic mAb was in the location of the amide 1 peak, which was consistent with collagen denaturation, and there was little or no change in most components of the matrix, as judged by the lack of changes in other regions of the spectra (Figure 3). However, analysis of the second derivatives provided more information than was obtained using the primary spectra, for which the cartilage contained living chondrocytes. Whatever the treatment

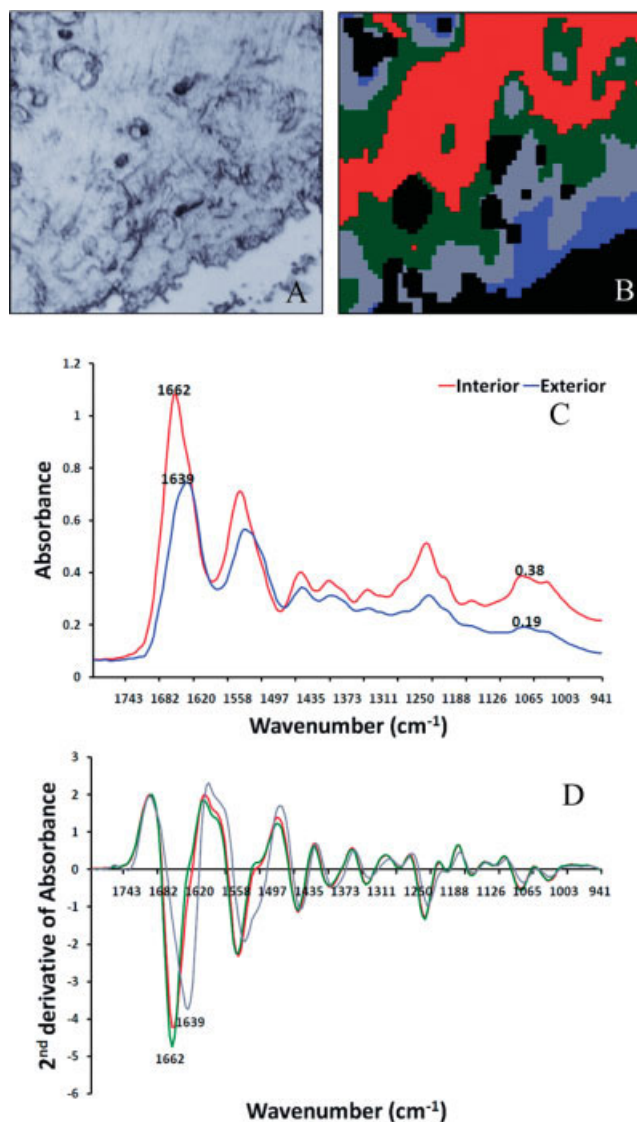


Figure 3. Fourier transform infrared microspectroscopy (FTIRM) of freeze-thawed cartilage sections cultured for 7 days with monoclonal antibodies (mAb) M2139 and CIIC1, showing a comparison of the results obtained by direct analysis and by unsupervised hierarchical cluster analysis (UHCA) using second derivative spectra. Both techniques showed peaks located in similar positions, but the direct spectra showed loss of cartilage components. **A**, Light microscopy image of an unstained cartilage section on a Kevley reflective slide (original magnification $\times 200$). **B**, Infrared image processed by UHCA using second derivative spectra with 4 clusters (4 different colors). Pixels with poor signal-to-noise ratios are shown as black. **C**, Mean FTIRM spectra obtained by direct analysis of 10 pixels from the interior and exterior of the cartilage. **D**, Second derivative spectra corresponding to the clusters shown in **B**. Pixels colored blue were judged to be artifacts and were removed during analysis.

used, the spectra derived from living cartilage were more complex than those derived from freeze-thawed carti-

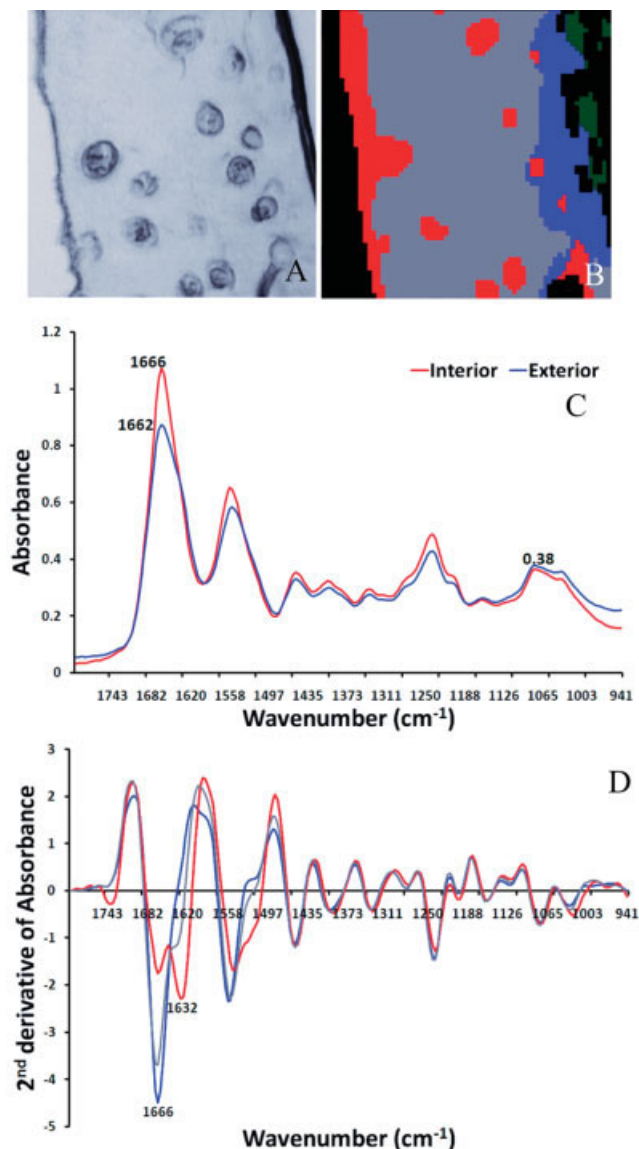


Figure 4. Fourier transform infrared microspectroscopy (FTIRM) of a section of living cartilage cultured for 7 days with monoclonal antibodies (mAb) M2139 and CIIC1 plus mAb CIIF4, showing a comparison of the results obtained by direct analysis and by unsupervised hierarchical cluster analysis (UHCA) using second derivative spectra. Both techniques showed the normal appearance of the cartilage spectra in the presence of CIIF4, but the use of second derivatives highlighted the appearance of a peak at $\sim 1632\text{--}1635\text{ cm}^{-1}$, in the region of living chondrocytes that did not appear in the freeze-thawed cartilage samples. **A**, Light microscopy image of unstained cartilage section on a Kevley reflective slide (original magnification $\times 200$). **B**, Infrared image processed by UHCA using second derivative spectra with 4 clusters (4 different colors). Pixels with poor signal-to-noise ratios are shown as black. **C**, Mean FTIRM spectra obtained by direct analysis of 10 pixels from the interior and exterior of the cartilage. **D**, Second derivative spectra corresponding to the clusters shown in **B**. Pixels colored green were judged to be artifacts and were removed during analysis.

lage, particularly in the region above 1500 cm^{-1} (Figure 4). The most prominent and consistent feature was the appearance of a second derivative minimum at $1632\text{--}1635\text{ cm}^{-1}$, either as a separate peak or as a shoulder on another peak in the amide 1 region. This component could not be identified but was consistent with likely chondrocyte metabolic activation. It was seen particularly in spectra from all samples of CIIF4-treated living cartilage, as well as in untreated controls and in cartilage treated with arthritogenic mAb, although less prominently.

Assessment of the role of MMPs in the cartilage damage mediated by anti-CII mAb. To assess whether MMPs affected the matrix destruction observed in the presence of arthritogenic mAb, and whether MMP-3 could determine the counterdestructive effect of CIIF4, we investigated the use of the broad-spectrum MMP inhibitor GM6001 (15, 25, and $35\ \mu\text{M}$) in combination with M2139 and CIIC1 ($25\ \mu\text{g/ml}$ each) in bovine cartilage explant cultures. At all concentrations, the addition of the MMP inhibitor GM6001 reduced the cartilage damage seen in response to the arthritogenic mAb, but the changes differed from the protective effects of CIIF4. Fragmentation at the surface of the antibody-treated cartilage was seen histologically, but it had a fibrillar appearance and followed the orientation of collagen fibrils within the tissue, being parallel with the joint surface, but perpendicular to the cut surface of the cartilage. The substantial loss of proteoglycans normally seen in cartilage treated with the arthritogenic mAb did not occur, and the intensity of the toluidine blue staining was maintained (Figure 5). By FTIRM, there was little evidence of collagen denaturation, as judged by the location of the amide 1 peak, which remained above 1660 cm^{-1} , and the area under the proteoglycan peak was similar to that of the controls (data not shown). Similar effects were seen in freeze-thawed cartilage. Taken together, these results suggest that blocking MMP activity in the cartilage prevented degradation of the damaged collagen fibrils and loss of proteoglycan but did not prevent the initial damage mediated by antibodies.

DISCUSSION

This study was designed to examine the effects on bovine cartilage explants of 3 mAb to native CII that bind to well-identified and structurally different conformational epitopes (16). Two of these mAb, M2139 and CIIC1, are arthritogenic upon passive transfer in vivo (9,14), and whether used individually (15) or in combination, they caused progressive denaturation of CII and

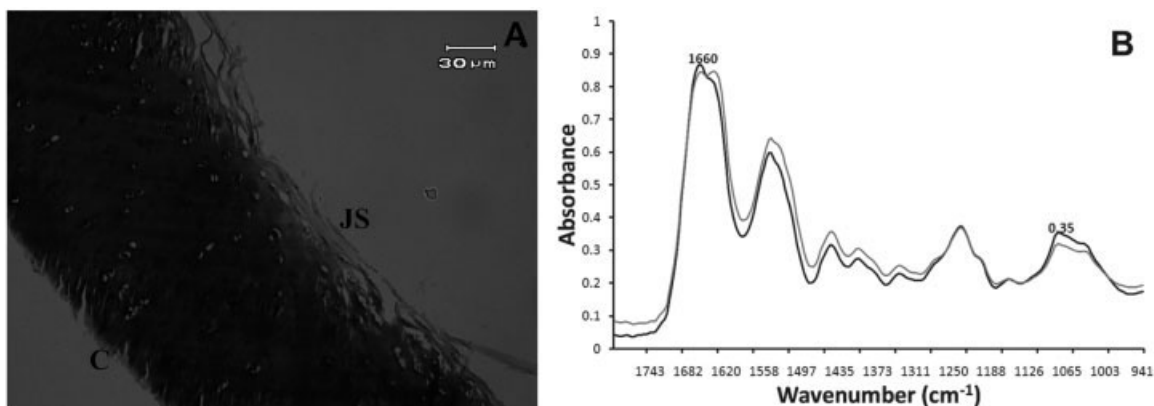


Figure 5. **A**, Toluidine blue-stained cartilage sample cultured for 14 days with monoclonal antibodies (mAb) M2139 and CIIC1 in the presence of the broad-spectrum matrix metalloproteinase inhibitor GM6001. The intensity of the staining was maintained, but there was fragmentation at the joint surface (JS) and the cut surface (C) that approximately aligned with the expected direction of the collagen fibrils. **B**, Spectra obtained by Fourier transform infrared microspectroscopy. The proteoglycan peak at $\sim 1076\text{ cm}^{-1}$ was maintained, and the amide 1 peak remained above 1660 cm^{-1} . Measurements were taken from the central areas (thick line) and near the surface of the tissue (thin line).

substantial loss from cartilage of both CII and proteoglycans in vitro. By contrast, the third mAb, CIIF4, which is nonarthritogenic and protective in vivo when given with other mAb (14,17), had no adverse effect in vitro when used alone on cultured cartilage and countered the adverse effects of arthritogenic mAb, even promoting the regeneration of cartilage matrix components. Thus, this counterdestructive effect of CIIF4 in vitro parallels its antiarthritogenic effects in vivo. It is notable that whereas the destructive effects of the arthritogenic mAb were independent of the presence of viable chondrocytes, the protective effect of CIIF4 required viable chondrocytes, since it was abrogated by freeze-thawing of the cultured cartilage explant.

The effector role of autoantibodies in the development of arthritis has been extensively studied in the context of murine CAIA. The bound antibodies have been shown to trigger and enhance inflammation by activating the complement cascade and Fc γ R-bearing cells, with release of proinflammatory cytokines by mononuclear cells within the synovium, leading to recruitment of neutrophils and macrophages that amplify the response by the further release of cytokines and tissue-degrading enzymes (31). Moreover, preceding or in parallel with these nonspecific effects of immune complex cellular activation, there is increasing evidence that autoantibodies to CII can have specific destructive effects within the cartilage (15,16,17). In addition to the degradative effects on preformed cartilage seen in the present study, the arthritogenic mAb have been shown to impair the synthesis of new matrix and disrupt

collagen fibril formation in chondrocyte cultures in vitro (17,32–34), changes that would directly affect the processes of cartilage repair following damage to the matrix.

The mechanism by which CIIF4 exerts its effects is currently unknown. The nonarthritogenic mAb CIIF4 was derived in a manner similar to that of the arthritogenic mAb from a DBA/1 mouse immunized with CII, and it is an IgG2a mAb, as is the arthritogenic mAb CIIC1. It binds strongly to CII, as demonstrated by ELISA, as well as to cartilage, both in vitro and in vivo. Hence, CIIF4 should activate complement and bind to Fc γ R-bearing cells to trigger immune complex-mediated inflammation. Nonetheless, it is not arthritogenic, but is actually protective in vivo, reducing the arthritis in mice injected with otherwise arthritogenic mAb (14,17). CIIF4 is reactive with a conformational epitope at the COOH-terminus of the CII triple helix (aa 932–936), and within the assembled collagen fibrils, it is close to one of the cleavage sites of MMP-3 (stromelysin 1) (14) that is located within the NH₂ telopeptide region in the collagen fibril (30). Moreover, its effects differ from those of other mAb, in that they were only seen when viable chondrocytes remained in the cartilage.

Our hypothesis was that CIIF4 exerts its protective effect by steric hindrance, blocking the cleavage of CII by MMP-3, which is produced by chondrocytes and by synovial fibroblasts, and is associated with cartilage degradation in osteoarthritis and in RA (35,36). MMP-3 primarily targets proteoglycans and is not a conventional collagenase, but it acts as a telopeptidase by cleaving CII

at a site inside its NH₂-telopeptide crosslinking residue (30) and most likely also cleaving off the C-telopeptide. MMP-3 plays an essential role in the degradation of not only aggrecan, but also collagen fibrils in the cartilage (35), so that MMP-3-knockout mice are resistant to cartilage degradation in antigen-induced arthritis (37). The use of a broad-spectrum MMP inhibitor to block MMP-3 activity in the cultures, however, did not mimic the effect of the addition of the mAb CIIF4. Thus, the MMP inhibitor did not prevent cartilage damage as assessed histologically, and there were no apparent differences in the cultures that contained living or dead chondrocytes, indicating that the protective effect of CIIF4 was not merely a result of steric hindrance of MMP-3 activity, although steric hindrance of the binding of one or other of the arthritogenic mAb could not be discounted.

The use of the MMP inhibitor GM6001 in culture provided further information about the likely mechanism of damage by the arthritogenic mAb. By FTIRM, it appeared that the MMP inhibitor prevented both the denaturation of collagen and the loss of proteoglycans seen in cartilage cultured with the arthritogenic mAb, indicating that MMPs do play a role in the cartilage degradation induced by the antibodies. The fibrillar nature of the cartilage damage in the presence of the inhibitor suggests that the initial effect of the binding of the arthritogenic mAb on the surface of the collagen fibrils was to cause disaggregation of the collagen fibrils, but the lack of collagen denaturation or proteoglycan loss in the presence of the MMP inhibitor indicates that these enzymes play an important role in further cartilage degradation. The results suggest that the disruption of the collagen matrix causes the release of the MMPs known to be sequestered in the intact matrix (38,39), and these MMPs are responsible for the ongoing loss of proteoglycans and collagen degradation, without any requirement for further MMP inhibitor synthesis.

A striking observation from these studies is the importance of living chondrocytes in the maintenance of cartilage integrity in the presence of arthritogenic mAb and in the protective effect of CIIF4. In each case, the arthritogenic mAb caused more damage to the freeze-thawed cartilage, as judged by the greater shift in the position of the amide 1 peak and the loss of proteoglycans on both day 7 and day 14. This augmented damage was also seen in the freeze-thawed cartilage even in the presence of CIIF4. The appearance of chondrocyte dimers, or clumps of cells in the antibody-treated cartilage, which were absent in the freeze-thawed cartilage,

suggested that cell division was occurring in response to the treatment, and the appearance of an additional peak at 1632–1635 cm⁻¹ in the living cartilage was consistent with cellular activation. Taken together, these observations suggest that there is a balance between damage and regeneration within the cartilage.

The use of FTIRM, a technique that allows the examination of localized chemical changes within tissue without any requirement of a priori knowledge of the likely mechanism has allowed definitive detection of the protective effect of CIIF4. Determination of the mechanism of the protective effect of CIIF4 will require the use of different techniques and is beyond the scope of the current study, but we are investigating the gene expression profiles in chondrocytes treated with CIIF4 and other antibodies.

The major question that arises from these studies is whether there is any connection with the pathogenesis of RA. RA is generally considered to be an immune complex-mediated disease, and its features are well accounted for by the formation and deposition in joint structures of immune complexes that are operative by complement activation and by Fc binding and Fcγ activation. In CIA in animals, the antigenic component is clearly CII, but in RA in humans, there is uncertainty (noting that an antibody response to ALL of the epitopes recognized by the mAb in this study also occur in RA). If antibodies to CII of the same specificity as the arthritogenic mAb also occur in human sera (14), the mechanisms of joint damage that occur in CIA could also occur in RA. Interestingly, both proteoglycan and CII destruction and secretion into the synovium occur in RA (40–42). It is striking that antibodies to CII of the same specificity as CIIF4 also occur in human sera, but they are associated with osteoarthritis rather than rheumatoid arthritis (14), and it is tempting to speculate that such antibodies may also prevent the inflammatory damage seen in human RA.

ACKNOWLEDGMENTS

We thank Ian Mackay and Senga Whittingham for helpful discussions and editorial comments. Part of this research was undertaken using the infrared microspectroscopy beamline at the Australian Synchrotron (Clayton, Victoria, Australia).

AUTHOR CONTRIBUTIONS

All authors were involved in drafting the article or revising it critically for important intellectual content, and all authors approved the final version to be published. Dr. Rowley had full access to all of

the data in the study and takes responsibility for the integrity of the data and the accuracy of the data analysis.

Study conception and design. Croxford, McNaughton, Holmdahl, Rowley.

Acquisition of data. Croxford, Crombie, Rowley.

Analysis and interpretation of data. Croxford, Crombie, McNaughton, Nandakumar, Rowley.

REFERENCES

- Alamanos Y, Drosos AA. Epidemiology of adult rheumatoid arthritis. *Autoimmun Rev* 2005;4:130–6.
- Manz RA, Hauser AE, Hiepe F, Radbruch A. Maintenance of serum antibody levels. *Ann Rev Immunol* 2005;23:367–86.
- Rowley MJ, Nandakumar KS, Holmdahl R. The role of collagen antibodies in mediating arthritis. *Mod Rheumatol* 2008;18:429–41.
- Trentham DE, Townes AS, Kang AH. Autoimmunity to type II collagen an experimental model of arthritis. *J Exp Med* 1977;146:857–68.
- Courtenay JS, Dallman MJ, Dayan AD, Martin A, Mosedale B. Immunisation against heterologous type II collagen induces arthritis in mice. *Nature* 1980;28:666–8.
- Holmdahl R, Andersson M, Goldschmidt TJ, Gustafsson K, Jansson L, Mo JA. Type II collagen autoimmunity in animals and provocations leading to arthritis. *Immunol Rev* 1990;118:193–232.
- Terato K, Hasty KA, Reife RA, Cremer MA, Kang AH, Stuart JM. Induction of arthritis with monoclonal antibodies to collagen. *J Immunol* 1992;148:2103–8.
- Nandakumar KS, Holmdahl R. Antibody-induced arthritis: disease mechanisms and genes involved at the effector phase of arthritis. *Arthritis Res Ther* 2006;8:223.
- Nandakumar KS, Svensson L, Holmdahl R. Collagen type II-specific monoclonal antibody-induced arthritis in mice: description of the disease and the influence of age, sex, and genes. *Am J Pathol* 2003;163:1827–37.
- Holmdahl R, Rubin K, Klareskog L, Larsson E, Wigzell H. Characterization of the antibody response in mice with type II collagen-induced arthritis, using monoclonal anti-type II collagen antibodies. *Arthritis Rheum* 1986;29:400–10.
- Hogarth PM. Fc receptors are major mediators of antibody based inflammation in autoimmunity. *Curr Opin Immunol* 2002;14:798–802.
- Nandakumar KS, Johansson BP, Bjorck L, Holmdahl R. Blocking of experimental arthritis by cleavage of IgG antibodies in vivo. *Arthritis Rheum* 2007;56:3253–60.
- Nandakumar KS, Collin M, Olsen A, Nimmerjahn F, Blom AM, Ravetch JV, et al. Endoglycosidase treatment abrogates IgG arthritogenicity: importance of IgG glycosylation in arthritis. *Eur J Immunol* 2007;37:2973–82.
- Burkhardt H, Koller T, Engstrom A, Nandakumar KS, Turnay J, Kraetsch HG, et al. Epitope-specific recognition of type II collagen by rheumatoid arthritis antibodies is shared with recognition by antibodies that are arthritogenic in collagen-induced arthritis in the mouse. *Arthritis Rheum* 2002;46:2339–48.
- Crombie DE, Turer M, Zuasti BB, Wood B, McNaughton D, Nandakumar KS, et al. Destructive effects of murine arthritogenic antibodies to type II collagen on cartilage explants in vitro. *Arthritis Res Ther* 2005;7:R927–37.
- Schulte S, Unger C, Mo JA, Wendler O, Bauer E, Frischholz S, et al. Arthritis-related B cell epitopes in collagen II are conformation-dependent and sterically privileged in accessible sites of cartilage collagen fibrils. *J Biol Chem* 1998;273:1551–61.
- Nandakumar KS, Bajtner E, Hill L, Bohm B, Rowley MJ, Burkhardt H, et al. Arthritogenic antibodies specific for a major type II collagen triple-helical epitope bind and destabilize cartilage independent of inflammation. *Arthritis Rheum* 2008;58:184–96.
- Camacho NP, West P, Torzilli PA, Mendelsohn R. FTIR microscopic imaging of collagen and proteoglycan in bovine cartilage. *Biopolymers* 2001;62:1–8.
- Potter K, Kidder LH, Levin IW, Lewis EN, Spencer RG. Imaging of collagen and proteoglycan in cartilage sections using Fourier transform infrared spectral imaging. *Arthritis Rheum* 2001;44:846–55.
- Payne KJ, Veis A. Fourier transform IR spectroscopy of collagen and gelatin solutions: deconvolution of the amide I band for conformational studies. *Biopolymers* 1988;27:1749–60.
- Bi X, Li G, Doty SB, Camacho NP. A novel method for determination of collagen orientation in cartilage by Fourier transform infrared imaging spectroscopy (FT-IRIS). *Osteoarthritis Cartilage* 2005;13:1050–8.
- West PA, Torzilli PA, Chen C, Lin P, Camacho NP. Fourier transform infrared imaging spectroscopy analysis of collagenase-induced cartilage degradation. *J Biomed Opt* 2005;10:14015.
- George A, Veis A. FTIRS in H₂O demonstrates that collagen monomers undergo a conformational transition prior to thermal self-assembly in vitro. *Biochemistry* 1991;30:2372–7.
- Lazarev YA, Grishkovsky BA, Khromova TB. Amide I band of IR spectrum and structure of collagen and related polypeptides. *Biopolymers* 1985;24:1449–78.
- Bhargava R, Levin IW. Fourier transform infrared imaging: theory and practice. *Anal Chem* 2001;73:5157–67.
- Wood BR, Tait B, McNaughton D. Fourier-transform infrared spectroscopy as a tool for detecting early lymphocyte activation: a new approach to histocompatibility matching. *Hum Immunol* 2000;61:1307–14.
- Lasch P, Haensch W, Naumann D, Diem M. Imaging of colorectal adenocarcinoma using FT-IR microspectroscopy and cluster analysis. *Biochim Biophys Acta* 2004;1688:176–86.
- Clements KM, Bee ZC, Crossingham GV, Adams MA, Sharif M. How severe must repetitive loading be to kill chondrocytes in articular cartilage? *Osteoarthritis Cartilage* 2001;9:499–507.
- Malemud CJ. Matrix metalloproteinases (MMPs) in health and disease: an overview. *Front Biosci* 2006;11:1696–701.
- Wu JJ, Lark MW, Chun LE, Eyre DR. Sites of stromelysin cleavage in collagen types II, IX, X, and XI of cartilage. *J Biol Chem* 1991;266:5625–8.
- Nandakumar KS, Holmdahl R. Therapeutic cleavage of IgG: new avenues for treating inflammation. *Trends Immunol* 2008;29:173–8.
- Amirahmadi SF, Pho MH, Gray RE, Crombie DE, Whittingham SF, Zuasti BB, et al. An arthritogenic monoclonal antibody to type II collagen, CII-C1, impairs cartilage formation by cultured chondrocytes. *Immunol Cell Biol* 2004;82:427–34.
- Gray RE, Seng N, Mackay IR, Rowley MJ. Measurement of antibodies to collagen II by inhibition of collagen fibril formation in vitro. *J Immunol Methods* 2004;285:55–61.
- Amirahmadi SF, Whittingham S, Crombie DE, Nandakumar KS, Holmdahl R, Mackay IR, et al. Arthritogenic anti-type II collagen antibodies are pathogenic for cartilage-derived chondrocytes independent of inflammatory cells. *Arthritis Rheum* 2005;52:1897–906.
- Yoshihara Y, Nakamura H, Obata K, Yamada H, Hayakawa T, Fujikawa K, et al. Matrix metalloproteinases and tissue inhibitors of metalloproteinases in synovial fluids from patients with rheumatoid arthritis or osteoarthritis. *Ann Rheum Dis* 2000;59:455–61.

36. Kobayashi A, Naito S, Enomoto H, Shiomi T, Kimura T, Obata K, et al. Serum levels of matrix metalloproteinase 3 (stromelysin 1) for monitoring synovitis in rheumatoid arthritis. *Arch Pathol Lab Med* 2007;131:563–70.
37. Van Meurs J, van Lent P, Stoop R, Holthuysen A, Singer I, Bayne E, et al. Cleavage of aggrecan at the Asn³⁴¹–Phe³⁴² site coincides with the initiation of collagen damage in murine antigen-induced arthritis: a pivotal role for stromelysin 1 in matrix metalloproteinase activity. *Arthritis Rheum* 1999;42:2074–84.
38. Okada Y, Nagase H, Harris ED Jr. A metalloproteinase from human rheumatoid synovial fibroblasts that digests connective tissue matrix components: purification and characterization. *J Biol Chem* 1986;261:14245–55.
39. Van Meurs J, van Lent P, Holthuysen A, Lambrou D, Bayne E, Singer I, et al. Active matrix metalloproteinases are present in cartilage during immune complex-mediated arthritis: a pivotal role for stromelysin-1 in cartilage destruction. *J Immunol* 1999;163:5633–9.
40. Klareskog L, Johnell O, Hulth A, Holmdahl R, Rubin K. Reactivity of monoclonal anti-type II collagen antibodies with cartilage and synovial tissue in rheumatoid arthritis and osteoarthritis. *Arthritis Rheum* 1986;29:730–8.
41. Lohmander LS, Atley LM, Pietka TA, Eyre DR. The release of crosslinked peptides from type II collagen into human synovial fluid is increased soon after joint injury and in osteoarthritis. *Arthritis Rheum* 2003;48:3130–9.
42. Uysal H, Bockermann R, Nandakumar KS, Sehnert B, Bajtner E, Engstrom A, et al. Structure and pathogenicity of antibodies specific for citrullinated collagen type II in experimental arthritis. *J Exp Med* 2009;206:449–62.

CHAPTER THREE

THE EFFECTS OF MONOCLONAL ANTIBODIES TO CII ON CARTILAGE *IN VIVO*

A. CHEMICAL CHANGES DEMONSTRATED IN CARTILAGE BY SYNCHROTRON INFRARED MICROSPECTROSCOPY

3.1. Preface

Although the arthritogenic mAbs have been clearly shown to cause cartilage damage *in vitro* the relevance of this *in vivo* is unclear. Various single mAbs to CII have been shown to induce mild arthritis in naïve mice⁽⁶⁾ and combinations of mAbs induce more severe arthritis with longer lasting effects, exacerbated by injection with lipopolysaccharide (LPS) at day 5^(6, 153). CAIA induced with mAbs to CII has a rapid onset. Swelling of joints in the paws may appear at 24 hrs post immunisation, and histological changes including bone and cartilage erosions, synovial influx of neutrophils and macrophages in the articular cavity and pannus formation are observable within 8-48 hours after immunisation^(6, 176, 195). Although various mAbs to CII differ in their arthritogenicity, the injection of LPS, which is a strong inducer of pro-inflammatory cytokines, overcomes epitope specificity of the response, and increases the severity of CAIA^(153, 188, 196).

The inflammatory cells that infiltrate the joint produce degradative enzymes which cause cartilage damage⁽¹⁹⁷⁾. Antibodies in the form of immune complexes are considered to play a central role in triggering the inflammatory cascade by activating the complement system or by direct engagement of cells containing Fc-receptors^(198, 199). However my data from *in vitro* experiments suggests that we should be able to see changes similar to those seen *in vitro* in cartilage in mice that have been injected with the mAbs but do not develop inflammation.

To test this, *in vivo* experiments were performed in two strains of mice. The first strain B10.Q develops CAIA but rarely develops inflammation until given an injection of LPS at day 5⁽⁶⁾. The second strain B10.Q C5 δ lacks complement factor C5 and doesn't develop CAIA⁽¹⁸⁵⁾. The assumption is that if the cartilage damage seen by these mAbs *in vitro* is directly mediated by the mAbs it should also be detectable *in vivo* by FTIRM.

Animal experiments were carried out in Sweden by Prof. Rikard Holmdahl and A/Prof. Kutty Selva Nandakumar. Mice were killed at day 3 after injection and

paws were removed, fixed and decalcified and embedded in paraffin. The tissue tested was sent to Monash University either as prepared slides containing serial sections from hind paws from mice, unstained for FTIRM, and also stained with haematoxylin and eosin or, in a separate experiment as paraffin embedded blocks, 6 per mouse, containing all four paws with the hind-paws cut in two and separately embedded to allow examination of both phalanges and tarsal joints.

In this case, I cut 5 μm sections at Monash University for analysis by histology and infrared microspectroscopy. To illustrate the sections obtained, a low power image of an H & E stained section from a paw from a control mouse injected only with saline is shown in **Figure 3.1**.

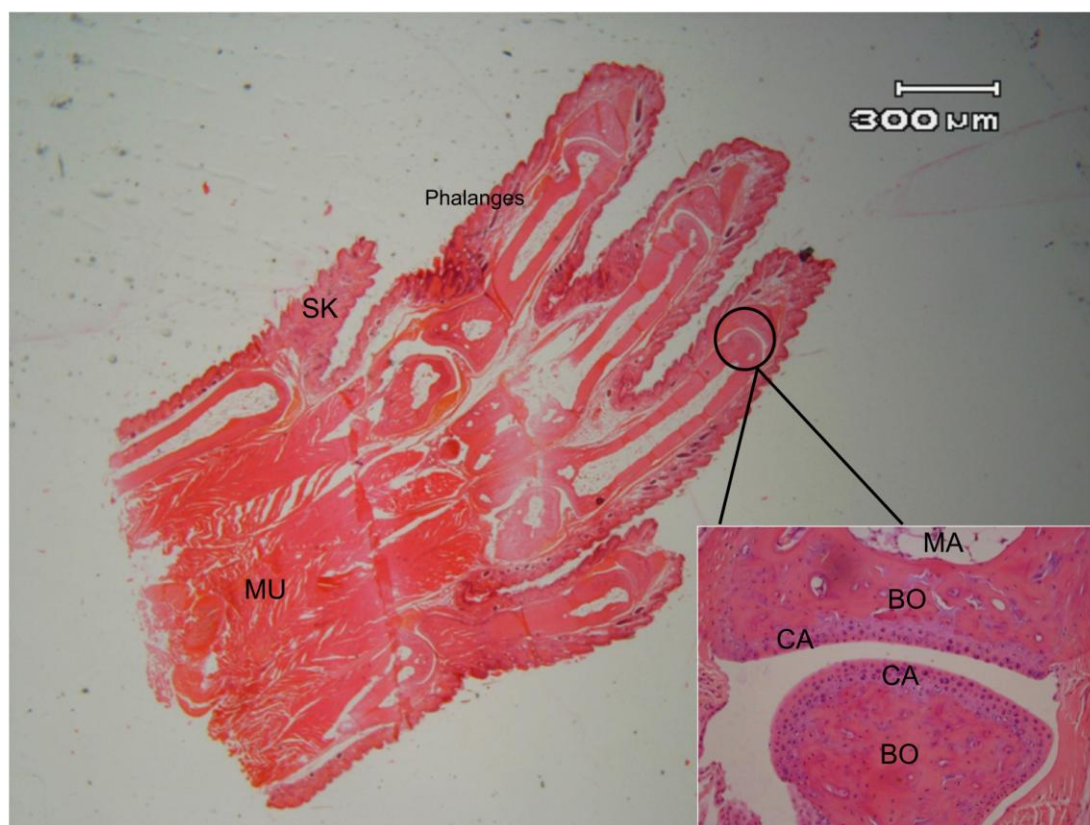


Figure 3.1. H&E stained section of a representative mouse paw at x 4 magnification showing the major features of the tissue, muscle (MU) and skin (SK), marrow cavity (MA), bone (BO) and cartilage (CA). Inset: section from a joint (x 20 magnification)

Initially cartilage analysis was performed by FTIRM using a Stingray Digilab FTS 7000 series spectrometer coupled to a UMA 600 microscope equipped with a 64 x 64 focal plane array detector as described in chapter 2. However the resolution obtained was not sufficient to clearly distinguish between bone and cartilage, noting that the IR spectrum of the decalcified bone was dominated by CI which is almost identical to that of CII in the cartilage. To obtain the required resolution to clearly distinguish between bone and cartilage subsequent experiments were conducted using the IR beamline at the Australian Synchrotron, and these are the results reported in this chapter.

For synchrotron analysis, an overview image of the unstained mouse paw was first collected to select the joints of interest (**Figure 3.2**). Chemical changes within selected joints were examined using two different methods. First, ten single point spectra were selected from the chondrocytes and from the cartilage matrix close to the cartilage surface in the area of direct mAb penetration and then from the chondrocytes and cartilage deeper in the joints (40 single point spectra in total). Secondly large maps (grids) were overlaid in selected areas of the joints to encompass spectra from the bone, cartilage and chondrocytes. An overview image, example of selection of single point spectra and grids obtained from the IR beamline at the Australian Synchrotron are shown in **Figure 3.2**.

The results of FTIRM analysis are presented in the following manuscript.

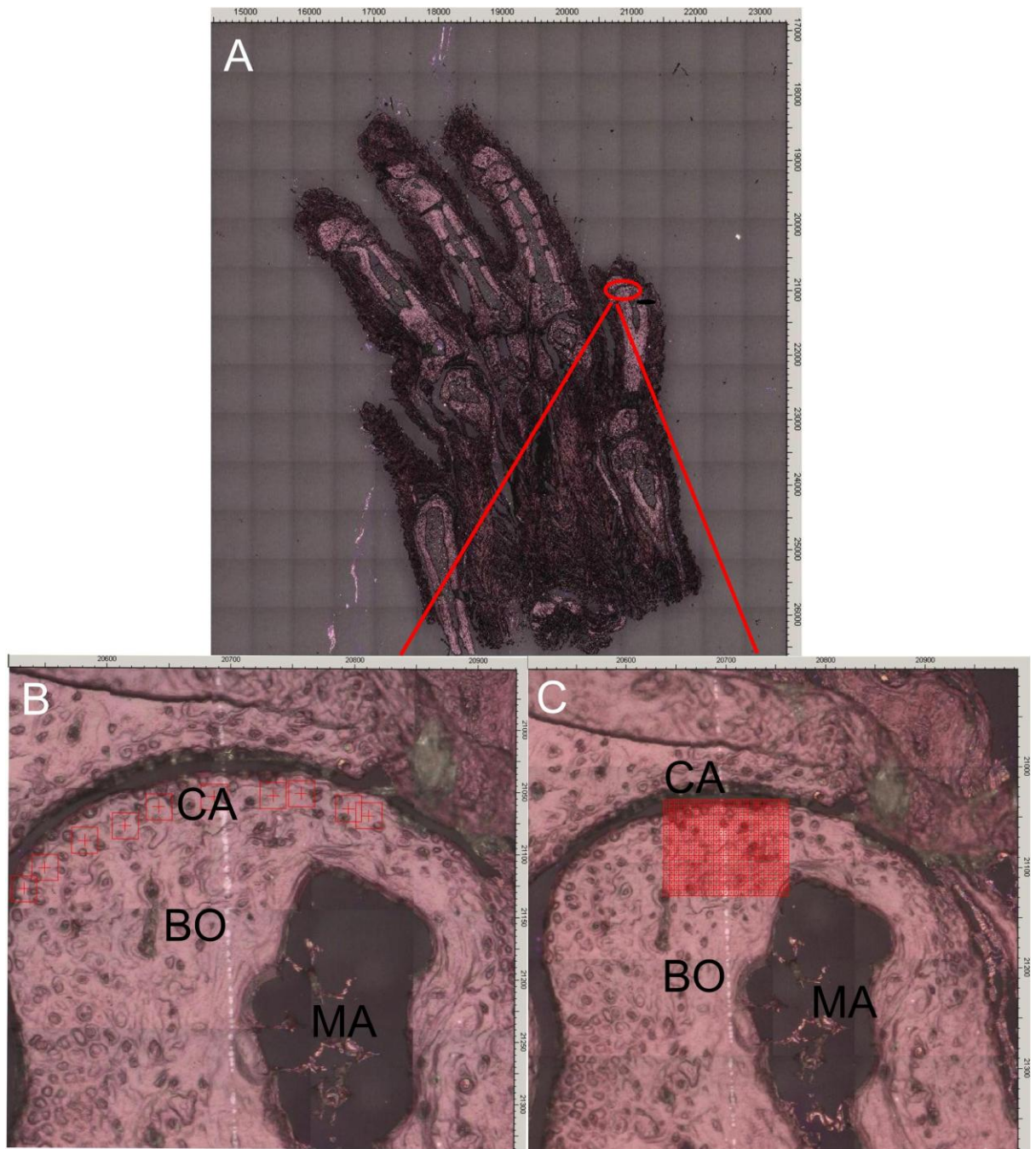


Figure 3.2. Light images of unstained control mouse paw showing an overview image **(A)**, image highlighting the location of selection of single point spectra of cartilage matrix close to the surface (centre of cross) **(B)** and **(C)** image showing overlay of grid of interest encompassing cartilage, bone and chondrocytes. BO represents bone, CA is cartilage and MA shows the marrow cavity. Note: The selected single point spectra are not to scale.

Chemical changes demonstrated in cartilage by synchrotron infrared microspectroscopy in an antibody-induced murine model of rheumatoid arthritis

Allyson M. Croxford,^{a,b} Kutty Selva Nandakumar,^c Rikard Holmdahl,^c Mark J. Tobin,^d Don McNaughton,^b and Merrill J. Rowley^a

^aMonash University, Department of Biochemistry and Molecular Biology, Clayton, Victoria, Australia

^bMonash University, Centre for Biospectroscopy and School of Chemistry, Clayton, Victoria, Australia

^cKarolinska Institute, Medical Inflammation Research, MBB, Stockholm, Sweden

^dAustralian Synchrotron, Clayton, Victoria, Australia

Abstract. Collagen antibody-induced arthritis develops in mice following passive transfer of monoclonal antibodies (mAbs) to type II collagen (CII) and is attributed to effects of proinflammatory immune complexes, but transferred mAbs may react directly and damagingly with CII. To determine whether such mAbs cause cartilage damage *in vivo* in the absence of inflammation, mice lacking complement factor 5 that do not develop joint inflammation were injected intravenously with two arthritogenic mAbs to CII, M2139 and CIIC1. Paws were collected at day 3, decalcified, paraffin embedded, and 5- μm sections were examined using standard histology and synchrotron Fourier-transform infrared microspectroscopy (FTIRM). None of the mice injected with mAb showed visual or histological evidence of inflammation but there were histological changes in the articular cartilage including loss of proteoglycan and altered chondrocyte morphology. Findings using FTIRM at high lateral resolution revealed loss of collagen and the appearance of a new peak at 1635 cm^{-1} at the surface of the cartilage interpreted as cellular activation. Thus, we demonstrate the utility of synchrotron FTIRM for examining chemical changes in diseased cartilage at the microscopic level and establish that arthritogenic mAbs to CII do cause cartilage damage *in vivo* in the absence of inflammation. © 2011 Society of Photo-Optical Instrumentation Engineers (SPIE). [DOI: 10.1117/1.3585680]

Keywords: synchrotron Fourier-transform infrared microspectroscopy; cartilage; monoclonal antibodies; collagen antibody-induced arthritis; type II collagen.

Paper 10568RR received Oct. 21, 2010; revised manuscript received Mar. 29, 2011; accepted for publication Apr. 11, 2011; published online Jun. 1, 2011.

1 Introduction

Collagen-induced arthritis (CIA) is an animal model of human rheumatoid arthritis (RA) induced by immunization with type II collagen (CII), the most abundant protein in the cartilage.^{1–4} Autoantibodies to CII occur in both CIA and RA, and intravenous injection of particular monoclonal antibodies (mAbs) to CII can induce arthritis in naïve mice.^{5–8} This passively transferred collagen antibody-induced arthritis (CAIA) develops within two to four days, depending on the genetic background of the mice, although a further injection of lipopolysaccharide may be required for enhanced incidence and severity. Mice injected with the mAbs develop swollen joints with an influx of inflammatory and synovial cells into the joint cavity, and accompanying cartilage degradation. It is a highly efficient model of inflammatory arthritis that is used widely, commercially, to assess the efficiency of potential anti-inflammatory drugs.

CAIA is generally considered to result from an inflammatory response to immune complexes of antibody and CII formed on the surface of the joint as mice that are unable to develop an inflammatory response do not develop macroscopic arthritis, and the cartilage degradation has been attributed to the action of

degradative enzymes released by the inflammatory cells. However, we have previously shown using *in vitro* systems based on cartilage explants, that two mAbs to CII, M2139 and CIIC1, which are arthritogenic *in vivo*^{7,8} adversely affect the cartilage matrix integrity and cause changes to the chemical structure of the cartilage as measured by Fourier-transform infrared microspectroscopy (FTIRM), including loss of proteoglycans, and progressive denaturation and loss of collagen from the surface where the antibodies penetrated.⁹ These changes occurred *in vitro* in the absence of any inflammatory cells, but their significance *in vivo* remained unclear.

Articular cartilage is an avascular tissue that consists of sparsely located individual chondrocytes in an abundant extracellular matrix (ECM), which represents ~95% of the cartilage tissue volume.¹⁰ The ECM comprises a network of collagen fibers, mainly CII, in which are enmeshed a variety of sulphated glycoproteins, particularly aggrecan and the unsulphated glycosaminoglycan hyaluronan.^{10,11} Collagen, primarily CII, comprises approximately 10–20% of the wet weight of the cartilage¹⁰ and provides the tensile strength of the cartilage matrix.^{10,12} These interactions are essential for the structural stability of cartilage, and we postulate that arthritogenic mAbs cause cartilage damage by binding specifically to critical structural regions on collagen fibrils that are sites of interaction between CII and matrix components or chondrocytes. If so, such

Address all correspondence to: Merrill J Rowley, Department of Biochemistry and Molecular Biology, Monash University, Wellington Road, Clayton Vic 3800 Australia. Tel: +61 3 9905 1438; Fax: +61 3 9905 3726; E-mail: Merrill.Rowley@monash.edu.

damage should be also detectable *in vivo*, in the absence of inflammation.

In the present study, we examined whether the mAbs M2139 and CIIC1 cause direct damage *in vivo* to the cartilage matrix in the absence of any inflammation, following injection of mice that lack complement factor C5, and hence are resistant to the development of inflammatory arthritis with these mAbs. Because of a lack of other appropriate biochemical or histological techniques, synchrotron FTIR-microspectroscopy was used to provide the lateral resolution necessary to examine changes to the cartilage matrix and cells in the small distal interphalangeal joints in the presence of mAbs without any prior knowledge of the chemical changes occurring.

2 Materials and Methods

2.1 Monoclonal Antibodies

The mAbs used were derived from hybridomas developed from CII-immunized mice as described previously.⁸ Briefly, hybridomas were cultured in CL-1000 flasks (Integra Biosciences, Wallisellen, Switzerland) using Dulbecco's Glutamax-I medium containing ultralow bovine IgG (Gibco BRL, Invitrogen AB, Stockholm, Sweden). Antibodies were purified using γ -Bind Plus affinity gel matrix (GE Healthcare Bio-Sciences AB, Uppsala, Sweden). The IgG content was determined from the weight of freeze-dried preparations. The antibody solutions were sterile filtered and stored at -80°C until used. M2139 and CIIC1 are arthritogenic mAbs that bind to separate well-defined conformational epitopes within the helical region of the collagen molecule, at the J1 epitope, amino acids 551–564 for M2139 and the C1¹ epitope, amino acids 359–363 for CIIC1.

2.2 Injection of Arthritogenic mAbs into Mice

To determine whether the arthritogenic mAbs cause cartilage damage *in vivo* in the absence of inflammation, paws were examined from mice three days after intravenous injection with a mixture of the two mAbs, M2139 and CIIC1 in phosphate-buffered saline (PBS) pH 7.4. Four mice from two strains were used: B10.Q mice that develop CAIA but require a further injection of lipopolysaccharide for enhanced incidence and severity of arthritis⁷ and B10.Q C5-congenic mice that lack complement factor C5 (C5 δ) and hence do not develop CAIA.¹³ C5 δ congenic mice were generated using the speed congenic technique.¹⁴ The congenic fragment from non-obese diabetic mice (NOD) in the B10.Q genetic background was ~ 54 Mb, ranging from D2Mit116 to D2Mit91. None of the mice used in this study developed macroscopic arthritis by day 3. The mixture of M2139 and CIIC1 contained 4.5 mg of each of the sterile-filtered antibody solutions in a final volume of 0.4 ml. Mice of the same strains injected with PBS alone were used as controls. Mice were killed at day 3 after injection, and paws were fixed in 4% phosphate-buffered paraformaldehyde solution for 24 h, decalcified for three to four weeks in an ethylenediaminetetraacetic acid-polyvinylpyrrolidone-Tris solution (pH 6.9), dehydrated, and embedded in paraffin using standard protocols for processing for histology and for synchrotron FTIRM.

2.3 Examination of the Cartilage

2.3.1 Histology

To examine the cartilage in the small joints, the paws of the mice were sectioned to a depth that allowed examination of both the bone and the cartilage surface within the joints. Then, 5- μm sections were stained with haematoxylin and eosin (H&E) to examine the appearance and integrity of the cartilage and chondrocytes, or with toluidine blue to examine proteoglycan loss. The thickness of the cartilage in various joints was measured using MCIDTM Image Analysis Software (M4 3.0 Rev 1.1, Imaging Research Inc., St. Catharines, Ontario, Canada). Images were captured at 200 \times magnification on H&E stained sections, and the autoselect tool was used to designate and create a line at the bone-cartilage junction. Using the two-point straight-line measurement tool, the distance of loss was measured from the edge of the tissue, through to the line created by the autoselect tool. The measurement was performed six times on each image captured.

2.3.2 Fourier-transform infrared microscopy

For examination by synchrotron FTIRM, 5- μm sections of paraffin-embedded tissue were placed onto MirrIR low-e microscope slides (Kevley Technologies, Chesterland, Ohio). To obtain the requisite resolution, measurements were performed on the IR beamline at the Australian Synchrotron (Melbourne, Victoria, Australia). Spectra were collected with a Bruker Hyperion 2000 IR microscope (Bruker Optik GmbH, Ettlingen, Germany) equipped with a liquid-nitrogen-cooled narrowband HgCdTe (MCT) detector with a 36 \times (0.5 NA) IR objective. The Hyperion 2000 microscope is coupled to a Bruker Vertex 80 spectrometer. For FTIR mapping and single-point measurements, the aperture was set at 5 \times 5 μm . For each sample examined, single-point measurements and spectral maps (grids) were collected in transmittance mode by scanning the computer-controlled microscope stage in a raster pattern with a 5- μm step size in both the x and y directions for the maps.

Because the mAbs bind to the cartilage surface^{8,15,16} for each joint examined, 10 single-point spectra were collected from chondrocytes close to the cartilage surface and 10 spectra were collected from the cartilage matrix between the cells at the surface. Similarly, 10 spectra were collected from chondrocytes and the cartilage matrix deeper within the cartilage, to compare changes associated with direct mAb penetration at the cartilage surface and changes beyond the area of direct mAb penetration. Single-point spectra were examined using OPUS 6.5 spectroscopic software (Bruker, Germany), where second-derivative spectra were used to enable the spectral resolution of bands that contribute to either inflection points or shoulders in the original spectrum¹⁷ while also greatly reducing the contribution of sloping baselines observed in some absorbance spectra.

Grids were defined over the distal interphalangeal joints that encompassed regions of the cartilage surface and included the bone beyond the cartilage surface. The spectra obtained from the grids were analyzed using CytoSpec (CytoSpec, Inc., Berlin, Germany), performing unsupervised hierarchical cluster analysis (UHCA)¹⁸ to generate false color maps based on spectral variation. UHCA is a multivariate approach to analyzing a data set of spectra collected from tissue by FTIRM and has been well

described in literature.^{18–20} It provides an objective means for determining variations in the tissue without any prior knowledge of changes that may be occurring. A “quality test” was performed to remove spectra with poor signal-to-noise ratios and spectra of very high or low absorbance and analysis was directed toward the spectral region $940\text{--}1800\text{ cm}^{-1}$, where the major macromolecular spectral bands appear. Spectra at the tissue periphery that showed dispersion effects and hence confound analysis of the amide bands were also removed.

Because the major components of the cartilage matrix are collagen, sulphated proteoglycans, and the nonsulphated glycosaminoglycan hyaluronan, analysis was directed particularly to the location of the amide I peak ($1640\text{--}1670\text{ cm}^{-1}$), representing total protein and to peaks within the region of $960\text{--}1175\text{ cm}^{-1}$ derived from carbohydrate moieties.⁹ The amide I peak for native triple helical collagen is unusual, being $>1660\text{ cm}^{-1}$, compared to most other proteins for which the peak is $\sim 1650\text{ cm}^{-1}$, and there is a characteristic shift to lower wavenumber on denaturation.^{21–24} The “collagen triplet” of peaks at 1203 , 1234 , and 1280 cm^{-1} often used to identify collagen in other tissues is of limited utility in the analysis of cartilage, as it overlaps the peak at $1240\text{--}1245\text{ cm}^{-1}$ derived from sulphates,^{22,25} which are a major component of the highly sulphated glycosaminoglycans of the cartilage matrix. For the analysis of chondrocytes, particular attention was paid to bands in the second-derivative spectra that could be attributed to nuclear deoxyribose nucleic acid (DNA), or ribonucleic acid (RNA), which may be increased in activated cells. These include bands at 1240 and 1080 cm^{-1} attributed to the asymmetric and symmetric phosphate stretching vibrations ($\nu_{\text{as}}\text{PO}_2^-$ and $\nu_{\text{s}}\text{PO}_2^-$) of cellular nucleic acids, bands at 1050 and 1015 cm^{-1} characteristic of ribose sugars, and a band at 970 cm^{-1} , characteristic of phosphodiester main chain vibrations.¹⁷ An important component of this study was the need for optimum lateral resolution and careful comparison of the visual images to localize the IR spectra obtained, to examine the chondrocytes, and to discriminate the cartilage from bone, noting that the major protein in decalcified bone is type I collagen, which has an almost identical IR spectrum to that of the type II collagen in cartilage.

3 Results

3.1 Histology of Joints

Sections of paws from mice treated with mAbs and from control mice were examined by light microscopy. Whereas the cartilage surface in the joints of control mice was smooth, shown by H&E staining [Fig. 1(a)] and the proteoglycans stained strongly with toluidine blue [Fig. 1(c)], the cartilage of mice of both strains treated with the mAbs showed considerable variability in appearance [Fig. 1(b) and 1(d)]. Unlike the cartilage surface in the control mice, the cartilage surface in the mice treated with mAbs was often uneven, with cells protruding from the cartilage surface [Fig. 1(b)]. There was a dramatic reduction in the intensity of staining of proteoglycans in the majority of joints, particularly in the small distal interphalangeal joints where there were cells protruding from the cartilage surface and dark “ringing” of stain around the cells suggestive of new proteoglycan synthesis [Fig. 1(d)]. By MCID analysis of 17 distal interphalangeal joints from six mice of the two strains

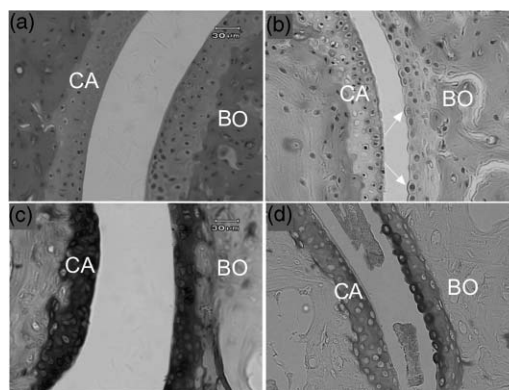


Fig. 1 Histological sections through joints from control and mAb-treated mice showing the cartilage: (a) Control joint stained with H&E, showing a smooth cartilage surface; (b) joint from mAb-treated mouse stained with H&E, showing an uneven cartilage surface, due to cells protruding from the cartilage surface; (c) control joint stained with toluidine blue to show dark, uniform staining of proteoglycans; and (d) joint from mAb-treated mouse stained with toluidine blue, showing loss of proteoglycan staining and dark “ringing” of stain around protruding surface chondrocytes. All images in this figure are on the same scale. CA: cartilage, BO: bone, arrows indicate protruding chondrocytes.

treated with mAb, the cartilage that showed these “protruding” cells was significantly thinner than cartilage from joints in which the surface remained smooth (mean \pm standard deviation, 33 ± 7 versus $49 \pm 6\ \mu\text{m}$, $p = 0.004$), suggesting that there was loss of matrix from the cartilage surface. The changes following mAb injection were similar in both strains of mice tested.

3.2 Synchrotron FTIRM Analysis of the Cartilage: Comparison of Chondrocytes and Matrix

Single-point spectra of the cartilage matrix were compared from interphalangeal joints from mAb-treated mice and from control mice. For both groups, the averaged absorbance spectra after baseline correction were very similar and characteristic of cartilage [Fig. 2(a)], but the groups differed in two characteristics. First, there was a substantial decrease in absorbance in peaks of $<1500\text{ cm}^{-1}$, including the peak at $1240\text{--}1245\text{ cm}^{-1}$ derived from sulphates and peaks within the region $960\text{--}1175\text{ cm}^{-1}$ derived from carbohydrate moieties; these changes were consistent with the loss of proteoglycans shown by histological staining in treated mice. Second, there was a shift in location of the amide I peak, from 1670 to 1656 cm^{-1} in the mAb-treated mice, taken to represent collagen denaturation. Spectra from the chondrocytes were very similar to those from the matrix in both groups, and no peaks could be identified that occurred only in the chondrocytes.

Individual spectra were further analyzed using second-derivative analysis to assign bands. Overall, spectra from both chondrocytes and matrix were very similar and the proteoglycan loss identified by toluidine blue staining and seen in the underivatized spectra was not apparent using second-derivative spectra, suggesting that the proteoglycan loss was not associated with any major changes in those components. Moreover, second-derivative spectra from the chondrocytes did not show any bands that could be unequivocally assigned to nucleic acid bands of either DNA or RNA.

Chapter 3: Research Paper 2

Croxford et al.: Chemical changes demonstrated in cartilage by synchrotron...

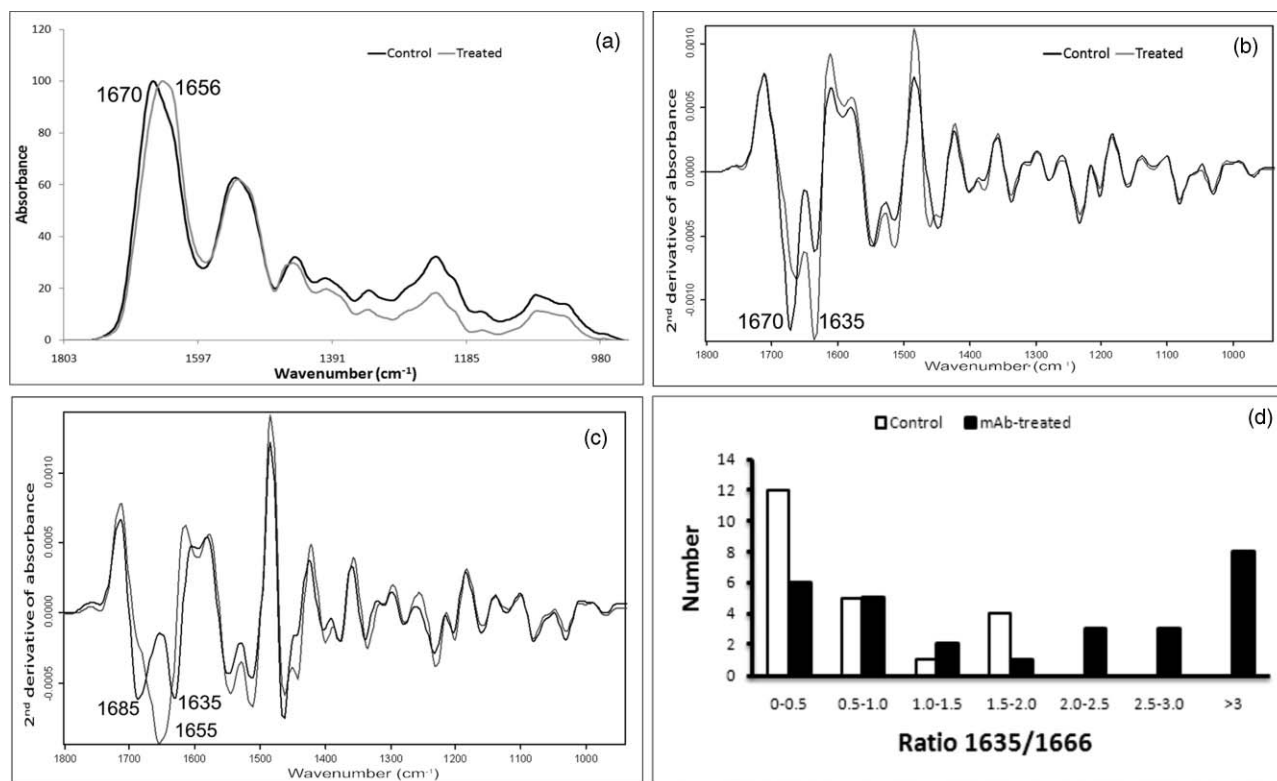


Fig. 2 Patterns of spectra from control and mAb-treated mice: (a) Mean absorbance spectra from matrix from control mice and a mAb-treated mouse after background correction and normalization based on the Amide I peak; (b) mean second-derivative spectra from the same mice, showing the most frequently seen pattern with two bands at 1666–1670 cm^{-1} and at 1635–1637 cm^{-1} ; (c) uncommon patterns of second-derivative spectra, a single peak at 1655 cm^{-1} corresponding to an underivatized absorbance peak in the same position (light gray) or two peaks with a marked shift of one to 1685 cm^{-1} (black); and (d) differing distribution of spectra of control mice and mAb-treated mice according to ratios 1635/1666 calculated based on the value of the minima in second-derivative spectra.

The major differences in the second-derivative spectra were in the amide I region, $>1600 \text{ cm}^{-1}$. In $>90\%$ of all spectra, two bands were identified as components of the amide I peak, one in the region of $1660\text{--}1670 \text{ cm}^{-1}$ and a second at $1635\text{--}1637 \text{ cm}^{-1}$ [Fig. 2(b)]. The band at $1635\text{--}1637 \text{ cm}^{-1}$ could be identified as a shoulder on the amide I peak in the underivatized spectrum, and an increase in its intensity when compared to the $1660\text{--}1670 \text{ cm}^{-1}$ band, which corresponded to a shift in the amide I peak to a lower wavenumber in the original spectrum. This pattern was seen in $>90\%$ of all individual spectra from either matrix or chondrocytes, and either control or mAb-treated mice, but there were differences in the relative intensity of the two bands according to the source of the spectrum.

Two further patterns of bands in the amide I region also occurred infrequently [Fig. 2(c)]. In one, the band at $1660\text{--}1670 \text{ cm}^{-1}$ was replaced by a band at $1680\text{--}1685 \text{ cm}^{-1}$, often with a small band at $1635\text{--}1637 \text{ cm}^{-1}$. In the other, there was a band around 1654 cm^{-1} , usually alone, but sometimes associated with bands at $1666\text{--}1670$ and/or 1635 cm^{-1} , and seen as an amide I peak in the underivatized spectrum at $\sim 1655 \text{ cm}^{-1}$. This pattern was rare in the mouse spectra but corresponded to spectra we have attributed to collagen denaturation in cartilage explants treated with the mAbs *in vitro*.^{9,26} These two patterns of bands occurred too rarely for analysis, but may provide information about the secondary structure of the collagen matrix

(see Sec. 4). In a preliminary experiment, a ratio 1635/1666 was calculated from the value of minima in the second-derivative spectra at each wavenumber for 22 surface-located cells from control mice and 28 cells from mAb-treated mice [Fig. 2(d)]. The mean ratio 1635/1666 for the control cells was 0.65 (range 0–2), which was significantly lower than 3.4 (range 0.12–11) for the mAb-treated cells ($p < 0.001$, Mann-Whitney U test). Overall, only 5 of the 22 second-derivative spectra from control mice showed a ratio 1635/1666 > 1 , compared to 19 of 28 of the spectra from mAb-treated mice ($p = 0.0015$, χ^2). Because ratios > 1 were readily identified from individual second-derivative spectra, in all further analysis results have been expressed as the number in each group > 1 .

Table 1 and Fig. 3 show the results of analysis of cells or matrix that showed the common pattern of reactivity in controls and mAb-treated mice. For the control mice, the spectra differed little between the surface and deep in the cartilage [Fig. 3(a) and 3(c)]. The spectra from the mAb-treated mice were more variable, and there were differences between the spectra derived at the cartilage surface and deep within the cartilage, particularly for the chondrocytes [Fig. 3(b) and 3(d)]. The major spectral changes in the treated mice were seen in the amide I region, $>1600 \text{ cm}^{-1}$; although in all cases, loss of peak height was clearly apparent in the nonderivatized spectra (data not shown). At or near the cartilage surface, the band at 1635 cm^{-1} was prominent in all spectra and, for the chondrocytes, this band

Chapter 3: Research Paper 2

Croxford et al.: Chemical changes demonstrated in cartilage by synchrotron...

Table 1 Relative prominence of second-derivative bands in the amide 1 region at 1635 and 1666 cm^{-1} for cells and matrix from mAb-treated and control mice.

	mAb-treated (n = 8 mice)	Control (n = 3 mice)	p (χ^2)
Surface cells			
Spectra examined	106	30	
Ratio > 1	57 (54%) ¹	9 (30%)	0.0214
Mean ratio ²	1.3	0.55	
Surface matrix			
Spectra examined	69	30	
Ratio > 1	24 (35%)	4 (13%)	0.0199
Mean ratio	1.7	0.32	
Deep cells			
Spectra examined	80	30	
Ratio > 1	8 ³ (10%)	0 (0%)	ns
Mean ratio	1.7	0.13	
Deep matrix			
Spectra examined	80	30	
Ratio > 1	0 (0%)	0 (0%)	ns
Mean ratio	0.02	0.04	

1. Number (%) of individual spectra in which 1635 cm^{-1} was the major band (ratio > 1).
 2. Ratio 1635/1666 based on the value of the minima in the mean second-derivative spectrum.
 3. From a single mouse.
- ns: Not significant.

was often stronger than the band at 1666 cm^{-1} (Table 1). Thus, for 106 surface chondrocytes examined from eight mAb-treated mice, the mean ratio 1635/1666 bands for the treated mice was 1.25 (range 0.36–3.3), compared to 0.55 (range 0.08–1.2) for 28

chondrocytes from three control mice, and the 1635 cm^{-1} was the major band in significantly more of the mAb-treated mice (57/106, 54% versus 9/30, 30% $p = 0.0214$, χ^2). Deeper in the cartilage, the spectra for both chondrocytes and matrix were similar to those of controls and, the band at 1635 cm^{-1} seen at the surface, was noticeably reduced (mean ratio 1635/1666, 0.038, range 0.038–0.068).

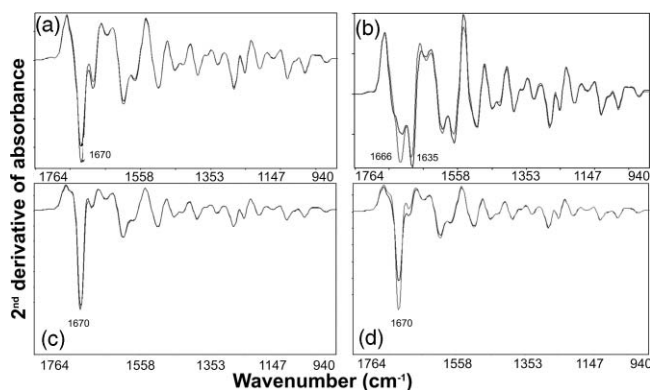


Fig. 3 Representative single point synchrotron FTIRM spectra collected from control and mAb-treated mice, comparing the spectra obtained from the chondrocytes and from the cartilage matrix at the edge of the cartilage (a,b) and deeper in the cartilage (c,d). The bold line represents the chondrocytes and the pale line indicates cartilage matrix. (a) Spectra at the cartilage surface in a control mouse, (b) spectra at the cartilage surface in an mAb-treated mouse, (c) spectra deeper in the cartilage in a control mouse, and (d) spectra deeper in the cartilage in an mAb-treated mouse.

3.3 Unsupervised Hierarchical Cluster Analysis of the Cartilage

Spectral maps spanning from the cartilage surface through to the bone in the distal interphalangeal joints were collected and examined using UHCA on either standard spectra or second-derivative spectra. Despite using varying numbers of clusters and performing a quality test to eliminate poor quality spectra, UHCA did not clearly distinguish between the bone and the cartilage, and spectra collected from control mice were very similar across the entire grid (Fig. 4), noting that the characteristic bands representing mineralization of the bone have been removed by decalcification. The major amide I band in each cluster was located above 1660 cm^{-1} , characteristic of collagen, whether the type II collagen in the cartilage, or the type I collagen of bone, and there were bands at 1203, 1234, and 1280 cm^{-1} that could be ascribed to the “collagen triplet.” In several joints from the control mice, cluster analysis discriminated a cluster

Chapter 3: Research Paper 2

Croxford et al.: Chemical changes demonstrated in cartilage by synchrotron...

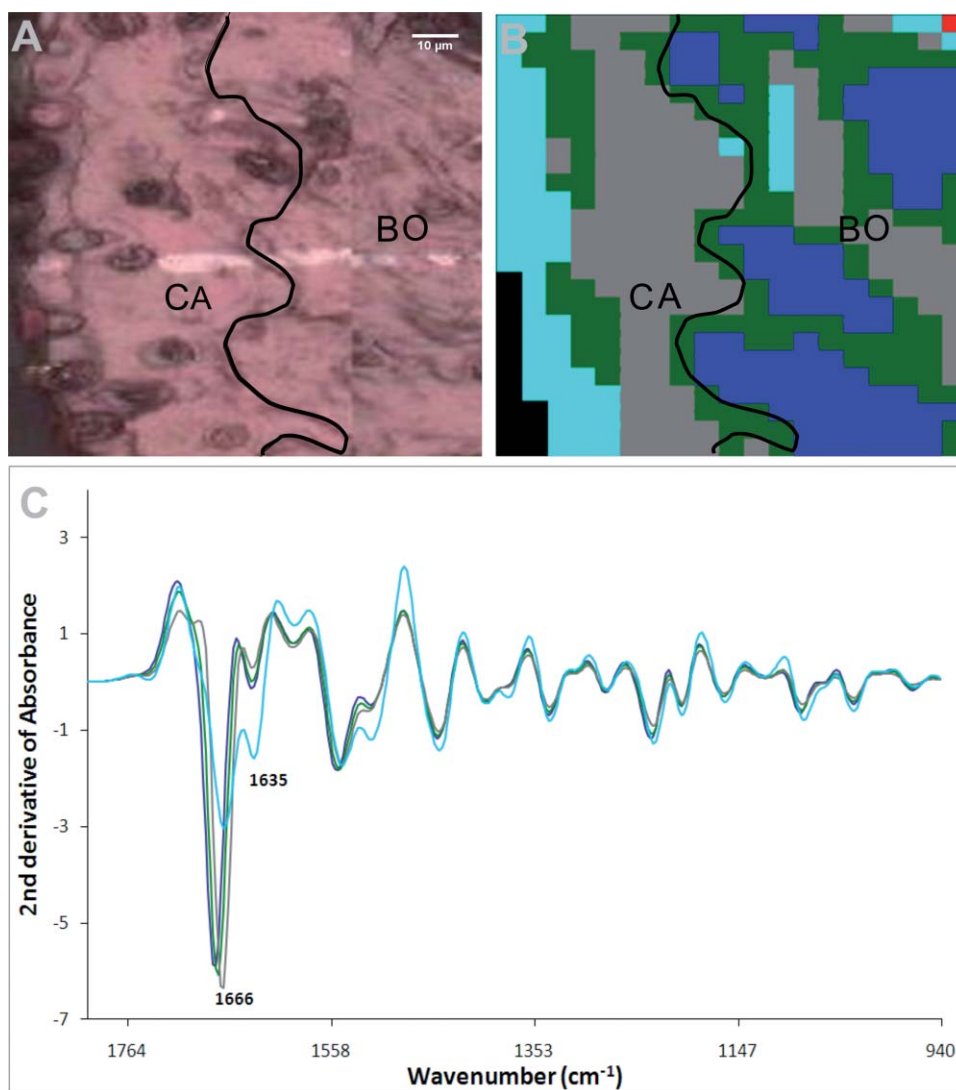


Fig. 4 Representative result obtained by synchrotron FTIRM on a grid from a control mouse. (a) Light microscopy image of unstained section on Kevley reflective slide. CA: cartilage, BO: bone, \blacktriangledown cartilage border. (b) IR image processed by UHCA over the range 940–1800 cm^{-1} using second-derivative spectra with five clusters. (c) Second-derivative spectra for the clusters, corresponding to the image in (b), showing a band at 1635 cm^{-1} in the cluster corresponding to the cartilage surface (1635/1666 ratio 0.5, based on peak height). Pixels of poor quality were excluded from analysis. Original magnification of (a) and (b) are $\times 200$.

localized to a surface layer of the cartilage that contained a relatively high proportion of chondrocytes in which the amide I band at 1666 cm^{-1} was reduced and the minor band at 1635 cm^{-1} was prominent (Fig. 4).

The grids collected from the mice treated with mAbs were more complex. Overall spectra showed more “noise” at the cartilage surface, leading to loss of pixels, when quality tested for UHCA, and clusters at the cartilage surface were often uninformative. Figure 5 shows the results obtained from a representative mouse paw. In this sample, close to the surface, the amide I band at 1666 cm^{-1} was markedly reduced and considerably smaller than the band at 1635 cm^{-1} .

4 Discussion

This study examined the histological and chemical changes by synchrotron FTIRM in the cartilage of paws from mice injected

with two mAbs to CII, M2139, and CIIC1, which can induce arthritis.^{7,27} Until day 3, when samples were collected, none of the mice transferred with mAb showed macroscopic joint swelling or histological evidence of any infiltrating inflammatory cells. Nonetheless, there was clear histological damage to the cartilage, including proteoglycan loss and cartilage thinning in the small joints, and matrix changes identified by synchrotron FTIRM that included loss of the 1660 cm^{-1} amide I band characteristic of native CII and the appearance of an unidentified band at 1635 cm^{-1} in both the complement factor C5 sufficient and deficient mice. These results provide clear evidence that the mAbs that cause the cartilage damage *in vitro*^{9,26} also have damaging effects on the cartilage *in vivo* in the absence of inflammation.

In contrast to our previous studies using the cartilage explants *in vitro*^{9,26} in which the shift in the position of the amide I band to below 1660 cm^{-1} in absorbance spectra was accompanied

Chapter 3: Research Paper 2

Croxford et al.: Chemical changes demonstrated in cartilage by synchrotron...

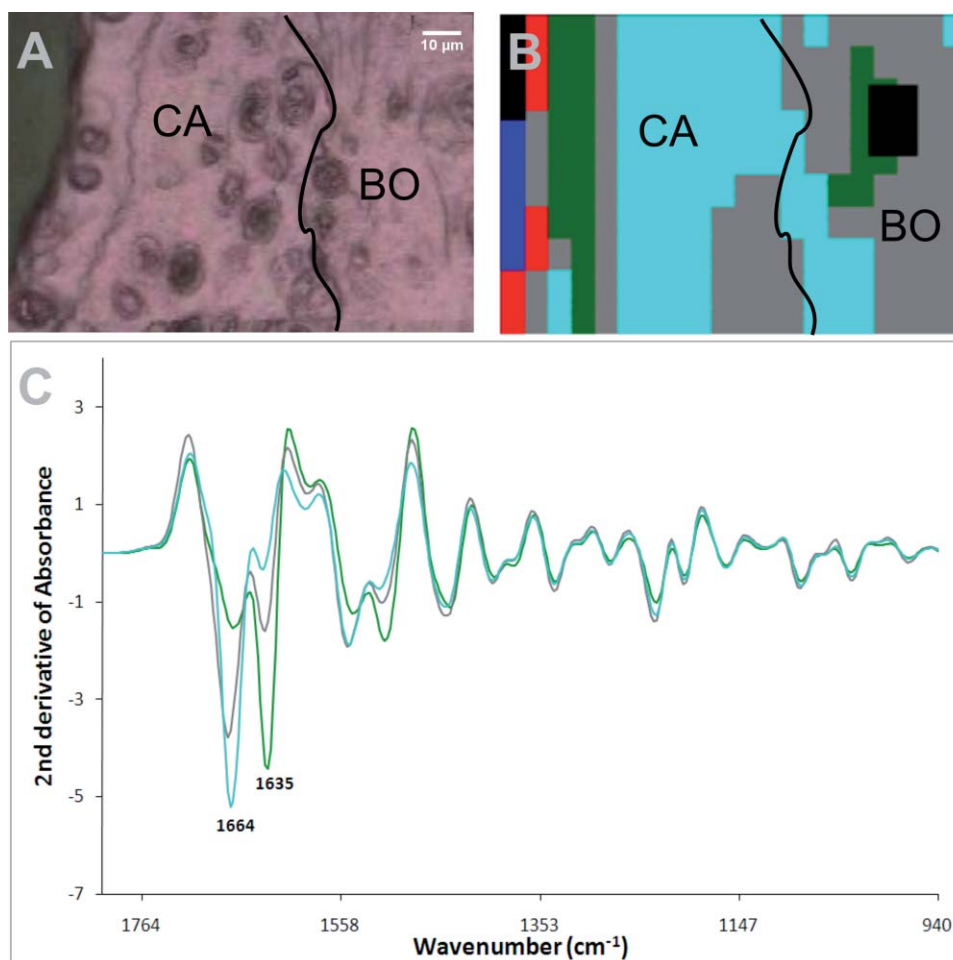


Fig. 5 Representative result obtained by synchrotron FTIRM on a grid from a mouse injected with two mAb. (a) Light microscopy image of unstained section on Kevley reflective slide CA: cartilage, BO: bone, \curvearrowright cartilage border. (b) IR image processed by UHCA over the range 940–1800 cm^{-1} using second-derivative spectra for the clusters with five clusters. (c) Second-derivative spectra for the clusters, corresponding to the image in (b). Pixels of poor quality were excluded from analysis. At the cartilage surface the band at 1635 cm^{-1} was more prominent than the band at 1664 cm^{-1} (1635/1664 ratio 3.1). Original magnification of (a) and (b) are $\times 200$.

by a similar shift in second-derivative spectra in the cartilage cultured with mAbs, this shift representative of collagen denaturation was much less prominent *in vivo*. Instead, there was evidence of complete loss of collagen, seen as a decrease in the strength of the amide I band, particularly at the cartilage surface, and measurable thinning of the cartilage. This may represent differences in the processing of denatured collagen in the tissue *in vivo* and *in vitro*. Although native collagen is highly resistant to degradation by proteases other than collagenases, denatured collagen is readily degraded by a variety of enzymes. *In vivo*, denatured collagen would be rapidly removed by various matrix metalloproteinases (MMPs) not only by the gelatinases MMP-2 and 9,²⁸ but also by MMP-3 (stromelysin-1), which by degrading the pericellular extracellular matrix components further activates the cartilage-degrading enzymes such as proMMP-1, proMMP-9, and proMMP-13²⁹ with the result that there is complete loss of matrix. By contrast, *in vitro*, these enzymes may be less abundant, leading to less rapid removal of the denatured collagen and, hence, its appearance in spectra.

Despite the use of the high lateral resolution of the synchrotron to examine the spectra of the chondrocytes, the spectra obtained from both the chondrocytes and matrix were very sim-

ilar. The abundance of the ECM means that the IR spectrum of cartilage primarily represents its major components, particularly CII, with little contribution from cellular components such as DNA, RNA, or other proteins. Because chondrocytes are the cells that synthesize, assemble, and secrete the components of the ECM,¹² these components are likely to contribute to the cellular spectra also.

A major difference from previous *in vitro* studies was the appearance of a band at 1635 cm^{-1} that appeared as a shoulder on the amide I band in the nonderivatized spectra. This was distinct from the shift in the amide I peak we have previously observed in the cartilage explant cultures,^{9,26} and attributed to collagen denaturation,^{30–32} and the two bands could be discriminated in second-derivative spectra. Moreover, as spectra at the tissue periphery that showed dispersion effects were removed, and a similar band was occasionally seen deep in the tissue, this distinct peak could not be explained by a shift of the amide I band resulting from scattering effects close to the edge of tissue samples, as has been reported elsewhere.³³ In some mAb-treated mice, the band at 1635 cm^{-1} was the dominant band in the spectrum at the cartilage surface. The nature of this peak is unknown, but a similar peak has been associated with

living chondrocytes in cartilage explants and may be associated with matrix regeneration.²⁶ In the mouse cartilage where the 1635-cm⁻¹ band occurred, surface chondrocytes often showed evidence of proteoglycan synthesis, seen as ringing in the toluidine blue-stained sections. In healthy cartilage, the turnover of the matrix is normally very slow and the half-life of CII in adult cartilage has been estimated to be 1000 days,¹¹ although there is some loss and repair of the ECM evidenced by turnover of proteoglycans, particularly aggrecan, at the joint surface, and this is increased following damage.^{11,34} Taken together, these results suggest that the 1635-cm⁻¹ band is a marker of activated chondrocytes in the cartilage.

Although the 1635 cm⁻¹ band was associated with regions that contain activated chondrocytes in the mouse cartilage, it has not been conclusively identified. Despite the heightened resolution obtained by use of synchrotron radiation, it appeared in both the spectra of chondrocytes and also extracellularly. The major protein of the cartilage is CII, a fibril forming collagen synthesized by chondrocytes, and comprising three α -helical polypeptide chains twisted tightly into a right-handed triple helix to form a ropelike structure stabilized by strong covalent bonds.^{10,12} The amide I peak of this collagen helix is characteristically above 1658–1660 cm⁻¹, appearing in deconvoluted or second-derivative spectra as three distinct bands at 1657–1661, 1630–37 cm⁻¹, and above 1670 cm⁻¹.^{23,31,32,35–37} These bands appear to be characteristic of a triple helix and also occur in other molecules that contain a collagen-like triple helix, including the nonfibrillar collagens that contain one or several small triple-helical domains interrupted by short nonhelical domains, and the complement component C1q that comprises a collagen-like triple helix at the N-terminus, with C-terminal globular heads.³⁸ In all these proteins, the band at 1657–61 cm⁻¹ is normally the strongest of the three. The 1635-cm⁻¹ band in the mouse cartilage could represent the 1630–37 cm⁻¹ band of the collagen triple helix, although it is unclear why it would be much stronger in the cartilage of the mAb-treated mice than in the control mice.

Alternatively, the 1635cm⁻¹ could represent the appearance of another band within the amide I region as a result of new protein synthesis. Bands below 1640 cm⁻¹ and particularly at 1637 cm⁻¹ are characteristic of β -strand secondary structures.^{39,40} Such structures may reflect marked increases in other unknown cartilage proteins, but they may also arise from collagen itself. Mature collagen fibrils are almost entirely triple helical in structure and hence are unlikely to contain significant β -strand secondary structures, but collagen precursors are synthesized with large C- and N-terminal extensions, which may contain β -sheet and β -turns. These extension propeptides are involved in the chain assembly necessary for the triple-helical formation that takes place within the cell prior to secretion and are cleaved by specific peptidases after secretion but prior to formation of fibrils in which the major structural unit is triple helical collagen.^{10,12} The fibrils of triple helical collagen are then aligned in a quarter-staggered array to form thicker fibrils and stabilized by cross-linking residues, including lysine. The IR spectrum of purified collagen derived by pepsin extraction reflects this triple helical secondary structure without any contribution from β -sheet structures, as pepsin cleavage removes any remaining nontriple-helical regions at the N- and C-terminus of the collagen but does not digest the triple helix itself.³⁸ However, in this study, the band at 1635 cm⁻¹ may rep-

resent β -secondary structures within the globular heads of newly synthesized collagen produced by activated chondrocytes, both within the cells and also in the matrix before fibril formation occurs. A similar change in the relative intensity of second-derivative spectra has been described for C1q where there is a strong band at 1637 cm⁻¹ for the intact molecule, taken to represent β -secondary structures within the globular domains, and only a weak band at 1661 cm⁻¹, representing the relatively low proportion of triple helix, whereas for the triple helical C1q stalks remaining after removal of the globular domains by pepsin digestion. The major band was at 1655 cm⁻¹ and assigned to the triple helical structure, with only a weak band at 1636 cm⁻¹.³⁸

Finally, this study illustrates the utility of IR microspectroscopy for examining chemical changes in cartilage by providing information that can only be deduced indirectly otherwise. In the absence of other markers of cartilage damage, the combination of standard histological analysis and FTIRM analysis should provide important new information in studies of arthritis and cartilage repair. By utilizing the higher lateral resolution available for infrared microspectroscopy at the Australian synchrotron, it has been possible to look at individual cells and areas of matrix in different joints, and at different depths in the cartilage, and to discern differences that cannot be measured by any currently available biochemical or histological techniques. We have demonstrated damage to the cartilage structure and matrix by mAbs to CII directly both *in vitro*²⁶ and in the current study *in vivo* in the absence of inflammation. Autoantibodies play an essential role in the pathogenesis of CIA and most likely also in RA.^{13,41} The exact mechanism and cause for the cartilage damage and destruction seen in RA is yet to be fully elucidated. However, these same antibodies to CII are present in RA and its murine model and may explain the cartilage damage that occurs in the human disease. Furthermore, understanding the direct damage caused by antibodies on target tissues without any major inflammatory events will stimulate further research in several antibody dependent immune pathologies.

Acknowledgments

We thank Ian Mackay and Senga Whittingham for helpful discussions and editorial comments. The work was supported by grants from the National Health and Medical Research Council of Australia, the Barbara Cameron Grant, and a project grant from Arthritis Australia, the Swedish Research Council, the Swedish Strategic Science Foundation, and the European Union Grant Masterswitch (Grant No. HEALTH-F2-2008-223404). Part of this research was undertaken on the Infrared Microspectroscopy beamline at the Australian Synchrotron, Victoria, Australia.

References

1. J. S. Courtenay, M. J. Dallman, A. D. Dayan, A. Martin, and B. Mosedale, "Immunisation against heterologous type II collagen induces arthritis in mice," *Nature* **283**, 666–668 (1980).
2. R. Holmdahl, M. Andersson, T. J. Goldschmidt, K. Gustafsson, L. Jansson, and J. A. Mo, "Type II collagen autoimmunity in animals and provocations leading to arthritis," *Immunol. Rev.* **118**, 193–232 (1990).
3. C. Steffen, "Consideration of pathogenesis of rheumatoid arthritis as collagen autoimmunity," *Z. Immunitätsforsch. Allerg. Klin. Immunol.* **139**, 219–227 (1970).

Chapter 3: Research Paper 2

Croxford et al.: Chemical changes demonstrated in cartilage by synchrotron...

4. D. E. Trentham, A. S. Townes, and A. H. Kang, "Autoimmunity to type II collagen an experimental model of arthritis," *J. Exp. Med.* **146**, 857–868 (1977).
5. K. Terato, K. A. Hasty, R. A. Reife, M. A. Cremer, A. H. Kang, and J. M. Stuart, "Induction of arthritis with monoclonal antibodies to collagen," *J. Immunol.* **148**, 2103–2108 (1992).
6. K. S. Nandakumar and R. Holmdahl, "Antibody-induced arthritis: disease mechanisms and genes involved at the effector phase of arthritis," *Arthritis Res. Ther.* **8**, 223–233 (2006).
7. K. S. Nandakumar, L. Svensson, and R. Holmdahl, "Collagen type II-specific monoclonal antibody-induced arthritis in mice: description of the disease and the influence of age, sex, and genes," *Am. J. Pathol.* **163**, 1827–1837 (2003).
8. R. Holmdahl, K. Rubin, L. Klareskog, E. Larsson, and H. Wigzell, "Characterization of the antibody response in mice with type II collagen-induced arthritis, using monoclonal anti-type II collagen antibodies," *Arthritis Rheum.* **29**, 400–410 (1986).
9. D. E. Crombie, M. Turer, B. B. Zuasti, B. Wood, D. McNaughton, K. S. Nandakumar, R. Holmdahl, M. P. Van Damme, and M. J. Rowley, "Destructive effects of murine arthritogenic antibodies to type II collagen on cartilage explants *in vitro*," *Arthritis Res. Ther.* **7**, R927–937 (2005).
10. E. E. Coates and J. P. Fisher, "Phenotypic variations in chondrocyte subpopulations and their response to *in vitro* culture and external stimuli," *Ann. Biomed. Eng.* **38**, 3371–3388 (2010).
11. H. Muir, "The chondrocyte, architect of cartilage: biomechanics, structure, function and molecular biology of cartilage matrix macromolecules," *Bioessays* **17**, 1039–1048 (1995).
12. K. E. Kuettner, "Biochemistry of articular cartilage in health and disease," *Clin. Biochem.* **25**, 155–163 (1992).
13. K. S. Nandakumar, E. Bajtner, L. Hill, B. Bohm, M. J. Rowley, H. Burkhardt, and R. Holmdahl, "Arthritogenic antibodies specific for a major type II collagen triple-helical epitope bind and destabilize cartilage independent of inflammation," *Arthritis Rheum.* **58**, 184–196 (2008).
14. A. C. Johansson, M. Sundler, P. Kjellen, M. Johannesson, A. Cook, A. K. Lindqvist, B. Nakken, A. I. Bolstad, R. Jonsson, M. Alarcon-Riquelme, and R. Holmdahl, "Genetic control of collagen-induced arthritis in a cross with NOD and C57BL/10 mice is dependent on gene regions encoding complement factor 5 and FcγRIIb and is not associated with loci controlling diabetes," *Eur. J. Immunol.* **31**, 1847–1856 (2001).
15. R. Holmdahl, J. A. Mo, R. Jonsson, K. Karlstrom, and A. Scheynius, "Multiple epitopes on cartilage type II collagen are accessible for antibody binding *in vivo*," *Autoimmunity* **10**, 27–34 (1991).
16. J. A. Mo, A. Scheynius, S. Nilsson, and R. Holmdahl, "Germline-encoded IgG antibodies bind mouse cartilage *in vivo*: epitope- and idiotype-specific binding and inhibition," *Scand. J. Immunol.* **39**, 122–130 (1994).
17. B. R. Wood, B. Tait, and D. McNaghton, "Fourier transform infrared spectroscopy as a method for monitoring the molecular dynamics of lymphocyte activation," *Appl. Spectrosc.* **54**, 353–359 (2000).
18. P. Lasch, W. Haensch, D. Naumann, and M. Diem, "Imaging of colorectal adenocarcinoma using FT-IR microspectroscopy and cluster analysis," *Biochim. Biophys. Acta.* **1688**, 176–186 (2004).
19. M. Diem, L. Chiriboga, and H. Yee, "Infrared spectroscopy of human cells and tissue. VIII. Strategies for analysis of infrared tissue mapping data and applications to liver tissue," *Biopolymers* **57**, 282–290 (2000).
20. B. R. Wood, L. Chiriboga, H. Yee, M. A. Quinn, D. McNaughton, and M. Diem, "Fourier transform infrared (FTIR) spectral mapping of the cervical transformation zone, and dysplastic squamous epithelium," *Gynecol. Oncol.* **93**, 59–68 (2004).
21. X. Bi, G. Li, S. B. Doty, and N. P. Camacho, "A novel method for determination of collagen orientation in cartilage by Fourier transform infrared imaging spectroscopy (FT-IRIS)," *Osteoarthritis Cartilage* **13**, 1050–1058 (2005).
22. N. P. Camacho, P. West, P. A. Torzilli, and R. Mendelsohn, "FTIR microscopic imaging of collagen and proteoglycan in bovine cartilage," *Biopolymers* **62**, 1–8 (2001).
23. K. J. Payne and A. Veis, "Fourier transform IR spectroscopy of collagen and gelatin solutions: deconvolution of the amide I band for conformational studies," *Biopolymers* **27**, 1749–1760 (1988).
24. P. A. West, P. A. Torzilli, C. Chen, P. Lin, and N. P. Camacho, "Fourier transform infrared imaging spectroscopy analysis of collagenase-induced cartilage degradation," *J. Biomed. Opt.* **10**, 14015 (2005).
25. K. Potter, L. H. Kidder, I. W. Levin, E. N. Lewis, and R. G. Spencer, "Imaging of collagen and proteoglycan in cartilage sections using Fourier transform infrared spectral imaging," *Arthritis Rheum.* **44**, 846–855 (2001).
26. A. M. Croxford, D. Crombie, D. McNaughton, R. Holmdahl, K. S. Nandakumar, and M. J. Rowley, "Specific antibody protection of the extracellular cartilage matrix against collagen antibody-induced damage," *Arthritis Rheum.* **62**, 3374–3384 (2010).
27. H. Burkhardt, T. Koller, A. Engstrom, K. S. Nandakumar, J. Turnay, H. G. Kraetsch, J. R. Kalden, and R. Holmdahl, "Epitope-specific recognition of type II collagen by rheumatoid arthritis antibodies is shared with recognition by antibodies that are arthritogenic in collagen-induced arthritis in the mouse," *Arthritis Rheum.* **46**, 2339–2348 (2002).
28. C. J. Malemud, "Matrix metalloproteinases (MMPs) in health and disease: an overview," *Front. Biosci.* **11**, 1696–1701 (2006).
29. A. Kobayashi, S. Naito, H. Enomoto, T. Shiomi, T. Kimura, K. Obata, K. Inoue, and Y. Okada, "Serum levels of matrix metalloproteinase 3 (stromelysin 1) for monitoring synovitis in rheumatoid arthritis," *Arch. Pathol. Lab. Med.* **131**, 563–570 (2007).
30. R. Bhargava and I. W. Levin, "Fourier transform infrared imaging: theory and practice," *Anal. Chem.* **73**, 5157–5167 (2001).
31. A. George and A. Veis, "FTIRS in H₂O demonstrates that collagen monomers undergo a conformational transition prior to thermal self-assembly *in vitro*," *Biochemistry* **30**, 2372–2377 (1991).
32. Y. A. Lazarev, B. A. Grishkovsky, and T. B. Khromova, "Amide I band of IR spectrum and structure of collagen and related polypeptides," *Biopolymers* **24**, 1449–1478 (1985).
33. P. Bassan, A. Kohler, H. Martens, J. Lee, H. J. Byrne, P. Dumas, E. Gazi, M. Brown, N. Clarke, and P. Gardner, "Resonant Mie scattering (RMieS) correction of infrared spectra from highly scattering biological samples," *Analyst* **135**, 268–277 (2010).
34. M. A. Campbell, C. J. Handley, and S. E. D'Souza, "Turnover of proteoglycans in articular-cartilage cultures: characterization of proteoglycans released into the medium," *Biochem. J.* **259**, 21–25 (1989).
35. R. D. Fraser, T. P. MacRae, and E. Suzuki, "Chain conformation in the collagen molecule," *J. Mol. Biol.* **129**, 463–481 (1979).
36. K. Okuyama, S. Arnott, M. Takayanagi, and M. Kakudo, "Crystal and molecular structure of a collagen-like polypeptide (Pro-Pro-Gly)₁₀," *J. Mol. Biol.* **152**, 427–443 (1981).
37. C. Petitbois, G. Gousspillou, K. Wehbe, J. P. Delage, and G. Deleris, "Analysis of type I and IV collagens by FT-IR spectroscopy and imaging for a molecular investigation of skeletal muscle connective tissue," *Anal. Bioanal. Chem.* **386**, 1961–1966 (2006).
38. K. F. Smith, P. I. Haris, D. Chapman, K. B. Reid, and S. J. Perkins, "Beta-sheet secondary structure of the trimeric globular domain of C1q of complement and collagen types VIII and X by Fourier-transform infrared spectroscopy and averaged structure predictions," *Biochem. J.* **301**(Pt 1), 249–256 (1994).
39. D. M. Byler and H. Susi, "Examination of the secondary structure of proteins by deconvolved FTIR spectra," *Biopolymers* **25**, 469–487 (1986).
40. W. K. Surewicz, H. H. Mantsch, and D. Chapman, "Determination of protein secondary structure by Fourier transform infrared spectroscopy: a critical assessment," *Biochemistry* **32**, 389–394 (1993).
41. K. S. Nandakumar, "Pathogenic antibody recognition of cartilage," *Cell Tissue Res.* **339**, 213–220 (2010).

CHAPTER FOUR

THE EFFECTS OF MONOCLONAL ANTIBODIES TO CII ON CARTILAGE *IN VIVO*

B. HISTOLOGICAL CHANGES

4.1. Preface

In addition to the use of infrared spectroscopy to analyse the changes in the cartilage *in vivo* in mice injected with mAbs that did not develop CAIA, all paws from the mice were examined histologically. Detail on the strains of mice and immunization are described in chapter three. Mice were injected with either two (M2139 and CIIC1) or four (M2139, CIIC1, UL-1 and CIIC2) arthritogenic mAbs to CII. Morphological changes were identified using histology. To determine whether there was non-inflammatory cartilage damage such that occurs in osteoarthritis, a scoring system based on a modified Mankin score was developed. This analysis focused particularly on analysis of cartilage structure, chondrocyte integrity and organization. Proteoglycan loss was measured using toluidine blue staining in the cartilage of the phalangeal and tarsal joints in these mice. The modified Mankin score applied in these studies has been used previously for scoring cartilage changes in osteoarthritis^(61, 200).

For cartilage analysis, all four paws from each mouse were collected and processed. The hind paws were embedded in two blocks to allow examination of both phalangeal and tarsal joints (total of 6 blocks per mouse). Each paw was sectioned longitudinally to a depth that allowed examination of both bone and cartilage surfaces of multiple joints within each section. The hind paws of a further 4 mice of each strain that had been injected with two mAbs were also examined.

The results are presented in the form of a manuscript being prepared for publication.

Abstract

Cartilage damage that occurs in murine collagen induced arthritis (CIA) and human rheumatoid arthritis is taken to result from inflammation and the effects of degradative enzymes. However monoclonal antibodies (mAb) to type II collagen (CII) that induce collagen antibody induced arthritis (CAIA) after passive transfer *in vivo* cause cartilage damage *in vitro* in the absence of inflammation. To determine whether arthritogenic mAbs cause non-inflammatory cartilage damage *in vivo*, strains of mice with impaired capacity to develop inflammation (B10.Q C5 δ) and the parental strain (B10.Q) that are CAIA sufficient but require an injection of lipopolysaccharide for enhanced incidence and severity, were injected intravenously with either two or four potentially arthritogenic mAbs to induce CAIA, or with saline only for controls. At day 3, mice were killed and the cartilage in joints of all paws was scored histologically. Analysis included that of cartilage structure, chondrocyte integrity and organization, proteoglycan loss using toluidine blue, and synchrotron-enhanced Fourier Transform Infrared Microspectroscopy to assess collagen changes. No macroscopic or microscopic inflammation was evident in any of the mice, yet all mAb-treated mice showed cartilage damage, marked by loss of cartilage structure, chondrocyte hyperplasia and/or loss and loss of proteoglycans in all joints. Such changes in inflammation-intact mice would readily enhance the exposure of damaged collagen fibrils to immune complexes containing collagen antibodies, and to the degradative enzymes released by inflammatory cells. Hence antibody-induced cartilage damage is a potential mechanism for initiation and perpetuation of cartilage damage in both murine arthritis and, possibly, in human RA wherein anti-CII antibodies of the same specificity are known to be present.

1. Introduction

B cells and secreted antibodies clearly participate in the pathogenesis of rheumatoid arthritis (RA), and depletion of B cells using monoclonal antibodies (mAb) to CD20 (Rituximab) ameliorates the disease. However autoantibody levels are not completely depleted in patients with RA undergoing B cell depletion therapy with Rituximab⁽²⁰¹⁾, therefore an understanding of the regulatory mechanisms at the effector level is important for the design of improved therapies.

An autoimmune response to native articular CII develops in patients with RA in whom IgG antibodies to CII are demonstrable in blood, cartilage and synovium⁽¹⁾. The arthritis induced by immunization of animals with CII, CIA, resembles RA in showing destruction of the articular cartilage matrix, and accompanying T and B cell immune responses to CII that are required for disease development⁽¹⁶¹⁾. Moreover certain mAb to CII from strains of mice susceptible to CIA can, on passive transfer, induce an acute arthritis in recipients. This is termed CAIA and occurs independently of any direct activity of B and T cells, so allowing effector processes to be studied independently of events during disease induction⁽⁵⁾. Articular inflammation characteristic of the effector stage is attributable to deposited immune complexes and activation of complement and Fc receptors (FcRs)⁽²⁰²⁾. However not all CII-specific antibodies are equally arthritogenic, inferring that the epitope of CII that is recognized modulates the response⁽¹⁶⁷⁾.

Studies on the effects of mAbs to CII *in vitro* have shown that two mAbs M2139 and CIIC1 that are potently arthritogenic *in vivo* affected cartilage matrix integrity in cartilage explant cultures⁽¹¹⁾, and impaired synthesis of new matrix and disrupted collagen fibril formation in chondrocyte cultures⁽⁹⁾, whereas a non-arthritogenic mAb CIIF4 had no such effect^(9, 11). Notably, in the culture systems used, cartilage damage must occur independently of immune cells or their small molecular mediators.

These *in vitro* studies suggest that antibodies to CII may participate in the cartilage damage that accompanies articular inflammation; and that such cartilage damage should be discernable *in vivo* after injection with arthritogenic mAbs, in mice that are unable to develop CAIA⁽¹⁸⁵⁾. Accordingly, the present study was to verify that mice that are incapable of developing inflammation characteristic of CAIA nonetheless show evidence of cartilage damage after receiving arthritogenic mAbs.

2. Materials and Methods

2.1. Monoclonal antibodies

The mAbs used were derived from hybridomas developed from CII-immunized mice^(4, 179, 193, 203). M2139, CIIC1, UL-1 and CIIC2 are arthritogenic mAbs that each bind to separate well-defined conformational epitopes on one or another of the cyanogen bromide (CB) cleaved peptides of native CII, including CB11 (C1^I epitope, ARGLT, aa 359-369)^(4, 193, 203), CB8 (U1 epitope, GLVGPRGERGF, aa 494-504)⁽¹⁷⁹⁾ and CB10 (J1 epitope, MPGERGAAGIAGPK, aa 551-564, and D3 epitope, RGAQGPPGATGF, aa 687-698)⁽¹⁸⁴⁾. Previous experiments *in vivo* were performed using a mixture of two mAbs, M2139 + CIIC1 for passive transfer of CAIA, but a mixture of four mAbs, (M2139+CIIC1+UL1+CIIC2), representing a polyclonal mAb response proved even more arthritogenic^(6, 184). The mAbs were purified from culture supernatants using γ -bind plus affinity gel matrix (Amersham Pharmacia Biotech Inc, Uppsala, Sweden)⁽¹⁸⁴⁾.

2.2. Mice

Two strains of mice were used, B10.Q C5-congenics that lack complement factor C5 (B10.Q C5 δ) and hence cannot develop CAIA⁽¹⁸⁵⁾, and the parental strain B10.Q that

are C5 sufficient and do develop CAIA upon antibody transfer, however require further injection of lipopolysaccharide for enhancement of arthritis⁽⁶⁾. The B10.Q C5 δ congenic mice were generated using the speed congenic technique⁽¹⁸⁸⁾; the congenic fragment from NOD in the B10.Q genetic background was approximately 54 Mb ranging from D2Mit116 to D2Mit91. Local (Lund-Malmö region, Sweden) animal welfare authorities permitted all the animal experiments.

2.3. Effects on cartilage of passive transfer of mAb to CII

Cartilage changes after passive transfer of mAbs to CII in the absence of inflammation were examined in groups of 4 four-month old mice injected intravenously with either 2 (M2139 + CIIC1) or 4 (M2139 + CIIC1 + UL-1 + C2) arthritogenic mAbs, or PBS alone (total 24 mice). The mixture of M2139 and CIIC1 contained 4.5 mg of each of the sterile-filtered antibody solutions in a final volume of 0.4 ml, and the mixture of CIIC1+M2139+UL1+C2 contained 1 mg of each mAb in a final volume of 0.4 ml. Mice were killed at day 3 after injection at a time when none had developed arthritis macroscopically⁽⁶⁾.

Paws were fixed in 4% phosphate buffered paraformaldehyde solution for 24 hours, decalcified for 3 to 4 weeks in an ethylenediaminetetraacetic acid-polyvinylpyrrolidone-Tris solution (pH 6.9), dehydrated, and embedded in paraffin for processing for histology and for synchrotron FTIRM. All four paws from each mouse were collected and processed, with the hind paws embedded in two blocks to allow examination of both phalangeal and tarsal joints. Each paw was sectioned longitudinally to a depth that allowed examination of both bone and cartilage surfaces of multiple joints within each section.

To compare the cartilage changes in the small joints of the phalanges, and the larger tarsal joints, serial sections of tissue from the hind paws of a further 4

mice of each strain that had been injected with two mAbs were also examined by histology and FTIRM.

2.4. Histology

For histological examination, 5µm serial sections of tissue were cut and stained with haematoxylin and eosin (H&E), or with toluidine blue to provide a semi-quantitative examination of proteoglycan loss from the cartilage⁽⁶²⁾. For most mice it was possible to compare the intensity of the staining of the cartilage within growth plates of the radial and ulna epiphyses with that of the cartilage at the joint surfaces of the carpal, metacarpal and phalangeal joints in the same section.

2.4.1. Histomorphometry

Histomorphometry to measure cartilage thickness and mean chondron size was performed on H&E-stained sections using MCIDTM Image Analysis Software (M4 3.0 Rev 1.1, Imaging Research Inc, St Catherines, Ontario, Canada), on images captured at 200 X magnification, as described previously⁽¹¹⁾. For chondrocyte size, individual chondrocytes were manually outlined using the MCIDTM software, which then calculated the chondrocyte area.

2.4.2. Scoring of cartilage changes

Scoring of cartilage changes was based on a modified Mankin score which has been used for scoring cartilage in osteoarthritis⁽²⁰⁰⁾ and is shown in Table 1, however the scale was reduced to exclude scoring for the more extreme structural changes, pannus and fissures into the calcified cartilage layer, seen in long-standing osteoarthritis. A combined score was derived for the joints by assessing cartilage structure (0-2 points), cellular abnormalities (0-3 points), and matrix staining (0-4 points), such that scores of 0 reflect normal cartilage and 9 the most severe

cartilage lesions. The scores for the structure of the cartilage, and cellular abnormalities were assessed from sections stained with H&E, and scores for matrix staining were assessed from toluidine blue-stained sections. For each mouse, scores were derived from at least three different sections, 111 joints in total, with selection based on the quality of the histology. Scores obtained for each joint were ranked, expressed as median and range, and statistical analysis was performed using the nonparametric Kruskal-Wallis Analysis of Variance by Ranks, or the Mann Whitney U test, as appropriate.

2.5. *Chemical composition of the cartilage by synchrotron FTIRM*

Chemical changes in the cartilage, particularly changes to CII were examined by synchrotron FTIRM. The IR spectrum of collagen is characterized by a triplet of peaks at 1203, 1234 and 1280 cm^{-1} , but in cartilage this collagen triplet coincides with a major peak at 1240-1245 cm^{-1} which is derived from sulphated glycosaminoglycans in the cartilage matrix. Therefore, analysis of CII was concentrated on the location of the amide I peak (1640-1670 cm^{-1}) which for native triple helical collagen is $>1660\text{cm}^{-1}$. However this amide I peak is complex due to contributions from the secondary structure of the proteins; for collagen a shoulder at $\sim 1637\text{ cm}^{-1}$ that has been attributed to the triple helix absorption of collagen⁽¹²¹⁾, or possibly to new collagen⁽²⁰⁴⁾ and there is a characteristic shift to lower wavenumber on denaturation^(71, 112, 139, 205). For proteoglycans, analysis was based on peaks within the region of 1175-960 cm^{-1} derived from carbohydrate moieties.

Details of this methodology have been published previously^(11, 206), but briefly, 5 μm sections of paraffin-embedded tissue were placed onto MirrIR low-e microscope slides (Kevley Technologies, Chesterland, OH), and to obtain the requisite resolution, measurements were performed on the IR beamline at the Australian Synchrotron (Melbourne, Victoria), as described previously⁽²⁰⁴⁾.

Grids were defined that encompassed regions of the cartilage surface, chondrocytes and included the bone beyond the cartilage surface. The spectra obtained from the grids were analysed using Cytospec (CytoSpec, Inc, <http://www.cytospec.com>), performing unsupervised hierarchical cluster analysis (UHCA)⁽¹³²⁾ using second derivative spectra with 5 clusters. Analysis was performed using second derivatives which measures changes in the slope of the spectra, where minima peaks in the second-derivative spectra correlated with the maxima peaks in the non-derivatized spectra⁽²⁰⁷⁾. This provided more information about the changes in cartilage components by allowing the resolution of bands that contribute to inflection points or shoulders in the original spectra, and eliminated problems with sloping baselines arising from loss of cartilage components. A “quality test” was performed to remove spectra with poor signal-to-noise ratios and spectra of low absorbance, and analysis encompassed the region 940-1800 cm⁻¹, where the major macromolecular spectral bands appear.

3. Results

3.1. *Histology of Joints*

At day 3, none of the mice showed macroscopic or histological evidence of inflammation or cellular infiltration, yet there were clear differences between treated mice and control mice, with histological abnormalities varying in degree for different joints, even within a single mouse.

3.1.1. *Cartilage structure*

In the control mice the cartilage had a smooth surface, and was highly cellular, with evenly spaced chondrocytes with rounded nuclei that contained 2-3 nucleoli (**Figure 4.1A**). In the mAb-treated mice some areas of the cartilage appeared

normal, but in many joints the cartilage surface was irregular, with surface fissures or apparent loss of cells from the surface, or the surface was uneven with apparent protrusions of chondrocytes (**Fig 4.1B,C**). The appearance of the chondrocytes differed, with regions of both hypercellularity with cell clusters suggestive of cell division, or hypocellularity, with areas of empty chondrons, particularly deep in the cartilage (**Fig 4.1D**).

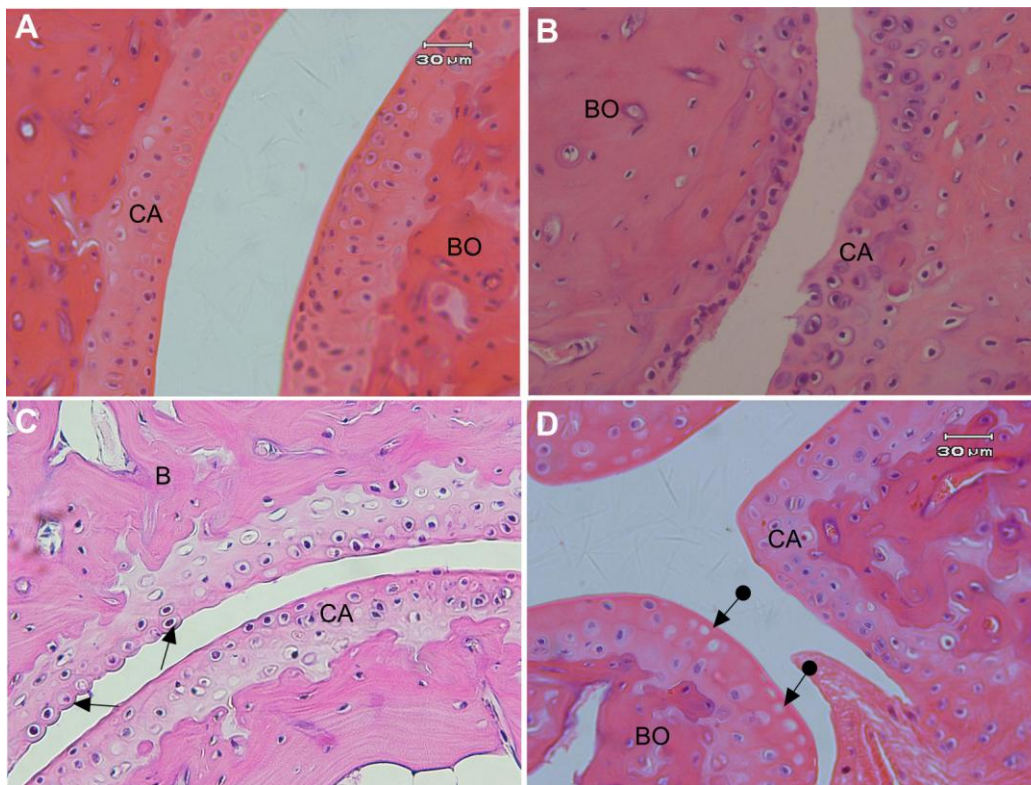


Figure 4.1. Histological sections stained with H & E through joints from control and mAb-treated mice showing the cartilage. **A.** Control joint showing a smooth cartilage surface and rounded nuclei. **B.** Joint from mAb-treated mouse, showing an uneven cartilage surface. **C.** Joint from a mAb-treated mouse showing an uneven cartilage surface and protruding cells. **D.** Joint from mAb-treated mouse, showing the hypocellularity with areas of empty chondrons. All images in this figure are on the same scale. CA indicates cartilage, BO shows bone, bold arrows indicate protruding chondrocytes, and double ended arrows indicate the presence of empty chondrons.

3.1.2. Proteoglycan loss

It was mostly possible to use the intensity of staining of the cartilage within growth plates of the radial and ulnar epiphyses as an internal control for loss of staining in cartilage at the joint surfaces of the carpals, metacarpals and phalanges in the same section (**Figure 4.2**). In the articular cartilage of control mice there was strong even intensity of staining similar to that of the growth plate (**Figure 4.2A**). By contrast, the intensity of staining of cartilage from the mAb-treated mice varied, with the articular cartilage being in most instances substantially weaker than that of the growth plate (**Figure 4.2B**); this pertained particularly in the distal interphalangeal joints of the forepaws with regions in which there was an intensely stained ring of matrix around chondrocytes. This was particularly evident when there were protrusions of chondrocytes from the cartilage surface (**Figure 4.2C**). In other areas there was complete loss of staining over part of the cartilage, often corresponding to areas containing empty chondrons (**Figure 4.2D**).

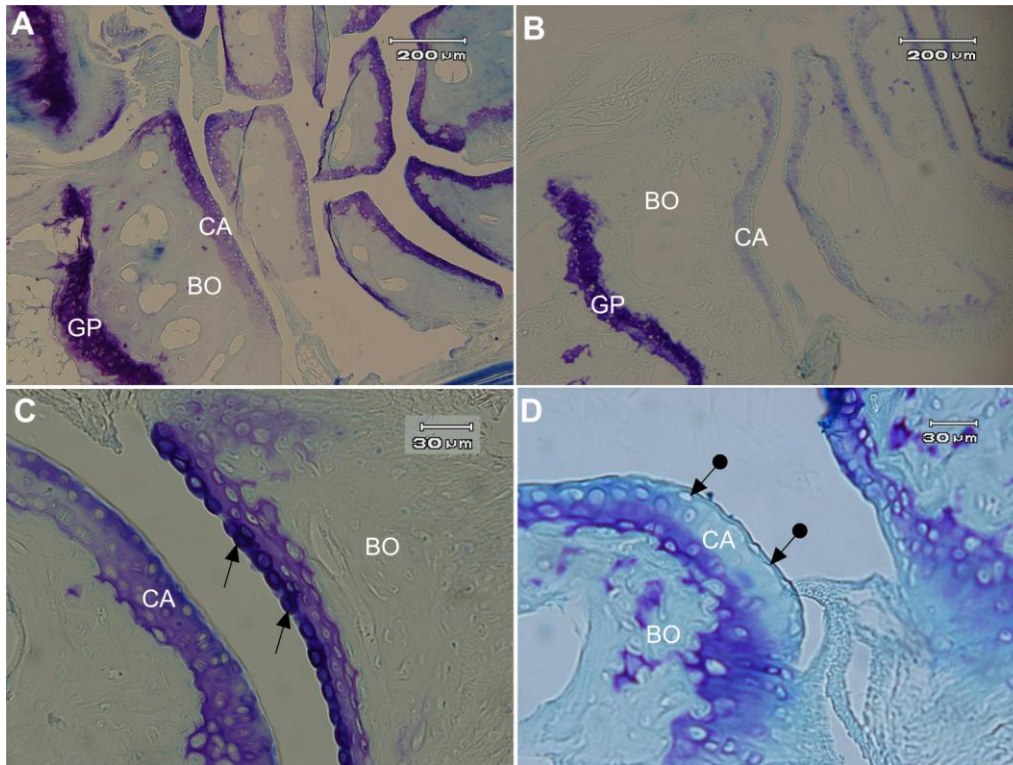


Figure 4.2. Histological sections stained with toluidine blue through joints from control and mAb-treated mice showing the cartilage. **A.** Control joint showing strong evenly stained cartilage surfaces which stained similarly to the growth plate. **B.** Joint from mAb-treated mouse, showing substantial loss of staining in the cartilage matrix, comparable to that of the growth plate which is stained strongly. **C.** Joint from a mAb-treated mouse showing loss of toluidine blue staining at the cartilage surface and protruding cells. **D.** Joint from mAb-treated mouse, showing complete loss of staining and empty chondrons. Images **A** and **B** are at x 10 magnification and images **C** and **D** are at x 40 magnification. CA indicates cartilage, BO shows bone, bold arrows indicate protruding chondrocytes, and double ended arrows indicate the presence of empty chondrons.

3.1.3. Comparison of histological changes in groups of mice.

A modified Mankin score was used to examine variations due to different combinations of mAbs, and mouse strains, in the degree of cartilage abnormality in

multiple joints. For each mouse, cartilage structure, chondrocyte abnormalities, and degree of proteoglycan loss in the matrix of multiple joints were scored. For each mouse a median score for all joints assessed was derived, and used to calculate group medians and ranges (**Table 1**).

For each of the features examined, scores for mice that received mAbs exceeded those of control mice. The eight control mice gave essentially normal scores (median score overall, and for each characteristic measured = 0) and none showed any substantial cartilage damage. In the mice treated with mAb, in contrast, the median score and the score for each characteristic measured in the mice treated with mAbs was higher than that of the control mice (**Table 2**). All mice showed changes in some joints, and median scores for individual mice that received mAbs were 2 to 8. Although there was considerable variation both in the score derived between joints in a single mouse, and between mice, only two tarsal joints, from two different animals, were assessed as being normal. The most consistent change was the loss of proteoglycan staining, which was present in all of the mAb-treated mice. Although loss of staining was occasionally seen in joints that lacked surface or cellular changes, the reverse did not occur, since histological changes were not observed without loss of matrix staining. Considering the two mouse strains there were no significant differences in the results although in the two different mAb-treated groups, the scores were slightly higher in the B10.Q C5 δ inflammation-incompetent than in the B10.Q inflammation-competent mice.

To compare changes in different joints, serial sections were examined from the hindpaws of eight mice, four from each strain which had been injected with two mAbs, for comparison of the small distal interphalangeal joints and the larger tarsal joints. The median and range of the overall Mankin scores for the two joints were similar, 5 (2-6) for the tarsal joints, and 5.5 (4-6) for the interphalangeal joints, but there were differences in the abnormalities observed. In the larger tarsal joints,

the surface of the cartilage was normal for 7 of the 8 mice, but most of the mice showed areas of complete cell loss and in such areas there was complete loss of proteoglycan staining, whereas in the interphalangeal joints, the cartilage surface was irregular in 5 of 8 mice, with protruding cells, and in these areas there was strong proteoglycan staining, although there was loss of staining deeper in the matrix. Chondrocytes within the cartilage that showed an uneven surface were significantly larger than those from cartilage with a smooth surface (145 ± 35 vs. $74 \pm 30 \mu\text{m}^2$), and the thickness of the cartilage was significantly reduced in the small distal interphalangeal joints, but not in larger joints.

Table 1. Grading scale for cartilage

	Point score
Structure	
Normal	0
Irregular surface, including bumps, fissures into radial layer	1
Slight disorganisation	2
Chondrocyte abnormalities	
Normal	0
Hypercellularity including small superficial clusters	1
Clusters, or protruding cells	2
Hypocellularity	3
Matrix staining	
Normal	0
Slight reduction	1
Moderate reduction	2
Severe reduction	3
Absent	4

Chapter 4: Research Paper 3

Table 2. Histological scores for the groups of mice tested, shown as median score, and the range of medians for individual mice in the group. The range of scores for all joints assessed from all mice in each group are shown **

Characteristics analysed (score)	Treatment group					
	4 mAb		2 mAb		Control	
	B10.Q	B10.Q C5δ-	B10.Q	B10.Q C5δ-	B10.Q ³	B10.Q C5δ-
Structure	1 (0-1)	1 (1)	1 (0-1)	1 (1)	0 (0-0.5)	0 (0)
	(0-2)**	(0-2)**	(0-2)**	(0-2)**	(0-1)**	(0-1)**
Cellular abnormalities	2.25 (0-2.5)	3 (2.5-3)	2 (0-2)	2 (0-2)	0 (0)	0 (0)
	(0-3)**	(0-3)**	(0-3)**	(0-3)**	(0-3)**	(0-3)**
Matrix staining	2.5 (1-4)	3 (1.5-3)	2 (1-3)	3 (1.5-4)	0 (0-0.5)	0 (0)
	(0-4)**	(1-4)**	(0-3)**	(1-4)**	(0-1)**	(0-2)**
Total score²	4 (4-7)	6.5 (3-7)	4 (4-5)	4.5 (5-7)	0 (0-1)	0 (0)
	(3-7)**	(2-8)**	(0-6)**	(4-7)**	(0-1)**	(0-3)**
	6 (3-7)³		5 (4-7)		0 (0-1)	

1. Including small superficial clusters
2. Calculated using only those joints for which data were available for both H&E and toluidine blue staining
3. Statistically significant results: Kruskal-Wallis ANOVA by Ranks P=0.0009, Mann Whitney U test Controls vs 4 mAb-treated P=0.00051, controls vs 2 mAb-treated P=0.00108; 2 mAb vs 4 mAb-treated ns

3.2. *Cartilage changes measured by synchrotron FTIRM*

To examine the chemical changes in the cartilage in the mAb-treated mice, spectra were obtained by synchrotron FTIRM for comparison between small distal interphalangeal joints and larger tarsal joints using control and mAb-treated mice. Spectral grids that spanned the cartilage surface to bone were analysed by UHCA using 5 clusters on second derivative spectra, and compared with the light microscopic image of the same section. UHCA did not clearly distinguish between the bone and the cartilage, and spectra collected from control mice were very similar across the entire grid (**Figure 4.3**), noting that the characteristic bands representing mineralization of the bone are removed by decalcification. The major amide I band in each cluster was located above 1660cm^{-1} , characteristic of collagen, whether type II collagen in cartilage or type I in bone, and there were bands at 1203 , 1234 and 1280 cm^{-1} that represented the “collagen triplet”. In several joints from control mice, UHCA discriminated a cluster localized to a surface layer of the cartilage that contained a relatively high proportion of chondrocytes in which the amide I band at 1666 cm^{-1} was reduced, and the minor band at 1635 cm^{-1} that is associated with activated chondrocytes⁽²⁰⁶⁾ was prominent (ratio $1635/1666$: 0.52) (**Figure 4.3**).

The grids collected from the mAb-treated mice were more complex. Overall there was more “noise” at the cartilage surface, leading to loss of pixels, and clusters at the cartilage surface were often uninformative. For the remaining clusters, the most striking feature was a decrease in the amide I band above 1660 cm^{-1} , and the increase in the band at 1635 cm^{-1} , which often became the most prominent band in the spectrum, shown in **Figure 4.4**, derived from a representative mouse paw. In this sample, close to the surface, the amide I band at 1666 cm^{-1} was markedly reduced, and considerably smaller than the band at 1635 cm^{-1} (ratio $1635/1666$:2.8). There were no changes in the location of bands in the region $1175\text{-}960\text{ cm}^{-1}$ that would indicate changes of proteoglycan composition, but decreases in heights of peaks in that region corresponding to proteoglycan loss

were seen in the non-derivatized spectra (data not shown). Taken together, these results obtained by synchrotron-enhanced FTIRM confirm the cartilage damage and proteoglycan loss seen histologically, and provide clear evidence both of changes to the collagenous matrix and also of marked cellular activation.

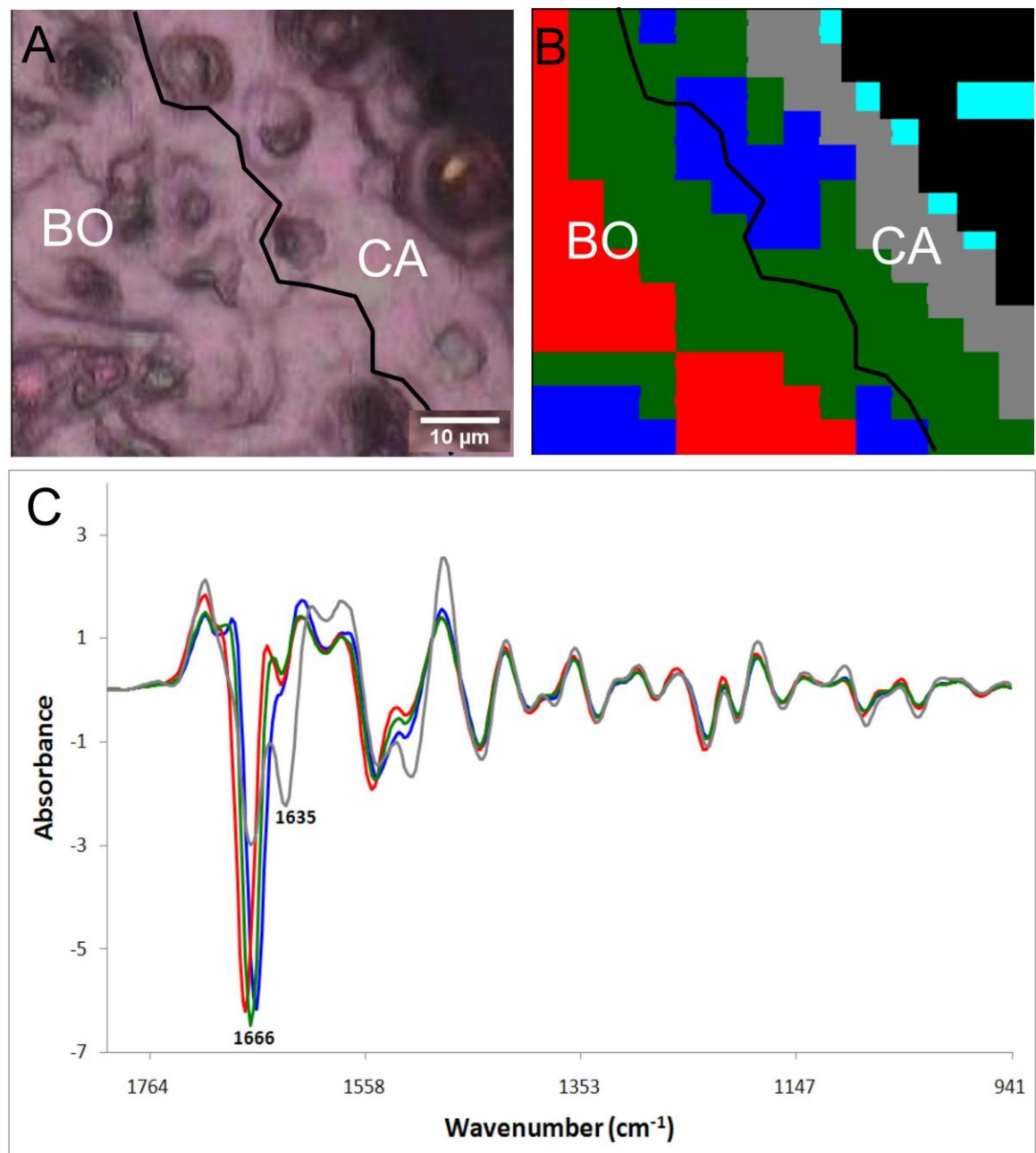


Figure 4.3. Representative result obtained by synchrotron FTIRM on a grid from a control mouse. **(A)** Light microscopy image of unstained section on Kevley reflective slide. CA is cartilage, BO is bone, \surd represents the cartilage border. **(B)** IR image processed by UHCA over the range 940-1800 cm⁻¹ using second-derivative spectra with five clusters. **(C)** Second-derivative spectra for the clusters, corresponding to the image in **(B)**, showing amide 1 bands at 1666 cm⁻¹ in each cluster, and a band at 1635 cm⁻¹ in the cluster corresponding to the cartilage surface. The aqua coloured pixels were of poor quality and hence excluded from analysis. Original magnification of **(A)** and **(B)** are x 200.

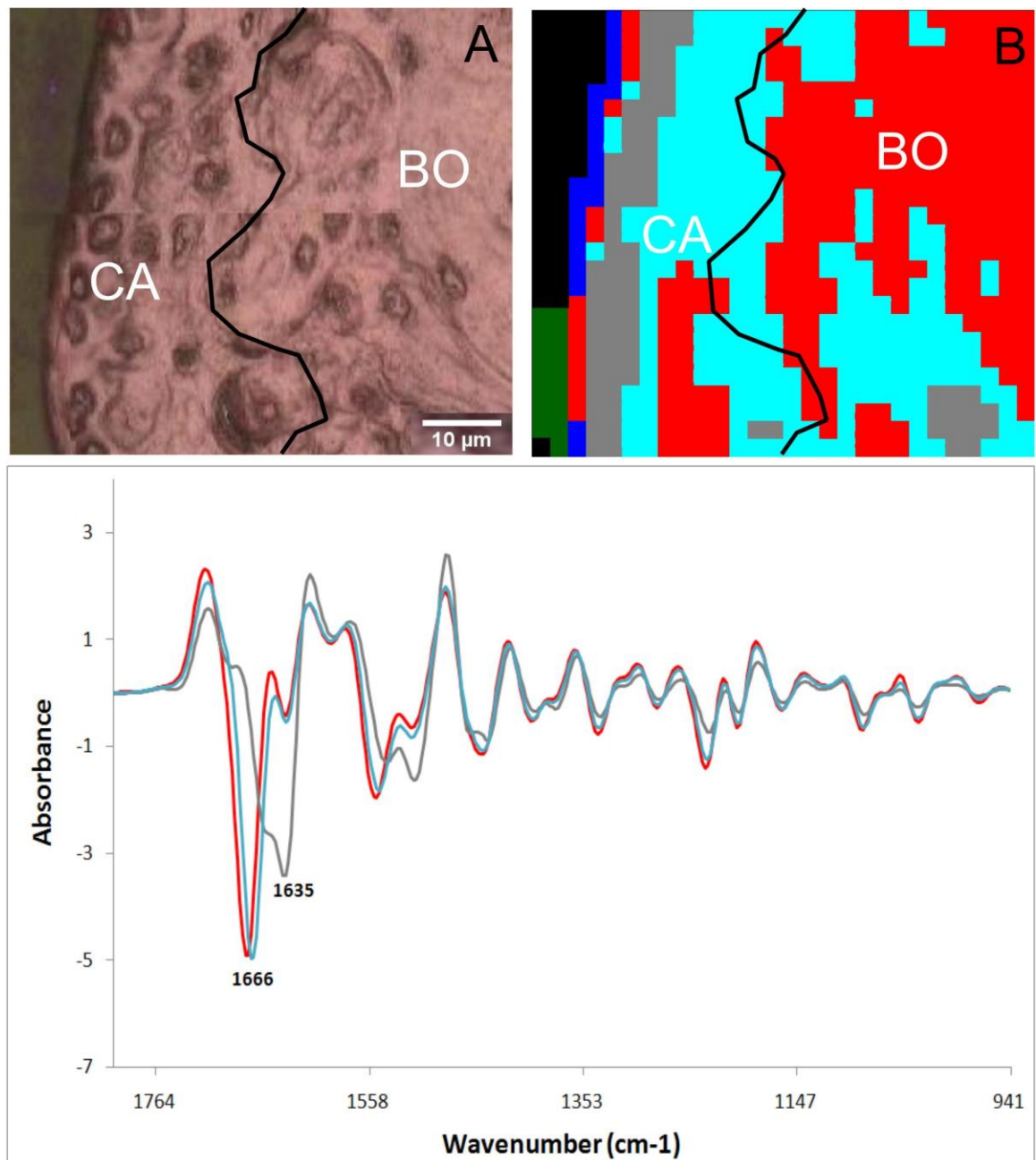


Figure 4.4. Representative result obtained by synchrotron FTIRM on a grid from a mAb treated mouse. **(A)** Light microscopy image of unstained section on Kevley reflective slide. CA is cartilage, BO is bone, \blacktriangledown represents the cartilage border. **(B)** IR image processed by UHCA over the range 940-1800 cm^{-1} using second-derivative spectra with five clusters. **(C)** Second-derivative spectra for the clusters, corresponding to the image in **(B)**, showing amide 1 bands at 1666 cm^{-1} in each of the clusters except at the cartilage surface, where there is a band at 1635 cm^{-1} . The green and blue coloured pixels were of poor quality and hence excluded from analysis. Original magnification of **(A)** and **(B)** are x 200.

4. Discussion

Autoantibodies to CII are readily demonstrable in serum, cartilage and synovial fluid of patients with RA^(1, 151), yet the significance of CII as an autoantigen and the detrimental effect of these autoantibodies on the integrity and function of articular cartilage in RA is poorly understood. Arthritis induced in experimental animals by immunization with CII closely mimics the human disease and murine models in particular provide a means of studying the evolution of arthritis and the mechanisms that underlie its development.

One informative observation in the murine model is the ease with which arthritis can be transferred from arthritic to naïve mice by arthritogenic monoclonal antibodies. The mAbs used in the transfer are well-characterized in terms of IgG subclass, fine specificity and capacity to induce arthritis, and collectively represent the polyclonal response of human disease. Accordingly, this model provides a useful means of analysing the immunopathology that is a consequence of the antibody response to CII.

In a series of experiments *in vitro* we developed various strategies and a range of techniques to examine the effects of these mAbs on articular cartilage. These strategies included the seeding of chondrocytes at high density in culture to examine the effect of antibody on newly-synthesized matrix^(8, 9), the study of the behaviour of collagen fibrils when assembling in the presence of mAb⁽⁷⁾, and the isolation of mature cartilage to observe the effect of antibody on it *in situ*^(11, 206). This approach allowed us to isolate any deleterious effects attributed to antibody that could be masked *in vivo* by the inflammatory response.

In brief, antibodies to CII induced subtle morphological changes in chondrocytes, and aggregation and thickening of collagen fibrils in their newly synthesized matrix^(8, 9), there was significant inhibition of the self-assembly of triple-helical CII monomers to insoluble polymeric fibrils⁽⁷⁾, and, in mature articular cartilage, there was loss of proteoglycans, denaturation and loss of CII, and overall

disruption of the topography and chemistry of the articular cartilage^(11, 206).

Moreover, the effects could be titrated according to concentration and duration of exposure to antibody and were more pronounced when F(ab)₂ fragments replaced whole antibody⁽¹¹⁾.

This study revealed abnormalities in cartilage in paws of mice injected with combinations of arthritogenic mAbs to CII that are well defined in terms of epitopes recognized, immunoglobulin subclass and capacity to induce CAIA in many mouse strains^(6, 167, 184). Collectively these mAb mixtures can be considered to be representative of antibodies induced in the arthritogenic response to CII, and so simulate the polyclonal antibody response to CII in CIA. The inflammatory arthritis induced *in vivo* by these mAbs requires complement activation and Fc-receptor binding⁽⁵⁾, and the associated cartilage damage is attributable to degradative enzymes produced by monocytes and macrophages within the joint⁽¹⁹⁷⁾. Knowing that these mAbs cause damage *in vitro* in cartilage independent of inflammation we ascertained whether the same mAb caused such damage *in vivo* as well.

Articular cartilage consists of a complex network of collagen fibrils, primarily of CII, in which are entrapped negatively charged proteoglycans and other matrix proteins. Together these interactions are essential to maintain the structural stability of cartilage^(10, 17). In chondrocyte cultures, the arthritogenic mAbs were shown to interfere with new matrix synthesis resulting in altered collagen fibril formation and chondrocyte morphology^(7, 8). In cartilage explants, the same mAbs caused cartilage breakdown in regions wherein the mAbs are bound, with ensuing collagen denaturation and loss of both proteoglycans and collagen from the matrix^(11, 206). Since these changes occurred in the absence of inflammatory mediators, the interpretation was that the mAbs bound specifically to, and damaged, critical structural regions on collagen fibrils that are sites of interaction between CII and matrix components or chondrocytes. Our present study established that the mAbs cause damage to cartilage *in vivo* likewise in the absence of inflammation, noting that paws from mice injected with arthritogenic mAbs were

examined before inflammatory changes would be expected. Of the two mouse strains examined, the parental strain, B10.Q, is C5 sufficient and mice develop typical CAIA upon antibody transfer, albeit at a low intensity unless there is a further injection of lipopolysaccharide to enhance incidence and severity of arthritis⁽⁶⁾. However the C5 insufficient B10.Q C5 δ mice cannot develop inflammation. None of the mice receiving the mAb showed macroscopic joint swelling nor histological evidence of inflammation at day 3 when samples were collected, but there was clear evidence of histological damage to the cartilage consistent with the changes seen in the explants cultures, notably cartilage thinning in the small joints, extensive proteoglycan loss, changes to the cartilage structure and chondrocyte morphology, and changes indicative of chondrocyte activation and new CII synthesis identified by synchrotron FTIRM⁽²⁰⁴⁾. The changes were the same in both strains of mice, indicating that they were independent of inflammation.

The changes seen *in vivo* aligned well with those seen *in vitro* in cartilage explants cultured with the mAbs^(11, 206). The apparent thinning of the cartilage seen in the small joints at the tips of the paws correlates with the observation *in vitro* of collapse of the cartilage matrix that follows loss of proteoglycans and denaturation of collagen demonstrable by FTIRM⁽¹¹⁾. Disruption of the matrix *in vivo* would result in direct mechanical loss of cartilage protein that could then be readily taken up into the surrounding synovial tissues. Such uptake has been shown for citrullinated CII⁽²⁰⁸⁾ as well as for native triple helical CII⁽¹⁷²⁾, where fragments of CII are detectable by immunohistochemical procedures in both synovial fluid and synovial tissue in human RA.

Although the mAbs used are reactive only with CII, the most prominent change observed within the joints of the mice treated with the arthritogenic mAbs was loss of proteoglycans from the cartilage. This occurred in all joints from both strains of mice, and also occurs *in vitro* in cartilage explants cultured with the same mAbs^(11, 206). The mAbs to CII do not react directly with proteoglycans, but may cause proteoglycan loss by binding to critical structural regions on collagen fibrils

that are sites of interactions between CII and matrix components or chondrocytes. Loss of proteoglycan is an early marker of cartilage disruption in both human osteoarthritis⁽²⁰⁹⁾ and RA, and is attributed to the activation of matrix metalloproteinases and aggrecanases that are released after disruption of the molecular interactions between matrix constituents^(209, 210). This loss of the proteoglycans, which provide 'cushioning' of the cartilage in the joint, in turn allows a greater susceptibility to damage from compressive forces, and greater penetration of degradative molecules, whether these be enzymes released by inflammatory cells, or arthritogenic mAb to CII as used in the present study.

The proteoglycan loss induced by the arthritogenic mAb could well contribute to the development of CAIA by facilitating immune complex deposition. In healthy cartilage, there is only minimal binding *in vivo* of mAb to CII to the surface of the cartilage⁽¹⁹⁴⁾, and the mAbs scarcely penetrate into the cartilage matrix, but they do bind strongly when the matrix is disrupted by treatment *in vitro* with hyaluronidase⁽¹¹⁾. In cartilage explant cultures wherein there is progressive loss of matrix, the penetration of the mAbs extends as the cartilage matrix is destroyed⁽¹¹⁾. Although there was abrogation of the inflammatory changes that normally accompany immune complex deposition and complement activation in our present study, the proteoglycan loss itself induced by the arthritogenic mAbs could enhance immune complex deposition within the joint and potentiate the degradative response.

Loss of proteoglycans in the cartilage is associated also with non-inflammatory arthritis^(211, 212), and in animals osteoarthritis can be induced by intra-articular injection of papain which causes degradation of proteoglycans^(60, 213, 214). Interestingly, van der Kraan *et al*⁽⁶⁰⁾ showed in mice that 3 days after a single injection of papain into the knee joints there was pronounced proteoglycan loss, damage at the cartilage surface, and chondrocyte changes including proliferation and/or cell death, and residual chondrocytes were often surrounded by a pericellular halo of strongly staining matrix; such changes closely resemble those in

the joints of mice injected with arthritogenic mAb to CII. The cartilage damage after papain injection progressed without further treatment, and by day 42 were typical of early osteoarthritis, including cartilage fragmentation and osteophyte formation, but there was no inflammation, suggesting that the mAb to CII might also induce changes akin to osteoarthritis in the longer term.

In conclusion, the results of this study have important connotations for the pathogenesis of human RA. Serum autoantibodies are present in RA^(1, 151), they bind to cartilage and can be released from immune complexes deposited within the cartilage by treatment with collagenase⁽²¹⁵⁾, and are reactive with the same epitopes that are arthritogenic in mice⁽¹⁶⁷⁾. Both CIA and RA are highly complex polygenic diseases in which overall pathology depends on both cell- and antibody-mediated inflammation. Our demonstration in mice that arthritogenic mAb to CII contribute directly to cartilage destruction in the absence of any inflammatory component implies an involvement of non-inflammatory as well as inflammatory components in the disease process. It may even be that injurious effects of antibody to CII on articular cartilage may precede, perhaps initiate, subsequent inflammatory events that lead ultimately to joint destruction. Whereas in healthy cartilage proteoglycans lost from the cartilage surface are normally rapidly resynthesised and replaced. Antibody-mediated cartilage damage and accompanying proteoglycan loss provides a further rationale for the successful use of combination therapies.

CHAPTER FIVE

GENERAL DISCUSSION

The experiments presented in this thesis were designed to examine the direct effects on pre-existing cartilage of various mAbs to CII derived from mice immunised with CII. The mAbs used are well characterised and have known effects in mice following passive transfer^(6, 186, 190). Moreover, antibodies of the same specificity have also been described human RA^(170, 188, 197). Each of the studies in this thesis was investigated using a combination of conventional and synchrotron FTIRM to identify chemical changes to the major components of the cartilage matrix, as cartilage changes are not readily detectable using standard histological techniques and require complex quantitative biochemical and/or immunohistochemical analysis for detection. By contrast, FTIRM allows the examination of all components of the cartilage matrix in a single sample.

Previous studies have shown that a combination of the mAbs M2139 and CIIC1 which induce a clinically severe arthritis in mice *in vivo*^(6, 186, 190-192) are also destructive *in vitro*, causing both damage to pre-existing cartilage in culture and adversely affecting collagen fibril formation and the synthesis of new matrix by chondrocytes^(7-9, 11). Furthermore, the mAb CIIF4 which does not cause cartilage damage either *in vivo* or *in vitro* has been shown to inhibit the pathogenesis of CAIA in combination with two arthritogenic mAbs, M2139 and CIIC1 *in vivo*⁽¹⁷⁰⁾.

The first part of the present study has shown that two arthritogenic mAbs, M2139 and CIIC1, that bind to well-defined conformational epitopes on the CII molecule^(170, 174, 187) used either individually or in combination cause direct damage to the pre-existing cartilage matrix *in vitro*, causing substantial loss of proteoglycans seen both by FTIRM and toluidine blue staining and progressive denaturation and loss of CII shown by FTIRM. This cartilage damage was mAb mediated, as it was greater in the absence of living chondrocytes. Loss of proteoglycans, and changes to collagen can be induced by MMPs which may be sequestered in the intact cartilage matrix^(220, 221), but changes in the presence of the mAbs were not prevented by the addition of the MMP inhibitor GM6001. Additional evidence to support the direct destructive effects of the arthritogenic mAbs to CII come from

previously published data from our laboratory⁽¹¹⁾ showing that mAb-mediated cartilage destruction was increased with F(ab)₂ was used instead of the intact CIIC1 mAb. In that study the F(ab)₂ penetrated the cartilage more deeply and caused greater loss of CII and complete loss of proteoglycans⁽¹¹⁾. The removal of the Fc region of the mAb was considered likely to prevent uptake and removal of the mAbs from the matrix by the chondrocytes, resulting in greater damage.

A striking observation from the current study was that the mAb CIIF4, which alone had no adverse effect on cartilage *in vitro* and countered the adverse effects of the arthritogenic mAb, promoting the regeneration of the cartilage matrix components, both CII and proteoglycans when administered in combination with two arthritogenic mAbs. This counter-destructive effect is only seen in the presence of living chondrocytes and parallels its protective effects previously observed on cartilage in CAIA *in vivo*⁽¹⁷⁰⁾. Interestingly, the protection by CIIF4 is delayed, being maximal at days 10 and 14 in culture as seen by FTIRM, where there is a dramatic increase in the level of proteoglycans and also seen as increased proteoglycan synthesis, including dark 'ringing' of toluidine blue stain around the chondrocytes at the surface of the cartilage. As primary cultures of chondrocytes take approximately 3 days after removal from the matrix for the cells to become stable and begin to synthesise matrix⁽⁹⁾, it is not unusual that the protective effect of CIIF4 may be delayed slightly from the onset of culture. It is therefore likely that there is a balance between the cartilage damage caused by the arthritogenic mAbs and the new matrix synthesis by chondrocytes, which is stimulated by the protective mAb CIIF4. The protective effect of the otherwise inert mAb CIIF4, which is of the same IgG subclass as the arthritogenic mAb CIIC1, and of similar affinity, highlights the fact that the epitope to which mAbs bind to CII determines both its arthritogenicity *in vivo* and adverse effects both *in vitro* and *in vivo*.

The effects of combinations of mAbs to CII on pre-existing cartilage *in vitro* suggested that similar changes should also be identifiable in mice injected with arthritogenic mAbs that do not develop inflammation *in vivo*. This was tested in

two strains of mice, and there was clear evidence of cartilage damage by both FTIRM and histology in mouse paws that showed no macroscopic damage. Furthermore, synchrotron infrared microspectroscopy identified chemical changes to the cartilage matrix, namely loss of the 1660 cm^{-1} amide I band and the subsequent appearance of an unidentified band at 1635 cm^{-1} and appeared to be associated with cellular activation. This could represent new synthesis of an unknown protein, but may result from β -secondary structures within the globular telopeptides of newly synthesized collagen produced by activated chondrocytes^(10, 17, 117, 222). These results were consistent with the changes seen *in vitro*.

The major question that arises from these studies and the demonstration that antibodies to CII cause direct cartilage damage both *in vitro* and *in vivo* in the absence of any confounding inflammatory mediators is whether there is any relevance of these results in the pathogenesis of RA. Antibodies of the same epitope specificity as the arthritogenic mAbs used in these studies also occur in human sera, and the C1 and U1 epitopes recognised by the arthritogenic mAbs CII C1 and UL-1 respectively are major immunodominant epitopes in RA^(170, 172) and therefore, the mechanisms of joint damage that occur in CAIA may also occur in RA. Furthermore, it has been shown that, with increasing cartilage damage in inflamed joints, the frequency of antibodies to CII detectable in serum reduces, suggesting that the antibody response to CII in RA is not simply a secondary effect of cartilage damage^(194, 195). Instead, newly synthesized mAb may bind to the cartilage, and contribute to pathogenesis.

The data presented in this thesis, suggest that there is interference with the integrity of the cartilage matrix, caused by the arthritogenic mAbs, which may lead to exposure of CII and release of cartilage breakdown products, including MMPs, and enhancing the production and exposure of immune complexes to cells which are capable of stimulating an inflammatory response. It is evident from these studies, that CII-reactive mAbs can cause direct cartilage damage or be protective both *in vitro* and *in vivo*. As CII antibodies of the same epitope specificity

to those used in these experiments, occur in human RA, this study is an important step in developing our understanding of the pathogenesis of RA and more detailed studies should expose the regulatory mechanisms which are operating at the effector level of arthritis pathogenesis. Furthermore, the data presented suggest that antibodies to CII may participate in the cartilage damage that accompanies articular inflammation in human RA since cartilage damage is observable after injection with arthritogenic mAbs in mice. The destructive effects of these anti-CII antibodies may therefore precede and perhaps initiate subsequent inflammatory events in the joints ultimately leading to joint destruction.

The cartilage destruction shown in these studies which is in the absence of any inflammatory component implies involvement of both inflammatory and non-inflammatory components in the perpetuation of the disease process in CIA which is an animal model of human RA, and suggests that similar effects may occur in RA. The use of combinations of mAbs to CII provides a valuable tool towards understanding the polyclonal response occurring in human RA. Moreover, understanding the direct damage caused by antibodies on target tissues without the influence of inflammatory mediators will likely stimulate further research into other antibody dependent immune diseases and pathologies such as systemic lupus erythematosus.

It should be emphasized that the use of both conventional FTIRM and synchrotron FTIRM in these studies has allowed the definitive demonstration that mAbs to CII can cause direct cartilage damage in the absence of inflammation both *in vitro* and *in vivo*. FTIRM has allowed examination of the localised chemical changes within the cartilage matrix without any prior knowledge of the likely mechanism of action of the mAbs. Such changes are very difficult to demonstrate using other techniques. Although FTIRM is increasingly being used to examine other tissues such as the brain⁽²²³⁾, it has proved to be particularly useful for the analysis of cartilage, which is an unusual tissue made up of a small number of cells in an abundant extracellular matrix⁽¹⁷⁾ particularly since it is made up of

components that have been extensively studied by IR spectroscopy^(122, 123, 125-130). Utilisation of the higher lateral resolution available for infrared microspectroscopy at the Australian synchrotron has made it possible to identify changes to individual cells and the cartilage matrix in several different joints, at different depths of the cartilage, discerning differences which are unable to be measured by any currently available biochemical or histological technique.

FTIRM has been increasingly used to examine changes to biological tissues, including examination of pre-cancerous and cancerous changes in cervical cancer studies^(136, 138, 139). FTIRM was used successfully in one of these studies to identify chemical changes to the amide I and amide II regions, glycogen and carbohydrate peaks and in the phosphodiester bands of nucleic acids that corresponded to the changes that were identified by histology, also highlighting pre-cancerous changes which were not yet visible by histology⁽¹³⁶⁾. Cartilage is an ideal tissue for analysis by FTIRM, as it is a tissue with relatively little components, each of which have previously been studied using infrared spectroscopy and the individual spectra have been well characterised^(36, 72, 127, 209). FTIRM is also a valuable tool for examining changes to cartilage not only in RA⁽¹³²⁾ but also in osteoarthritis^(73, 141-143, 224), joint injuries⁽¹⁴⁰⁾ and osteoporosis⁽¹⁴⁴⁾.

In conclusion, these studies have clearly demonstrated the utility of FTIRM for the analysis of cartilage and should have wide applicability not only in RA but also in OA, biomaterials and cartilage replacement therapies by identifying changes to the components of cartilage within its native state in the cartilage matrix. Whilst there are tissue engineering procedures which have been developed for cartilage repair and replacement therapies based on implantation of autologous chondrocytes following expansion *in vitro*, a major ongoing problem is the de-differentiation of chondrocytes. Cell culture in monolayers provides a convenient and an effective method for increasing cell numbers, but during cell culture the cell phenotype is mostly lost, and the biochemical characteristics of the matrix produced changes. Thus chondrocytes lose their rounded phenotype, assume a

fibroblastic appearance and switch to producing CI rather than CII characteristic of hyaline cartilage⁽²²⁵⁾. There is therefore a requirement for identifying improved conditions for culture of chondrocytes in preparation for implantation that will retain their phenotype. To obtain further information and develop more stable cartilage for replacement therapies, further information is required on the distribution and quality of cartilage components including proteoglycans and collagen. Particular reference to defining whether CI or CII is produced by chondrocytes in culture and FTIRM would assist in providing direct information about the chemical structure of the components of cartilage.

These studies suggest that antibodies to CII may participate in the cartilage damage that accompanies articular inflammation and that such cartilage damage is independent of, and possibly precedes damage that results from inflammation. Since antibodies of similar epitope specificity to the mAbs used in these studies occur in RA the data presented in this thesis provide new evidence demonstrating the involvement of CII specific antibodies in the pathogenesis and possibly initiation of human RA.

The FTIRM studies have identified changes to the cartilage matrix in the presence of mAbs to CII, however in order to completely understand the mechanisms of damage cause by anti-CII specific mAbs, the binding sites of these mAbs on the CII molecule and the importance of these epitopes in terms of other important matrix interactions should be investigated. The epitopes recognised by the arthritogenic mAbs M2139 and UL-1 are also binding sites for $\alpha 1\beta 1$ and $\alpha 2\beta 1$ integrins on the CII molecule^(226, 227) and therefore may block signalling between chondrocytes and the ECM affecting the morphology of the chondrocytes observed in the presence of these arthritogenic mAbs. The epitope binding site of the arthritogenic mAb ClIC1 is close to the binding site of chondroadherin, where interaction between chondroadherin and CII has been shown to inhibit fibrillogenesis⁽²²⁸⁾. The epitope where M2139 binds is within the region of CII that is

involved in the binding of CII with CIX^(174, 229), and therefore binding of M2139 to its epitope on CII could quite possibly interfere with the interaction of CII and CIX.

Determination of the protective effect of CIIF4 will require additional experiments including analysis of the effect of its addition to cartilage cultures after initial incubation with the arthritogenic mAbs to determine the protective capacity of CIIF4 against pre-existing cartilage damage. Other experiments may include investigation of gene expression profiles in chondrocytes which have been treated with CIIF4 and the arthritogenic mAbs to identify any inflammatory mediators, including pro-inflammatory cytokines such as IL-1, TNF- α and whether the expression of certain genes differs in the presence of the protective mAb CIIF4.

REFERENCES

1. Rowley MJ, Nandakumar KS, Holmdahl R. The role of collagen antibodies in mediating arthritis. *Mod Rheumatol*. 2008;18(5):429-41.
2. Alamanos Y, Drosos AA. Epidemiology of adult rheumatoid arthritis. *Autoimmun Rev*. 2005;4(3):130-6.
3. Feldmann M, Brennan FM, Maini RN. Role of cytokines in rheumatoid arthritis. *Annu Rev Immunol*. 1996;14:397-440.
4. Holmdahl R, Rubin K, Klareskog L, Larsson E, Wigzell H. Characterization of the antibody response in mice with type II collagen-induced arthritis, using monoclonal anti-type II collagen antibodies. *Arthritis Rheum*. 1986;29(3):400-10.
5. Nandakumar KS, Holmdahl R. Antibody-induced arthritis: disease mechanisms and genes involved at the effector phase of arthritis. *Arthritis Res Ther*. 2006;8(6):223.
6. Nandakumar KS, Svensson L, Holmdahl R. Collagen type II-specific monoclonal antibody-induced arthritis in mice: description of the disease and the influence of age, sex, and genes. *Am J Pathol*. 2003;163(5):1827-37.
7. Gray RE, Seng N, Mackay IR, Rowley MJ. Measurement of antibodies to collagen II by inhibition of collagen fibril formation in vitro. *J Immunol Methods*. 2004;285(1):55-61.
8. Amirahmadi SF, Pho MH, Gray RE, Crombie DE, Whittingham SF, Zuasti BB, et al. An arthritogenic monoclonal antibody to type II collagen, CII-C1, impairs cartilage formation by cultured chondrocytes. *Immunol Cell Biol*. 2004;82(4):427-34.
9. Amirahmadi SF, Whittingham S, Crombie DE, Nandakumar KS, Holmdahl R, Mackay IR, et al. Arthritogenic anti-type II collagen antibodies are pathogenic for cartilage-derived chondrocytes independent of inflammatory cells. *Arthritis Rheum*. 2005;52(6):1897-906.
10. Muir H. The chondrocyte, architect of cartilage. *Biomechanics, structure, function and molecular biology of cartilage matrix macromolecules*. *Bioessays*. 1995;17(12):1039-48.
11. Crombie DE, Turer M, Zuasti BB, Wood B, McNaughton D, Nandakumar KS, et al. Destructive effects of murine arthritogenic antibodies to type II collagen on cartilage explants in vitro. *Arthritis Res Ther*. 2005;7(5):R927-37.
12. Heinegard D, Paulsson M. *Cartilage*. *Methods Enzymol*. 1987;145:336-63.
13. Stockwell RA. *Biology of cartilage cells*. Cambridge: Cambridge University Press; 1979.
14. Kiani C, Chen L, Wu YJ, Yee AJ, Yang BB. Structure and function of aggrecan. *Cell Res*. 2002;12(1):19-32.
15. Mackay IR, Rowley MJ. Collagen of articular cartilage: the neglected autoantigen of rheumatoid arthritis. *J Rheumatol*. 2008;35(5):731-3.
16. Cremer MA, Rosloniec EF, Kang AH. The cartilage collagens: a review of their structure, organization, and role in the pathogenesis of experimental arthritis in animals and in human rheumatic disease. *J Mol Med*. 1998;76(3-4):275-88.
17. Coates EE, Fisher JP. Phenotypic variations in chondrocyte subpopulations and their response to in vitro culture and external stimuli. *Annals of biomedical engineering*. 2010;38(11):3371-88.
18. Buchwalter JA, Hunziker EB. *Articular Cartilage Morphology and Biology*. In: Archer CW, Caterson B, Benjamin M, Ralphs JR, editors. *Biology of the Synovial Joint*. The Netherlands: Harwood Academic Publishers; 1999. p. 75-100.
19. Smith KF, Haris PI, Chapman D, Reid KB, Perkins SJ. Beta-sheet secondary structure of the trimeric globular domain of C1q of complement and collagen types VIII and X by

- Fourier-transform infrared spectroscopy and averaged structure predictions. *Biochem J.* 1994;301 (Pt 1) , , :249-56.
20. Sellar GC, Blake DJ, Reid KB. Characterization and organization of the genes encoding the A-, B- and C-chains of human complement subcomponent C1q. The complete derived amino acid sequence of human C1q. *Biochem J.* 1991;274 (Pt 2):481-90.
21. Reid KB. Molecular cloning and characterization of the complementary DNA and gene coding for the B-chain of subcomponent C1q of the human complement system. *Biochem J.* 1985;231(3):729-35.
22. Shoulders MD, Raines RT. Collagen structure and stability. *Annu Rev Biochem.* 2009;78:929-58.
23. Myllyharju J, Kivirikko KI. Collagens and collagen-related diseases. *Ann Med.* 2001;33(1):7-21.
24. Brinckmann J. Collagens at a Glance. *Topics in Current Chemistry.* 2005;247:1-6.
25. Veit G, Kobbe B, Keene DR, Paulsson M, Koch M, Wagener R. Collagen XXVIII, a novel von Willebrand factor A domain-containing protein with many imperfections in the collagenous domain. *J Biol Chem.* 2006;281(6):3494-504.
26. Kuettner KE. Biochemistry of articular cartilage in health and disease. *Clin Biochem.* 1992;25(3):155-63.
27. Eyre DR, Wu JJ. Collagen structure and cartilage matrix integrity. *J Rheumatol Suppl.* 1995;43:82-5.
28. Poole CA, Ayad S, Schofield JR. Chondrons from articular cartilage: I. Immunolocalization of type VI collagen in the pericellular capsule of isolated canine tibial chondrons. *J Cell Sci.* 1988;90 (Pt 4):635-43.
29. Schmid TM, Popp RG, Linsenmayer TF. Hypertrophic cartilage matrix. Type X collagen, supramolecular assembly, and calcification. *Ann N Y Acad Sci.* 1990;580:64-73.
30. Kadler KE, Holmes DF, Trotter JA, Chapman JA. Collagen fibril formation. *Biochem J.* 1996;316 (Pt 1):1-11.
31. Campbell MA, Handley CJ, D'Souza SE. Turnover of proteoglycans in articular-cartilage cultures. Characterization of proteoglycans released into the medium. *Biochem J.* 1989;259 , , :21-5.
32. Ng L, Grodzinsky AJ, Patwari P, Sandy J, Plaas A, Ortiz C. Individual cartilage aggrecan macromolecules and their constituent glycosaminoglycans visualized via atomic force microscopy. *J Struct Biol.* 2003;143(3):242-57.
33. Gaffney J, Matou-Nasri S, Grau-Olivares M, Slevin M. Therapeutic applications of hyaluronan. *Mol Biosyst.* 2010;6(3):437-43.
34. Volpi N, Schiller J, Stern R, Soltes L. Role, metabolism, chemical modifications and applications of hyaluronan. *Curr Med Chem.* 2009;16(14):1718-45.
35. Theocharis AD, Skandalis SS, Tzanakakis GN, Karamanos NK. Proteoglycans in health and disease: novel roles for proteoglycans in malignancy and their pharmacological targeting. *FEBS J.* 2010;277(19):3904-23.
36. Fraser JR, Laurent TC, Laurent UB. Hyaluronan: its nature, distribution, functions and turnover. *J Intern Med.* 1997;242(1):27-33.
37. Bianco P, Fisher LW, Young MF, Termine JD, Robey PG. Expression and localization of the two small proteoglycans biglycan and decorin in developing human skeletal and non-skeletal tissues. *J Histochem Cytochem.* 1990;38(11):1549-63.
38. Mason RM, Levick R, Coleman P, Scott D. Biochemistry of the Synovium and Synovial Fluid. In: Archer CW, Caterson B, Benjamin M, Ralphs JR, editors. *Biology of the Synovial Joint.* The Netherlands: Harwood Academic Publishers; 1999. p. 254-6.

39. Hildebrand A, Romaris M, Rasmussen LM, Heinegard D, Twardzik DR, Border WA, et al. Interaction of the small interstitial proteoglycans biglycan, decorin and fibromodulin with transforming growth factor beta. *Biochem J.* 1994;302 (Pt 2):527-34.
40. Ralphs JR, Benjamin M. Cell and Matrix Organisation in Tendons and Ligaments. In: Archer CW, Caterson B, Benjamin M, Ralphs JR, editors. *Biology of the Synovial Joint.* The Netherlands: Harwood Academic Publishers; 1999. p. 272.
41. Archer CW, Francis-West P. The chondrocyte. *Int J Biochem Cell Biol.* 2003;35(4):401-4.
42. Verzijl N, DeGroot J, Thorpe SR, Bank RA, Shaw JN, Lyons TJ, et al. Effect of collagen turnover on the accumulation of advanced glycation end products. *J Biol Chem.* 2000;275:39027-31.
43. Mankin HJ. Localisation of tritiated thymidine in articular cartilage of rabbits III: Mature articular cartilage. *J Bone Joint Surg.* 1963;45A:529-40.
44. Venn M, Maroudas A. Chemical composition and swelling of normal and osteoarthrotic femoral head cartilage. I. Chemical composition. *Ann Rheum Dis.* 1977;36(2):121-9.
45. Van Damme MP, Sinnaya P, Derry K, Murphy WH, Preston BN. Temporal changes in charge content of cultured chondrocytes from bovine cartilaginous tissues. *Matrix Biol.* 1997;15(7):495-502.
46. Oakes BW, Handley CJ, Lisner F, Lowther DA. An ultrastructural and biochemical study of high density primary cultures of embryonic chick chondrocytes. *J Embryol Exp Morphol.* 1977;38:239-63.
47. Kuettner KE, Memoli VA, Pauli BU, Wrobel NC, Thonar EJ, Daniel JC. Synthesis of cartilage matrix by mammalian chondrocytes in vitro. II. Maintenance of collagen and proteoglycan phenotype. *J Cell Biol.* 1982;93(3):751-7.
48. Buschmann MD, Gluzband YA, Grodzinsky AJ, Kimura JH, Hunziker EB. Chondrocytes in agarose culture synthesize a mechanically functional extracellular matrix. *J Orthop Res.* 1992;10(6):745-58.
49. Goldring MB, Birkhead JR, Suen LF, Yamin R, Mizuno S, Glowacki J, et al. Interleukin-1 beta-modulated gene expression in immortalized human chondrocytes. *J Clin Invest.* 1994;94(6):2307-16.
50. Kokenyesi R, Tan L, Robbins JR, Goldring MB. Proteoglycan production by immortalized human chondrocyte cell lines cultured under conditions that promote expression of the differentiated phenotype. *Arch Biochem Biophys.* 2000;383(1):79-90.
51. Mukhopadhyay K, Lefebvre V, Zhou G, Garofalo S, Kimura JH, de Crombrughe B. Use of a new rat chondrosarcoma cell line to delineate a 119-base pair chondrocyte-specific enhancer element and to define active promoter segments in the mouse pro-alpha 1(II) collagen gene. *The Journal of biological chemistry.* 1995;270(46):27711-9.
52. Saas J, Lindauer K, Bau B, Takigawa M, Aigner T. Molecular phenotyping of HCS-2/8 cells as an in vitro model of human chondrocytes. *Osteoarthritis Cartilage.* 2004;12(11):924-34.
53. Takigawa M, Tajima K, Pan HO, Enomoto M, Kinoshita A, Suzuki F, et al. Establishment of a clonal human chondrosarcoma cell line with cartilage phenotypes. *Cancer Res.* 1989;49(14):3996-4002.
54. Xu X, Urban JP, Tirlapur U, Wu MH, Cui Z. Influence of perfusion on metabolism and matrix production by bovine articular chondrocytes in hydrogel scaffolds. *Biotechnol Bioeng.* 2006;93(6):1103-11.

55. Erggelet C, Sittinger M, Lahm A. The arthroscopic implantation of autologous chondrocytes for the treatment of full-thickness cartilage defects of the knee joint. *Arthroscopy*. 2003;19(1):108-10.
56. Chiang H, Kuo TF, Tsai CC, Lin MC, She BR, Huang YY, et al. Repair of porcine articular cartilage defect with autologous chondrocyte transplantation. *J Orthop Res*. 2005;23(3):584-93.
57. Thissen H, Chang KY, Tebb TA, Tsai WB, Glattauer V, Ramshaw JA, et al. Synthetic biodegradable microparticles for articular cartilage tissue engineering. *J Biomed Mater Res A*. 2006;77(3):590-8.
58. Werkmeister JA, Adhikari R, White JF, Tebb TA, Le TP, Taing HC, et al. Biodegradable and injectable cure-on-demand polyurethane scaffolds for regeneration of articular cartilage. *Acta Biomater*. 2010;6(9):3471-81.
59. Munteanu SE, Ilic MZ, Handley CJ. Highly sulfated glycosaminoglycans inhibit aggrecanase degradation of aggrecan by bovine articular cartilage explant cultures. *Matrix Biol*. 2002;21(5):429-40.
60. Bullough PG, Jagannath A. The morphology of the calcification front in articular cartilage. Its significance in joint function. *J Bone Joint Surg Br*. 1983;65(1):72-8.
61. van der Kraan PM, Vitters EL, van de Putte LB, van den Berg WB. Development of osteoarthritic lesions in mice by "metabolic" and "mechanical" alterations in the knee joints. *The American journal of pathology*. 1989;135(6):1001-14.
62. Mankin HJ, Dorfman H, Lippiello L, Zarins A. Biochemical and metabolic abnormalities in articular cartilage from osteo-arthritic human hips. II. Correlation of morphology with biochemical and metabolic data. *J Bone Joint Surg Am*. 1971;53(3):523-37.
63. Kiraly K, Lapvetelainen T, Arokoski J, Torronen K, Modis L, Kiviranta I, et al. Application of selected cationic dyes for the semiquantitative estimation of glycosaminoglycans in histological sections of articular cartilage by microspectrophotometry. *Histochem J*. 1996;28(8):577-90.
64. Gruber HE, Ingram JA. Basic Staining and Histochemical Techniques and Immunohistochemical Localizations Using Bone Sections. In: An YH, Martin KL, editors. *Handbook of Histology Methods for Bone and Cartilage*. New Jersey: Humana Press; 2010. p. 281-6.
65. Otterness IG, Downs JT, Lane C, Bliven ML, Stukenbrok H, Scampoli DN, et al. Detection of collagenase-induced damage of collagen by 9A4, a monoclonal C-terminal neoepitope antibody. *Matrix Biol*. 1999;18(4):331-41.
66. Little CB, Flannery CR, Hughes CE, Mort JS, Roughley PJ, Dent C, et al. Aggrecanase versus matrix metalloproteinases in the catabolism of the interglobular domain of aggrecan in vitro. *Biochem J*. 1999;344 Pt 1:61-8.
67. Lark MW, Bayne EK, Flanagan J, Harper CF, Hoerrner LA, Hutchinson NI, et al. Aggrecan degradation in human cartilage. Evidence for both matrix metalloproteinase and aggrecanase activity in normal, osteoarthritic, and rheumatoid joints. *J Clin Invest*. 1997;100(1):93-106.
68. Janusz MJ, Little CB, King LE, Hookfin EB, Brown KK, Heitmeyer SA, et al. Detection of aggrecanase- and MMP-generated catabolic neoepitopes in the rat iodoacetate model of cartilage degeneration. *Osteoarthritis Cartilage*. 2004;12(9):720-8.
69. Felice BR, Chichester CO, Barrach HJ. Type II collagen peptide release from rabbit articular cartilage. *Annals of the New York Academy of Sciences*. 1999;878:590-3.

70. Fosang AJ, Last K, Gardiner P, Jackson DC, Brown L. Development of a cleavage-site-specific monoclonal antibody for detecting metalloproteinase-derived aggrecan fragments: detection of fragments in human synovial fluids. *The Biochemical journal*. 1995;310 (Pt 1):337-43.
71. Fosang AJ, Last K, Jackson DC, Brown L. Antibodies to MMP-cleaved aggrecan. *Methods Mol Biol*. 2001;151:425-49.
72. Camacho NP, West P, Torzilli PA, Mendelsohn R. FTIR microscopic imaging of collagen and proteoglycan in bovine cartilage. *Biopolymers*. 2001;62(1):1-8.
73. Bi X, Yang X, Bostrom MP, Camacho NP. Fourier transform infrared imaging spectroscopy investigations in the pathogenesis and repair of cartilage. *Biochim Biophys Acta*. 2006;1758(7):934-41.
74. Sherman Hsu CP. Infrared Spectroscopy. In: Settle FA, editor. *Handbook of Instrumental Techniques for Analytical Chemistry*
Upper Saddle River, New Jersey: Prentice Hall; 1997. p. 247-83.
75. Berthomieu C, Hienerwadel R. Fourier transform infrared (FTIR) spectroscopy. *Photosynth Res*. 2009;101(2-3):157-70.
76. Jackson RS. Continuous Scanning Interferometers for Mid-infrared Spectrometry. In: Chalmers JM, Griffiths PR, editors. *Handbook of Vibrational Spectroscopy*. West Sussex: John Wiley & Sons; 2002. p. 264-5.
77. Silverstein RM, Webster FX, Kiemle DJ. *Infrared Spectrometry*. 7 ed. USA: John Wiley & Sons; 2005.
78. Duygu D, Baykal T, Acikgoz I, Yildiz K. Fourier Transform Infrared (FT-IR) Spectroscopy for Biological Studies. *GU Journal of Science*. 2009;22(3):17-121.
79. Wetzel KB. Near-Infrared Spectrophotometry. *Applied Spectroscopy Reviews*. 1968;2(1):1-67.
80. Kong J, Yu S. Fourier transform infrared spectroscopic analysis of protein secondary structures. *Acta Biochim Biophys Sin (Shanghai)*. 2007;39(8):549-59.
81. Lewis EN, Treado PJ, Reeder RC, Story GM, Dowrey AE, Marcott C, et al. Fourier transform spectroscopic imaging using an infrared focal-plane array detector. *Anal Chem*. 1995;67(19):3377-81.
82. Hannah RW. Standard Sampling Techniques for Infrared Spectroscopy. In: Chalmers JM, Griffiths PR, editors. *Handbook of Vibrational Spectroscopy*. West Sussex: John Wiley & Sons; 2002. p. 933-52.
83. Colthup NB, Daly LH, Wiberley SE. *Introduction to Infrared and Raman Spectroscopy*. New York: Academic Press; 1964.
84. Hanst PL. Long Path Gas Cells. In: Chalmers JM, Griffiths PR, editors. *Handbook of Vibrational Spectroscopy*. West Sussex: John Wiley & Sons; 2002. p. 961-8.
85. PE. FT-IR Spectroscopy- Attenuated Total Reflectance (ATR). Technical Note. USA: Perkin Elmer Life and Analytical Sciences; 2005.
86. Miller LM, Dumas P. Chemical imaging of biological tissue with synchrotron infrared light. *Biochim Biophys Acta*. 2006;1758(7):846-57.
87. Quinteiro-Rodriguez MP. Fourier Transform Infrared (FTIR) Technology for the Identification of Organisms. *Clinical Microbiology Newsletter*. 2000;22(8):57-61.
88. Aparicio S, Doty SB, Camacho NP, Paschalis EP, Spevak L, Mendelsohn R, et al. Optimal methods for processing mineralized tissues for Fourier transform infrared microspectroscopy. *Calcif Tissue Int*. 2002;70(5):422-9.

89. Nasse MJ, Ratti S, Giordano M, Hirschmugl CJ. Demountable liquid/flow cell for in vivo infrared microspectroscopy of biological specimens. *Appl Spectrosc*. 2009;63(10):1181-6.
90. Petibois C, Piccinini M, Guidi MC, Marcelli A. Facing the challenge of biosample imaging by FTIR with a synchrotron radiation source. *J Synchrotron Radiat*. 2010;17(Pt 1):1-11.
91. Miller LM, Carlson CS, Carr GL, Chance MR. A method for examining the chemical basis for bone disease: synchrotron infrared microspectroscopy. *Cellular and molecular biology*. 1998;44(1):117-27.
92. Miller LM, Smith GD, Carr GL. Synchrotron-based biological microspectroscopy: from the mid-Infrared through the far-infrared regimes. *Journal of Biological Physics* 2003;29:219-30.
93. Reffner JA, Martoglio PA, Williams GP. Fourier transform infrared microscopical analysis with synchrotron radiation: the microscope optics and system performance. *RevSci Instr* 1995;66:1298.
94. Dumas P, Sockalingum GD, Sule-Suso J. Adding synchrotron radiation to infrared microspectroscopy: what's new in biomedical applications? *Trends Biotechnol*. 2007;25(1):40-4.
95. Petibois C. Imaging techniques with synchrotron radiation. *Anal Bioanal Chem*. 2010;397(6):2031-2.
96. Wetzel DL, Post GR, Lodder RA. Synchrotron infrared microspectroscopic analysis of collagens I, III, and elastin on the shoulders of human thin-cap fibroatheromas. *Vibrational Spectroscopy*. 2005;38:53-9.
97. Smith TI. The source issue in infrared microspectroscopy. *Nuclear Instruments and Methods in Physics Research A*. 2002;483:565-70.
98. Nasse MJ, Mattson EC, Reininger R, Kubala T, Janowski S, Hirschmugl CJ. Multi-beam synchrotron infrared chemical imaging with high spatial resolution: Beamline realization and first reports on image restoration. *Nuclear Instruments and Methods in Physics Research A*. 2010.
99. Nasse MJ, Reininger R, Kubala T, Janowski S, Hirschmugl CJ. Synchrotron infrared microspectroscopy imaging using a multi-element detector (IRMSI-MED) for diffraction-limited chemical imaging. *Nuclear Instruments and Methods in Physics Research A*. 2007;582:107-10.
100. Ferraro JR, Basile LJ, editors. *Fourier Transform Infrared Spectroscopy*. New York: Academic Press; 1978.
101. Tsuboi M. Application of Infrared Spectroscopy to Structure Studies of Nucleic Acids. *Applied Spectroscopy Reviews*. 1970;3(1):45-90.
102. Benedetti E, Bramanti E, Papineschi R, Rossi I, Benedetti E. Determination of the Relative Amount of Nucleic Acids and Proteins in Leukemic and Normal Lymphocytes by Means of Fourier Transform Infrared Microspectroscopy. *Applied Spectroscopy*. 1997;51(6):792-7.
103. Wong PTT, Wong RK, Fung Kee Fung M. Pressure-Tuning FT-IR Study of Human Cervical Tissues. *Applied Spectroscopy*. 1993;47(7):1058-63.
104. Wong PT, Cadrin M, French SW. Distinctive infrared spectral features in liver tumor tissues of mice: evidence of structural modifications at the molecular level. *Exp Mol Pathol*. 1991;55(3):269-84.

105. Jackson M, Choo LP, Watson PH, Halliday WC, Mantsch HH. Beware of connective tissue proteins: assignment and implications of collagen absorptions in infrared spectra of human tissues. *Biochim Biophys Acta*. 1995;1270(1):1-6.
106. Darmon SE, Sutherland GBBM. Infrared spectra and structure of natural and synthetic polypeptides. *Journal of American Chemical Society*. 1947;69(8):2074.
107. Wong PT, Siminovitch DJ, Mantsch HH. Structure and properties of model membranes: new knowledge from high-pressure vibrational spectroscopy. *Biochim Biophys Acta*. 1988;947(1):139-71.
108. Surewicz WK, Mantsch HH. New insight into protein secondary structure from resolution-enhanced infrared spectra. *Biochim Biophys Acta*. 1988;952(2):115-30.
109. Wood B, Tait B, McNaughton D. Fourier Transform Infrared Spectroscopy as a Method for Monitoring the Molecular Dynamics of Lymphocyte Activation. *Applied Spectroscopy*. 2000;54(3):353-9.
110. Taillandier E, Liquier J, Taboury JA. Infrared Spectral Studies of DNA Conformations. *Advances in infrared and Raman Spectroscopy*. 1985;12:65-114.
111. Fabian H, Jackson M, Murphy L, Watson PH, Fichtner I, Mantsch HH. A comparative infrared spectroscopic study of human breast tumors and breast tumor cell xenografts. *Biospectroscopy*. 1995;1:37-45.
112. Diem M, Boydston-White S, Chiriboga L. Infrared Spectroscopy of cells and Tissues: Shining Light onto a Novel Subject. *Applied Spectroscopy*. 1999;53(4):148A-61A.
113. Rieppo L, Saarakkala S, Narhi T, Holopainen J, Lammi M, Helminen HJ, et al. Quantitative analysis of spatial proteoglycan content in articular cartilage with Fourier transform infrared imaging spectroscopy: Critical evaluation of analysis methods and specificity of the parameters. *Microsc Res Tech*. 2010;73(5):503-12.
114. Synder RG, Strauss HL, Elliger CA. C-H Stretching Modes and the Structure of n-Alkyl Chains. 1. Long, Disordered Chains. *Journal of Physical Chemistry*. 1982;86:5145-50.
115. Payne KJ, Veis A. Fourier transform IR spectroscopy of collagen and gelatin solutions: deconvolution of the amide I band for conformational studies. *Biopolymers*. 1988;27(11):1749-60.
116. Kauppinen JK, Moffatt DJ, Mantsch HH, Cameron DG. Fourier Self-Deconvolution: A Method for Resolving Intrinsically Overlapped Bands. *Applied Spectroscopy*. 1987;35(3):271-6.
117. Surewicz WK, Mantsch HH, Chapman D. Determination of protein secondary structure by Fourier transform infrared spectroscopy: a critical assessment. *Biochemistry*. 1993;32(2):389-94.
118. Kennedy DF, Crisma M, Toniolo C, Chapman D. Studies of peptides forming 3(10)- and alpha-helices and beta-bend ribbon structures in organic solution and in model biomembranes by Fourier transform infrared spectroscopy. *Biochemistry*. 1991;30(26):6541-8.
119. Kauppinen JK, Moffatt DJ, Cameron DG, Mantsch HH. Noise in Fourier self-deconvolution. *Appl Opt*. 1981;20(10):1866-79.
120. Dong A, Huang P, Caughey WS. Protein secondary structures in water from second-derivative amide I infrared spectra. *Biochemistry*. 1990;29(13):3303-8.
121. Cameron DG, Moffat DJ. A generalized approach to derivative spectroscopy. *Applied Spectroscopy*. 1986 41:539-44.
122. George A, Veis A. FTIRS in H₂O demonstrates that collagen monomers undergo a conformational transition prior to thermal self-assembly in vitro. *Biochemistry*. 1991;30(9):2372-7.

123. Lazarev YA, Grishkovsky BA, Khromova TB. Amide I band of IR spectrum and structure of collagen and related polypeptides. *Biopolymers*. 1985;24(8):1449-78.
124. Petibois C, Gouspillou G, Wehbe K, Delage JP, Deleris G. Analysis of type I and IV collagens by FT-IR spectroscopy and imaging for a molecular investigation of skeletal muscle connective tissue. *Anal Bioanal Chem*. 2006;386(7-8):1961-6.
125. Lazarev YA, Grishkovsky BA, Khromova TB, Lazareva AV, Grechishko VS. Bound water in the collagen-like triple-helical structure. *Biopolymers*. 1992;32(2):189-95.
126. Bychkov SM, Bogatov VN, Kharlamova VN. Infrared spectra of certain proteoglycans. *Biull Eksp Biol Med*. 1980;89(6):680-2.
127. Bychkov SM, Bogatov VN, Kuz'mina SA. Infrared spectra of cartilage proteoglycans. *Biull Eksp Biol Med*. 1980;90(11):561-3.
128. Bychkov SM, Kuz'mina SA. Study of tissue proteoglycans by means of infrared spectroscopy. *Biull Eksp Biol Med*. 1992;114(9):246-9.
129. Bychkov SM, Kuz'mina SA. The comparative study of the IR spectra of proteoglycans. *Biull Eksp Biol Med*. 1991;112(11):480-2.
130. Bychkov SM, Bogatov VN, Kuz'mina SA. Comparative study of the IR-spectra of glycosaminoglycans and their monomers. *Biull Eksp Biol Med*. 1981;91(4):442-5.
131. Fraser RDB, P MT. Conformation in Fibrous Proteins and Related Synthetic Polypeptides. In: Horecker B, Kaplan NO, Marmur J, Scheraga HA, editors. *Conformation in Fibrous Proteins and Related Synthetic Polypeptides*: Academic New York; 1973. p. 344-402.
132. Bychkov SM, Zakharova MM, Kuz'mina SA, Pavlov VP. Study of articular cartilage and the synovial membrane using IR spectroscopy. *Biull Eksp Biol Med*. 1987;104(11):554-6.
133. Potter K, Kidder LH, Levin IW, Lewis EN, Spencer RG. Imaging of collagen and proteoglycan in cartilage sections using Fourier transform infrared spectral imaging. *Arthritis Rheum*. 2001;44(4):846-55.
134. Diem M, Chiriboga L, Yee H. Infrared spectroscopy of human cells and tissue. VIII. Strategies for analysis of infrared tissue mapping data and applications to liver tissue. *Biopolymers*. 2000;57(5):282-90.
135. Lasch P, Haensch W, Naumann D, Diem M. Imaging of colorectal adenocarcinoma using FT-IR microspectroscopy and cluster analysis. *Biochim Biophys Acta*. 2004;1688(2):176-86.
136. Wood BR, Chiriboga L, Yee H, Quinn MA, McNaughton D, Diem M. Fourier transform infrared (FTIR) spectral mapping of the cervical transformation zone, and dysplastic squamous epithelium. *Gynecol Oncol*. 2004;93(1):59-68.
137. Crombie DE, Mackay IR, Wood BR, McNaughton D, Rowley MJ. Images of interest. Hepatobiliary and pancreatic: Liver histopathology: Fourier transform infrared microspectroscopic imaging for objective and quantifiable assessment of liver biopsies. *J Gastroenterol Hepatol*. 2005;20(3):485.
138. Romeo MJ, Wood BR, Quinn MA, McNaughton D. Removal of blood components from cervical smears: implications for cancer diagnosis using FTIR spectroscopy. *Biopolymers*. 2003;72(1):69-76.
139. El-Tawil SG, Adnan R, Muhamed ZN, Othman NH. Comparative study between Pap smear cytology and FTIR spectroscopy: a new tool for screening for cervical cancer. *Pathology*. 2008;40(6):600-3.
140. Saadat E, Lan H, Majumdar S, Rempel DM, King KB. Long-term cyclical in vivo loading increases cartilage proteoglycan content in a spatially specific manner: an infrared

- microspectroscopic imaging and polarized light microscopy study. *Arthritis Res Ther.* 2006;8(5):R147.
141. West PA, Bostrom MP, Torzilli PA, Camacho NP. Fourier transform infrared spectral analysis of degenerative cartilage: an infrared fiber optic probe and imaging study. *Appl Spectrosc.* 2004;58(4):376-81.
142. West PA, Torzilli PA, Chen C, Lin P, Camacho NP. Fourier transform infrared imaging spectroscopy analysis of collagenase-induced cartilage degradation. *J Biomed Opt.* 2005;10(1):14015.
143. Ueno M, Shibata A, Yasui S, Yasuda K, Ohsaki K. A proposal on the hard tissue remineralization in osteoarthritis of the knee joint investigated by FT-IR spectrometry. *Cell Mol Biol (Noisy-le-grand).* 2003;49(4):613-9.
144. Boskey A, Pleshko Camacho N. FT-IR imaging of native and tissue-engineered bone and cartilage. *Biomaterials.* 2007;28(15):2465-78.
145. Heraud P, Wood BR, Tobin MJ, Beardall J, McNaughton D. Mapping of nutrient-induced biochemical changes in living algal cells using synchrotron infrared microspectroscopy. *FEMS Microbiol Lett.* 2005;249(2):219-25.
146. Jamin N, Dumas P, Moncuit J, Fridman WH, Teillaud JL, Carr GL, et al. Highly resolved chemical imaging of living cells by using synchrotron infrared microspectrometry. *Proc Natl Acad Sci U S A.* 1998;95(9):4837-40.
147. Burghardt AJ, Wang Y, Elalieh H, Thibault X, Bikle D, Peyrin F, et al. Evaluation of fetal bone structure and mineralization in IGF-I deficient mice using synchrotron radiation microtomography and Fourier transform infrared spectroscopy. *Bone.* 2007;40(1):160-8.
148. Huang RY, Miller LM, Carlson CS, Chance MR. In situ chemistry of osteoporosis revealed by synchrotron infrared microspectroscopy. *Bone.* 2003;33(4):514-21.
149. Miller LM, Novatt JT, Hamerman D, Carlson CS. Alterations in mineral composition observed in osteoarthritic joints of cynomolgus monkeys. *Bone.* 2004;35(2):498-506.
150. Miller LM, Vairavamurthy V, Chance MR, Mendelsohn R, Paschalis EP, Betts F, et al. In situ analysis of mineral content and crystallinity in bone using infrared microspectroscopy of the $\nu(4) PO(4)(3-)$ vibration. *Biochim Biophys Acta.* 2001;1527(1-2):11-9.
151. Ruppel ME, Burr DB, Miller LM. Chemical makeup of microdamaged bone differs from undamaged bone. *Bone.* 2006;39(2):318-24.
152. Tobin MJ, Chesters MA, Chalmers JM, Rutten FJ, Fisher SE, Symonds IM, et al. Infrared microscopy of epithelial cancer cells in whole tissues and in tissue culture, using synchrotron radiation. *Faraday Discuss.* 2004;126:27-39; discussion 77-92.
153. Petibois C, Cestelli-Guidi M, Piccinini M, Moenner M, Marcelli A. Synchrotron radiation FTIR imaging in minutes: a first step towards real-time cell imaging. *Anal Bioanal Chem.* 2010;397(6):2123-9.
154. Trentham DE, Townes AS, Kang AH. Autoimmunity to type II collagen an experimental model of arthritis. *J Exp Med.* 1977;146(3):857-68.
155. Steffen C. Consideration of pathogenesis of rheumatoid arthritis as collagen autoimmunity. *Z Immunitatsforsch Allerg Klin Immunol.* 1970;139(3):219-27.
156. Terato K, Hasty KA, Reife RA, Cremer MA, Kang AH, Stuart JM. Induction of arthritis with monoclonal antibodies to collagen. *J Immunol.* 1992;148(7):2103-8.
157. Courtenay JS, Dallman MJ, Dayan AD, Martin A, Mosedale B. Immunisation against heterologous type II collagen induces arthritis in mice. *Nature.* 1980;283:666-8.
158. Yoo TJ, Kim SY, Stuart JM, Floyd RA, Olson GA, Cremer MA, et al. Induction of arthritis in monkeys by immunization with type II collagen. *J Exp Med.* 1988;168(2):777-82.

159. Brand DD, Kang AH, Rosloniec EF. The mouse model of collagen-induced arthritis. *Methods Mol Med.* 2004;102:295-312.
160. Brand DD, Latham KA, Rosloniec EF. Collagen-induced arthritis. *Nat Protoc.* 2007;2(5):1269-75.
161. Brand DD, Kang AH, Rosloniec EF. Immunopathogenesis of collagen arthritis. *Springer Semin Immunopathol.* 2003;25(1):3-18.
162. Myers LK, Rosloniec EF, Cremer MA, Kang AH. Collagen-induced arthritis, an animal model of autoimmunity. *Life Sci.* 1997;61(19):1861-78.
163. Holmdahl R, Andersson ME, Goldschmidt TJ, Jansson L, Karlsson M, Malmstrom V, et al. Collagen induced arthritis as an experimental model for rheumatoid arthritis. Immunogenetics, pathogenesis and autoimmunity. *APMIS.* 1989;97(7):575-84.
164. Holmdahl R, Andersson M, Goldschmidt TJ, Gustafsson K, Jansson L, Mo JA. Type II collagen autoimmunity in animals and provocations leading to arthritis. *Immunol Rev.* 1990;118:193-232.
165. Moder KG, Nabozny GH, Luthra HS, David CS. Immunogenetics of collagen induced arthritis in mice: a model for human polyarthritis. *Reg Immunol.* 1992;4(5):305-13.
166. Griffiths MM. Immunogenetics of collagen-induced arthritis in rats. *Int Rev Immunol.* 1988;4(1):1-15.
167. Holmdahl R, Jansson L, Larsson E, Rubin K, Klareskog L. Homologous type II collagen induces chronic and progressive arthritis in mice. *Arthritis Rheum.* 1986;29(1):106-13.
168. Brand DD. Rodent models of rheumatoid arthritis. *Comp Med.* 2005;55(2):114-22.
169. Trentham DE, Dynesius-Trentham R. Collagen-induced Arthritis. In: Henferson B, Edwards JCW, Pettipher ER, editors. *Mechanisms and Models in Rheumatid Arthritis.* San Diego, CA: Academic Press Limited; 1995. p. 447-56.
170. Burkhardt H, Koller T, Engstrom A, Nandakumar KS, Turnay J, Kraetsch HG, et al. Epitope-specific recognition of type II collagen by rheumatoid arthritis antibodies is shared with recognition by antibodies that are arthritogenic in collagen-induced arthritis in the mouse. *Arthritis Rheum.* 2002;46(9):2339-48.
171. Burkhardt H, Sehnert B, Bockermann R, Engstrom A, Kalden JR, Holmdahl R. Humoral immune response to citrullinated collagen type II determinants in early rheumatoid arthritis. *Eur J Immunol.* 2005;35(5):1643-52.
172. Kraetsch HG, Unger C, Wernhoff P, Schneider C, Kalden JR, Holmdahl R, et al. Cartilage-specific autoimmunity in rheumatoid arthritis: characterization of a triple helical B cell epitope in the integrin-binding-domain of collagen type II. *Eur J Immunol.* 2001;31(6):1666-73.
173. Holmdahl R, Bailey C, Enander I, Mayer R, Klareskog L, Moran T, et al. Origin of the autoreactive anti-type II collagen response. II. Specificities, antibody isotypes and usage of V gene families of anti-type II collagen B cells. *J Immunol.* 1989;142(6):1881-6.
174. Schulte S, Unger C, Mo JA, Wendler O, Bauer E, Frischholz S, et al. Arthritis-related B cell epitopes in collagen II are conformation-dependent and sterically privileged in accessible sites of cartilage collagen fibrils. *J Biol Chem.* 1998;273(3):1551-61.
175. Klareskog L, Johnell O, Hulth A, Holmdahl R, Rubin K. Reactivity of monoclonal anti-type II collagen antibodies with cartilage and synovial tissue in rheumatoid arthritis and osteoarthritis. *Arthritis Rheum.* 1986;29(6):730-8.
176. Michaelsson E, Andersson M, Engstrom A, Holmdahl R. Identification of an immunodominant type-II collagen peptide recognized by T cells in H-2q mice: self tolerance at the level of determinant selection. *European journal of immunology.* 1992;22(7):1819-25.

177. Michaelsson E, Malmstrom V, Reis S, Engstrom A, Burkhardt H, Holmdahl R. T cell recognition of carbohydrates on type II collagen. *The Journal of experimental medicine*. 1994;180(2):745-9.
178. Di Paola R, Cuzzocrea S. Predictivity and sensitivity of animal models of arthritis. *Autoimmun Rev*. 2008;8(1):73-5.
179. Holmdahl R, Jansson L, Larsson A, Jonsson R. Arthritis in DBA/1 mice induced with passively transferred type II collagen immune serum. Immunohistopathology and serum levels of anti-type II collagen auto-antibodies. *Scand J Immunol*. 1990;31(2):147-57.
180. Wooley PH, Luthra HS, Singh SK, Huse AR, Stuart JM, David CS. Passive transfer of arthritis to mice by injection of human anti-type II collagen antibody. *Mayo Clin Proc*. 1984;59(11):737-43.
181. Nandakumar KS. Pathogenic antibody recognition of cartilage. *Cell Tissue Res*. 2010;339(1):213-20.
182. Bajtner E, Nandakumar KS, Engstrom A, Holmdahl R. Chronic development of collagen-induced arthritis is associated with arthritogenic antibodies against specific epitopes on type II collagen. *Arthritis Res Ther*. 2005;7(5):R1148-57.
183. Wu G, Zhu L, Dent JE, Nardini C. A comprehensive molecular interaction map for rheumatoid arthritis. *PLoS One*. 2010;5(4):e10137.
184. Koczan D, Drynda S, Hecker M, Drynda A, Guthke R, Kekow J, et al. Molecular discrimination of responders and nonresponders to anti-TNF alpha therapy in rheumatoid arthritis by etanercept. *Arthritis research & therapy*. 2008;10(3):R50.
185. Kagari T, Tanaka D, Doi H, Shimozato T. Essential role of Fc gamma receptors in anti-type II collagen antibody-induced arthritis. *Journal of immunology*. 2003;170(8):4318-24.
186. Nandakumar KS, Andren M, Martinsson P, Bajtner E, Hellstrom S, Holmdahl R, et al. Induction of arthritis by single monoclonal IgG anti-collagen type II antibodies and enhancement of arthritis in mice lacking inhibitory Fc gammaRIIB. *Eur J Immunol*. 2003;33(8):2269-77.
187. Nandakumar KS, Holmdahl R. Efficient promotion of collagen antibody induced arthritis (CAIA) using four monoclonal antibodies specific for the major epitopes recognized in both collagen induced arthritis and rheumatoid arthritis. *J Immunol Methods*. 2005;304(1-2):126-36.
188. Nandakumar KS, Bajtner E, Hill L, Bohm B, Rowley MJ, Burkhardt H, et al. Arthritogenic antibodies specific for a major type II collagen triple-helical epitope bind and destabilize cartilage independent of inflammation. *Arthritis Rheum*. 2008;58(1):184-96.
189. Fietzek PP, Kuhn K. Information contained in the amino acid sequence of the alpha1(I)-chain of collagen and its consequences upon the formation of the triple helix, of fibrils and crosslinks. *Mol Cell Biochem*. 1975;8(3):141-57.
190. Hietala MA, Nandakumar KS, Persson L, Fahlen S, Holmdahl R, Pekna M. Complement activation by both classical and alternative pathways is critical for the effector phase of arthritis. *Eur J Immunol*. 2004;34(4):1208-16.
191. Svensson L, Nandakumar KS, Johansson A, Jansson L, Holmdahl R. IL-4-deficient mice develop less acute but more chronic relapsing collagen-induced arthritis. *Eur J Immunol*. 2002;32(10):2944-53.
192. Johansson AC, Hansson AS, Nandakumar KS, Backlund J, Holmdahl R. IL-10-deficient B10.Q mice develop more severe collagen-induced arthritis, but are protected from arthritis induced with anti-type II collagen antibodies. *J Immunol*. 2001;167(6):3505-12.

193. Cook AD, Gray R, Ramshaw J, Mackay IR, Rowley MJ. Antibodies against the CB10 fragment of type II collagen in rheumatoid arthritis. *Arthritis research & therapy*. 2004;6(5):R477-83.
194. Cook AD, Rowley MJ, Mackay IR, Gough A, Emery P. Antibodies to type II collagen in early rheumatoid arthritis. Correlation with disease progression. *Arthritis Rheum*. 1996;39(10):1720-7.
195. Cook AD, Rowley MJ, Stockman A, Muirden KD, Mackay IR. Specificity of antibodies to type II collagen in early rheumatoid arthritis. *The Journal of rheumatology*. 1994;21(7):1186-91.
196. Fujii K, Tsuji M, Kitamura A, Murota K. The diagnostic significance of anti-type II collagen antibody assay in rheumatoid arthritis. *Int Orthop*. 1992;16(3):272-6.
197. Wernhoff P, Unger C, Bajtner E, Burkhardt H, Holmdahl R. Identification of conformation-dependent epitopes and V gene selection in the B cell response to type II collagen in the DA rat. *Int Immunol*. 2001;13(7):909-19.
198. Holmdahl R, Mo JA, Jonsson R, Karlstrom K, Scheynius A. Multiple epitopes on cartilage type II collagen are accessible for antibody binding in vivo. *Autoimmunity*. 1991;10(1):27-34.
199. Kerwar SS, Englert ME, McReynolds RA, Landes MJ, Lloyd JM, Oronsky AL, et al. Type II collagen-induced arthritis. Studies with purified anti-collagen immunoglobulin. *Arthritis Rheum*. 1983;26:1120-31.
200. Terato K, Harper DS, Griffiths MM, Hasty DL, Ye XJ, Cremer MA, et al. Collagen-induced arthritis in mice: synergistic effect of E. coli lipopolysaccharide bypasses epitope specificity in the induction of arthritis with monoclonal antibodies to type II collagen. *Autoimmunity*. 1995;22(3):137-47.
201. Malemud CJ. Matrix metalloproteinases (MMPs) in health and disease: an overview. *Front Biosci*. 2006;11:1696-701.
202. Colten HR. Immunology. Drawing a double-edged sword. *Nature*. 1994;371(6497):474-5.
203. Ravetch JV, Clynes RA. Divergent roles for Fc receptors and complement in vivo. *Annual review of immunology*. 1998;16:421-32.
204. van der Sluijs JA, Geesink RG, van der Linden AJ, Bulstra SK, Kuyer R, Drukker J. The reliability of the Mankin score for osteoarthritis. *J Orthop Res*. 1992;10(1):58-61.
205. Manz RA, Hauser AE, Hiepe F, Radbruch A. Maintenance of serum antibody levels. *Annu Rev Immunol*. 2005;23:367-86.
206. Hogarth PM. Fc receptors are major mediators of antibody based inflammation in autoimmunity. *Curr Opin Immunol*. 2002;14(6):798-802.
207. Mo JA, Holmdahl R. The B cell response to autologous type II collagen: biased V gene repertoire with V gene sharing and epitope shift. *J Immunol*. 1996;157(6):2440-8.
208. Croxford AM, Nandakumar K, Holmdahl R, Tobin MJ, McNaughton D, Rowley MJ. Chemical changes demonstrated in cartilage by synchrotron infrared microspectroscopy in an antibody-induced murine model of rheumatoid arthritis. *J Biomed Opt*. 2011.
209. Bi X, Li G, Doty SB, Camacho NP. A novel method for determination of collagen orientation in cartilage by Fourier transform infrared imaging spectroscopy (FT-IRIS). *Osteoarthritis Cartilage*. 2005;13(12):1050-8.
210. Croxford AM, Crombie D, McNaughton D, Holmdahl R, Nandakumar K, Rowley MJ. Specific antibody protection of the extracellular cartilage matrix against collagen antibody-induced damage. *Arthritis Rheum*. 2010.

211. Wood BR, Tait B, McNaughton D. Fourier-transform infrared spectroscopy as a tool for detecting early lymphocyte activation: a new approach to histocompatibility matching. *Hum Immunol.* 2000;61(12):1307-14.
212. Uysal H, Bockermann R, Nandakumar KS, Sehnert B, Bajtner E, Engstrom A, et al. Structure and pathogenicity of antibodies specific for citrullinated collagen type II in experimental arthritis. *J Exp Med.* 2009;206:449-62.
213. Lin PM, Chen CT, Torzilli PA. Increased stromelysin-1 (MMP-3), proteoglycan degradation (3B3- and 7D4) and collagen damage in cyclically load-injured articular cartilage. *Osteoarthritis Cartilage.* 2004;12(6):485-96.
214. Fosang AJ, Stanton H, Little CB, Atley LM. Neoepitopes as biomarkers of cartilage catabolism. *Inflamm Res.* 2003;52(7):277-82.
215. Angyal A, Egelston C, Kobezda T, Olasz K, Laszlo A, Glant TT, et al. Development of proteoglycan-induced arthritis depends on T cell-supported autoantibody production, but does not involve significant influx of T cells into the joints. *Arthritis research & therapy.* 2010;12(2):R44.
216. Glant TT, Finnegan A, Mikecz K. Proteoglycan-induced arthritis: immune regulation, cellular mechanisms, and genetics. *Crit Rev Immunol.* 2003;23(3):199-250.
217. Murat N, Karadam B, Ozkal S, Karatosun V, Gidener S. [Quantification of papain-induced rat osteoarthritis in relation to time with the Mankin score]. *Acta Orthop Traumatol Turc.* 2007;41(3):233-7.
218. Kopp S, Mejersjo C, Clemensson E. Induction of osteoarthrosis in the guinea pig knee by papain. *Oral Surg Oral Med Oral Pathol.* 1983;55(3):259-66.
219. Foidart JM, Abe S, Martin GR, Zizic TM, Barnett EV, Lawley TJ, et al. Antibodies to type II collagen in relapsing polychondritis. *N Engl J Med.* 1978;299(22):1203-7.
220. Okada Y, Nagase H, Harris ED, Jr. A metalloproteinase from human rheumatoid synovial fibroblasts that digests connective tissue matrix components. Purification and characterization. *The Journal of biological chemistry.* 1986;261(30):14245-55.
221. van Meurs J, van Lent P, Holthuysen A, Lambrou D, Bayne E, Singer I, et al. Active matrix metalloproteinases are present in cartilage during immune complex-mediated arthritis: a pivotal role for stromelysin-1 in cartilage destruction. *Journal of immunology.* 1999;163(10):5633-9.
222. Byler DM, Susi H. Examination of the secondary structure of proteins by deconvolved FTIR spectra. *Biopolymers.* 1986;25:469-87.
223. Heraud P, Caine S, Campanale N, Karnezis T, McNaughton D, Wood BR, et al. Early detection of the chemical changes occurring during the induction and prevention of autoimmune-mediated demyelination detected by FT-IR imaging. *Neuroimage.* 2010;49(2):1180-9.
224. Sato M, Wada M, Miyoshi N, Imamura Y, Noriki S, Uchida K, et al. Hydroxyapatite Maturity in the Calcified Cartilage and Underlying Subchondral Bone of Guinea Pigs with Spontaneous Osteoarthritis: Analysis by Fourier Transform Infrared Microspectroscopy. *Acta Histochem Cytochem.* 2004;37(2):101-7.
225. Henderson I, Lavigne P, Valenzuela H, Oakes B. Autologous chondrocyte implantation: superior biologic properties of hyaline cartilage repairs. *Clin Orthop Relat Res.* 2007;455:253-61.
226. Knight CG, Morton LF, Peachey AR, Tuckwell DS, Farndale RW, Barnes MJ. The collagen-binding A-domains of integrins alpha(1)beta(1) and alpha(2)beta(1) recognize the same specific amino acid sequence, GFOGER, in native (triple-helical) collagens. *The Journal of biological chemistry.* 2000;275(1):35-40.

227. Siljander PR, Hamaia S, Peachey AR, Slatter DA, Smethurst PA, Ouwehand WH, et al. Integrin activation state determines selectivity for novel recognition sites in fibrillar collagens. *The Journal of biological chemistry*. 2004;279(46):47763-72.
228. Mansson B, Wenglen C, Morgelin M, Saxne T, Heinegard D. Association of chondroadherin with collagen type II. *The Journal of biological chemistry*. 2001;276(35):32883-8.
229. Fertala A, Sieron AL, Adachi E, Jimenez SA. Collagen II containing a Cys substitution for Arg-alpha1-519: abnormal interactions of the mutated molecules with collagen IX. *Biochemistry*. 2001;40(48):14422-8.

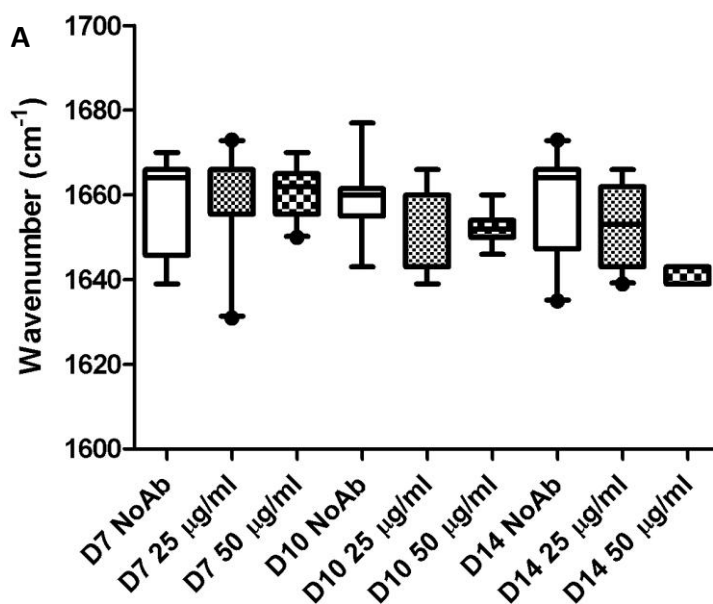
APPENDIX

The effects of two concentrations of arthritogenic mAbs to CII in cartilage.

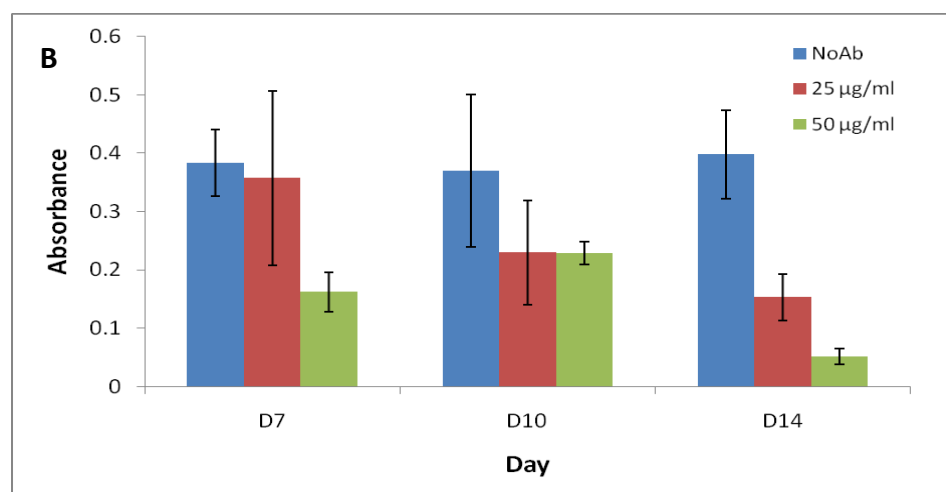
The effects of two different concentrations of two arthritogenic CII specific mAbs M2139 and CIIC1 on pre-existing cartilage *in vitro* were analysed using FTIRM.

Two separate experiments were conducted where bovine cartilage explants were cultured in the presence of M2139 and CIIC1 using two antibody concentrations, 25 µg/ml or 50 µg/ml or without mAb and data was collected at days 7, 10 and 14. Chemical changes to cartilage focussed on changes to CII and proteoglycans and were assessed by FTIRM. The location of the amide 1 peak was used for CII, where a shift to a wavenumber below 1660 cm⁻¹ indicates denaturation and changes to the height of the peak at 1080 cm⁻¹ was used for proteoglycan content. Ten individual spectra were collected from the exterior of the cartilage in each experiment at each time point and a median location of amide 1 peak and a mean proteoglycan absorbance at 1080 cm⁻¹ for the combined experiments (n=20) were calculated and compared with a no antibody control.

A progressive shift in the location of the amide 1 peak to a lower wavenumber was observed with both 25 µg/ml and 50 µg/ml arthritogenic mAb; however, this occurred to a larger degree with 50 µg/ml arthritogenic mAb. The greatest shift in the position of the amide 1 peak occurred at day 14, where the median location had shifted from 1660 to 1639 cm⁻¹. A similar pattern was observed by examining the height of the proteoglycan peak at 1080 cm⁻¹, where there was a progressive decrease in proteoglycans from day 7 to 14 with both 25 µg/ml but more so with 50µg/ml arthritogenic mAb.



A: Median location of amide 1 peak (line), box is interquartile range and the whiskers represent 95% confidence interval at days 7, 10 and 14 with no antibody, 25 µg/ml or 50 µg/ml arthritogenic mAbs M2139 and CIIC1. The location of the amide 1 peak shifts below 1660 cm⁻¹ with increasing concentration of mAb and time in culture.



B: Mean \pm SD absorbance of proteoglycans (1080 cm⁻¹) at days 7, 10 and 14 with no antibody, 25 µg/ml or 50 µg/ml of arthritogenic mAbs M2139 and CIIC1. With increasing concentration of mAb the amount of proteoglycans decreases.

The data presented indicate that increasing concentrations of mAbs cause an increase in cartilage damage, and therefore a concentration of 25 µg/ml of each arthritogenic mAbs giving a combined final concentration of 50 µg/ml was selected for future mAb experiments to examine changes to cartilage.